MOLECULAR BIOLOGY AND PATHOGENESIS OF CORONAVIRUS: VIRUS AND HOST FACTORS INVOLVED IN VIRAL RNA TRANSCRIPTION

TAN YONG WAH

(B. SC., NATIONAL UNIVERSITY OF SINGAPORE)

A THESIS SUBMITTED FOR THE DEGREE OF

DOCTOR OF PHILOSOPHY

DEPARTMENT OF BIOCHEMISTRY

NATIONAL UNIVERSITY OF SINGAPORE

2012

Acknowledgements

I would like to thank Associate Professor Liu Ding Xiang for his mentorship and unceasing guidance for the past five years working on this thesis. I would also like to thank Professor Hong Wanjin and Associate Professor Zhang Lianhui for their critical feedback during the annual progress review meetings which have definitely made a positive impact on the work that has been done.

I would like to express my gratefulness for the help and guidance provided by the members of the Molecular Virology and Pathogenesis Lab in IMCB. Special thanks to Dr. Xu Linghui for her advice on yeast-related work and Dr. Fang Shouguo for his advice on molecular techniques. My heartfelt gratitude goes to Felicia, Huihui, Yanxin, Siti, Selina, Dr. Nasir, Dr. Yamada and Dr. Wang Xiaoxing for their everyday advice on my experiments and support when difficulties were encountered.

I would also like to thank IMCB for providing me with an opportunity to further my studies under the Scientific Staff Development Scheme, Dr. Shanthi Wasser for allowing me to continue using the BSL2+ containment facility after the lab has moved out and Associate Professor Tan Yee Joo for allowing me to work in her lab at IMCB for several months. Lastly, I would like to thank my husband for his unceasing love and understanding for the past five years which has allowed me to focus on my research.

Table of Contents

Summary

A successful coronavirus infection is characterized by the release of infectious progeny particles which entails the replication of the viral genome and its packaging into infectious particles by its structural proteins. These two processes are dependent upon its ability to synthesize both the positive-sense genomic mRNA and a set of positive-sense subgenomic mRNAs for genome replication and viral proteins expression respectively.

The cleavage products from the coronavirus replicase gene, also known as the non-structural proteins (nsps), are believed to make up the major components of the viral replication/transcription complex. Although viral RNA synthesis is thought to be one of the most important parts of the virus life cycle, it is still not fully understood with respect to how the complex functions as a whole, or the degree of cellular protein involvement. Till date, only a number of enzymatic functions have been assigned to several nsps and a handful of host proteins have been identified so far to play a role in coronavirus RNA synthesis.

Zinc finger CCHC-type and RNA binding motif 1 (ZCRB1 alias MADP1) has been identified as a possible host protein involved in RNA synthesis of coronaviruses. The protein has found to interact with the positive-sense 5'untranslated region (UTR) of infectious bronchitis virus (IBV) but weakly with that of severe acute respiratory syndrome coronavirus (SARS-CoV) and human coronavirus OC43 (HCoV-OC43). Further characterization of this interaction confirmed it to be specific and the interacting domains have been subsequently mapped to the RNA recognition motif domain of MADP1 and stem-loop I of the positive-sense IBV 5'-UTR. It was

observed that upon virus infection, MADP1 translocated to the cytoplasm, a deviation from its regular nuclear localization pattern, an indication of possible involvement in the virus life cycle.

Functional analyses using small interfering RNA to silence the gene has elucidated the function of MADP1, a determinant of efficient negative-sense RNA synthesis. A confirmation of the role of MADP1 in virus infection was obtained when it was shown that the expression of MADP1 resistant to the silencing effects of the hairpin RNA targeting MADP1 enhanced virus infection in stable MADP1 knock-down cells.

While progress has been made on host involvement in coronavirus RNA synthesis, the role of viral proteins has not been forgotten. Several nsps encoded by IBV were screened for RNA-binding activity and interaction with its RNA-dependent RNA polymerase, nsp12. Four non-structural proteins, nsp2, nsp8, nsp9 and nsp10 were found to bind to either of the UTRs assessed and nsp8 was confirmed to interact with nsp12. Nsp8 had been reported to form a complex with nsp7 which was functionally assigned as the primase synthesizing RNA primers for nsp12.

Further characterization of the interaction between nsp8 and nsp12 revealed that the interaction is independent of the presence of RNA was subsequently shown that nsp8 interacts with both the N- and C-termini of nsp12. These results have prompted a proposal of how the nsp7-nsp8 complex could possibly function in tandem with nsp12, forming a highly efficient complex which could synthesize both the RNA primer and viral RNA during coronavirus infection. (507 words)

List of Tables

List of Figures

List of Publications

1. Tan, Y.W., Hong, W. and Liu, D.X. (2012) Binding of the 5'-untranslated region of coronavirus RNA to zinc finger CCHC-type and RNA-binding motif 1 enhances viral replication and transcription. *Nucleic Acids Res*.

2. Tan, Y.W., Fang, S., Fan, H., Lescar, J. and Liu, D.X. (2006) Amino acid residues critical for RNA-binding in the N-terminal domain of the nucleocapsid protein are essential determinants for the infectivity of coronavirus in cultured cells. *Nucleic Acids Res*, **34**, 4816-4825.

3. Fan, H., Ooi, A., Tan, Y.W., Wang, S., Fang, S., Liu, D.X. and Lescar, J. (2005) The nucleocapsid protein of coronavirus infectious bronchitis virus: crystal structure of its N-terminal domain and multimerization properties. *Structure*, **13**, 1859-1868.

Chapter 1 Literature Review: The Biology of Coronavirus

1.1 Overview of Coronaviruses

1.1.1 Taxonomy, genomic and physical properties of Coronaviruses

Coronaviruses are a group of enveloped RNA viruses whose genome is in the form of a positive-sense single stranded RNA molecule. They are classified under the order of *Nidovirales,* family of *coronaviridae* and subfamily of *coronavirinae*. Within this subfamily, the coronaviruses are divided into three genera, the *alpha-*, *beta-* and *gammacoronavirus*, based on their antigenic and genetic properties.

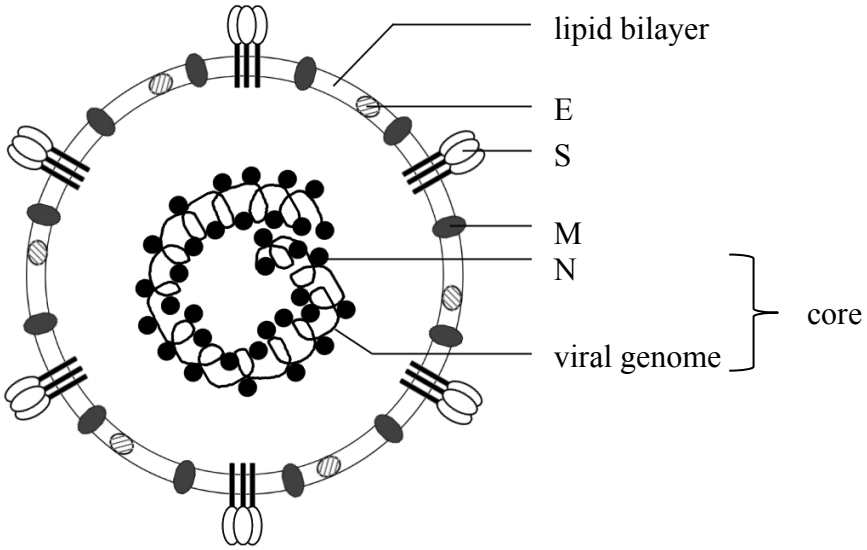

Figure 1.1: Schematic diagram of a coronavirus particle.

The outermost layer of the coronavirus particle, as depicted in the Figure 1.1 is a double-membrane envelope, embedded with the virus structural proteins spike (S), membrane (M) and envelope (E). Some betacoronaviruses are able to encode an additional structural protein, the haemagglutinin-estarase (HE), which is also represented on the double-membrane envelope. Encompassed within the virus envelope is the ribonucleocapsid core, which comprised of two components: the viral

mRNA genome and the structural protein, nucleocapsid (N). The N protein packages and compact the fairly large viral genomic RNA into the relatively small sized virus particle through RNA-protein interactions.

The coronavirus genome is a 5'-capped, single-stranded positive-sense mRNA, which is the largest known of its kind, ranging from 27 to 32 kb in length (1). The mRNA is

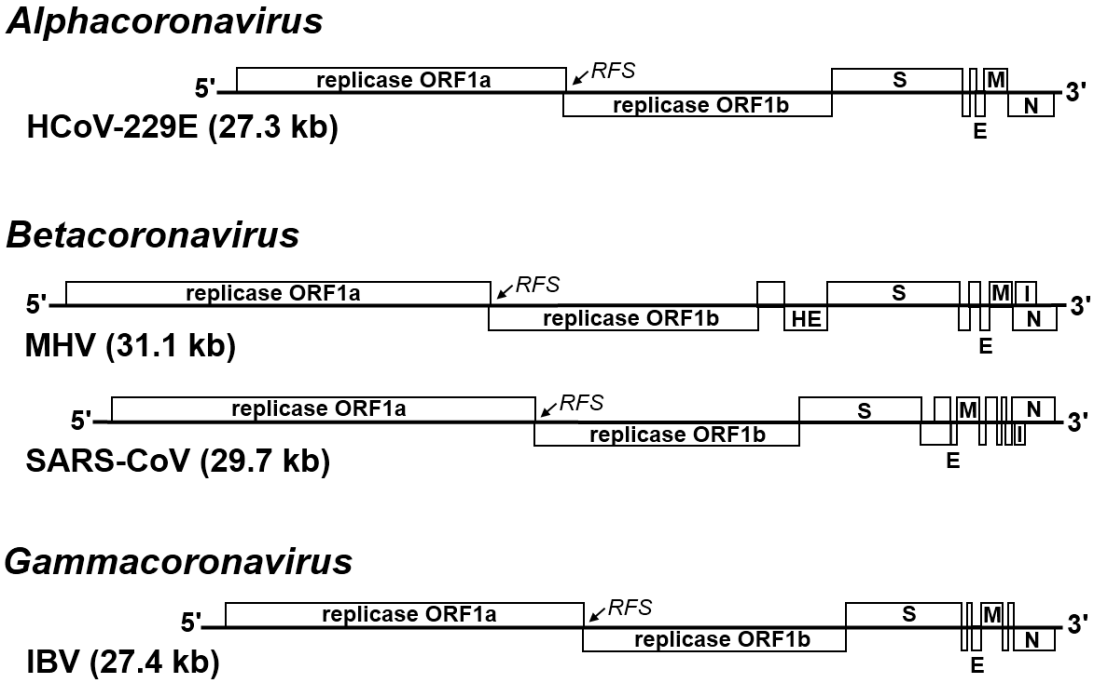

Figure 1.2: Genome Organization of selected coronaviruses. Replicase and structural genes and ribosomal frameshift site (RFS) are indicated. Internal ORF within N gene encoded by betacoronaviruses is denoted I. Unlabeled blocks represent accessory genes.

flanked by two untranslated regions, the 5'-UTR, which ranges from 209 – 528 nucleotides (nt) in length, contains the leader sequence (65 – 98 nt) and the 3'-UTR (288 – 506 nt), contains an octameric sequence of GGAAGAGC (beginning at residue 73 – 81) upstream of the poly(A) tail. As shown in Figure 1.2, coronaviruses have an extremely large gene 1 (ORF 1), spanning about two-thirds of the entire genome, which encodes for the non-structural proteins involved in viral RNA transcription.

ORF 1 is translated into two poly proteins, pp1a and pp1ab via a pseudoknot-induced frameshifting event upstream at the ORF1a/1b junction.

The structural genes are encoded in the order of S, E, M, N, 5' – 3', within the 3' one-third of the genome. Interspersed between these structural genes is a variable number of ORFs encoding accessory proteins including HE. Some of these accessory genes, like ORF 4, 5a (2,3), have been proven to be dispensable for virus replication in cultured cells or even in their natural host (4).

The most prominent feature of the virus particle, and that which gives the coronavirus its name, is the S protein, a large (≈180 kDa) class I virus fusion protein (5) embedded in the virus envelope. S is cleaved post-translationally into two fragments by cellular proteases (6,7), S1 (receptor binding domain) and S2 (transmembrane domain) that interacts with each other through non-convalent bonding (8). S1 is responsible for receptor recognition, defining cell tropism (9), whereas S2 mediates the fusion between viral and cellular membranes through the fusion peptide sequence.

In *betacoronavirus*, phylocluster A, an additional protein is present on the viral envelope, the HE protein. The ability to express the HE protein is lost in many laboratory strains of the murine coronavirus (MHV) (10), including the widely studied MHV-A59 (11), but is however retained in other laboratory strains like MHV-S, -JHM and –DVIM (10,12,13) as well as field strains. The coronavirus HE protein has been shown to exhibit both sialic acid binding and receptor-destroying enzymatic activity (RDE) (14,15). The significance of sialic acid binding activity of HE varies between coronaviruses, in bovine coronavirus (BCoV) and human coronavirus (HCoV) OC43, HEs appear to play only a modest role in viral attachment to sialic

acids (16,17). On the otherhand, hemagglutination activity of MHV-DVIM appears to depend upon the availability of HE.

The coronavirus N protein is a RNA chaperone (18) which is essential for the formation of the helical ribonucleoprotein (RNP) core with viral genomic RNA that which is also its primary function. The coronavirus N is composed of about 400 amino acid residues, contains two structural domains, the N-terminal RNA-binding domain and the C-terminal dimerization domain joined by a linker region (19). The coronavirus N has been shown to be capable of self-association, forming dimers or oligomers of higher orders through its C-terminal dimerization domain (20,21) in a concentration dependent manner (22). The ability of N to self-associate and its subsequent formation of oligomers is vital for the encapsidation of coronaviral genomic mRNA (23). It has also been reported that the dimerization domain exhibits strong RNA-binding activity (24) and its association with nucleic acids can promote the formation of higher-order oligomers (25) which may have been the mechanism for the long RNP formation.

Embedded within the viral envelope is another structural protein of the coronavirus, the integral membrane glycoprotein, M. In terms of its structure, the M protein has a short ectodomain in its N-terminus, followed by three transmembrane regions and a long endodomain at its C-terminus and functions in dimers. The main function of M is in the adaptation of regions in the intracellular membranes, at the endoplasmic reticulum-golgi intermediate compartment (ERGIC) (26), for virus assembly by capturing other structural proteins at the budding site through protein-protein interactions with other structural proteins, S and N (27) as well as the viral gRNA

(28). Its ability to self-associate (29,30) also allows it to form a network which may have excluded some host proteins from the viral envelope.

A small integral membrane protein, the coronavirus envelope protein, E, is the smallest structural protein encoded by the virus. The E protein plays an important role in the formation of virus particles, including budding and morphogenesis (31-34). Its importance is heightened by the observation of it being able to form virus-like particles alone, in the absence of M, when it is over-expressed in cells (31,35). Mutations of the E protein also results in the formation of virions with aberrant morphologies (36) which implied the importance of E in viral morphogenesis.

1.1.2 Coronaviruses and diseases

Coronaviruses have identified in a variety of domesticated animals, rodents as well as humans. As coronaviruses infect livestock, viral infections in farms have resulted in large scale economic losses in farming nations, and hence are of exceptional veterinary research value. Coronaviruses in fowls, exemplified by the highly contagious infectious bronchitis virus (IBV) in chickens, can be highly lethal to young chicks and are mainly associated with upper respiratory tract infections in adults, and to a lesser extent, nephrogenic infections. In larger livestock like pigs and cattle on the otherhand, coronaviruses typically establish enteric infections. In both cases, an infection or outbreak can cause severe economic losses from death of young, lifelong impact on the yield of animal produce (eggs and milk), weight losses and the general health of the population. With respect to their significance to the economy, vaccines have been developed for many coronaviruses in a bid to prevent localized infections

from progressing into serious outbreaks. This has however proved to be a hard battle as the vaccines are unable to provide complete cross-protection between the various serotypes of each coronavirus and have to be updated regularly to target emerging strains.

Murine coronaviruses, exemplified by MHV, can cause high mortality epidemic illness, which particularly impacts laboratory mice colonies which are kept in close proximity. As the murine coronavirus infections complicate research, it has been promptly picked up by researchers in order to exclude this disease from laboratories worldwide, and was the most extensively studied coronavirus before 2002.

Human coronaviruses have, in the recent years, been placed in the limelight with the emergence of severe acute respiratory virus (SARS-CoV) in late 2002, infecting more than 8000 people with a mortality rate of roughly 10%. Prior to the outbreak, human coronaviruses, being the etiologic agent responsible for 10-15% of common cold, have received little attention due to the mild display of symptoms although they may result in fatalities, especially in in weaker individuals complicated by other diseases. After the SARS-CoV epidemic, 2 new human coronaviruses have also been isolated, the alphacoronavirus HCoV-NL63 and betacoronavirus HCoV-HKU.

1.2 The Coronavirus Life Cycle

There are multiple stages in the coronavirus life cycle and the very first step would be its attachment to a suitable host cell via cellular receptors followed by the entry of the virus particle into the cytosol where the helical virus genome is released from the N protein it was packaged with. The virus genome is a 5'-methyl capped positive sense mRNA which mimics the eukaryotic mRNAs and hence is able to make use of the existing ribosomes to translate its genome. Only the ORF on the 5' most of the mRNA, the replicase gene, is translated, producing two polyproteins, pp1a and pp1ab via a (-1) ribosomal frame shift event. These two polyproteins are auto-proteolytically cleaved into the non-structural proteins co-translationally. The non-structural proteins make up the bulk of the replication/transcription complex (RTC) which is anchored onto double membrane vesicles (DMVs), the site where virus transcription/replication takes place (37-39).

The products of the RTCs is a nested set of mRNAs that are co-terminal at both their 5'- and 3'- ends and the longest being mRNA1, the genomic-sized mRNA (gRNA) and the sub-genome sized mRNAs (sgRNAs) which are destined to be packaged into progeny virus particles and used for viral structural and accessory gene expression respectively. Translation of the structural genes produces the viral S, E, M and N proteins which are assembled at the endoplasmic reticulum-golgi intermediate compartment (ERGIC) together with the gRNA into progeny viruses which are eventually exported out of the host cell via exocytosis.

Figure 1.3 is a diagrammatic representation of the key events in the coronavirus life cycle, a slightly modified version of that published by Stadler et al. (2003) (40).

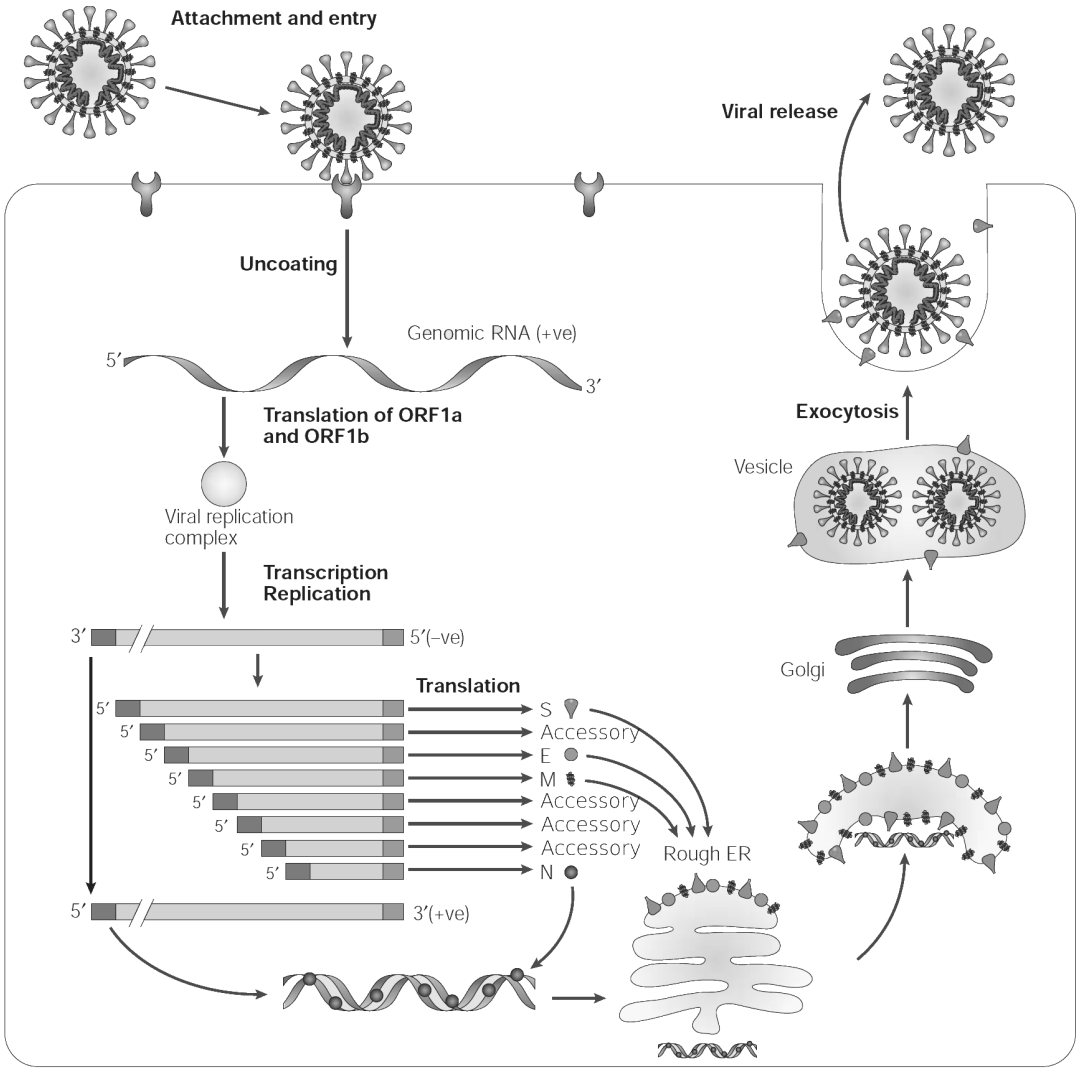

Figure 1.3: Life cycle of a coronavirus. Virus particle attached onto the host cell via cellular receptors on the surface and enters. Entry is followed by the uncoating of the ribonucleocapsid to expose the positive-sense genomic RNA which is translated by the host ribosomes to yield the viral replication complex. Viral transcription and replication of genome is achieved by the viral replication complex, yielding a nested set of positive-sense sub-genomic sized mRNAs as well as the full length virus genome. Sub-genomic sized mRNAs are translated by host ribosomes into viral structural (S, E, M, N) and accessory proteins. The N protein packages the positive-sense genomic RNA into a ribonucleocapsid and is assembled into the virus particles. The newly formed virus particles undergo maturation by passaging through the Golgi and exit the host cell via exocytosis.

1.2.1 Attachment and entry

Entry of the virus can take place either through direct entry when the viral envelope fuses with the cell membrane directly, or through the endosomal pathway where the virion enters by endocytosis and fusion occurs between the viral envelope and the endosomal membrane in an acidic pH environment (41,42). Most coronaviruses are able to utilize the endosomal pathway and some are able to engage in pH independent direct entry like most MHVs (43,44). The very first step of virus entry is the attachment of the virus particle onto host cells via their attachment protein, S, the receptor binding protein. S protein has two functional domains, the receptor binding domain, which defines the tropism of the virus as well as a membrane fusion domain, which mediates the fusion event between viral envelope and cell membrane during virus entry.

Many host cell proteins have been identified as receptors for the different coronaviruses including the angiotensin converting enzyme 2 (ACE2) for HCoV-NL63 and SARS-CoV (45-47), carcinoembryonic antigen-cell adhesion molecules (CEACAMs) for the MHV, aminopeptidase N for most alphacoronaviruses eg. feline infectious peritonitis virus (FIPV) and transmissible gastroenteritis virus (TGEV). Some betacoronaviruses, eg. BCoV and HCoV-OC43, employ a similar strategy to influenza viruses by using the N-acetyl-9-O-acetyl neuraminic acid as a receptor and encodes an additional non-structural protein, the HE, which possess receptor destroying activity, preventing the formation of virus aggregates as well as facilitating virus release.

On the otherhand, the receptor for some coronaviruses, in particular, that of gammacoronavirus IBV, has not been identified. The presence of α2, 3-linked sialic acids serves as a receptor determinant of IBV in primary attachment as it has been shown that neuraminidase treatment rendered the previously permissible host cells resistant to IBV infection (48). This however does not establish the identity of the receptor employed by IBV for virus entry as α2, 3-linked sialic acid has a broad distribution pattern in different tissues and varies between species, in contrast to the narrow host tropism exhibited by the virus. This implied the existence of another receptor in addition to the α2, 3-linked sialic acid (9), required for successful entry of the IBV particle into the host cell and primary attachment to sialic acid may have enhanced the probability of the virus S protein coming into close proximity of the actual receptor.

After the receptor-binding ectodomain of S protein on the surface of the viral envelope attaches onto the receptor presented on the host cell surface, a conformation change takes place to expose the protease cleavage site, which prepares for the second step in virus entry, membrane fusion. Whether the virus uses the direct entry pathway or the endosomal pathway, cellular proteases are required to cleave the virus S protein into two parts the S1 (receptor binding domain) and the S2 (membrane fusion domain). This in turn induces a conformation change in the S2 domain to expose the membrane fusion peptide (heptad repeat regions) which initiates the formation of a six-helix bundle, bringing viral and cellular membranes into close proximity, thereby facilitating membrane fusion.

From studies in the human coronavirus, SARS-CoV, several cellular proteases have been found to serve as fusion activators, including endosomal protease, cathepsin L (49), soluble proteases elastase, trypsin, thermolysin (50), factor Xa (51), furin (52) and transmembrane protease/serine subfamily member 11a (TMPRSS11a) (53). Some of these proteases have also been found to play a role in facilitating virus entry in other coronaviruses like trypsin and cathepsin L in MHV (54) and furin in IBV (55). Although soluble proteases have been identified to be fusion activators, the mechanism behind which these proteases may catalyze the proteolytic cleavage on the cell surface has not been established. It was however speculated that they can either function in the early endosome or are anchored near the receptors after being released onto the cell surface.

1.2.2 Translation and auto-proteolytic processing

Upon successful membrane fusion either at the cell surface or the endosomal membrane, the ribonucleocapsid is released into the cytosol and rapidly uncoats, releasing the viral genomic mRNA. The virus genomic mRNA is 5'-methylated capped and has a poly(A) tail which appears very similar to the host mRNA. This strategy allows the virus to make use of the host translation machinery directly for the translation of the replicase gene, the first ORF on the mRNA.

The replicase gene, which spans the 5'-two-thirds of the mRNA, is translated by the host ribosomes into two large polyproteins, pp1a and pp1ab via a (-1) frameshift event (56-58). Figure Figure 1.4 illustrates the domain organization of the two polyproteins. The polyproteins are auto-proteolytically processed into 15 or 16 non-structural

proteins (59) by means of the virus encoded proteases, the papain-like protease (PL^{pro}) nsp3 and the 3C-like protease or main protease (M^{pro}) nsp5 (60,61). The use of protease inhibitors specific to cysteine proteases, the class of protease nsp3 and nsp5 belongs to, blocks their protease activity and inhibits viral RNA synthesis, highlighting the importance of these two proteins (62). As the name suggests, the main protease (M^{pro}) or 3C-like protease, nsp5, is the major protease which is required for the processing of most non-structural proteins, except at the 3 cleavage sites at the

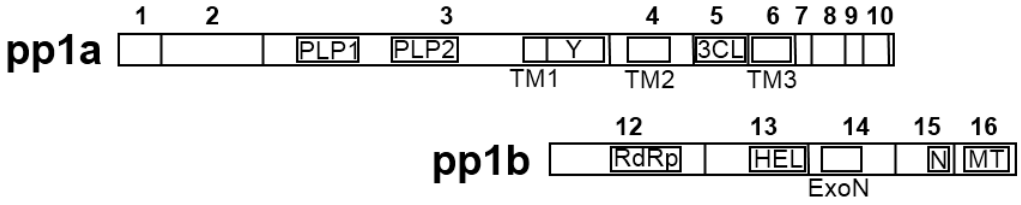

Figure 1.4: Domain organization of the replicase polyproteins pp1a and pp1ab (pp1a joined with pp1b). Major conserved domains of pp1a include: papain-like protease (PLP1 and PLP2), Y domain (Y), 3C-like protease (3CL) and transmembrane domains (TM1, TM2, TM3). Major conserved domains of pp1b include: RNA-dependent RNA polymerase (RdRP), RNA-helicase (HEL), exonuclease (ExoN), uridylate-specific endoribonuclease or NendoU (N) and methyltransferase (MT). Numbers indicate name of non-structural proteins (nsps) after complete protease cleavage. Note: IBV does not contain nsp1.

N-terminal (or 2 sites for IBV) which is performed by nsp3. A relatively well conserved and fairly large protein, nsp3 ranges between 180 to 210 kDa and contains a pair of paralogous papain-like protease (PL^{pro})domains, PLP1 and PLP2, the former non-functional in IBV (63).

Mature nsps as well as some processing intermediates (64-66) are incorporated into the replicase complex which is assembled on double membrane vesicles (DMVs) (37-39), the site of viral RNA synthesis.

1.2.3 Transcription and replication

The purpose of coronavirus transcription is the generation of mRNAs for viral protein expression downstream of the replicase gene. The sub-genome sized mRNAs encode for viral structural (S, E, M, N) and other accessory genes. Genome replication is achieved through the synthesis of mRNA1 or the gRNA which serves the primary purpose of genome duplication, producing new copies of the viral genome to be packaged into progeny virus particles, but may also serve as the mRNA for the replicase gene (pp1a and pp1ab). Central to the transcription and replication of the virus genome is the virus-encoded replicase complex made up of the non-structural proteins, auto-proteolytic products of the polyproteins 1a and 1ab in every coronavirus.

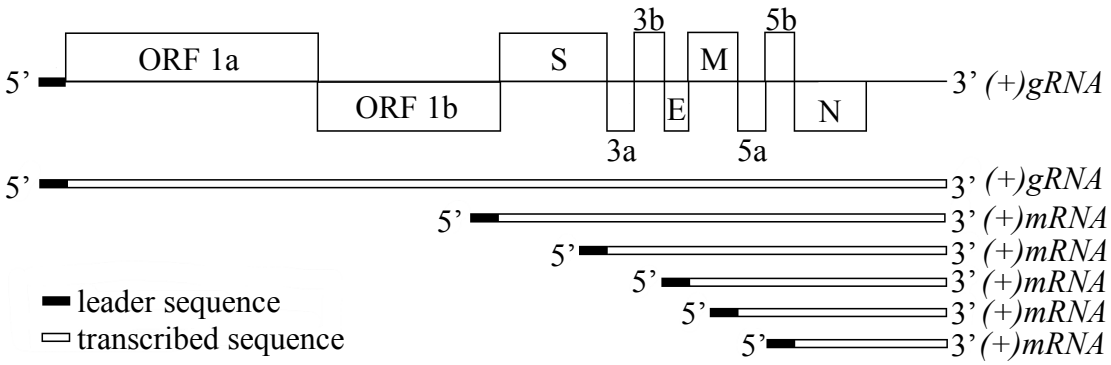

Figure 1.5: The transcription of gammacoronavirus IBV produces a nested set of 6 positive-sense mRNAs that are 5'- and 3'- co-terminal. (+) gRNA is mRNA1 and mRNAs 2 to 6 are (+) sgRNAs which become templates for translation of structural and accessory proteins.

The final product of coronavirus transcription is a nested set of sgRNAs, which varies between 6 for IBV, shown in Figure 1.5, to 9 for SARS-CoV including newly synthesized gRNA (or mRNA1), that are both 5' and 3' co-terminal. The sgRNAs

contain in their 5'-end a terminal leader sequence fused to distant RNA coding sequences, which is likely achieved through discontinuous transcription during negative strand synthesis (67-70).

With regards to transcription initiation, it was proposed that both the 5'- and 3'-UTR interact either directly or indirectly through RNA-protein and protein-protein interactions (71) to form the promoter for negative-strand synthesis, analogous to the picornavirus replication-transcription model (72). This model supports the observation that only genome length RNA is able to serve as a template in the process as the sgRNAs do not contain the entire 5'-UTR and the requirement of certain cis-acting sequences in the 5'-UTR in negative-strand transcription. The two ends of the genome, including some internal sequences in certain coronaviruses, contain multiple cis-acting sequences which have been shown to be important for the replication of defective interfering (DI) RNA.

The coronavirus 5'-UTR is predicted to fold into several stem loop structures. The extreme 5'-end of the coronavirus 5'-UTR is the leader sequence which is predicted to fold into two stem-loops, stem-loops I and II and the leader transcription regulatory sequence (TRS-L) is situated at the 3' end of the leader sequence. The first secondary structure, the thermodynamically unstable stem-loop I, is characterized by the presence of bulges and/or non-canonical base-pairing, and is especially unstable at its base (73). This characteristic instability of stem-loop I appear to be conserved in the absence of primary sequence conservation among the key members of the three genera (74). Also, the structural lability has been shown in MHV to be important, its function in both positive and negative-strand transcription, which is likely mediated

through an interaction with the viral 3'-UTR, at a site very close to the poly(A) tail (75). In contrast to stem-loop I, the coronavirus stem-loop II is predicted to fold into a highly conserved short U-turn motif but has also been experimentally shown to be important for viral sgRNA synthesis (both positive and negative-strand) but not in gRNA synthesis. In addition to its function in viral transcription, coronavirus stem-loop II appears to play a role in viral translation (74,76).

Downstream of the coronavirus 5'-leader lie a short ORF, which likely encodes a short peptide between 3 to 11 amino acid residues. This region has been experimentally shown in BCoV to fold into stem-loop III harbouring the AUG start codon of the ORF within its left stem. Using a defective interfering (DI) RNA system, the importance of structural integrity in stem-loop III as well as the presence of the short ORF in DI RNA replication had been highlighted (77). The same group also found another RNA structure, designated stem-loop IV in the publication (78), also known as stem-loop VII (74), to be required for the replication of BCoV DI RNA in its positive strand, as well as interacting with several unidentified cellular proteins. The structure was reported to be conserved in both in sequence and structure within betacoronaviruses (78). It is not known if the structure is present in alpha- and gammacoronaviruses.

Cis-acting signals at the 3'-UTR of the coronavirus genome, the start site of negative sense RNA synthesis, have been mapped for betacoronaviruses to a 5'-proximal segment corresponding to the mutually exclusive bulged stem loop structure and pseudoknot (stem-loops 1 and 2) as well as the last 29 nt of the 3'-UTR which base-pairs with loop 1 and sequences downstream of stem 2 (79). These structures are

highly conserved in betacoronaviruses and substitution within the genus produces no discernible defect, despite primary sequence heterogeneity (79-81). Hence, it is likely that alpha- and gammacoronaviruses possess similar secondary structures although evidence supporting the presence of the bulged stem loop and pseudoknot has been elusive for alphacoronaviruses (82) and gammacoronaviruses (83,84) respectively. Although it has been previously discovered in a promoter mapping experiment that only the poly-A tail as well as the last 55 nt at the 3' UTR are necessary for the initiation of negative strand synthesis (85) of DI RNA, it was unclear if the upstream sequences had been supplied in *trans* by the helper virus genome (79).

An important feature of coronavirus discontinuous transcription is the TRS, comprising of a highly conserved core sequence (CS), which varies between coronaviruses. The CS is flanked by relatively variable sequences (5'-TRS and 3'-TRS) which are regulatory factors for transcription (86,87). The TRSs are found at the 3'-end of the 5'-leader sequence (TRS-L) and immediately upstream of each gene or ORF, the body TRSs (TRS-Bs), as shown for IBV in Figure 1.6, and they share an identical CS. This similarity between the CS of TRS-L and TRS-B (CS-L and CS-B respectively) allows for complementary base pairing between the nascent negative sense CS-B (cCS-B) and the template CS-L, a key event which mediates discontinuous transcription (88-91). It is believed that the TRS is important for discontinuous transcription and not genome replication as its absence was found to impair template switching but not continuous transcription of the genome (92).

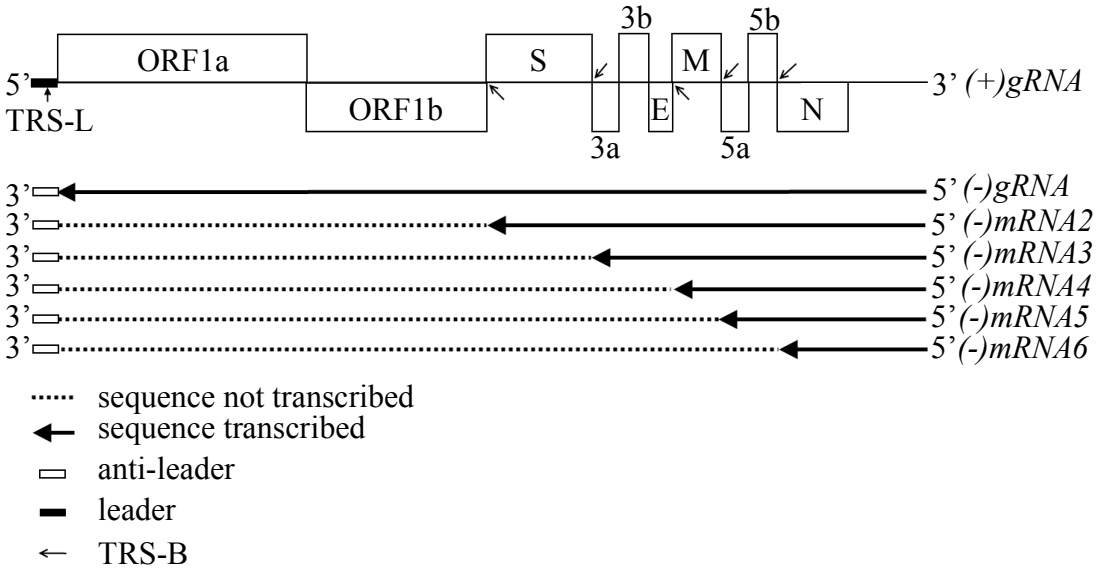

Figure 1.6: Discontinuous transcription in negative-strand synthesis of gammacoronavirus IBV. TRS is present in the 5'-leader (TRS-L) and upstream of each designated ORF (TRS-B) of the IBV genome. Each time a TRS-B is being transcribed by the replicase complex, the replicase complex may exchange its template for TRS-L, located at the 5'-end of the genome and transcribe the leader sequence or it may retain its template and continue transcribing from the 3'-end of the genome. This results in the generation of a set of negative-sense mRNAs bearing an identical 5'-terminus as well as an anti-leader at their 3'-end.

In a model of discontinuous transcription, the TRS-B is proposed to act as both an attenuation and dissociation signal for the transcription complex, the viral replicase complex. Template switching follows the pausing of the viral RdRP, upon transcribing CS-B, and the replicase complex, together with the nascent negative strand, containing the cCS-B, dissociates from TRS-B and associates with the TRS-L which is in close proximity. In the sequence context, TRS-L and TRS-B are distal sequences, and their induced proximity should most probably have been achieved through RNA-protein and protein-protein interactions. A diagrammatic representation of the key features in discontinuous transcription in coronaviruses presented by Enjuanes et al. (93) is shown in Figure 1.7.

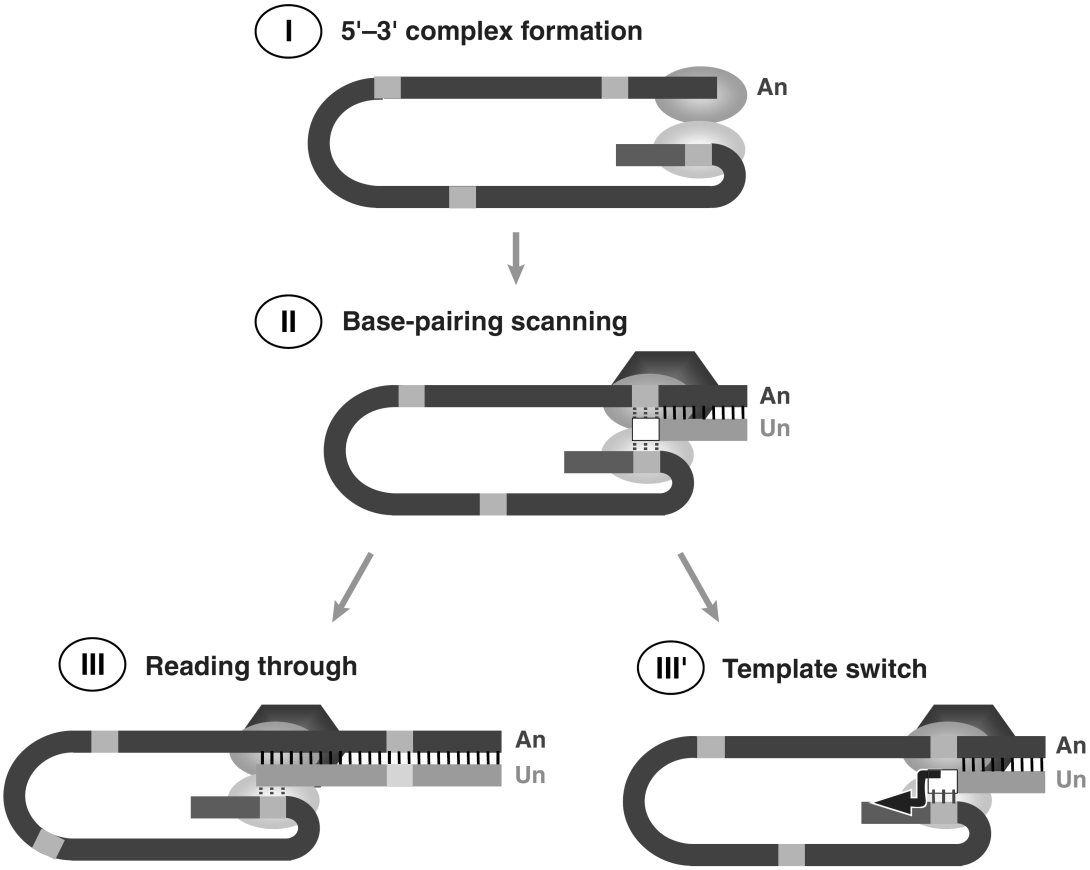

Figure 1.7: A model of discontinuous transcription in coronaviruses in three steps. (I) Initiation begins with genome circularization facilitated by RNA-binding proteins (ellipsoids) interacting with the 5'- and 3'-UTR respectively. (II) The replicase complex (hexagon) transcribes the genome from the 3'-UTR up to the first CS-B (grey block), synthesizing the cCS-B (white block). Complementarity between cCS-B and CS-L stalls the replicase and the replicase may either (III) read through the transcribed CS-B and continue transcription or it may (III') switch its template to CS-L and transcribe the leader sequence.

The relative abundance of the different sgRNA species is most probably influenced by the relative position of their TRS-B from the 3' end of the genome. The further the TRS-B is located from the 3' end, the more attenuation signals need to be passed over by the replicase before reaching it, resulting in a lower probability of that particular TRS-B being encountered, ie. longer sgRNAs are less abundant. That is however not the only contributing factor as a linear correlation could not be established between

3’-end proximity and mRNA abundance in all coronaviruses. The context in which the CS is situated, 5’- and 3’- TRS, is also an important factor as it determines the extent of complementarity between TRS-B and TRS-L and hence the likelihood that a template switching event occurs (86). The importance of these flanking sequences is highlighted through reports that sequences flanking the CS-L can act as acceptor sites for template switch, even in the absence of a canonical CS in the TRS-L (94,95) although it is still the preferred site.

In TGEV, the TRS-L was found to fold into a bulged stem-loop, presenting the CS-L in an apical heptaloop and both its low stability and secondary structure are essential for replication and transcription (96). This finding coincides well with the proposed mechanism for template switching as it promotes CS-L for complementary base-pairing with cCS-B. However, this hairpin structure of TRS-L is predicted not to be conserved and may have been unstructured or part of the stem of another stem-loop structure in other coronaviruses (73,74). This could have been due to the low thermal stability characteristic associated with the secondary structure resulting in a negative structure prediction and would require experimental confirmation.

1.2.4 The viral replication/transcription complex

It was proposed that the polyprotein intermediates (partially cleaved nsps) function in negative-strand synthesis while the fully processed nsps form the RTCs responsible for positive strand synthesis due to the instant ceasure of negative-strand synthesis upon cycloheximide treatment while positive strand synthesis is able to continue for a longer period of time (97).

Presumably central to the function of the RTC is the main enzyme, RNA-dependent RNA polymerase (RdRP) nsp12 (98) and the RNA helicase (99,100). Nsp12 is a primer dependent, RdRP (101), generates new gRNA for replication as well as sgRNAs to be used in translation to produce virus structural and other accessory proteins while nsp13 has been shown to be crucial for the function of nsp12 (102). A second RNA-dependent RNA polymerase, nsp8, has been proposed to be the primase (103) which produces primers required by nsp12. Nsp8 forms a channel-like hexadecameric complex with nsp7, has a positively charged cylindrical channel, presumably to facilitate interaction with the negatively charged phosphate backbone. Its capability to encircle RNA (both single and double stranded) coincides with its proposed role as a primase (104). The allowance of incomplete cleavage between nsp7-nsp8, nsp8-nsp9 and nsp9-nsp10 (65) is indicative that these proteins may function closely or even as a polyprotein (66). Indeed, both nsp9 and nsp10 have been reported to colocalize with nsp8 at the RTCs (105).

Individually, nsp9 has been reported to possess non-specific binding to single stranded RNA (ssRNA) and double stranded DNA (106-108). The structure of nsp10 reveals that it has two highly conserved zinc finger motifs and is able to bind both single- and double- stranded DNA and RNA non-specifically (109). It was also reported that through self-association, nsp10 forms a dodecameric structure with positive electrostatic potential on both its inner and outer surface (110). It has also been reported to be essential for coronavirus RNA synthesis (111).

The coronavirus genome is of an unprecedented scale among non-segmented single-stranded RNA viruses, hence, its highly sophisticated replicase complex does not just

possess the ability to synthesize RNA but also a number of RNA-modifying enzymatic activities. Nsp14 and 15 have been reported to possess 3'- to 5'-exonuclease (ExoN) and endoribonuclease (NendoU) respectively while nsp16 is reported to be a S-adenosyl methionine-dependent ribose 2'-O-methyltransferase. Universally conserved across *Nidovirales* (112), nsp15 represents a genetic marker of nidoviruses (113) critically involved in viral RNA synthesis, as illustrated by blocked viral RNA synthesis upon disruption of its endonucleolytic activity (113). Exonuclease activity of nsp14 was shown to be important in ensuring a high fidelity in viral genome replication, and hence a role in ensuring the stability of the large coronavirus genome (114,115).

Cap formation is yet another important post-transcriptional process in coronavirus RNA synthesis as it ensures that the viral RNAs can be translated by host ribosomes as well as being differentiated from the host mRNAs. Nsp13, the viral RNA helicase possesses NTPase activity which implies an additional role in capping viral RNAs (116). Nsp14 on the otherhand has been revealed to possess N7 methyltransferase activity, thereby producing a N7-methylated guanine cap (cap-0) (117). This could have been followed up by 2'-O-methyltransferase (nsp16), together with its activator nsp10 (118-120) catalyzing the conversion of the cap-0 structure to a cap-1 structure (121) of viral RNAs. Another RNA processing activity associated with the viral replicase rests upon the ADP-ribose-1" monophosphatase (ADRP) domain (122) of nsp3. The ADRP domain is assigned based on structural evidence (123) but binding of the protein to its canonical substrate, ADP-ribose, was found to be relatively weak (124) if not undetectable, in the case of IBV (122). Hence it is unclear whether the ADRP domain plays a major role in viral transcription.

The anchorage of the complex onto the membrane of DMVs is likely achieved by the transmembrane domains of nsp3, nsp4 and nsp6 (38,125-129) and that of nsp3 has been shown to be important for its protease function (130,131). Although they appear to be critical for coronavirus replication (132), no function has been assigned to nsp4 and nsp6 apart from anchoring the replicase complex to the membrane through their hydrophobic regions and likely interaction with other viral proteins (128,133).

Apart from the replicase gene products, viral structural protein, the nucleocapsid, has also been shown to be associated with the viral replication-transcription complexes (134). The presence of the N gene was found to be required for efficient replication coronavirus HCoV-229E vector RNAs which would otherwise only be able to complete transcription (135). In addition, it has also been reported to function as a chaperone protein, facilitating template-switching during discontinuous transcription (136), and therefore, is required for efficient transcription to take place.

1.2.5 Translation and cotranslational modification of structural proteins, viral assembly and release

The products of sgRNA transcription, positive-stranded mRNAs are translated in the cytosol by host ribosomes and only the 5'-proximal ORF is being translated from each mRNA. This produces the four virus structural proteins, S, E, M and N as well as a number of accessory proteins, which varies between coronaviruses. While the structural proteins are to be packaged into the progeny virus together with the viral gRNA, they have other functions in the pathogenesis of the virus. The accessory

proteins, on the otherhand, are believed to be dispensable for *in vitro* virus infections and function only in establishing infections in their natural hosts.

The viral S protein is cotranslationally modified via glycosylation and palmitoylation (137-139) and subsequently trimmed in the Golgi (140). A subset of the modified trimeric S protein gets transported to the plasma membrane directly (141,142) and engages in membrane fusion with adjacent cells, resulting in the spread of virus infection and eventually, the appearance of large fusion cells, the syncytia (143).

The key players in the budding of virus particles from the endoplasmic reticulum-golgi intermediate compartment (ERGIC), are the M and E proteins. As such, the coronavirus M protein is the most abundant protein in the viral envelope and together with the E protein in much smaller amounts, are the only viral proteins required to drive the efficient formation virus-like particles (VLPs) (32,33). To form an infectious virus particle, the other structural proteins, as well as the viral genome has to be packaged as well. E protein, is palmitoylated (144-146) post-translationally, accumulates in throughout the Golgi (31) when expressed alone exogeneously and carries in its C-terminal tail as well as the N-terminal hydrophobic domain, Golgi-targeting signals (144,147). M protein, on the otherhand, is glycosylated and localizes to the Golgi when expressed alone (26,148,149) by virtue of a Golgi-targeting signal in the first transmembrane domain for (150) IBV or C-terminal cytoplasmic tail for (151) MHV.

In virus-infected cells, N forms ribonucleoprotein complexes with all viral mRNAs (28,152) however only those comprised of the viral gRNA or mRNA 1 can be packaged into virions efficiently (153-159). An encapsidation signal that lies within

gene 1 (160-165), is unique to the viral gRNA, and is the prime factor in the specific incorporation of genome length mRNAs into the virions. The mechanism by which this is achieved is likely through specific interaction between M and the encapsidation signal (166), as well as the interaction of M with N in the presence of RNA (the nucleocapsid) (28). M has also been shown to interact with S (167) and non-structural protein HE (27), thereby incorporating these two membrane-spanning proteins into the budding virion. Although it has also been shown that IBV E protein interacts with (168), and retains M in the ERGIC (169), the general observation that the key players in viral assembly are not localized to the budding site by themselves point to the need of cooperative interaction between viral proteins and possibly unknown host proteins in this process.

Apart from its role in virion assembly at the budding site, the E has been demonstrated to be essential for virion maturation and release in TGEV (170). In addition, the coronavirus E protein has been shown to oligomerize through its hydrophobic domain (171), forming cation-selective channels (172), whose function is essential for the efficient production of progeny virus particles as demonstrated by the use of ion channel inhibitor hexamethylene amiloride (173). The same hydrophobic domain has been shown to be responsible for the disassembly of the Golgi apparatus, altering the host secretory pathway and promoting virion trafficking towards the plasma membrane for release (174). Although it is not known if the mutation introduced for the study disrupted E oligomerization, it has been proposed that the presence E protein ion channels may disrupt the luminal pH and homeostasis of the Golgi apparatus (175) resulting in its disassembly, thereby protecting the

virions from damage by Golgi proteases as well as altering the secretory pathway to promote virion release.

1.3 Virus-host interactions

In a coronavirus infection, the virus replicates in the host cytosol, amid a myriad of host signaling pathways and systems, interaction between the virus and the host systems is inevitable. This is especially true when coronaviruses are severely gene-poor in comparison to its mammalian hosts. Virus-host interplay occurs at multiple points during the virus replication cycle, from entry to exit. The nature of such interactions can range from a simple usage of existing machinery to destructive interactions that modulate the host environment to the advantage of the virus while inhibiting host activities. One of the most important interactions between virus and host is the modulation of host cell environment, converting it into one which the virus can replicate in safety. The significance of host components being used to supplement the gene-poor virus in various processes cannot be dismissed although they usually serve as enhancers, as they could become major pathogenicity factors.

1.3.1 Innate immune system

Upon infection by viruses, host cells could sense the invading pathogen through the recognition of pathogen-associated molecular patterns (PAMPs), present in viral genomes, by host pattern recognition receptors (PRRs) (176,177). Depending on host cell type and the invading pathogen, Toll-like receptors (TLR3, 7, 8 and 9) (178,179)

in endosomal compartments as well as cellular cytoplasmic helicases retinoic acid-inducible gene-I (RIG-I) and melanoma differentiation-associated gene 5 (Mda5) may be activated (180-182). Detection of PAMPs triggers signaling cascades via adaptor proteins TIR-domain containing adapter-inducing interferon β (TRIF), myeloid differentiation primary response gene 88 (MyD88) or virus-induced signaling adapter (VISA) (178-181) leading to the activation of non-canonical inhibitor of NF-κB (IκB) kinase homologues (IKK), IKKε (183) and TANK-binding kinase 1 (TBK1) (184,185). This activates interferon regulatory factor 3 (IRF3) (186), IRF7 (187) and nuclear factor kappa-light-chain-enhancer of activated B cells (NF-κB) (188-191) which translocate to the nucleus and activates transcription of type I interferons (IFNα and IFNβ) and inflammatory cytokines. The release of IFNs lead to the phosphorylation of Janus kinases (JAK) as well as signal transducers and activators of transcription (STAT) proteins which results in the transcription of anti-viral related genes (192,193). The viruses on the otherhand, have evolved multiple strategies to avoid elimination from the host which range from prevention of detection to inhibition of antiviral responses mounted by the host immune system. All these activities involve viral-host interactions at different levels.

The first step to defending itself against viruses is the detection of viral material. The exact nature of PAMPs recognized by RIG-I and Mda5 has not been firmly established but it has been reported that RIG-I recognizes 5'-triphosphate single stranded RNAs (ssRNAs) (ie. uncapped RNAs) (194,195) and short double stranded RNAs (dsRNAs) (196,197), Mda5 can specifically bind polyriboinosinic:polyribocytidylic acid or poly(I:C) (198) and long dsRNAs (196).

TLR3, 7 and 9 have established to recognize dsRNA, ssRNA and CpG DNA respectively.

A strategy coronaviruses have adopted to avoid detection of its newly synthesized mRNAs in the cytoplasm is to encode a 2'-O-methylase (nsp16), creating a 5'-cap structure analogous to the cellular mRNAs on their mRNAs, thereby escaping detection by Mda5 (199). However, during the course of viral transcription and replication, uncapped double-stranded RNA intermediates are generated and these may have served as ligands for the RIG-I and/or Mda5. Both RIG-I and Mda5 have been implicated in the detection of MHV infection (200) but conflicting evidence has been presented as well, especially when it is not understood how the cellular helicases could bind to viral replicative/transcriptive intermediates which should have been isolated by the DMVs (201).

Detection by the PRRs would activate signaling cascades leading to the production of type I IFNs, resulting in the establishment of an antiviral state. Thus, coronaviruses do not just avoid detection by the host immune system, which appears to be the main strategy of ensuring successful replication (202), but some also encode proteins that function to disrupt the downstream signaling cascades at various points, preventing the establishment of an effective antiviral state when detection of the viral PAMPs has occurred. Indeed, the N protein has also been shown to interfere with the 2', 5'-oligoadenylate synthetase/RNaseL activation, downstream of IFN induction, inhibiting global translation shutdown (203). This activity is in addition to its inhibition of IFNβ induction by binding to viral RNAs, preventing their detection (204).

Another structural protein, the SARS-CoV M, has been reported to interact with multiple components of the IFN induction pathway, namely IKKβ, IKKε, TBK1, TNF-receptor associated factor 3 (TRAF3) and RIG-I, resulting in a suppression of NF-κB activity and IRF3/7 activation, thereby impairing type I IFN production (205,206).

In addition to processing the polyproteins, PLP2 domain of the nsp3 has been shown to possess deubiquitinating activity (207-209). PLP2 of nsp3 deubiquitinates both TBK1, the activating kinase for IRF3 and IRF3 itself, then sequesters the hypo-phosphorylated TBK1-IRF3 complex in the cytoplasm. This prevents IRF3 nuclear translocation (210,211), thereby inhibiting the transcription of type I interferons (212). The ADRP domain of nsp3 in also appears to confer resistance against the antiviral effect of IFNα (213) through an unknown mechanism.

Nsp1 is a highly divergent protein across sub-family *Coronavirinae* and absent in gammacoronaviruses. It has no known direct function in viral transcription, but SARS-CoV nsp1 was reported to cause a general suppression of host gene expression most likely by promoting host mRNA degradation (214-217) and in particular the inhibition of IRF3/7 activation, activities of NF-κB and IFN promoters as well as STAT1 phosphorylation (218). Similarly, nsp2, possesses highly divergent sequences across coronaviruses and has been reported to act as a weak protein kinase RNA-activated (PKR) antagonist, suppressing the phosphorylation of eukaryotic initiation factor 2 alpha (e-IF2α), which in turn blocks host translation while allowing viral translation to take place (219). There have been reports that both nsp1 and nsp2 are

dispensable for virus replication/transcription *in vitro* and mainly function as pathogenicity factors (215) and in other parts of the virus life cycle (220,221).

Accessory protein SARS-CoV ORF 3b and 6 have also been implicated as an IFN antagonist (222) by which the latter works by interacting and subsequently sequestering the nuclear import factor, karyopherin alpha 2 (KPNA2) in the ER/Golgi region, preventing the nuclear translocation of STAT1 (223). SARS-CoV ORF 3b on the otherhand appears to stimulate activator protein 1 (AP-1) dependent synthesis of proinflammatory cytokines by activating both c-Jun N terminal kinase (JNK) and extracellular signal-regulated kinase (ERK) pathways (224). SARS-CoV 3a targets IFNα receptor subunit 1 (IFNAR1) for ubiquitination and subsequent lysosomal degradation as a consequence of PKR-like ER kinase (PERK) activation (225). MHV ORF 5a was also reported to be an IFN antagonist but the mechanism of action has not been established (226). Gene 7 is only present in a subset of alphacoronaviruses, and that of TGEV has been shown to interact with protein phosphatase 1 catalytic subunit c (PP1c) and the interaction is vital for eIF2α dephosphorylation. The innate immune response which can be triggered and subsequently countered by the coronavirus-encoded proteins has been summarized in Figure 1.8.

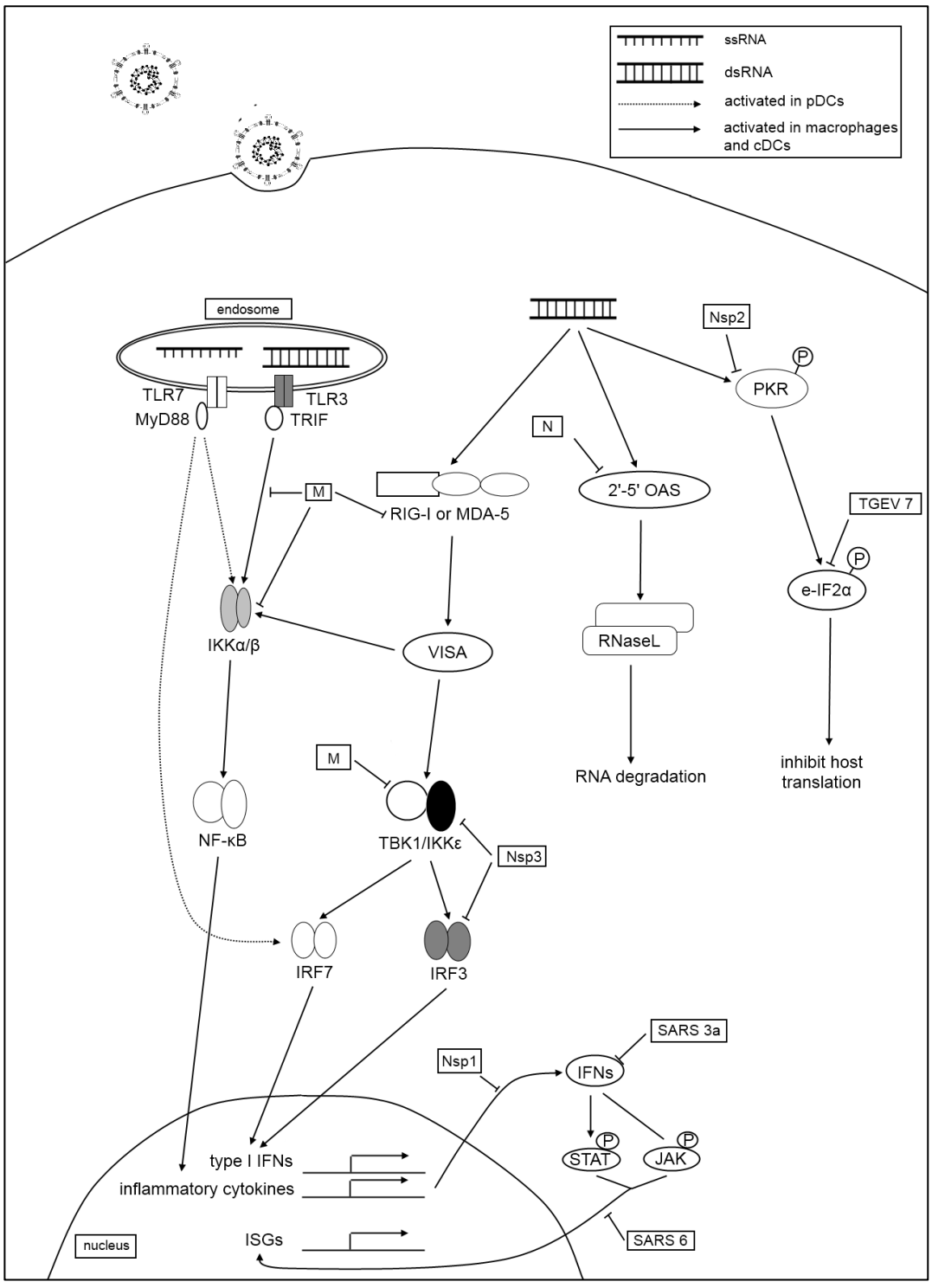

Figure 1.8: Virus-host interaction in innate immune response. The activation of toll-like receptors 3 and/or 7 as well as cytoplasmic helicases RIG-I and/or MDA-5 triggers signaling pathways resulting in the synthesis of type I interferons (IFNs), inflammatory cytokines and interferon-stimulated genes (ISGs) which acts in concert to establish an antiviral state. Activation of 2'-5' oligoadenylate synthesase (2'-5' OAS) and PKR results in global degradation of cellular RNA and inhibition of translation which can inhibit viral propagation. Coronaviruses encode many proteins that target multiple steps in the innate immune response mounted by the host cells, ensuring its successful replication in the host.

1.3.2 Cell cycle arrest, ER stress and apoptosis

Infections with viruses often result in cell cycle arrests, the activation of unfolded protein response (UPR) due to ER stress, both of which can be accompanied by the parallel activation of apoptosis in the infected cells. In this aspect, coronaviruses are no exception and Figure 1.9 summarizes how some coronavirus-encoded proteins interfere with the host cell cycle.

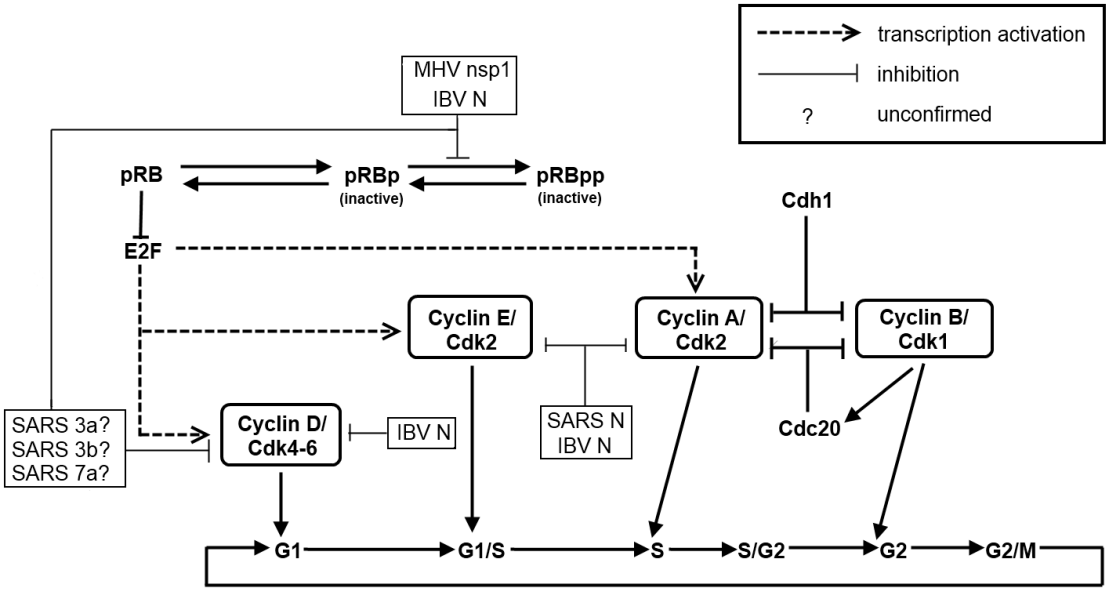

Figure 1.9: Coronavirus-encoded proteins interfere with the cell cycle. Cell cycle progression is mediated through the temporal expression levels of different cyclins and CDKs. Different coronavirus arrest the cell cycle at different stages. MHV and IBV have been confirmed to cause cell cycle arrest at G0/G1 and G2/M phases respectively. This arrest is mediated through the nucleocapsid protein (N) as well as other virus-encoded non-structural (replicase) and accessory proteins. The proposed point of interaction for some proteins has not been confirmed (as indicated by (?) although they have been linked to cell-cycle arrest.

Infection with MHV causes cell cycle arrest at G0/G1 phase (227) and IBV at S and G2/M phases (228,229). It has been observed that the N protein of several coronaviruses can localize in the nucleolus where it may have perturbed cell cycle activities of the host cell to benefit viral mRNA synthesis (230-233). SARS-CoV N

has been shown to interact with both cyclin D-CDK4 and cyclin A-CDK2 complexes, inhibiting their activities resulting in a block in S phase progression (234), despite being reported to localize to the nucleolus inefficiently (232,235,236). IBV N on the otherhand appears to target CDK2, cyclins A and D1 for proteasome-mediated degradation (229,237) and cause the accumulation of hypophosphorylated retinoblastoma (pRB), resulting in the downregulation of CDK1, cyclins E and B1 (229).

N is not the only viral-encoded protein implicated in causing cell cycle arrest in infected cells. MHV p28 (nsp1) over-expression was also linked to a reduction of pRb hyper-phosphorylation resulting in a G0/G1 cell cycle arrest (238). Over-expression of SARS CoV accessory proteins 3a, 3b and 7a has also been shown to lead to G0/G1 phase arrest (239-241) likely through the modulation of cyclin D3 expression level and pRB phosphorylation.

During virus replication, the newly translated viral proteins accumulating in the ER causes stress and activation of the UPR. The S protein of both MHV and SARS-CoV has been shown to be able to activate the UPR, albeit with differences in activation targets as MHV activates all three UPR transducers inositol-requiring enzyme 1 (IRE1), activating transcription factor 6 (ATF6) and PERK (242) while SARS-CoV selectively activates PERK signaling (243). In particular, activation of PERK leads to the activation of p38 mitogen-activated protein (MAP) kinase (244), which stimulates virus replication (245,246). Although MHV S protein activates UPR by all three transducers, other MHV encoded proteins negatively modulate the downstream

effectors as demonstrated by the lack of spliced X-box binding protein 1 (XBP-1) accumulation and decline in activated/cleaved ATF6α (242).

Coronavirus proteins tend to be multi-function in order to make up for their deficit in the number of genes the genome can contain. As such, the ER-localized SARS-CoV 3a has also been reported as an inducer of apoptosis (247) and ER stress (225) by activating the extrinsic and intrinsic apoptotic pathways as well as the p38 MAP kinase (245). The latter which is also activated by SARS S, can also promote apoptosis by increasing p53 levels leading to increased Bax oligomerization, releasing cytochrome c from the mitochondria (248).

SARS-CoV accessory proteins, 6 and 7a have been shown to induce apoptosis as well as UPR (249,250). SARS 7a has been shown to be able to interact and exhibit partial colocalization with anti-apoptotic protein Bcl-$_X$L to the mitochondria compartment, in addition to its interaction with other anti-apoptotic proteins of the Bcl-2 family (251). It was also reported to activate the p38 MAP kinase through an unknown mechanism which may have contributed to the induction of apoptosis (252). Interaction between SARS-CoV 7a and the human asymmetrical diadenosine tetraphosphate hydrolase (Ap$_4$A-hydrolase) (253), a signaling molecule that is proposed to function in multiple pathways including cell proliferation, RNA processing, apoptosis and DNA repair (254-259), has also been documented. This provides further evidence supporting the role of SARS-CoV 7a in modulating various signaling pathways in the infected cell. Like 7a, SARS-CoV 6 is also localized in the ER/Golgi compartment and has been shown to activate effector caspase 3 and induce ER-stress, triggering JNK-dependent apoptosis and UPR by unknown mechanisms (260). SARS-CoV 8a and 3b have also

been shown to induce apoptosis in host cells (241,261) and the latter may induce necrosis as well (262).

SARS-CoV E is also an inducer of apoptosis and has been shown to interact with anti-apoptotic protein Bcl-$_X$L (263). Similarly, MHV infections can also induce apoptosis (264-267) which can be blocked by Bcl-$_X$L over-expression (268) and the E protein is likely to be responsible for this activity (269). In IBV however, E protein was not shown to be an inducer of apoptosis, instead, nsp14 appears to trigger caspase-dependent apoptosis in over-expressing cells (270). Other coronaviruses TGEV, canine coronavirus (CCoV) and equine coronavirus (ECoV) have also been reported to induce apoptosis (271-273) but the mechanisms have not been established. Figure 10 highlights the roles played by some coronavirus-encoded proteins in the activation apoptosis.

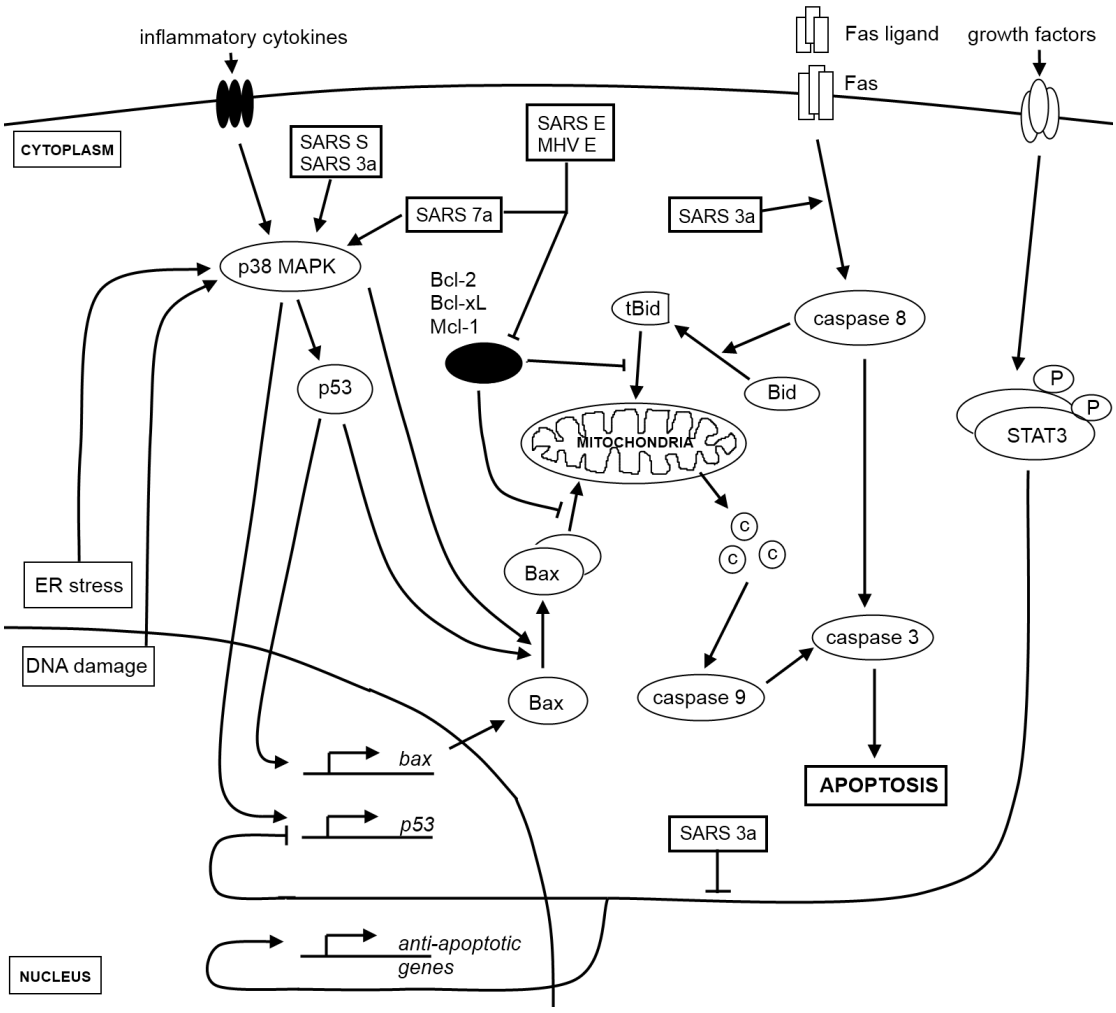

Figure 1.10: The activation of apoptosis by coronavirus-encoded proteins. Extrinsic signals from receptors (eg. Fas) culminate in the activation of caspase 8 which activates the effector caspase 3 while intrinsic signaling requires the participation of the mitochondria in releasing cytochrome c (shown as circles labeled "C") to activate caspase 9 in order to activate caspase 3. Key proteins in the intrinsic apoptosis signaling pathway are p53, both pro-apoptotic (eg. Bax, Bak) and anti-apoptotic proteins (eg. Bcl-2, Bcl-$_X$L) from the Bcl-2 family. Both extrinsic and intrinsic apoptosis signaling pathways are targeted by coronavirus proteins and viral proteins act at multiple points along the different signaling pathways, enhancing the pro-apoptotic effect brought upon by virus infection. Anti-apoptotic proteins (black oval) listed are key anti-apoptotic members from the Bcl-2 family of proteins. Other pathways triggered by coronavirus infections ie. ER stress and DNA damage response, also trigger apoptotic signaling.

1.3.3 Ubiquitin-proteasome system

The ubiquitin-proteasome system (UPS) plays a major role in regulating cellular protein levels (274,275). Viruses exploit and manipulate host metabolism to benefit their replication in permissive hosts, it is unsurprising that this system has been implicated in the replication of several other viruses (276-280), including coronaviruses. During a coronavirus infection, virus particles have been internalized through the endosomal pathway need to be transferred to the cytosol for viral replication to begin. This step as demonstrated in MHV, appears to require a functional proteasome as the application of proteasome inhibitors resulted in an accumulation of internalized particles in the lysosomes, lowering the progeny virus titre (281). This has been subsequently shown to be independent of ubiquitination activity (282). A later discovery that SARS-CoV N protein interacts colocalizes with the p42 subunit of the 26S proteasome in cultured cells affirms the significance of the UPS in coronavirus replication cycle (283).

Not only is the UPS implicated in the transfer of virus particles from the endosome into the cytosol, ubiquitination has also been shown to be important for viral RNA synthesis (282). The mechanism by which ubiquitination affects viral RNA synthesis could not be determined and considering that the UPS plays a central role in cellular protein homeostasis, it is likely that the disruption of ubiquitination may perturb multiple systems and signaling pathways (284), indirectly impacting viral RNA synthesis.

1.3.4 DMV biogenesis

Coronavirus infection induces the formation of DMVs in host cells, creating a protected environment for viral replication and transcription to take place (285). It is widely believed that the DMV membranes originate from the endoplasmic reticulum (ER) (37,129,286) but the mechanism by which they are derived remained elusive. Although the early secretory pathway has been shown to be linked to DMV biogenesis (287,288), the absence of marker proteins casts doubt on the extent of its involvement (288). On the otherhand, autophagy has also been reported to be likely involved in DMV biogenesis. However, in addition to the discovery that an essential component of the autophagy machinery is dispensable for MHV replication (289), contradictory findings have been presented with regards to the presence (289,290) or absence (37,291) of autophagosome marker microtubule-associated protein 1 light chain 3 (LC3) on the DMVs. A recent discovery that DMVs are coated with non-lipidated LC3-I, not autophagosome-associated LC3-II, has demystified the mechanism by which these virus-induces structures are derived from the ER (292). This study has elucidated the involvement of ER-derived vesicles exporting short-lived ER-associated degradation regulators (EDEMosomes) in DMV biogenesis and viral replication.

1.3.5 Viral RNA synthesis and translation

In virus RNA synthesis, the replicase complex is indispensable but not an exclusive participant, as cytoplasmic factors had to be supplied in *trans* for purified RTCs to function efficiently (293). One of the most obvious ways that host proteins can take

part in viral RNA synthesis would be sustaining interactions with cis-acting regulatory signals on the virus 5'- and 3'-UTRs. The ability of host proteins to form ribonucleoprotein complexes with genomic RNA of coronaviruses have long been reported (294,295), and their significance in the regulation of coronavirus RNA synthesis documented (296). However, despite their noteworthy participation in this vital part of the coronavirus replication cycle, only a handful of such cellular proteins have been identified.

The most well-studied host protein that interacts with the coronavirus genome is none other than heterogeneous nuclear ribonucleoprotein A1 (hnRNP A1), a nuclear protein, whose biological function is to regulate alternative splicing of cellular RNAs (297,298). In the first report, hnRNP A1 was shown to bind to both negative-sense leader sequence and negative-sense intergenic (IG) sequence of the MHV (299). Subsequently, the formation of a RNP complex between hnRNP A1, negative-sense leader and IG sequences has been demonstrated (300) and that the participation of hnRNP A1 is vital (301). In addition to its ability to interact with the coronavirus RNA, hnRNP A1 was also found to interact and colocalize with N protein (302,303), an important player in coronavirus RNA synthesis (91,136). It has also been highlighted that hnRNP A1 may be required to recruit other cellular proteins to the replicase complex (304). Information that diminishes the importance of hnRNP A1 were also presented (305) but that could have been explained by the subsequent discovery that other members of the hnRNP A/B family are able to substitute for hnRNP A1 in viral RNA synthesis (306).

In addition, it has also been reported that hnRNP A1 binds positive sense MHV 3'-UTR and the two binding sites overlap with that of another nuclear protein, polypyrimidine tract-binding protein (PTB), on the negative strand (307). In the same study, hnRNP A1 was also found to interact with PTB via protein-protein interactions and together form a RNP with the 5'- and 3'- ends of the MHV RNA.

PTB has been demonstrated to interact with both the positive-sense leader RNA (308,309) and negative-sense 3'-UTR (310) of MHV RNA and that the RNA-binding activity is required for viral RNA transcription. PTB was found to be interacting with the MHV N protein, as mentioned earlier, is required for coronavirus RNA synthesis (311). The role played by PTB is however, controversial, as it was found that excess PTB had an inhibitory effect on viral RNA synthesis (311). Further evidence had been presented using TGEV supporting the finding that PTB exerts a negative impact on coronavirus RNA synthesis and may sequester viral RNAs in cytoplasmic stress granules during infections (309,312).

Another protein belonging to the cellular splicing machinery, hnRNP Q, was also reported to exert a positive effect on coronavirus RNA synthesis, most likely through its interaction with the both positive and negative sense MHV 5'-UTR (313) as well as the 3' UTR (309). Poly(A)-binding protein (PABP) was also found to interact with the coronavirus extreme 3'-UTR including the poly(A)-tail (309,314). This finding establishes the importance of the poly(A)-tail as a cis-acting signal and the possibility of genome circularization during coronavirus RNA synthesis.

The MHV extreme 3'-UTR was reported in a separate study to form ribonucleoprotein complexes with at least four cellular proteins, one of which was

determined to be mitochondrial aconitase (m-aconitase) (315). The cytoplasmic counterpart of m-aconitase, iron-regulatory protein (IRP), functions as a translation regulator and binds to iron-responsive elements (IREs) on ferritin and transferrin mRNAs (316,317). Hence, although it was the first report of the RNA-binding capacity of m-aconitase, it is not surprising for the protein to possess such activity. Also, this work has demonstrated the partial colocalization of m-aconitase with viral RTCs, a crucial supporting evidence for the probability of a mitochondrial protein interacting with viral RNAs which are located at viral-induced DMVs.

Interactions with viral RNA is not the only way by which cellular proteins can take part in viral RNA synthesis, protein-protein interactions with the viral replicase complex can modulate this process as well. ATP-dependent RNA helicase 1 (DDX1), a cellular RNA helicase (318), was reported to be an interacting partner of the viral exonuclease, nsp14 from both IBV and SARS-CoV, and in addition, shown to relocate to the viral RTCs in the cytoplasm in the presence of nsp14, deviating from its regular, nuclear localization pattern (319).

1.3.6 Viral assembly and release

Late in the virus replication cycle, the secretory pathway is hijacked by the virus for the budding of virus particles and the exocytosis of vesicles containing the virus particles. The principle requirement for efficient virion assembly is the accumulation of viral structural proteins, as well as viral gRNA in the assembly or budding site, which in the case for coronaviruses, is the ERGIC (26). The coronavirus S, when expressed alone exogeneously, do not accumulate at the ERGIC and is found further

downstream along the secretory pathway as well as the plasma membrane (141,320,321). However, in a virus infection, most of it accumulates in the ERGIC and ER. The discovery of an ER retention signal in its C-terminus which could interact with coatomer complex I (COPI) (322-325) sheds light upon the mechanism by which S could be assembled into the virus particles at the ERGIC. COPI is a cytosolic coat protein involved in the retrograde transport of vesicles from the Golgi back to the ER (326,327). Therefore, an interaction between coronavirus S and COPI, and that the signal is required for ER/ERGIC localization of S protein (323), point to a role for retrograde transport in virion assembly.

On the otherhand, M protein has been reported to interact with actin, a cytoskeleton protein, and that the interaction is crucial for the budding or release of virus particles from the infected cells (328). It has however not been established which part of the process from virion assembly to exocytosis actin participates in. The observation that S protein interacts with M protein (167) as well as the involvement of actin microfilaments in retrograde transport of COPI coated vesicles from the Golgi (329-331) to the ER may imply a role for actin in facilitating virion assembly.

1.4 Objectives

As described in the preceding sections of the chapter, both cellular proteins and virus-encoded proteins, in particular, the nsps are important in ensuring the efficient production of the virus progeny. Also, one of the early steps of the coronavirus replication cycle is the synthesis of mRNAs, the efficiency of which can influence the outcome of the infection. Despite its significance, coronavirus RNA synthesis is still

poorly understood. Hence, this work has been dedicated to the identification of a cellular protein, zinc finger CCHC-type and RNA binding motif 1 (ZCRB1 alias MADP1), that could participate in coronavirus RNA synthesis through its interaction with the coronavirus UTRs and an investigation of the nsps in close contact to RNA or the RdRP (nsp12).

The main objectives can be summarized as follows:

- Identification of cellular proteins that could interact with the UTRs of SARS-CoV
- Characterization of the interaction between MADP1, a candidate protein identified from the screen with IBV 5'-UTR (+)
- Elucidation of the functional role played by MADP1 in coronavirus infection
- Investigation of the RNA-binding activity of nsps
- Identification of virus-encoded proteins that could interact with nsp12

Chapter 2 Materials and Methods

2.1 Chemicals and Reagents

2.1.1 Chemicals

Diethyl pyrocarbonate (DEPC), polysorbate 20 (Tween® 20), sodium dodecyl sulphate (SDS), 4-morpholinepropanesulfonic acid (MOPS), sterile dimethyl sulfoxide (DMSO), actinomycin D and 5-bromouridine 5'-triphosphate (BrUTP) were purchased from Sigma-Aldrich (St. Louis, MO, USA). IGEPAL CA-630 (Nonidet P-40 substitute) was purchased from US Biological (Marblehead, MA, USA). Formaldehyde (37% minimum), formamide and chloroform were purchased from Merck (Darmstadt, Germany) TRIzol® Reagent, UltraPure™ Phenol:Chloroform:Isoamyl Alcohol (25:24:1, v/v), UltraPure™ Agarose was purchased from Invitrogen (Carlsbad, CA, USA). Ethidium Bromide (10 mg/ml) and acrylamide/bis (29:1) solution were purchased from Bio-Rad (Hercules, CA, USA). PCR digoxigenin (DIG) labeling mix, biotin RNA labeling mix, Protector RNase inhibitor were purchased from Roche Applied Science (Penzberg, Upper Bavaria, Germany).

2.1.2 Culture medium and reagents

Mammalian Cell Culture

Roswell Park Memorial Institute (RPMI) 1640 medium with 2 mM L-glutamine and Dulbecco's Modified Eagle Medium (DMEM) containing 4500 mg/L D-glucose, both containing 2 mM L-glutamine and phenol red indicator were purchased from Invitrogen (Carlsbad, CA, USA). Fetal Bovine Serum (FBS), US Origin, was

purchased from Thermo Scientific HyClone (Waltham, MA, USA). Penicillin-streptomycin solution (PS), containing 10000 units (U) and 10000 µg of penicillin and streptomycin respectively was purchased from Invitrogen Gibco (Carlsbad, CA, USA). 0.25% Trypsin-EDTA solution containing phenol red was purchased from Invitrogen Gibco (Carlsbad, CA, USA). G418 disulphate salt solution (50 mg/ml) and carboxymethyl cellulose (CMC) were purchased from Sigma-Aldrich (St. Louis, MO, USA).

Yeast and Bacteria Culture

Bacto™-peptone, Bacto™-yeast extract, Bacto™-tryptone, Bacto™-agar and Difco™ nitrogen base without amino acids were purchased from Becton, Dickinson and Company (Franklin Lakes, NJ, USA). Drop-out media supplements were purchased from Clontech (Mountain View, CA, USA). 5-fluoroorotic acid (5-FOA) was purchased from US Biological (Marblehead, MA, USA). Antibiotics ampicillin, kanamycin, amino acid leucine and bovine serum albumin (BSA) were purchased from Sigma-Aldrich (St. Louis, MO, USA).

2.1.3 Antibodies, enzymes and other reagents

Polyclonal rabbit antibody to MADP1 (serum) was produced by BioGenes (Berlin, Germany) using a peptide sequence in its N-terminus as the antigen. Antibodies to actin, histone H1 and HIS-probe were purchased from Santa Cruz (Santa Cruz, CA, USA). Antibodies to β-tubulin, FLAG and HA tags were purchased from Sigma-Aldrich (St. Louis, MO, USA). Antibody to bromodeoxyuridine (BrdU) was purchased from Roche Applied Science (Penzberg, Upper Bavaria, Germany) and

antibody to green fluorescent protein (GFP) was purchased from Clontech (Mountain View, CA, USA). All horseradish peroxidase (HRP) conjugated secondary antibodies were purchased from Dako (Glostrup, Denmark) and Alexa Fluor® conjugated secondary antibodies were purchased from Invitrogen Molecular Probes® (Eugene, OR, USA). Zymolase was purchased from Zymo Research (Irvine, CA, USA) and lysozyme was purchased from Sigma-Aldrich (St. Louis, MO, USA).

All restriction enzymes and calf intestinal phosphatase (CIP) were purchased from New England Biolabs (Ipswich, MA, USA). T4 DNA ligase and ribonucleotide triphosphates (NTPs) were purchased from Promega (Fitchburg, WI, USA). T7 RNA polymerase, Expand Reverse Transcriptase (RT), PCR DIG Labeling Mix, DIG RNA Labeling Mix and Biotin RNA Labeling Mix were purchased from Roche Applied Science (Penzberg, Upper Bavaria, Germany). *Taq* polymerase was purchased from KAPA Biosystems (Cambridge, MA, USA). KOD Hot Start DNA Polymerase was purchased from Merck (Darmstadt, Germany). Deoxyribonucleotide triphosphates (dNTPs) were purchased from Thermo Scientific Fermentas (Vilnius, Lithuania).

All primers (100 μM) and siRNAs (100μM) were synthesized by Proligo, Sigma-Aldrich (St. Louis, MO, USA) or purchased from Thermo Scientific Dharmacon (Lafayette, CO, USA). Acid-washed glass beads of particle size between 425 to 600 μm, anti-FLAG® M2 affinity gel, 3X FLAG® peptide were purchased from Sigma-Aldrich (St. Louis, MO, USA). Fluorescence Mounting Medium was purchased from Dako (Glostrup, Denmark).

2.1.4 Molecular weight references

BenchMark™ Prestained Protein Ladder used as a molecular weight standard for most SDS-PAGE gels was purchased from Invitrogen (Carlsbad, CA, USA). Precision Plus Protein® Kaleidoscope Prestained ladder used in some SDS-PAGE gels was purchased from Bio-Rad (Hercules, CA, USA). 2-log, 1 kb and 100 bp DNA ladders used in all native agarose gels were purchased from New England Biolabs (Ipswich, MA, USA). DIG-labeled RNA Molecular Weight Marker I used in all denaturing agarose gels was purchased from Roche Applied Science (Penzberg, Upper Bavaria, Germany).

2.1.5 Buffers

Phosphate buffered saline (PBS) used in all experiments contained 8 mM Na_2HPO_4, 2 mM KH_2PO_4, 150 mM NaCl, 3 mM KCl and pH was adjusted to 7.4. Lysis buffer used in all experiments contained 140 mM NaCl, 10 mM Tris (pH 8.0), 1% IGEPAL CA-630 unless otherwise stated. DEPC-treated water was prepared with 0.1% DEPC (v/v) deactivated by auto-claving.

2.1.6 Membranes

Nitrocellulose membrane, Hybond-C Extra, and nylon membrane, Hybond-N^+, were purchased from Amersham (Amersham, United Kingdom). Polyvinylidene fluoride (PVDF) membrane was purchased from Bio-Rad (Hercules, CA, USA).

2.2 Yeast three-hybrid Screening

2.1.1 Basis of the three-hybrid system

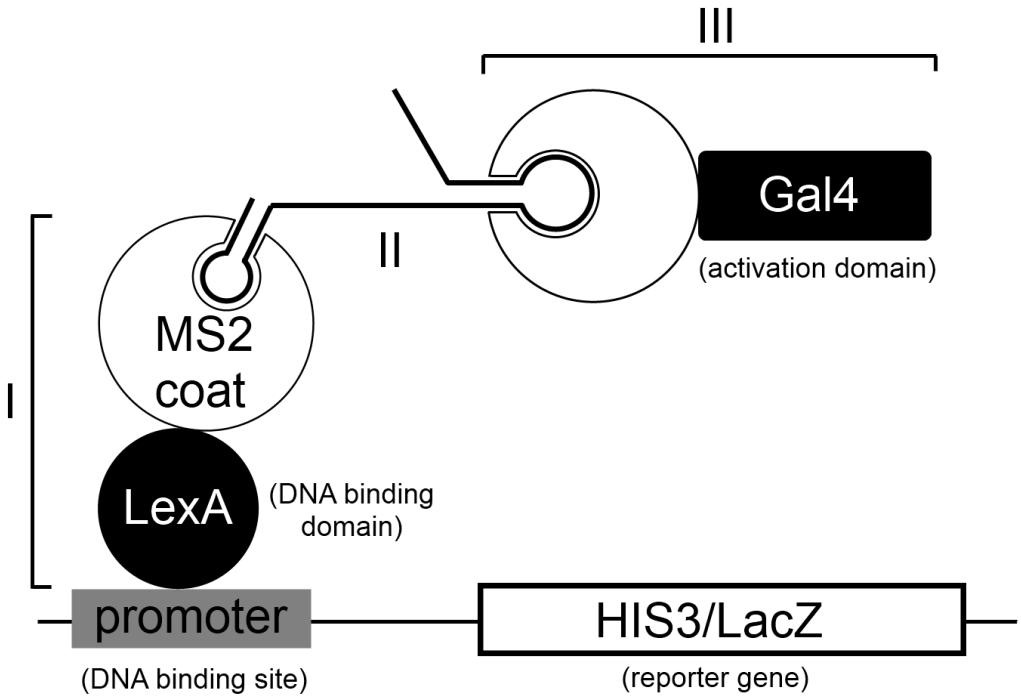

Figure 2.1: An overview of the yeast three-hybrid system. The system is based on the successful interaction between three hybrids (labeled I, II and III) resulting in the transcriptional activation of a reporter gene (*HIS3*). Hybrid I is a fusion protein of LexA DNA-binding domain and the coat protein of bacteriophage MS2. Hybrid II is a fusion RNA of the MS2 coat binding sequence and any other protein binding sequence. Hybrid III is a fusion protein of a RNA-binding protein and the Gal4 transcriptional activation domain. Interactions between the three components bring the activation domain in close proximity to the promoter and activate the transcription of the reporter gene under its control.

The three-hybrid system was a gift from Marvin Wickens (University Of Wisconsin-Madison, USA), the corresponding author of the original publication (332) and employed as the strategy to detect RNA-protein interactions between SARS CoV UTRs and human proteins. As depicted in Figure 1 above, hybrid I is a fusion protein,

which comprised of the LexA DNA-binding domain, tethers the bacteriophage MS2 coat protein to the promoter. Hybrid III is fusion protein comprised of a RNA-binding domain and the Gal4 transcription activation domain. Hybrid II on the otherhand is a fusion RNA and the MS2 coat binding sequence on it binds to the MS2 coat protein with high affinity, therefore anchoring hybrid II to the promoter region. Thus, an interaction between hybrid II and the RNA-binding domain on hybrid III would result in the Gal4 transactivation domain being brought into close proximity to the promoter, resulting in reporter gene *HIS3* or *LacZ* expression. The variable components of the system are designated to be the RNA-binding domain on hybrid III and hybrid II RNA sequence (apart from MS2 coat binding sites). The three hybrids required for the assay are supplied by the yeast strain (hybrid I) and plasmids (hybrids II and III).

2.2.2 Yeast plasmids

To create the fusion RNA hybrid II, the vector pIIIA/MS2-2 which was enclosed as part of the three-hybrid system obtained was used to express the SARS 5'- and 3'-UTR in yeast cells. The vector is a yeast/*Escherichia coli (E. coli)* shuttle vector which contains a polymerase III promoter that can direct the transcription of a RNA containing two MS2 coat binding sequences in tandem and selection markers URA3 for yeast and ampicillin for *E. coli*. Unique restriction sites Sma1 used was 5' to the MS2 coat binding sequences (MS2s) which allowed for the expression of hybrid RNAs of the SARS UTR-MS2s-MS2s, 5' to 3'.

Hybrid III for the screening was provided by a human cDNA library extracted from HeLa cells and cloned into the vector pGADT7. The library cloning was pre-prepared by another lab member. The pGADT7 vector carried the yeast genetic marker LEU2 which conferred leucine autotrophy, and fuses the GAL4 activation domain as well as a HA-epitope tag to the human cDNA fragment.

2.2.3 Yeast strain

The yeast (*Saccharomyces cerevisiae*) strain L40-coat which was supplied with the system was constructed by the authors who integrated a plasmid encoding hybrid I (LexA-MS2coat) into the genome of yeast strain L40-ura (*MAT***a**, *ura3-52, leu2-3, 112, his3Δ200, trp1Δ1, ade2, LYS2*::(lexAop)-*HIS3, ura3*::(lexAop)-*LacZ*). The resultant L40-coat is an auxotrophic strain for uracil, leucine, histidine, tryptophan and lysine, containing reporter genes *HIS3* and *LacZ* under the control of LexA promoter and expressing hybrid I fusion protein (LexA-MS2coat).

2.2.4 Yeast culture

Yeast strain L40-coat was cultured in yeast peptone dextrose (YPD) medium composed of 20 grams per litre (g/L) Bacto^{TM}-peptone, 10 g/L Bacto^{TM}-yeast extract and 2% (w/v) glucose. SD media for culturing yeast transformants was composed of 6.7 g nitrogen base without amino acids, 1X DO supplement, 2% (w/v) galactose, 1% (w/v) raffinose. For both types of media, an additional 20 g/L of Bacto^{TM}-agar was included.

2.2.5 Screening process

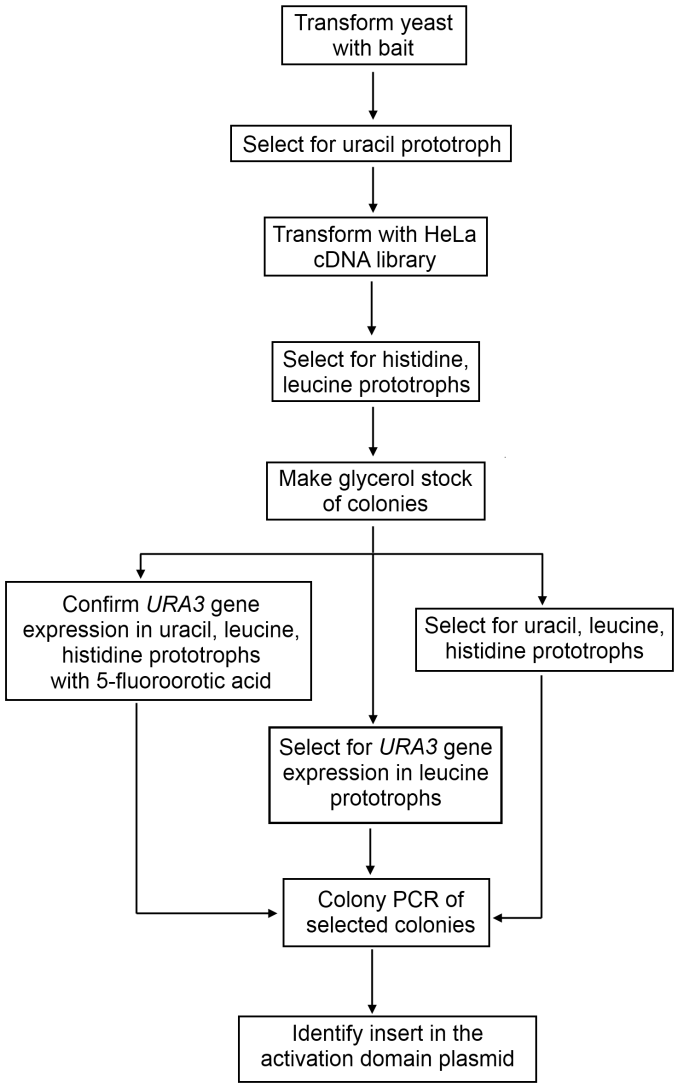

Figure 2.2: Screening process using the yeast three-hybrid system

The bait plasmid which carried the positive sense SARS 5' untranslated region sequence (5'-UTR), MS2 coat binding site and marker gene *URA3* was first transformed into yeast strain *L40-coat.* The transformants were selected for uracil prototrophy using SD/-ura plates. One single colony was selected for use in library transformation and the clone was expanded. This was followed by the transformation of the HeLa cell cDNA library which bears the marker gene *LEU2* into the selected

clone. The transformants were selected for prototrophy of leucine and uracil first using SD/-leu/-ura agar plates and incubated for 7 days when the colonies have grown to substantial size. The colonies were transferred from the agar plates with 1 µl disposable inoculating loops, to 75 µl of freezing media and dispersed evenly in the solution by vortexing to create a liquid stock. 2 µl of each colony stock was dotted on SD/-his/-leu/-ura agar to screen for reporter gene, *HIS3* activation. To verify that the activation of reporter gene *HIS3* was accompanied by the expression of *URA3* gene from the bait plasmid, 5-FOA, a negative selector for *URA3* gene expression, was required. Hence, 2 µl of each colony stock was dotted on SD/-his/-leu/-ura/5-FOA agar as well. An additional selection criterion was imposed to confirm URA3 gene expression in leucine prototrophs, and 2 µl of each colony stock was dotted on SD/-leu/5-FOA plates as well. The remaining colony stocks were frozen at -80°C and the plates were incubated until colonies on SD/-his/-leu/-ura have grown to a minimum of 2 millimeters (mm). Colonies which appeared on SD/-his/-leu/-ura but not on SD/-his/-leu/-ura/5-FOA were sequenced and the insert identified by alignment with the human transcript library using basic local alignment search tool (BLAST) from National Center for Biotechnology Information(NCBI). The key procedures of the screen had been summarized in Figure 2.2.

2.1.6 Yeast transformations

For the initial transformations of bait plasmids, 1 ml of YPD medium was inoculated with L40-coat strain of *S. cerevisiae* and vortexed to eliminate clumping. The resuspended yeast was transferred into a conical flask containing 25 ml of YPD medium and incubated at 30°C with shaking at 250 revolutions per minute (rpm) for

16 hours. 100 ml of YPD medium was inoculated with the overnight culture such that the optical density at 600 nm (OD_{600}) fell between 0.2 and 0.3. The culture was incubated at 30°C with shaking at 230 rpm until its OD_{600} fell between 0.5 and 0.6. The cell suspension was then transferred into 50 ml polypropylene centrifuge and centrifuged at 1000 g for 5 minutes at room temperature with a table-top centrifuge. The pellet was resuspended with 30 millilitres (ml) of 1X TE buffer (10 milimolar (mM) Tris (pH 7.5), 1 mM ethylenediaminetetraacetic acid (EDTA)) then centrifuged at 1000 g for 5 minutes. The pellet was then resuspended in 1.5 ml of sterile 1X TE/Lithium acetate (LiAc) (1X TE, 0.1 molar (M) LiAc) solution to yield transformation-competent yeast cells.

In a 1.5 ml polypropylene snap-cap tube, 0.1 micrograms (µg) of the bait plasmid and 0.1 milligram (mg) of salmon testes carrier deoxyribonucleic acid (DNA) (Millipore; Billerica, MA, USA) was mixed with 0.1 ml of competent yeast cells vigorously. 0.6 ml of PEG/LiAc solution (40% PEG, 1X TE, 0.1 M LiAc) was added and the mixture was mixed thoroughly then incubated at 30°C for 30 minutes with shaking at 200 rpm. After which, 70 µl of DMSO was mixed in by gentle inversion.

To perform heat shock, the tube was placed in a 42°C water bath for 15 minutes then chilled on ice for 2 minutes and centrifuged at 14000 rpm for 5 seconds at room temperature using a table-top microcentrifuge. The supernatant was removed carefully and the cells were resuspended in 0.5 ml of 1X TE buffer, of which, 0.1 ml was plated on a SD/-ura agar plate and incubated at 30°C for 16 hours.

For the transformation of the cDNA library, a 150 ml overnight culture of each confirmed transformant bearing the bait plasmid was prepared. 1 L of SD/-ura

medium was inoculated with the overnight culture and once the OD_{600} fell between 0.5 and 0.6 the cells were pelleted. It was then washed with 500 ml of 1X TE buffer and resuspended in 8 ml of TE/LiAc solution. 0.5 mg of the HeLa cell cDNA library (pre-constructed by another lab member using pGADT7 vector), 20 mg of salmon testes carrier DNA and 8 ml of competent cells were mixed in a 50 ml polypropylene centrifuge tube. Half of the mixture was transferred to a new tube and 30 ml of PEG/LiAc solution was added to each tube then incubated at 30°C with shaking at 200 rpm for 30 minutes. 3.5 ml of DMSO was then added to each tube and mixed gently. Heat shock was performed by incubating both tubes in a 42°C water bath for 15 minutes with occasional swirling then chilled on ice for 2 minutes. The cells were then pelleted, resuspended in 10 ml of 1X TE buffer, and plated on SD/-leu/-ura agar plates. The plates were incubated at 30°C for 5 to 7 days until colonies appear.

2.1.7 Yeast colony PCR

A matchhead amount of yeast cells from each selected colony was washed with 500 µl of de-ionized water in a 1.5 ml snap-cap eppendorf tube and pelleted by centrifugation at 5000 rpm for 1 minute using a microcentrifuge. The pellet was resuspended in 100 µl of water containing 6 U of zymolyase. 25 µl of glass beads was added to each sample and the tube was incubated at 37°C using a heating block for 30 minutes. The samples were vortexed vigorously for 1 minute and incubated at 95°C on a heating block for 10 minutes then chilled immediately on ice for 5 minutes. The cell debris and glass beads were pelleted by centrifugation at 5000 rpm for 1 minute and the supernatant was transferred to a clean 1.5 ml snap-cap eppendorf tube. 10 µl

of supernatant for each sample was used in a 50 µl PCR reaction for amplification of the insert with the following primers:

AD_5' (5'-CTATTCGATGATGAAGATACCCCACCAAACCC-3');

AD_3' (5'-GTGAACTTGCGGGGTTTTTCAGTATCTACGAT-3')

The PCR product of each sample was then purified and sequenced using the AD_3' primer.

2.3 Mammalian Cell Culture

2.3.1 Cell lines

Human lung cancer epithelial cell line, H1299, was cultured in RPMI-1640 medium supplemented with 5% FBS, 100 units (U) of penicillin and 100 µg of streptomycin. African green monkey kidney epithelial cell line, Vero, was cultured in DMEM supplemented with 5% FBS, 100 U of penicillin and 100 µg of streptomycin. Human liver cancer epithelial-like cell line, HuH-7, was also cultured in DMEM supplemented with 5% FBS, 100 U of penicillin and 100 µg of streptomycin.

All cell lines were cultured at 37°C with an atmosphere of 5% carbon dioxide (CO_2) and 95% air using an incubator.

2.3.2 Sub-culturing of adherent cell lines

All adherent cell lines were maintained in flasks and sub-cultured once they have reached a minimum of 95% confluency. Culture medium was first removed and the cells were rinsed with sterile PBS once to remove traces of the culture medium. Trypsin-EDTA solution was then used to rinse the cells and excess was removed. The flask was allowed to sit at room temperature or incubated at 37°C in the incubator to allow trypsin to dissociate the cells from the flask surface. Once the cells had started to dissociate from the surface, fresh culture medium was added to resuspend the cells evenly. The cell suspension was then redistributed to new flasks, culture dishes or well-plates and topped up with fresh medium.

2.3.3 Sub-culturing of suspension cell lines

Suspension cell lines were maintained in culture dishes and sub-cultured when required. Culture medium and the suspended cells were centrifuged at 600 rpm using table-top centrifuge (Sorvall Legend RT Plus) for 5 minutes. The supernatant was removed and the pellet was resuspended in fresh culture medium and redistributed to new dishes or well-plates, then topped up with fresh medium.

2.4 Virology Methods

2.4.1 Creating virus stocks

IBV virus stock

Monolayer Vero cells grown to a confluency of 100% in 180 cm^2 culture flasks were washed twice with serum-free medium and inoculated with wild-type IBV at a multiplicity of infection (MOI) of approximately 1 in serum-free medium. The cells were incubated at 37°C with 5% CO_2 for 16 hours until all cells exhibit cytopathic effects (CPE). The infected cells with the culture medium were then frozen at -80°C and thawed at room temperature for three cycles. The medium containing released virus particles was clarified by centrifugation at 1000 rpm at 4°C for 5 minutes with a table-top centrifuge. Clarified virus medium was divided into 1 ml aliquots and stored at -80°C.

Vaccinia/T7 virus stock

Monolayer Vero cells grown to a confluency of 100% in 180 cm^2 culture flasks were washed twice with serum-free medium and inoculated with 1 ml of Vaccinia/T7 recombinant virus in 20 ml of serum-free medium. The cells were incubated at 37°C with 5% CO_2 for 16 hours and subjected to three freeze-thaw cycles. The virus-containing medium was clarified by centrifugation at 1000 rpm at 4°C for 5 minutes with a table-top centrifuge. Clarified virus medium was divided into 1 ml aliquots and stored at -80°C.

Mock virus stock

Monolayer Vero cells grown to a confluency of 100% in 180 cm^2 culture flasks were washed twice with serum-free medium and incubated with 20 ml of fresh serum-free medium at 37°C with 5% CO_2 for 16 hours then subjected to three freeze-thaw cycles. The medium was clarified by centrifugation at 1000 rpm at 4°C for 5 minutes with a table-top centrifuge then stored at -80°C in 1 ml aliquots.

2.4.2 Virus infections

IBV and IBV-Luc recombinant virus infections

A monolayer of cells grown to a confluency of 100% was washed with serum-free medium twice and inoculated with the virus at a MOI of approximately 1, unless specified. The cells were incubated at 37°C with 5% CO_2 until it was ready to be harvested. For time-course experiments, 0h samples were harvested after the cells were incubated for 5 minutes.

IBV infection using suspension cells

Cells were collected in a sterile centrifuge tube by centrifugation at 600 rpm for 5 minutes with a table-top centrifuge. The cells were resuspended in fresh serum-free medium and approximately 2.5 x 10^6 cells were seeded into a new 60 mm culture dish. The culture medium was inoculated with the virus at a MOI of approximately 1. The cells were incubated at 37°C with 5% CO_2 until it was ready to be harvested.

Vaccinia/T7 infections

A monolayer of H1299 cells grown to a confluency of 100% was washed with serum-free medium twice and inoculated with 120 µl of virus in 3 ml of serum-free medium or 250 µl of virus in 8 ml of serum-free medium in a 60 mm or 100 mm dish respectively. The cells were incubated at 37°C with 5% CO_2 for 90 minutes before the virus-inoculated medium was removed and replaced with fresh serum-free medium.

2.4.3 Virus titration

Plaque assay

Viruses to be titrated were serially ten-fold diluted with serum-free medium up to a dilution factor of 1:10000X. Monolayers of Vero cells grown in 6-well plates to a confluency of 100% were washed twice with serum-free medium and the medium completely removed after the second wash. 200 µl of neat virus or diluted virus was added into each well and incubated at 37°C with 5% CO_2 for 1 hour with regular agitation to make sure the cells were covered with the virus medium. The virus medium was then removed completely, washed once with serum-free medium gently and overlaid with serum-free medium containing 0.6% CMC was added. The plates were incubated at 37°C with 5% CO_2 for 72 hours when plaques became visible.

For easy visualization, the medium was removed and the cells were carefully washed twice with PBS then fixed with 4% formaldehyde for 15 minutes at room temperature. The cells were then washed three times with PBS and stained with 0.1% toluidine blue solution. Assays were performed in triplicates and results were averaged.

End-point dilution assay: 50% tissue culture infectious dose ($TCID_{50}$)

A

$$\text{index} = \frac{(\%\text{ infected at dilution immediately above 50\%}) - 50\%}{(\%\text{ infected at dilution immediately above 50\%}) - (\%\text{ infected at dilution immediately below 50\%})}$$

B

$$\text{dilution immediately above 50\%} = 10^{-x}$$

$$1\ TCID_{50} = 10^{-(x + \text{index})}$$

$$\text{amount of virus in 0.1 ml} = 10^{(x + \text{index})} TCID_{50}$$

$$\text{amount of virus in 1 ml} = 10^{(1 + x + \text{index})} TCID_{50}$$

Figure 2.3: $TCID_{50}$ calculation by Reed-Muench method. (A) Calculation for index or proportionate distance from the closest dilution factor above that which 50% of the cells were infected. (B) Calculation of the $TCID_{50}$ value and conversion to virus titre per ml.

Viruses to be titrated were serially ten-fold diluted with serum-free medium up to a dilution factor of 1:100000X. Monolayers of Vero cells were grown in 96-well plates to a confluency of 100% using serum-free medium. The medium was removed and 100 µl of each diluted virus was added to each of 5 wells of cells. The cells were incubated at 37°C with 5% CO_2 for 5 days and the number of wells exhibiting CPE out of 5 for each dilution of each virus was recorded. Calculation of $TCID_{50}$ was performed using Reed-Muench calculation method.

The percentage (%) of wells infected at each dilution of each virus sample were tabulated and used to calculate an index using the formula as shown in Figure 2.3, panel A. For each sample, the calculated index was applied to the dilution factor at which the percentage (%) of infected wells was immediately above 50% as shown in Figure 2.3, panel B, to obtain the $TCID_{50}$ of the virus sample. The reciprocal of $TCID_{50}$ was taken to be the amount of virus present in 0.1 ml of the virus.

2.5 Polymerase Chain Reaction (PCR)

2.5.1 Regular PCR

PCR was used for the amplification of DNA for use in cloning as well as the detection of specific mRNAs when used in combination with reverse transcription (RT-PCR). Amplification of DNA not exceeding 2000 base pairs (bp) was achieved using either KAPA *Taq* DNA polymerase (Kapa Biosystems Inc, USA) or Fermentas *Taq* DNA polymerase (recombinant) (Thermo Scientific, USA). For amplification of DNA from plasmids using Fermentas Taq DNA polymerase, 150 ng of plasmid was mixed with 2 picomoles (pmol) of each specific primer, 2 nanomoles (nmol) of each deoxyribonucleotide triphosphate (dATP, dTTP, dCTP, dGTP) (Fermentas, USA), 2 mM $MgCl_2$ and 5 U of polymerase in 1X reaction buffer.

2.5.2 Site-directed mutagenesis

Primers for mutagenesis were designed to be complementary to each other, harbouring the desired mutations in the middle of the base-pairing region. In a 50 µl reaction, 150 ng of template DNA was mixed with 1.5 pmol of each primer, 2 nmol of each dexoyribonucleotide triphosphate, 1 mM $MgSO_4$ and 1.5 U of KOD Hot Start DNA polymerase in 1X PCR buffer. 18 to 20 thermal cycles was used for amplification and each product was kit purified, digested with *DpnI* to remove template DNA and kit purified again before it was transformed into DH5alpha *E. coli* for selection.

2.6 Nucleic Acid Manipulation Techniques

2.6.1 Restriction digestion

To perform restriction digestion on plasmid vectors, 3 µg of plasmid DNA was incubated in a 50 µl reaction with 15 units (U) of restriction enzyme, its supplied buffer, 100 µg/ml bovine serum albumin (BSA) (if required) for 2 hours at 37°C on a heating block. 20 U of calf intestinal phosphatase (CIP) (New England Biolabs, USA) was added into the reaction mixture and incubated for 1 hour at 37°C. Digestion products were purified with a kit.

For the preparation of cloning insert from existing plasmids, 5 µg of plasmid DNA was incubated with 20 U of restriction enzyme in a similar manner as stated above. The insert fragment was purified from the rest of the DNA using gel extraction.

For the preparation of PCR amplified fragments bearing flanking restriction sites as cloning insert, the PCR product was purified and 2 µg of purified DNA was incubated with 20 U of each required restriction enzyme, including *DpnI* (to remove the template DNA used in the PCR reaction). Digestion products were purified with a kit.

CIP was omitted if digestion was performed to generate insert DNA. Kit purifications were performed using QiaQuick PCR Purification Kit and DNA concentrations were determined using NanoDrop 1000.

For digestion with *SmaI* restriction enzyme, the reaction was left on the bench-top for 2 hours instead of incubating at 37°C. Multiple enzyme digestion was performed

either simultaneously when a common buffer was available for all restriction enzymes, or sequentially, if no common buffer was available. In a sequential digestion, the reaction mixture was purified before it was digested with the next enzyme.

2.6.2 Nucleic acid purification

Kit purifications were performed using QIAquick PCR Purificaation Kit from Qiagen (Hilden, Germany). 5 volumes of buffer PB was added to 1 volume of nucleic acid and applied onto the column. The column was washed with buffer PE and the nucleic acid was eluted with nuclease-free water. The concentration of the nucleic acid was determined using a spectrophotometer.

Nucleic acid purifications were also performed using UltraPure™ Phenol:Chloroform:Isoamyl Alcohol (25:24:1 v/v). The reagent was mixed vigorously with the nucleic acid at a 1:1 ratio (v/v) and centrifuged at 12000 rpm for 10 minutes at 4°C. The aqueous phase was transferred to a new tube and mixed vigorously with chloroform at a 1:1 ratio (v/v). The emulsion was centrifuged and the aqueous phase was transferred to a new tube. Sodium acetate (0.3 M final concentration) was added to the aqueous phase and mixed well. Isopropanol was added to the mixture at a ratio of 2:1 (v/v) and mixed by gentle inversion. Nucleic acid precipitation was allowed to proceed for up to one hour at -20°C and pelleted by centrifugation. The pellet was washed with 70% ethanol, air-dried and resuspended in nuclease-free water.

2.6.3 Gel extraction

The digested DNA was resolved by agarose gel electrophoresis with an agarose gel of an appropriate concentration between 1 to 1.5%, which contained ethidium bromide for visualization. The resolved DNA was visualized under ultraviolet illumination (UV) and the band corresponding to the desired fragment was excised with a clean scapel blade. The mass of the excised gel fragment was determined using a weighing scale. Nucleic acid extraction was performed using QIAquick Gel Extraction Kit from Qiagen (Hilden, Germany). Buffer QG was added into the tube containing the excised gel fragment and incubated at 50°C for 10 minutes or until the agarose dissolved completely. The dissolved gel was applied onto the column, washed with buffer PE and eluted with nuclease-free water. The nucleic acid concentration was determined using a spectrophotometer.

2.6.4 Agarose gel electrophopresis

Agarose gels were prepared by dissolving UltraPure^{TM} agarose in 1X Tris-acetate-EDTA (TAE) buffer (40 mM Tris, 1 mM EDTA (pH 8.0), 20 mM glacial acetic acid) by boiling. Ethidium bromide was added for visualization of the resolved nucleic acids. Nucleic acid was mixed with at a volume ratio of 5:1 with 6X gel loading dye (0.25% bromophenol blue, 0.25% xylene cyanol, 30% glycerol) and loaded onto the agarose gel. Electrophoresis was performed using 1X TAE as the running buffer.

2.6.5 DNA ligation

50 µg of linearized vector and insert DNA were mixed at a molar ratio of 1:3 with 1 U of T4 DNA ligase and 10X ligase buffer supplied with the enzyme. Minimum volume of reaction was 10 µl and the maximum was 20 µl. Ligation reactions were performed at 16°C in a water-bath for 16 to 18 hours and stored at 4°C or -20°C thereafter before they were transformed into bacteria.

2.6.6 Crude plasmid DNA extraction from *E. Coli*

200 µl of overnight bacteria culture was pelleted by centrifugation at 14000 rpm for 1 minute in a microcentrifuge. The pellet was resuspended in 4 µl of nuclease-free water and 8 µl of sodium chloride-Tris-EDTA-Triton-X (STET) buffer (0.1 mM NaCl, 10 mM Tris (pH 8.0), 1 mM EDTA, 5% (v/v) Trixon X-100). The resuspended cells were incubated at 100°C for 5 minutes and centrifuged at 14000 rpm for 2 minutes. The supernatant was transferred to a new tube and used for restriction digestion in the presence of RNase A. Plasmid DNA prepared by this method was only used in restriction enzyme screening of clones.

2.6.7 RNA extraction from mammalian cells

Adherent cells were lysed in the culture vessel with 1 ml of TRIzol® (more reagent was added if complete lysis was not possible) for 15 minutes at room temperature with shaking. The lysed cells were transferred into 1.5 ml polypropylene snap-cap tubes and 200 µl of chloroform was added into the lysate and mixed vigorously and left to stand for 15 minutes at room temperature. The tube was centrifuged at 11000

rpm, 4°C for 10 minutes for phase separation and the aqueous layer was transferred to a clean tube (interphase and organic phase were saved for protein extraction). 500 µl of isopropanol was added to the aqueous layer and incubated for 8 minutes at room temperature to precipitate the RNA. The precipitated RNA was pelleted by centrifugation at 9000 rpm, 4°C for 10 minutes. The pellet was washed with 70% ethanol and air-dried. The dried pellet was incubated with DEPC-treated water at 55°C, using a heating block, up to 20 minutes for solubilization. All RNAs were stored at -80°.

2.7 Molecular Cloning Techniques Involving *E. coli*

2.7.1 Preparation of chemically-competent *E. coli*

Both DH5 alpha and BL-21 strains of *E. coli* were prepared with the same method. 3 ml of Luria-Bertani (LB) broth was inoculated with 5 µl of thawed competent cells and incubated 37°C for 16 hours with shaking (200 rpm). 100 ml of LB broth was inoculated with 1ml of the overnight culture each and incubated at 37°C with shaking (200 rpm) until OD_{660} fell between 0.65 and 0.75. The culture was transferred into 50 ml conical centrifuge tubes and incubated on ice for 30 minutes. The tubes were then centrifuged at 5000 rpm at 4°C for 15 minutes. The pellet in each tube was resuspended with 20 ml of ice-cold wash buffer (0.1 M $CaCl_2$). The resuspended cells were incubated on ice for 40 minutes then centrifuged again. Each pellet was resuspended with 1 ml of freezing buffer and aliquoted into 50 µl (DH5 alpha) or 100 µl (BL-21) fractions with pre-chilled 0.5 ml polypropylene snap-cap tubes. The tubes

were rapidly frozen with liquid nitrogen (LN_2) and transferred to the -80°C freezer for permanent storage.

2.7.2 Transformation of DNA into chemically-competent *E. coli*

For plasmid amplification transformations, 50 ng of plasmid DNA was mixed with 50 µl of competent DH5 alpha cells and for transformations involving *E. coli* strain BL-21, for bacterial protein expression, 100 ng of plasmid DNA was mixed with 100 µl of chemically-competent BL-21 cells. Each transformation mix was incubated on ice for 30 minutes in a 1.5ml tube before heat-shock. To perform heat-shock, the tube was incubated at 42°C for 1 minute followed by 2 minutes incubation on ice. The cells were then spread onto a LB agar plate containing the required antibiotic for selection. If the required antibiotic was kanamycin, the cells were recovered before plating. To perform recovery, 500 µl of SOC media (2% w/v Bacto^{TM}-tryptone, 0.5% Bacto^{TM}-yeast extract, 10 mM NaCl, 2.5 mM KCl, 20 mM glucose) was added to the tube and the mixture incubated at 37°C for 1 hour with shaking at 200 rpm. After which, it was centrifuged at 5000 rpm for 5 minutes at room temperature using a microcentrifuge and the pellet resuspended in 50 µl of SOC media. The cells were then spread onto a LB agar plate with antibiotics (100 µg/ml for ampicillin, 50 µg/ml for kanamycin) for selection.

For ligation mix transformations, 50 µl of chemically-competent DH5 alpha *E. coli* was mixed with 10 µl of ligation mixture. Heat-shock was performed as described above and the cells were recovered before plating. All agar plates were incubated at 37°C for 16 hours.

2.8 Construction of Clones

2.8.1 Yeast three-hybrid screening

SARS 5'-UTR and 3'-UTR were amplified by polymerase chain reaction (PCR) using the primer pairs SARS5'UTR_Fwd/SARS5'UTR_Rev and SARS3'UTR_Fwd/SARS3'UTR_Rev from pKT-SARSA1 (5'-most segment) and pKT-SARSN (3'-most segment from N gene) plasmids respectively (Primer sequence listed in Table 2.1). Both PCR products were ligated with vector pIIIA/MS2-2 and screened for clones in either orientation. Clones pIIIA/MS2-2-SARS5'UTR(+), pIIIA/MS2-2-SARS5'UTR(-) and pIIIA/MS2-2-SARS3'UTR(-) were obtained.

Table 2.1: List primers used to amplify SARS 5'- and 3'- untranslated regions. Restriction sites were underlined.

Primer Name	**Sequence**
SARS5'UTR_Fwd	5'-TGACCCGGGTACCCAGGAAAAGCCAACCAACCT-3'
SARS5'UTR_Rev	5'-GCACCCGGGCGTCTCTAACCTGAAGGA-3'
SARS3'UTR_Fwd	5'-AAACCCGGGTGAGTGGAGCTTCTGCTG-3'
SARS3'UTR_Rev	5'-CAGCCCGGGTTTTTTTTTTTTTTTGTCATT-3'

2.8.2 Cloning of full-length, wild-type MADP1 into Gateway® vectors

Total RNA was extracted from HeLa cells using Trizol® and 5 µg was used for reverse transcription (RT) with primer Madp1_RT (Table 2.3). The primers 5'Madp1attB and 3'Madp1attB (Table 2.2) were used to amplify MADP1 from the cDNA and the PCR product was inserted into pDONR^{TM}221 vector in a recombination reaction using BP Clonase^{TM} enzyme mix from Invitrogen () to obtain

the clone pDONR-Madp1. MADP1 was subsequently inserted into pDEST15 vector in a recombination reaction using LR Clonase™ enzyme mix from Invitrogen.

Table 2.2: Primers used to amplify MADP1 from HeLa cDNA for cloning into pDONR™221 vector.

Primer Name	**Primer Sequence**
5'Madp1attB	5'-GGGGACAAGTTTGTACAAAAAAGCAGGCTTCACCATGAGTGGTGGATTGGCTCCAAGT-3'
3'Madp1attB	5'-GGGGACCACTTTGTACAAGAAAGCTGGGTCTTAATCACTAAGTTCTTCCTCATC-3'

2.8.3 Cloning of full-length, wild-type MADP1

Primers used for the construction of all full-length wild-type MADP1 clones were tabulated in Table 2.3. Total RNA was extracted from HeLa cells using Trizol® and 5 µg was used for reverse transcription (RT) with primer Madp1_RT. The RT product was used to perform a PCR with primers 5'Madp1_Sma1 and 3'Madp1_Sma1 and the PCR product was ligated with pGEM-T Easy vector to construct the plasmid pGEM-Madp1.

For bacterial expression of MADP1, pGEX-Madp1 and pET-Madp1 were constructed to express N-terminal glutathione S-transferase tagged (GST-MADP1) and 6Xhistidine (HIS-MADP1) MADP1. The primers Madp1_EcoRIF and Madp1_Not1R were used to amplify MADP1 from pGEM-Madp1 and the fragment was cloned into vector pGEX-5X-1 to construct pGEX-Madp1. Primers Madp1_NdeIF and Madp1_NdeIR were used to generate the fragment from pGEM-Madp1 to be inserted into vector pET-16b to construct pET-Madp1.

Table 2.3: List of primer sequences used in the cloning of all full-length and truncated MADP1 constructs. Restriction sites were underlined.

Primer Name	**Primer Sequence**
Madp1_RT	5'-ACGGGGTCGTGTCATTATTTTT-3'
5'Madp1_Sma1	5'-ATACCCGGGATGAGTGGTGGATTGGC-3'
3'Madp1_Sma1	5'-ATACCCGGGTTAATCACTAAGTTCTTCTT-3'
Madp1_EcoRIF	5'-AGAATTCATGAGTGGTGGATTGGCTCC-3'
Madp1_NotIR	5'-AAAAGCGGCCGCTTAATCACTAAGTTCTTCCTCATC-3'
Madp1_NdeIF	5'-AAAAAAACATATGAGTGGTGGATTGGCTCC-3'
Madp1_NdeIR	5'-AAAAAAACATATGTTAATCACTAAGTTCTTCTCATC-3'
Madp1_HindIIIF	5'-TTTTTTAAGCTTATGAGTGGTGGATTGGCTCCA-3'
Madp1_BglIIR	5'-TTTAGATCTTTAATCACTAAGTTCTTCCTCATC-3'
Madp1_121-144HindIIIF	5'-TTTTTTAAGCTTATCATGAAAGATAAAGATACCAGG-3'
Madp1_300-280BglIIR	5'-TTTAGATCTTTAGTTTCGCCTTCGGATGAACTC-3'
Madp1_351-332BglIIR	5'-TTTAGATCTTTAACTTAAGTGTCCACTTTCCCC-3'

For the expression of MADP1 in mammalian cell systems, pXJ40-Madp1 and pXJ40Flag-Madp1 were constructed to either express untagged MADP1 or N-terminal FLAG-tagged MADP1 (FLAG-MADP1). The primers Madp1_HindIIIF and Madp1_BglIIR were used to amplify MADP1 from pGEM-Madp1. The fragment was cloned into the vectors pXJ40 and pXJ40Flag to generate the respective clones.

2.8.4 Cloning of MADP1 truncation mutants

All truncation mutants of MADP1 were generated by amplification of segments of MADP1 with primers listed in Table 2.3 from the plasmid pGEM-Madp1. The plasmids pXJ40Flag-Madp1n, pXJ40Flag-Madp1m and pXJ40Flag-Madp1c were

constructed to express FLAG-Madp1n, FLAG-Madp1m and FLAG-Madp1c respectively. The primer pairs used to amplify the inserts were Madp1_HindIIIF / Madp1_258-236BglIIR, Madp1_178-199HindIIIF / Madp1_529-497BglIIR and Madp1_430-451HindIIIF / Madp1_BglIIR respectively.

Plasmids pXJ40Flag-Madp1x, pXJ40Flag-Madp1y and pXJ40Flag-Madp1z were constructed to express FLAG-Madp1x, FLAG-Madp1y and FLAG-Madp1z respectively. The primer pairs used to amplify the inserts were Madp1_HindIIIF / Madp1_300-280BglIIR, Madp1_121-144HindIIIF / Madp1_300-280BglIIR and Madp1_HindIIIF / Madp1_352-332BglIIR respectively. All inserts were cloned into the mammalian expression vector pXJ40Flag.

2.8.5 Site-directed mutagenesis of MADP1

To create a vector which could express wild-type FLAG-MADP1 and not be sensitive to the silencing effects of the siRNA, siMadp1b, three site-directed mutagenesis PCRs were performed sequentially with the primers listed in Table 2.4. The first mutant construct, pXJ40Flag-Madp1mutA, was generated with the primers Madp1_TTG76CTT_F and Madp1_TTG76CTT_R using pXJ40Flag-Madp1 plasmid as the template. The mutant was screened in *E. coli* and confirmed by sequencing. The second mutant, pXJ40Flag-Madp1mutAB, was generated with the primers Madp1_T72C_F and Madp1_T72C_R using pXJ40Flag-Madp1mutA as the template. The mutant was again screened in *E. coli* and confirmed by sequencing. Then the final mutant, pXJ40Flag-Madp1mutABC, was generated with the primers Madp1_A87CF

and Madp1_A87CR using pXJ40Flag-Madp1mutAB as the template. Likewise, it was screened in *E. coli* and confirmed by sequencing.

Table 2.4: List of all primer sequences used in the generation of mutants of pXJ40Flag-MADP1.

Primer Name	**Primer Sequence**
Madp1_TTG76CTT_F	5'-CAAACAATGACCTTTACCGGATATTTTC-3'
Madp1_TTG76CTT_R	5'-GAAAATATCCGGTAAAGGTCATTGTTTG-3'
Madp1_T72C_F	5'-CCTGACAAACAACGACCTTTACCG-3'
Madp1_T72C_R	5'-CGGTAAAGGTCGTTGTTTGTCAGG-3'
Madp1_A87CF	5'-CTTTACCGGATCTTTTCCAAGTATG-3'
Madp1_A87CR	5'-CATACTTGGAAAAGATCCGGTAAAG-3'
Madp1mutY13A_F	5'-GAGCACAGTGGCTGTATCCAACT-3'
Madp1mutY13A_R	5'-AGTTGGATACAGCCACTGTTCTC-3'
Madp1mutV53F55A_F	5'-GAGTAAAGGGGCTGCAGCTATTTTATTTTTGG-3'
Madp1mutV53F55A_R	5'-CCAAAAATAAAATAGCTGCAGCCCCTTTACTC-3'

Several plasmids which could express point mutants of FLAG-MADP1 were also created using the primers listed in Table 2.4. Mutants FLAG-MADP1mutY, FLAG-MADP1mutVF and FLAG-MADP1mutYVF were expressed by the plasmids pXJ40Flag-Madp1mutY13A, pXJ40Flag-Madp1mutV53F55A and pXJ40Flag-Madp1mutY13V53Y55A respectively. The plasmid pXJ40Flag-Madp1 was subjected to site-directed mutagenesis PCRs with the primer pairs Madp1mutY13A_F / Madp1mutY13A_R and Madp1mutV53F55A / Madp1mutV53F55A to generate the mutant plasmids pXJ40Flag-Madp1mutY13A and pXJ40Flag-Madp1mutV53F55A respectively. The third mutant plasmid was generated via mutagenesis PCR using

pXJ40Flag-Madp1mutV53F55A as a template with primer pair Madp1mutY13A_F / Madp1mutY13A_R.

2.8.6 Site-directed mutagenesis of IBV stem-loop I

The mutant construct pKT-IBVA_SL1dsmut was created to serve as the template to generate the RNA probe 5'-UTRΔ2M1, a transcript of the IBV 5'-UTR which with a disrupted stem loop I. The primer pair i1-29_SL1dsmutF/i1-29_SL1dsmutR (Table 2.5) and template pKT-IBVA were used for this mutagenesis PCR.

Table 2.5: List of primers used in the generation of stem loop I mutant plasmids.

Primer Name	**Primer Sequence**
i1-29_SL1dsmutF	5'-ACTTAAGATACTTATTAATATATATCTAT-3'
i1-29_SL1dsmutR	5'-ATAGATATATATTAATAAGTATCTTAAGT-3'
i9_39SL1rsmutF	5'-TACTTATTAATATATAAGTATTATACTAGCC-3'
i39_9SL1rsmutR	5'-GGCTAGTATAATACTTATATATTAATAAGTA-3'

Mutant construct pKT-IBVA_SL1rsmut was created to be used as the template to generate RNA probe 5'-UTRΔ2M2, a transcript of the IBV 5'-UTR which contained a mutation in 5'-UTRΔ2M1 which restored the structure of stem loop I. The primer pair i9_39SL1rsmutF/i39-9_SL1rsmutR (Table 2.5) and template pKT-IBVA_SL1dsmut were used for the mutagenesis PCR.

2.8.7 Cloning of HCoV-OC43 5'-UTR

The 5'-UTR of the coronavirus was amplified by PCR from a cDNA sample using the primers T7_oc1-20 and pT_oc210-192 (Table 2.6). The PCR product was ligated with pGEM-T Easy vector to generate the plasmid pGEM-oc5UTR.

Table 2.6: Primers used to clone HCoV-OC43 5'-UTR.

Primer Name	**Primer Sequence**
T7_oc1-20	5'-TGTAATACGACTCACTATAGGGATTGTGAGCGATTTGCGTG-3'
pT_oc210-192	5'-TTTTTTTTTTTTTTTTTTTTTGTGACCTATGGGCGGGCC-3'

2.8.8 Cloning of Hairpin siRNA into p*Silencer*^{TM} 2.1 U6-Neo

Table 2.7: Oligonucleotide sequence used for generating hairpin siRNA insert.

Oligonucleotide Name	**Oligonucleotide Sequence**
shZCRB1sense	5'-GATCCGCAATGACTTGTACCGGATATTCAAGAGATATCCGGTACAAGTCATTGTTTTTTGGAAA-3'
shZCRB1antisense	5'-AGCTTTCCAAAAAACAATGACTTGTACCGGATATCTCTTGAATATCCGGTACAAGTCATTGCG-3'

Two oligonucleotides Table 2.7 were designed based on the target sequence 5'-CAAUGACUUGUACCGGAUA-3' (same as siMadp1b) according to the instructions supplied with the kit. Both oligonucleotides were diluted in TE buffer to a concentration of 1 µg/µl. In a 50 µl mixture, 2 µl of each oligonucleotide was mixed with 1X DNA annealing Solution (supplied in kit) in a clean 1.5 ml tube. The tube was heated at 90°C for 3 minutes then incubated at 37°C for 1 hour. The annealed

oligonucleotides (hairpin siRNA) were diluted at a factor of 1:10 with nuclease-free water and 1 µl was ligated with 1 µl of p*Silencer*^{TM} U6-neo vector.

2.8.9 Cloning of IBV nsp12 truncation mutants

All nsp12 truncation mutants were created by amplification of the desired fragment from pXL-IBVC (obtained from another lab member), which contained a fragment of the IBV genome from nucleotide to, with the primers listed in Table 2.8. The fragments amplified by the primer pairs i12339-12360BamHIF / i13538_13516_XhoIR, i13296-13316_BamHIF / i14498-14474_XhoIF and i13926-13948_BamHIF / i15128-15106_XhoIR were cloned into the vector pXJ40Myc generating plasmids that could express N-terminally tagged proteins Myc-iNsp12n, Myc-iNsp12m, Myc-iNsp12c.

Table 2.8: List of primers used in the cloning of IBV nsp 12 truncation mutants. Restriction sites were underlined.

Primer Name	**Primer Sequence**
i12339-12360_BamH1F	5'-TTGGATCCGAATTATTTAAACGGGTACGGG-3'
i13538013516_Xho1R	5'-TTCTCGAGTTATAACGCACAAACACTAAAACAAG-3'
i13296-13316_BamH1F	5'-TTGGATCCATACCGCAGACTTCTTTCGGT-3'
i14498-14474_Xho1R	5'-TTCTCGAGTTAGCTCTTAATATTATCATAGACAATA-3'
i13926-13948_BamH1F	5'-TTGGATCCAAGAAGAATGTCCTACCCACTAT-3'
i15128-15106_Xho1R	5'-TTCTCGAGTTATTGTAAAGTCGTAGGAGCTCTAT-3'

2.9 Generation Of Template DNA For *In vitro* Transcription Labeling of RNA Probes

2.9.1 DIG-labeled probes for north-western blots

All probes were transcribed from PCR products amplified using the primers listed in Table 2.9. IBV 5'-UTR (+) probe was transcribed from the PCR product amplified from plasmid pKT-IBVA with the primers T7_i1-27 and pT_i507-528R. The template for SARS-CoV 5'-UTR(+) probe was amplified from the plasmid pKT-SARSA1 with the primers T7proF and pT_s325-342R.

2.9.2 Biotin-labeled probes used in biotin pull-down assay

All probes were transcribed with the PCR products from the respective PCRs performed with the primers listed in Table 2.9. EGFP (-) was transcribed from the PCR product of plasmid pEGFP-N1 amplified by the primers pT-EGFP_F and T7-EGFP_510-528R. The PCR template for SARS-CoV 5'-UTR (+) probe was amplified from the plasmid pKT-SARSA1 with the primers T7proF and pT_s325-342R. The IBV 5'-UTR (+) and IBV 5'-UTR (-) probes were generated from PCR fragments amplified from the plasmid pKT-IBVA with the primer pairs T7_i1-27/pT_i507-528R and pT_i1-29/T7_i528-506R respectively. The IBV 3'-UTR (+) probe was transcribed from the PCR product amplified from pGEM-IBVE plasmid with the primers T7_i27106-27125 and LDX30. The transcription template of HCoV-OC43 5'-UTR (+) probe was amplified from pGEM-oc5UTR with the primers pGEM-E_T7F and p18T_oc210-202.

Table 2.9: List of primers used to amplify PCR fragments used as templates for transcription of biotin-labeled probes.

Primer Name	**Primer Sequence**
pT-EGFP_F	5'-TTTTTTTTTTTTTTTTTTTTTGTATGGTGAGCAAGGGCGAGG-3'
T7-EGFP_510-528R	5'-TGTAATACGACTCACTATAGGGCTGCCGTCCTCGATGTTG-3'
T7proF	5'-TGTAATACGACTCACTATAGGGC-3'
pT_s325-342R	5'-TTTTTTTTTTTTTTTTTTTTTGCACCCGGGCGTCTCTAA-3'
T7_i1-27	5'-TGTAATACGACTCACTATAGGACTTAAGATAGATATTAATATATATCT-3'
pT_i507-528R	5'-TTTTTTTTTTTTTTTTTTTTTGTTGTCACTGTCTATTGTATGT-3'
pT_i1-29	5'-TTTTTTTTTTTTTTTTTTTTTACTTAAGATAGATATTAATATATATGTAT-3'
T7_i528-506	5'-TGTAATACGACTCACTATAGGGTTGTCACTGTCTATTGTATGTC-3'
T7_i27106-27125	5'-TGTAATACGACTCACTATAGGGTAACATAATGGACCTGTTG-3'
LDX30	5’-TGATGCCGGCCACGATGCGTC-3’
pT_i140-121	5'-TTTTTTTTTTTTTTTTTTTTTCAGGTGCCATCCAGGGCACT-3'
pT_i99-80	5'-TTTTTTTTTTTTTTTTTTTTTCCTATGAGGACCAGCTGTAG-3'
T7_i30-51	5'-TGTAATACGACTCACTATAGGTACACTAGCCTTGCGCTAGATT-3'
T7_i141-162	5'-TGTAATACGACTCACTATAGGGCCACCTGTCAGGTTTTTGTTA-3'
T7_i1-27_SL1dsmut	5'-TGTAATACGACTCACTATAGGACTTAAGATACTTATTAATATATATGT-3'
T7_i1-26_SL1rsmut	5'-TGTAATACGACTCACTATAGGACTTAAGATACTTATTAATATATAAG-3'
pGEM-E_T7F	5'-GGGAATTCGATTTGTAATACGA-3'
p18T_oc210-202	5'-TTTTTTTTTTTTTTTTTTTGTGACCTA-3'

The truncated probes of IBV 5'-UTR (+), 5'UTRΔ1, 5'UTRΔ2, 5'UTRΔ3 and 5'UTRΔ4 were transcribed from PCR fragments amplified from pKT-IBVA using the primer pairs T7_i1-27/pT_i140-121, T7_i1-27/pT_i99-80, T7_i30-51/pT_i140-121 and T7_i141-162-pT_i507-528R respectively. The template for probe 5'UTRΔ2M1 was amplified from pKT-IBVASL1dsmut with the primers T7_i1-27SL1dsmut and pT_i99-80 while the template for probe 5'UTRΔ2M2 was amplified from pKT-IBVASL1rsmut with the primers T7_i1-36SL1rsmut and pT_i99-80.

2.10 *In-vitro* transcription

2.10.1 Template preparation

PCR templates were produced with a forward primer containing a T7 promoter sequence and a reverse primer containing 18 to 21 thymidine residues at their respective 5' ends. Plasmid DNA templates with a T7 promoter sequence were linearized by an enzyme cutting at the 3' end of the template strand. All nucleic acids were kit purified and eluted in DEPC-treated water.

2.10.2 Transcription

1 mg of linearized plasmid DNA or 200 ng of PCR fragment was incubated with 10 U T7 RNA polymerase, 10 U Protector RNase Inhibitor and NTPs (1 mM each of ATP, CTP, GTP, UTP) in 1X Transcription Buffer (provided with polymerase), at 37°C for 2 hours. The transcription mix was incubated with 5 U of DNase I at 37°C for 15 minutes to remove template DNA. For labeling of RNA products, NTPs were

replaced with either DIG RNA Labeling Mix (1 mM each of ATP, CTP, GTP, 0.65 mM UTP, 0.35 mM DIG-11-UTP) or Biotin RNA Labeling Mix (1 mM each of ATP, CTP, GTP, 0.65 mM UTP, 0.35 mM biotin-16-UTP). Transcripts were purified with UltraPure™ Phenol:Chloroform:Isoamyl Alcohol (25:24:1, v/v) and stored at -80°C.

2.11 Mammalian Gene Over-Expression and Gene Silencing

2.11.1 Transient protein over-expression for biochemical assays

H1299 cells were grown to a confluency of 100% and infected with Vaccinia/T7 recombinant virus for 1 hour at 37°C, 5% CO_2. Plasmid DNA was delivered into the infected cells with Effectene® Transfection Reagent, purchased from Qiagen (Hilden, Germany). The cells were incubated with the transfection mix for 20 hours in the 37°C incubator before they were lysed with Lysis buffer.

2.11.2 Transient protein over-expression and BrUTP labeling for immunofluorescence detection

Vero cells grown to 50% confluency in 4-chamber glass slides were transfected with either pXJ40Flag vector or pXJ40Flag-Madp1 using Effectene® Transfection Reagent for 16 h. Transfected cells were infected with wild-type IBV or mock-infected with Vero cell lysate for 1 hour and replaced with fresh serum-free medium. The infection was allowed to progress for another 2 hours and the cells were treated with actinomycin D at a concentration of 15μg/ml for 4 hours. 1mM of BrUTP (Sigma

Aldrich) was delivered into the cells with SuperFECT® purchased from Qiagen (Hilden, Germany), and incubated for 3 hours before they were fixed.

2.11.3 Transient gene silencing with Dharma*FECT*®

In each well of a 6-well plate, H1299 cells were grown to a confluency of 30% and 200 picomoles (pmoles) of homogeneous siRNA or 250 pmoles of prescribed siRNA pools (target sequences listed in Table 2.10) was delivered into the cells with 2 µl of Dharma*FECT*® 2 Transfection Reagent purchased from Thermo Scientific Dharmacon (Lafayette, CO, USA). The transfection was repeated 24 hours later and the cells were incubated with the transfection mix for a further 48 hours before they were lysed with Lysis buffer for analysis or infected with IBV. Vero cells were transfected using Dharma*FECT*® 3 Transfection Reagent with the same protocol.

Table 2.10: Target sequence of siRNAs used for silencing MADP1.

siRNA	**Target Sequence**
siMADP1	5'-CAAUGACUUGUACCGGAUA-3'
siEGFP	5'-GCAACGUGACCCUGAAGUUC-3'
si1	5'-GCAAUAAACAACAAACAGU-3'
si2	5'-CCAAGUAAGAGCACAGUGU-3'
si3	5'-GAGUUCAUCCGAAGGCGAA-3'
si4	5'-AAAUAUGCUCGGAGAACGU-3'

2.11.4 Transient gene silencing with Lipofectamine® RNAiMAX

Transfections were performed on Vero and H1299 cells grown to a confluency of 40% in 6-well plates. A 5 μM stock of the siRNAs was diluted with DEPC-treated water from the 50 μM stock solutions from the supplier. For each well, the siRNA was mixed with serum-free medium to a final volume of 250 μl and the 5 μl of transfection reagent, Lipofectamine® RNAiMAX purchased from Invitrogen (Carlsbad, CA, USA), was mixed with serum-free medium to a final volume of 250 μl in a different tube. The two tubes were them combined, mixed by vortexing and left to stand at room temperature for 15 minutes. Meanwhile, the cells were washed twice with serum-free medium and 2.5 ml of fresh serum-free medium was added to the cells. The transfection mixture was then added to the serum-free medium and incubated for 6 hours at 37°C, 5% CO_2. The medium was then replaced with fresh culture medium (with serum). The second transfection was performed 24 hours after the first transfection with the same procedure.

2.11.5 Stable gene silencing of MADP1

H1299 cells grown to a confluency of 60% on a 100 mm culture dish and 2 μg of the plasmid pSilencer-shMadp1 was delivered into the cells using Effectene® Transfection Reagent using serum-free medium. The cells were incubated with the transfection mixture for 24 hours and the medium was replaced with selection medium (RPMI with 500 μg/ml G418). The dosage of G418 was pre-determined to be lethal to 100% of non-transfected H1299 cells. The cells were cultured under the same

selection condition until most cells were killed and small colonies (diameter 1 to 2 mm) appeared.

The medium was removed and the colonies incubated with trypsin-soaked 3mm cloning discs purchased from Scienceware® Sigma-Aldrich (St. Louis, MO, USA) for 5 minutes. The cloning discs were then transferred into 24-plates containing 1 ml of selection medium in each well. The colonies that expanded were transferred into larger culture vessels and the expression of the hairpin siRNA was indirectly determined by the mRNA level of MADP1 (*madp1*) of each colony via RT-PCR. The colony with the highest percentage reduction of *madp1* (compared to non-transfected H1299 cells) was chosen to be used in subsequent experiments as the cell line H1299-shMADP1.

To setup a negative-knockdown control cell line, the plasmid pSilencer-2.1 U6-neo negative control (expressed hairpin siRNA that does not target any human gene sequence) was also used to create the cell line H1299-shNC screened alongside H1299-MADP1.

2.12 Gene over-expression in *E. coli* by induction

Inserts cloned into pDEST15, pGEX-5x-1 or pET-16b bacteria expression vectors were transformed into BL-21 *E. coli*. For each plasmid, one colony was picked and cultured with 3ml of LB broth containing the necessary antibiotic at 37°C, shaking at 200 rpm for 16 hours. The overnight culture was used to inoculate the desired volume of LB (with antibiotic) at a dilution of 1:100 and incubated at 37°C, shaking at 200 rpm until OD_{595} fell between 0.5 and 0.6. Isopropyl-1-thio-β-D-galactopyranoside

(IPTG) was added to the culture and incubation continued for another 3 to 4 hours. The bacteria was sedimented by centrifugation at 5000 rpm, 4°C for 5 minutes in 50 ml polypropylene centrifuge tubes and resuspended with PBS (containing 100 μg/ml of lysozyme). The suspension was frozen with dry-ice in ethanol for 20 seconds and thawed in a 37°C water-bath for 1 minute for 10 cycles. Cell debris (pellet) was sedimented at 13200 rpm, 4°C for 1 hour and the lysate (supernatant) was transferred to a new tube.

2.13 Immunofluorescence Detection

Cells were fixed with 4% paraformaldehyde for 15 minutes at room temperature and permeabilized with 0.2% Triton-X 100 for 10 minutes. Treated cells were blocked in 1X PBS with 10% goat serum, stained with primary antibodies mouse monoclonal anti-BrdU and rabbit polyclonal anti-Flag then probed with Alexa Fluor® 488 anti-rabbit and Alexa Fluor® 594 anti-mouse antibodies. The stained cells were embedded with fluorescence mounting medium and covered with a glass coverslip. Washings were performed with PBS before the addition of secondary antibodies and the application of mounting medium. Images were captured with Olympus Fluoview FV1000 Upright Confocal microscope using a sequential laser scanning protocol to minimize bleed-through.

2.14 Cell Fractionation

The extraction of nuclear proteins from mammalian cells was performed using reagents from the CelLytic^{TM} NuCLEAR^{TM} Extraction Kit purchased from Sigma-Aldrich (St. Louis, MO, USA). Cells were rinsed with PBS twice, scraped from the culture vessel in fresh PBS into a 1.5 ml microcentrifuge tube. The tube was centrifuged for 5 minutes at 450 x g, 4°C, the supernatant was removed and the packed cell volume (PCV) was estimated. For every 100 µl PCV, 500 µl of lysis buffer was added. Both H1299 and Vero cells were lysed with 1X Lysis Buffer, isotonic (10 mM Tris pH 7.5, 2 mM $MgCl_2$, 3 mM $CaCl_2$, 0.5 M sucrose, 0.1 mM DTT) with 1X Protease Inhibitor Cocktail. The cell pellet was resuspended in the lysis buffer and incubated on ice for 15 minutes until the cells swell (5 µl of the lysate was used to check for swelling under the microscope).

10% IGEPAL CA-630 was added to the swollen cells to a final concentration of 0.6% and the mixture was vortexed vigorously. The nuclear fraction was immediately sedimented at 10000 x g for 30 seconds at 4°C. The supernatant (cytoplasmic fraction) was transferred to a new tube and the pellet (nuclear fraction) was washed twice with 200 µl PBS and sedimented at 10000 x g for 30 seconds at 4°C. The pellet was boiled with 2X SDS loading dye (same volume as lysis buffer used) for 10 minutes to lyse the nuclei.

For analysis of the proteins in the respective fractions, 10% volume of the cytoplasmic fraction boiled for 5 minutes in an appropriate volume of 6X SDS loading dye (with DTT) and 10% volume of the nuclear fraction were resolved by SDS-PAGE and western blot with the required antibodies was performed.

2.15 Luciferase Assay

Firefly luciferase activity was determined with the Luciferase® Assay System purchased from Promega (Fitchburg, WI, USA). Cells grown in 6-well plates were lysed with either 200 µl of Lysis Buffer or 400 µl of Passive Lysis Buffer (supplied with kit). For each sample, 5 µl of lysate was added to 50 µl of Luciferase Assay Substrate (supplied with kit) and measured immediately using TD-20/20 single-tube luminometer from Turner Biosystems (Sunnyvale, CA, USA). The averaged reading of three independent measurements of each sample was recorded.

Dual-Luciferase® Reporter Assay System was used when both firefly and renilla luciferase activities were to be determined in a single sample. For each sample, 5 µl of lysate was added to 50 µl of Luciferase Assay Substrate and measured immediately using the luminometer to determine its firefly luciferase activity. 50 µl of Stop & Glo® Substrate (supplied with kit) was added into the same tube and measured immediately to determine its renilla luciferase activity. The averaged reading of three independent measurements of both luciferase activities was recorded.

2.16 Detection of IBV and Host mRNAs by RT-PCR

Total RNAs were prepared from the infected cells at their specified time points using Trizol Reagent (Invitrogen) and RT-PCRs were performed with the primers listed in Table 2.11. Reverse transcription (RT) was performed with Expand Reverse Transcriptase using the sense primer IBV leader for the detection of negative-stranded sgRNA and the antisense primer IBV24803-R for the detection of positive-stranded sgRNA. Both primers were then used for PCR. If transcription of sgRNAs did occur,

a 415-bp PCR product corresponding to the 5'-terminal region of mRNA 5 and a 648-bp fragment corresponding to the 5'-terminal region of mRNA 4 would be expected. Similarly, RT was carried out with the sense primer IBV14931-F for the detection of negative-stranded gRNA. Sense primer IBV14931-F and the antisense primer IBV15600-R were used for PCR. If replication of viral RNA occurred, a 670-bp PCR fragment would be expected.

Table 2.11: Primers used for amplifying IBV mRNAs, MADP1 mRNA and GAPDH mRNA.

Primer Name	**Primer Sequence**
IBV leader	5'-CTATTACACTAGCCTTGCGCT-3'
IBV24803-R	5'-CTCTGGATCCAATAACCTAC-3'
IBV14931-F	5'-GCTTATCCACTAGTACATC-3'
IBV15600-R	5'-CTTCTCGCACTTCTGCACTAGCA-3'
oligo-dT	5'-TTTTTTTTTTTTTTTTT-3'
5'Madp1_Sma1	5'-ATACCCGGGATGAGTGGTGGATTGGC-3'
3'Madp1_Sma1	5'-ATACCCGGGTTAATCACTAAGTTCTTCTT-3'
GAPDH-F	5'-GACAACTTTGGTATCGTGGAA-3'
GAPDH-R	5'-CCAGGAAATGAGCTTGACA-3'

For the detection of host mRNAs, oligo-dT primer was used for RT. Primers used to amplify MADP1 mRNA were 5'Madp1_Sma1 and 3'Madp1_Sma1. Glyceraldehyde 3-phosphate dehydrogenase (GAPDH) mRNA which was used as a housekeeping gene control was amplified with the primers GAPDH-F and GAPDH-R.

2.17 SDS Polyacrylamide Gel Electrophoresis (SDS-PAGE)

2.17.1 Protein extraction from TRIzol® lysed cells

The interphase and organic phase from the phase separation step (after removal of the aqueous layer for RNA extraction) were used to the preparation of denatured protein samples. For every 1 ml of TRIzol® treated cell lysate, 300 µl of ethanol was added into and mixed by gentle inversion with the interphase and organic phase. The sample was incubated at room temperature for 3 minutes and the DNA was pelleted by centrifugation at 4500 rpm, 4°C for 5 minutes. 400 µl of the supernatant was transferred to a new 2.0 ml tube containing 1.2 ml of acetone and mixed by inversion. The sample was incubated at room temperature for 10 minutes for protein precipitation. The precipitate was sedimented at 11000 rpm, 4°C for 10 minutes. The pellet was dispersed by mechanical stirring using a pipette in 0.5 ml of guanidine hydrochloride/ethanol/glycerol solution (0.3 M guanidine hydrochloride, 95% ethanol, 2.5% glycerol). An additional 0.5 of the same solution was added after the pellet was completely dispersed and the sample was left to stand at room temperature for 10 minutes before it was sedimented at 9000 rpm, 4°C for 5 minutes. This was repeated twice with vortexing to disperse the pellet instead then washed with ethanol/glycerol solution (97.5% ethanol, 2.5% glycerol). The pellet was air-dried and heated in 2X SDS loading dye at 100°C for 5 minutes before it was loaded onto the gel.

2.17.2 Sample preparation

Pellets were resuspended in 2X SDS loading dye and liquid samples were mixed with 6X SDS loading dye. Both types of samples were heated at 100°C for 10 minutes then cooled on ice before loading onto the gel.

2.17.3 Electrophoresis

Polyacrylamide gels were prepared with 30% acrylamide/bis solution (29:1) in 375 mM Tris and 0.1% SDS. The electrophoresis was performed using the Bio-Rad Mini-PROTEAN®II System from Bio-Rad (Hercules, CA, USA), with 1X Tris-Glycine running buffer (25 mM Tris, 250 mM glycine, 0.1% SDS) at a current of 20 milliampere (mA) per gel (1 mm thickness). Resolved proteins were visualized by coomassie blue staining or transferred onto a membrane for immune-detection.

2.17.4 Coomassie blue staining

Gels were immersed in Staining Solution (0.25% (w/v) Coomassie Brilliant Blue R-250, 20% methanol, 10% glacial acetic acid) for 30 minutes until they were stained completely. The stained gel was rinsed with de-ionized water and immersed in Destaining Solution (20% methanol, 10% glacial acetic acid). Destaining Solution was changed when it turned blue until the bands become visible. The destained gels were rinsed and stored in de-ionized water until it was ready to be dried.

2.18 Western Blot

2.18.1 Wet transfer

Gels were equilibrated in 1X Wet Transfer buffer (48 mM Tris, 39 mM glycine, 20% methanol) before they were transferred onto either nitrocellulose or PVDF membranes. Transfer was performed with a Mini Trans-Blot Cell purchased from Bio-Rad (Hercules, CA, USA) in 1X Wet Transfer buffer at 4°C and 110 volts (V) for 90 to 120 minutes.

2.18.2 Semi-dry transfer

Gels were equilibrated in 1X Semi-Dry Transfer buffer (24 mM Tris, 192 mM glycine, 20% methanol) before they were transferred onto nitrocellulose membranes. Transfer was performed with a Trans-Blot SD Semi-Dry Transfer Cell from Bio-Rad (Hercules, CA, USA) in 1X Semi-Dry Transfer buffer at 20 V for 40 minutes.

2.18.3 Antibody binding and detection

Membrane was blocked in Blocking Solution (10% (w/v) non-fat milk, 1X PBS) for 1 hour at room temperature then incubated with the primary antibody at the appropriate concentration in Blocking Solution for 1 hour with constant shaking. The membrane was washed with PBS-T (1X PBS, 0.1% Tween®-20) three times then incubated with the required secondary antibody at a 1:2000 X dilution factor in Blocking Solution for 1 hour with constant shaking. The membrane was washed again with PBS-T three

times and Western Lightning®-ECL from Perkin Elmer (Waltham, MA, USA) was applied onto the membrane.

2.19 Northern Blot

2.19.1 Probe preparation

DIG-labeled DNA probes used for the detection of specific nucleic acids were generated by PCR using PCR DIG labeling mix (2 mM dATP, 2 mM dCTP, 2 mM dGTP, 1.9 mM dTTP, 0.1 mM DIG-11-dUTP).

2.19.2 Denaturing agarose gel electrophoresis

Denaturing agarose gel was prepared with UltraPure™ agarose in 1X MOPS (20 mM MOPS, 5 mM NaOAc, 1 mM EDTA) with 0.7 M formaldehyde. RNA loading buffer (50% formamide (v/v), 17.5% formaldehyde (v/v), 11% glycerol (v/v), 1X MOPS, 0.025% bromophenol blue and 0.15 mg/ml ethidium bromide) was mixed with 20 μg of total RNA or 100 ng of DIG-labeled RNA molecular weight marker at a volume ratio of 1:4.5. The mixture was heated at 65°C for 15 minutes and cooled on ice before it was loaded. A voltage of 6 V/cm gel length was used to resolve the loaded RNA samples in 1X MOPS running buffer.

2.19.3 Blot transfer

The resolved RNA was transferred onto Hybond N+ nylon membrane from Amersham (Amersham, United Kingdom) with a capillary transfer setup using 20X SSC (3 M NaCl, 0.3 M sodium citrate, pH 7.0) as the transfer buffer for 24 hours. The transferred RNA was cross-linked to the membrane using a UV cross-linker from Stratagene (La Jolla, CA, USA).

2.19.4 Probe hybridization

The membrane was pre-hybridized in DIG Easy Hyb (without probe) for one hour at 50°C then hybridized with the probe (denatured at 100°C for 5 minutes then cooled on ice) for 16 hours at 50°C in a hybridization oven. The membrane was washed twice with 2X SSC, 0.1% SDS at room temperature, then twice with 0.2X SSC, 0.1% SDS at 68°C, followed by a single wash with Washing buffer (0.15 M NaCl, 0.1 M maleic acid, pH 7.5, 0.3% Tween-20) at room temperature.

2.19.5 Detection

For detection of DIG, the membrane was blocked in Blocking buffer (1% w/v Blocking Reagent, 0.15 M NaCl, 0.1 M maleic acid, pH 7.5) for 1 hour with shaking then incubated with anti-DIG-AP (1:10000X in Blocking buffer) for 30 minutes. Following which, the membrane was washed twice with Washing buffer and equilibrated in Detection buffer for 5 minutes. 1ml of CDP-Star substrate solution (1:100X in Detection buffer) was prepared and applied evenly onto the membrane for chemiluminescent detection.

2.20 North-Western Blot

2.20.1 Probe and blot preparation

Digoxigenin (DIG)-labeled RNA probes for both coronaviruses were produced by *in vitro* transcription. N-terminal Flag-epitope tagged MADP1 was over-expressed in Vaccinia-T7 infected H1299 cells on a 60 mm TC-treated culture dish (Corning, USA). The cells were lysed with 150 µl of Lysis Buffer (140 mM NaCl, 10 mM Tris (pH 8.0), 1% Nonidet P-40) containing protease inhibitors. 40 µl of total cell lysate was mixed with 8 µl of 6X SDS loading dye and incubated 100°C for 5 minutes and cooled at room temperature before it was loaded onto a 15% SDS-PAGE gel. The resolved proteins were transferred onto a Hybond C-Extra nitrocellulose membrane purchased from Amersham (Amersham, Great Britain) using a semi-dry transfer setup.

2.20.2 Probe binding

Fresh probe buffer (10 mM Tris-HCl, 50 mM NaCl, 1mM EDTA, 1x Denhardt's Reagent) was prepared from stock buffers 1 M Tris (pH 7.5), 5 M NaCl, 100 mM EDTA pH (8.0) and 50X Denhardt's Reagent (1% polyvinylpyrrolidone, 1% Ficoll 400, 1% BSA) in nuclease-free water. The membrane was equilibrated in probe buffer at room temperature for 10 minutes with shaking and blocked in 10 ml of fresh probe buffer containing 250 µg yeast tRNA (Ambion, USA) for 1 hour at room temperature with shaking. The blocking buffer was then discarded and membrane was incubated with fresh probe buffer containing 10 ug of DIG-labeled probe for 1 hour at room

temperature with shaking. The membrane was then washed 3 times, for 10 minutes each with shaking in probe buffer and procedures for DIG detection were performed (Section 2.10.5).

2.21 Biotin Pull-down Assay

2.21.1 Probe and lysate preparation

Biotin-labeled RNAs for this assay were produced by *in vitro* transcription. All proteins used in this assay were whole cell lysates of Vaccinia-T7 recombinant virus infected H1299 cells over-expressing N-terminal Flag-epitope tagged proteins. Enhanced green fluorescent protein (EGFP) over-expressed with the same method was used as a negative control.

2.21.2 Binding and Immunoprecipitation

In a 200 µl binding reaction, 0.1 µM of biotin-labeled RNA was mixed with 150 µl of total cell lysate in the presence of 10 mM DTT, 20 µg of yeast tRNA, 200 U of Protector RNase inhibitor and nuclease-free water in a 1.5 ml eppendorf tube. The tube was incubated at room temperature with gentle rotation for 30 minutes. 40 µl of streptavidin agarose beads (Sigma-Aldrich, USA) was added directly into the tube and the mixture was incubated at room temperature with gentle rotation for 30 minutes. The tube was centrifuged at 1000 rpm for 5 minutes with a microcentrifuge and placed upright on a tube rack for 1 minute to pack the beads before the supernatant was removed carefully using a micro-pipette. 500 µl of RNase P (RP) buffer (50mM

KCl, 1mM $MgCl_2$, 10mM Hepes) was used to wash the beads trice with gentle inversion and the beads were collected by centrifugation. The buffer was removed thoroughly by gently aspiration with a gel-loading pipette after the last wash. 25 µl of 2X SDS loading dye with DTT was mixed with the beads and the mixture incubated at 100°C for 10 minutes, cooled at room temperature before loading onto a PAGE gel of an appropriate concentration.

Chapter 3 Characterization of interaction between host protein MADP1 and coronavirus 5'-UTR

The ability of the coronavirus in carrying out replication and transcription of its genome is crucial to the establishment of an infection and its successful propagation. This is an important part of the coronavirus life cycle which is made possible by the virus-encoded replicase gene. Coronavirus RNA synthesis takes place in the host cytosol, on DMVs which are modified host membrane structures, possibly originating from the ER or, specifically EDEMosomes. Regulatory sequences are scattered throughout the coronavirus genome in the form of TRS-Bs at the 5'-end of each designated mRNA, the 5'-UTR (including TRS-L) and the 3'-UTR. As such, the role of RNA-binding proteins in viral RNA synthesis is of particular significance as a bridge between these regulatory signals on the viral RNAs and replicase proteins which possess the enzymatic activities required for synthesis.

The critical enzymatic activities associated with the various steps involved in the synthesis of positive-sense mRNAs from the positive-sense genome have been assigned to the various replicase gene products. However, set in a myriad of host proteins, host protein involvement in viral RNA synthesis is almost inevitable and could not be dismissed. This has been supported by several reports of host proteins participating in coronavirus RNA synthesis, in particular, the involvement of hnRNP A1 in MHV RNA synthesis through its interactions with multiple transcription regulatory sequences. Although several other host proteins were subsequently reported to be required for efficient coronavirus RNA synthesis, information pertaining to the involvement of host proteins in coronavirus RNA synthesis is still limited and not fully understood. Furthermore, prior studies were mostly conducted in alpha- and betacoronaviruses TGEV and MHV, no such information was available for

SARS-CoV, a betacoronavirus of certain medical significance, and the gammacoronavirus IBV, a pathogen of great veterinary significance.

Therefore, it was of great importance to study how host proteins may be involved in viral RNA synthesis in these two coronaviruses. However, due to the lack of a facility suitable for handling SARS-CoV, a strategy was devised to first screen for human proteins which could interact with regulatory signals of SARS-CoV (strain Sin2774, accession AY283798), confirm the interaction using biochemical methods in both SARS-CoV and IBV (strain Beaudette isolate IBV-p65, accession DQ001339), then validating the significance of interactions in IBV infections. As most of the regulatory signals were clustered on the 5'- and 3'-UTRs, it was decidedly the most appropriate to look for proteins that could participate in coronavirus replication/transcription by screening for human proteins that could interact with the 5'- and 3'-UTRs. Also, during replication and transcription, coronaviruses generate both positive and negative sense RNAs, so each orientation of the UTRs could interact with different proteins.

Hence, a screen for human proteins which could interact with both sense and antisense SARS-CoV 5'- and 3'-UTRs was finalized as the approach to study the involvement of host proteins in coronavirus RNA synthesis.

3.1 Human MADP1 Interacts with SARS-CoV 5'-UTR

3.1.1 Yeast three-hybrid screen for human proteins that could potentially interact with SARS-CoV transcription regulatory regions.

Using the yeast three-hybrid system that was obtained from Marvin Wickens of the University of Wisconsin, the corresponding author of the original publication by SenGupta et. al. (332), the human cDNA library was screened for RNA-binding proteins that could interact with both sense and antisense SARS-CoV 5'-and 3'-UTR. However, a clone for the sense 3'-UTR could not be obtained after screening 50 colonies, it was dropped off the screen and only the antisense 3'-UTR, as well as the 5'-UTR in both orientations were screened instead.

3.1.2 Candidates identified from yeast three-hybrid screen using 5'-UTR (+) as bait

Three groups of positive candidates of initial screen (SD/-his) were classified by second tier screen into three groups: Group I (strong positives), Group II (weak positives) and Group III (false positives). Colonies classified under Group I, A81, A83, A127 A250, B169 and B225 were subjected to colony PCR (Figure 3.1) with an annealing temperature of 58°C. The PCR fragments from clones A81 and B225 were gel purified and sequenced.

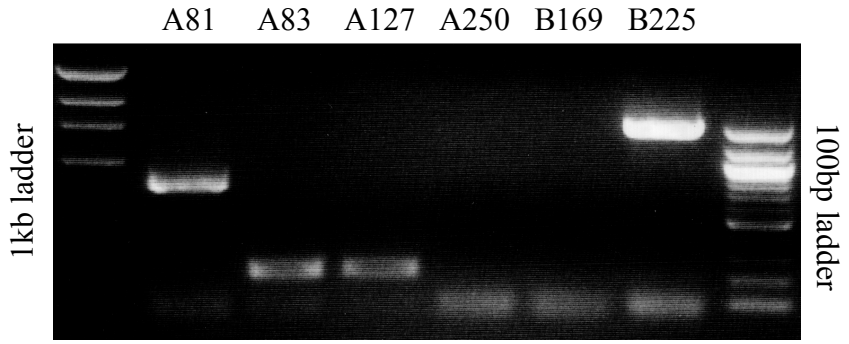

Figure 3.1: Colony PCR of colonies isolated from three-hybrid screen with SARS-CoV 5'-UTR (+). PCR products were resolved on a 1% agarose gel, stained by ethidium bromide. Clones A81 and B225 were gel-purified and sent for sequencing. A representative result of two experiments was shown.

The identity of the cDNA insert fragment was subsequently determined by performing a BLAST search on NCBI. Clone A81 was found to contain the N-terminal 408 nt of the zinc finger CCHC-type and RNA binding motif 1 protein (ZCRB1), also known as morphine (acute) dependence-related protein 1 (MADP1) (accession NM_033114). Clone B225 was found to have the cDNA fragment inserted in the wrong orientation on the library vector and was therefore invalid. Clones A83 and A127 were not sequenced as the PCR fragments were decided to be too short for consideration. As the primers used for the colony PCR bound roughly 200 to 300 nt apart on the vector (without insert), it was highly likely the two fragments were derived from the vector sequence. This was supported by the observation that both fragments were of an almost equal size.

The colony PCR was repeated at a different annealing temperature (61°C) (Figure 3.3) and an additional clone, B169, was gel purified and sequenced. The cDNA fragment in clone B169 was also found to be inserted in the reversed orientation and was invalid. No PCR fragment could be amplified from clone A250 so the clone was also considered as a false positive.

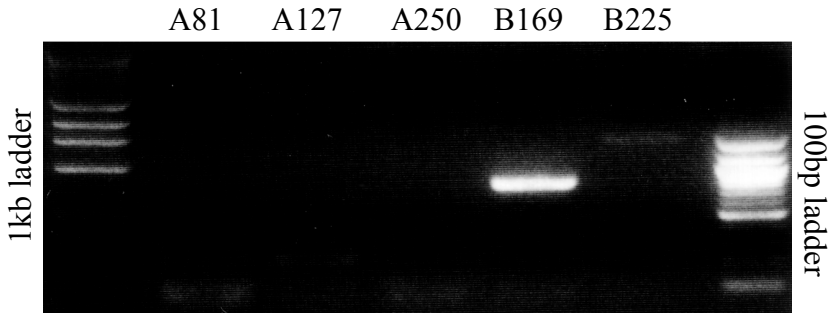

Figure 3.3: Repeat of colony PCR using a different annealing temperature with clones A83, A127, A250, B169, B225, isolated from three-hybrid screen with SARS-CoV 5'-UTR (+). PCR products were resolved on a 1% agarose gel, stained by ethidium bromide. Clone B169 produced a strong band and was subsequently gel purified then sent for sequencing. A representative result of two experiments was shown.

3.1.3 Candidates identified from yeast three-hybrid screen using 5'-UTR (-) as bait

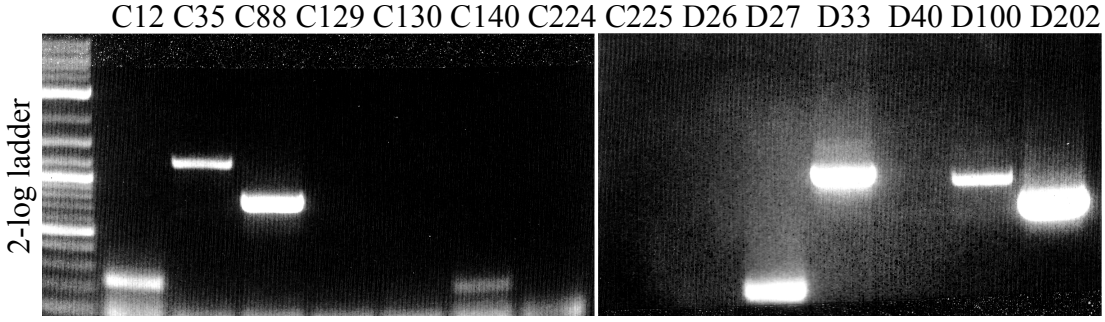

Figure 3.2: Colony PCR of colonies isolated from three-hybrid screen using SARS-CoV 5'-UTR (-) and 3'-UTR (-). PCR products were resolved on 1% agarose gel stained with ethidium bromide. Clones C35, C88, D27, D33, D100 and D202 were gel-purified and sent for sequencing. A representative result of two experiments was shown.

Group I (strong positives) colonies isolated from the screen using SARS-CoV 5'-UTR (-) as the bait were C12, C35, C88, C129, C130, C140, C224 and C225. The colonies were subjected to colony PCR at 58°C (Figure 3.2) and the PCR fragments from clones C35 and C88 were gel-purified and sent for sequencing. The cDNA fragment for clone C35 was found to be inserted with a cDNA fragment in the reverse orientation and was considered a false positive. The PCR fragment amplified from

Clone C88 was found to match nt 466 to 808 of hematopoietic cell-specific Lyn substrate 1 (HCLS1)-associated protein X-1 (HAX1) variant 2 mRNA (accession NM_001018837), within the coding sequence of the protein HAX1 isoform b.

3.1.4 Candidates identified from yeast three-hybrid screen using 3'-UTR (-) as bait.

Colonies classified under Group I (strong positives) isolated from the screen using SARS-CoV 3'-UTR (-) as the bait were D26, D27, D33, D40, D100 and D202. Colony PCR was performed for the 6 clones (Figure 3.2) and the PCR products from clones D27, D33, D100 and D202 were gel-purified and sequenced. Both clones D27 and D33 were found to contain similarity to only 33 nt of the X chromosome genome contig (accession NM_001842393) without similarity to any annotated protein coding sequence. For clone D100, it was found that the cDNA fragment was inserted in the reverse orientation so the clone was invalid. For clone D202 however, the sequence of the amplified PCR product matched that of ribosomal protein L27a (RPL27A) (accession NM_000990) with an identity of 98% spanning across 317 nt.

3.1.5 Consolidation of candidates from the screens

In total, only one protein was determined to be a valid candidate for interaction with each of the screened UTRs, that being MADP1, HAX1 (isoform b) and RPL27A for sense 5'-UTR, antisense 5'-UTR and antisense 3'-UTR respectively. HAX1 is a mitochondrial protein which functions as an anti-apoptotic protein (333-335) in the cell. The protein has been reported to interact with classical swine fever virus N-terminal protease (336), however, the absence of prior reports of an associated RNA-

binding activity and predicted RNA-binding domains deemed it less likely to be interacting with SARS-CoV 5'-UTR (-) specifically.

RPL27A being a component of the eukaryotic 60S ribosome, a ribonucleoprotein complex, is likely to possess RNA-binding activity. Although it was interesting to find RPL27A interacting with SARS-CoV 3'-UTR (-), which would not be required for viral protein translation, the ribosomal protein did not prove to be an attractive candidate as functional analysis could prove to be problematic. This problem would arise due to the fact that the virus relies heavily on the host translational machinery, which includes the host ribosomes, for the translation of viral proteins necessary for it to propagate.

MADP1 is a nuclear protein reported to be a member of the 18S U11/12 small nuclear ribonucleoprotein (snRNP), part of the minor spliceosome (337), and has been linked to morphine dependence, heat shock and hepatocarcinoma (338). It was also predicted to contain two conserved nucleic acid binding domains, the RNA recognition motif (RRM) and the provisional universal minicircle sequence binding protein domain, which is a zinc finger, CCHC-type. Although splicing had been ruled out as the mechanism by which discontinuous transcription could be achieved in coronaviruses, the RNA-binding domains on MADP1 which would likely interact with small nuclear RNAs (snRNAs) in the spliceosome complex, could also play a role in other processes. Hence, it was decided that the interaction between MADP1 and SARS-CoV 5'-UTR (+) would be studied in-depth.

3.2 MADP1 Interacts with IBV 5'-UTR

In order to validate the interaction between human MADP1 and SARS-CoV 5'-UTR as well as to verify if it could interact with the IBV counterpart as well, the interactions were assessed with a different method. The first method chosen for this purpose was North-Western Blotting using DIG-labeled RNA to probe for bacteria expressed human MADP1 immobilized on a membrane.

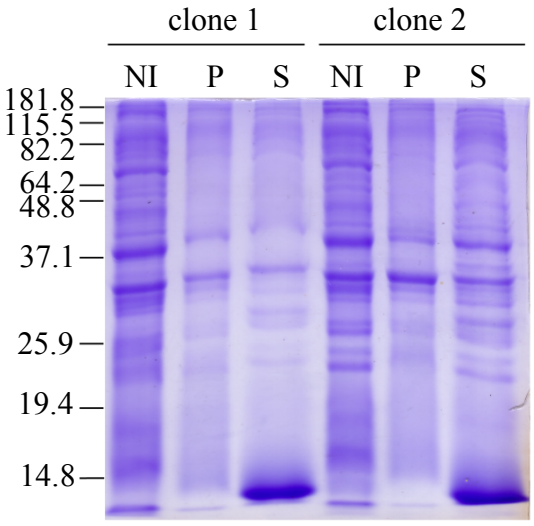

Figure 3.4: No expression of HIS-MADP1 was detected after induction at 1 mM IPTG for 3 hours at 37°C. BL-21 E. coli was transformed with 2 clones of plasmid pET-MADP1 and induced. Samples were resolved by a 12% SDS-PAGE gel. Non-induced samples (NI) were prepared from bacteria sedimented from 1 ml of each culture just before induction. Pellet (P) and supernatant (S) fractions were prepared from freeze/thaw lysed bacteria after induction. Unit for molecular weight reference is kilodaltons (kDa). A representative result of three independent experiments was shown.

3.2.1 Bacteria expression of MADP1 N-terminally tagged with HIS(X6) or GST

The bacteria expression system was chosen for its potential benefits of high protein yield and low cost. Also, a recombinant protein expressed with a small tag like HIS(X6) would not incur the additional step of tag removal as MADP1 was not a large protein, with an estimated molecular mass of 31 kilodaltons (kDa). Hence,

MADP1 was cloned into the vector pET-16b to express N-terminally HIS-tagged MADP1 (HIS-MADP1). The expression of HIS-MADP1 was induced by 1 mM IPTG at 37°C and its expression level was assessed coomassie blue staining as shown in Figure 3.4.

The expected band of HIS-MADP1 was not detected. However, it was noticed in the supernatant fraction of the lysed bacteria, that a strong band of an undetermined size, smaller than 14.8 kDa was present in both clones tested. This implied that the recombinant protein could have been unstable and the induction condition needed to be optimized. Hence, BL-21 transformed with clone 2 of pET-MADP1 was induced at a lowered temperature of 30°C, for a longer duration of 4 hours with either 0.8 mM or 1 mM of IPTG. The samples obtained were resolved and analyzed by western blot using anti-HIS or direct staining with coomassie blue (Figure 3.5).

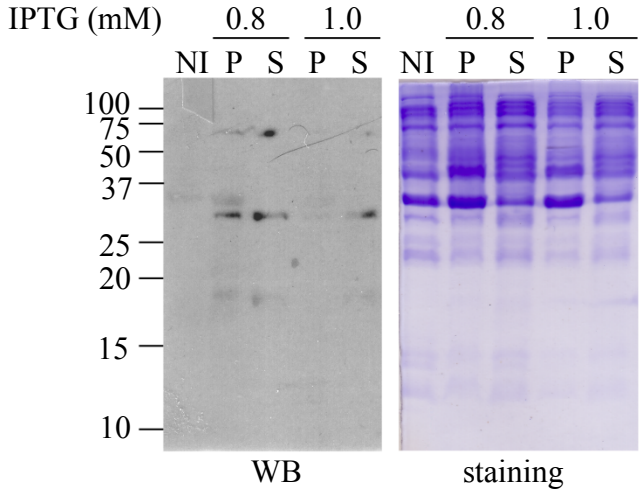

Figure 3.5: Expression of HIS-MADP1 was too low to be detected by coomassie blue staining. Optimization of HIS-MADP1 expression. E. coli transformed with clone 2 of pET-MADP1 plasmid was induced at 30°C for 4 hours with either 0.8 or 1.0 mM of IPTG. Samples were resolved by a 15% SDS-PAGE gel. WB: western blot was performed with anti-HIS antibody and total protein was visualized by coomassie blue staining. A representative result of two independent experiments was shown.

A dense band was observed in the stained gel with a molecular mass close to HIS-MADP1, but it did not belong to the protein as it was present in the non-induced sample as well. In addition, detection of the recombinant protein, HIS-MADP1, by anti-HIS antibody indicated that its expression was impossible to be visualized by coomassie blue staining. As the amount of protein was considered low even for western blot detection, it was decided that the fusion tag be changed to GST even though it could imply an additional tag-removal step if the protein could be successfully expressed. Hence, MADP1 was first cloned into Gateway® pDEST15 vector to express N-terminally GST-tagged MADP1 (GST-MADP1) of an estimated relative molecular mass of 57 kDa. However the expression level of the recombinant protein from the chosen clone (Figure 3.6, panel A) after 3 hours of induction with 1 mM IPTG at 37°C, appeared to be too low for detection by coomassie blue staining.

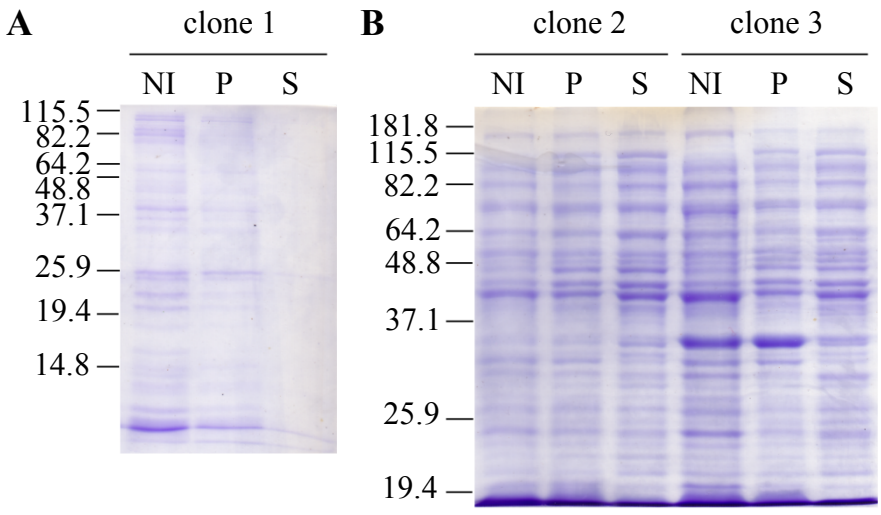

Figure 3.6: Expression of GST-MADP1 was too low for detection by coomassie blue staining. GST-MADP1 recombinant protein was expressed from from BL-21 *E. coli* transformed with three different clones of expression plasmid pDEST15-MADP1 induced by 1 mM IPTG for 3 hours at 37°C. (A) Samples from clone 1 resolved by a 12% SDS-PAGE gel. (B) Samples from clones 2 and 3 resolved by a 10% SDS-PAGE gel. A representative result of two independent experiments was shown.

Two more clones (clones 2 and 3) were assessed for their recombinant protein expression levels under the same induction condition, (Figure 3.6, panel B) but the result was still unsatisfactory although the total bacteria protein expression profiles differed from clone 1. The condition for induction was changed to 0.8 mM of IPTG for 4 hours at 37°C and the supernatant fraction (S) was concentrated by resuspending the sedimented bacteria in half the volume of PBS (with 100 µg/ml lysozyme). However, as shown in Figure 3.7, a clear induction of the recombinant protein expression was not detected as a band of the expected size, 57 kDa, remained conspicuously absent in all three clones tested.

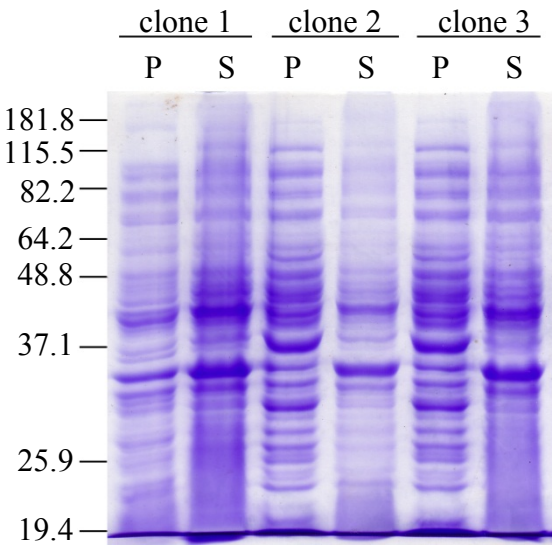

Figure 3.7: GST-MADP1 expression still could not be detected after reducing the concentration of IPTG to 0.8 mM. GST-MADP1 recombinant protein was expressed from BL-21 *E. coli* transformed with three different clones of expression plasmid pDEST15-MADP1 induced by 0.8 mM IPTG for 4 hours at 37°C. Samples were resolved by a 10% SDS-PAGE gel. A representative result of two independent experiments was shown.

Due to the lack of recombinant protein expression, the expression of GST with pDEST15 vector was assessed to rule out the possibility that the vector sequence was erroneous as this was the first time the vector was used in the laboratory. It was found that the expression of the GST tag, with an estimated relative molecular mass of 26 kDa, from pDEST15 plasmid following an induction with 1 mM IPTG for 3 hours at 37°C, was detectable in the insoluble fraction after freeze/thaw lysis, by coomassie

blue staining (Figure 3.8) which was much poorer than what could be achieved with the vector pGEX-5x-1, which was normally used in the laboratory for GST-recombinant protein expression in *E. coli*. Hence, MADP1 was cloned into the expression vector pGEX-5x-1.

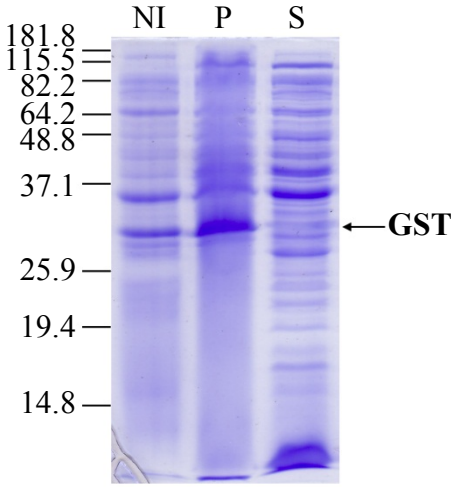

Figure 3.8: Expression of GST was confined to the insoluble fraction. Expression of GST protein from BL-21 *E. coli* transformed with vector pDEST15 induced by 1 mM IPTG for 3 hours at 37°C. Samples were resolved by a 12% SDS-PAGE gel. A representative result of three independent experiments was shown.

Expression of GST from vector pGEX-5x-1 and recombinant GST-MADP1 from two clones of plasmid pGEX-MADP1 following induction with 1 mM of IPTG for 3 hours at 37°C was assessed by SDS-PAGE followed by coomassie blue staining as shown in Figure 3.9. The expression of GST from vector pGEX-5x-1 transformed *E. coli* appeared normal. A band corresponding to the estimated molecular mass of GST-MADP1 was not detected in both clones transformed with the plasmid pGEX-MADP1. Instead, a dense band corresponding to the size of GST was observed to be induced.

This observation implied the possibility that translation of the recombinant protein was pre-maturely terminated just after the GST-tag was translated. This was not likely caused by the presence of a stop codon between the GST and MADP1 nucleotide sequences as reflected by the results from sequencing the plasmids used. Hence, the induction conditions were to be optimized.

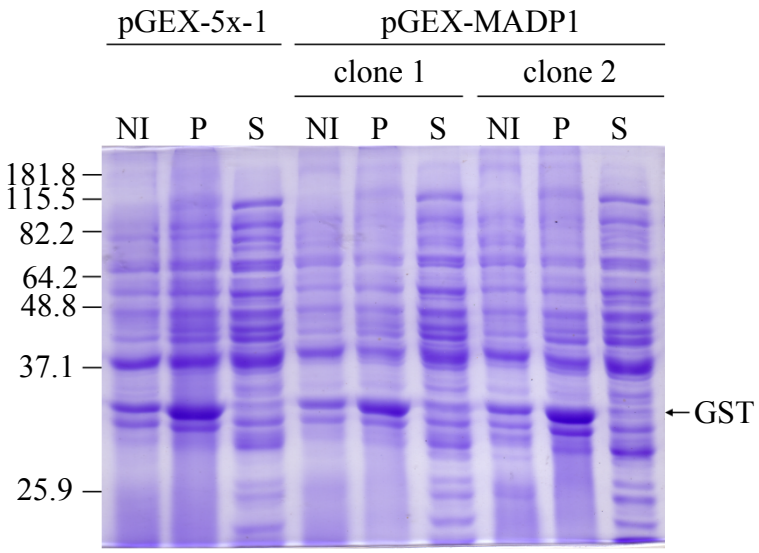

Figure 3.9: Expression profile of GST-MADP1 appeared to be similar to that of GST-tag only. Expression of GST and GST-MADP1 from BL-21 *E. coli* transformed with plasmid pGEX-5x-1 or pGEX-MADP1 induced by 1 mM IPTG for 3 hours at 37°C. Samples were resolved by a 10% SDS-PAGE gel. A representative result of two independent experiments was shown.

The induction duration was maintained at 3 hours, temperature was lowered to 30°C and IPTG concentrations 0.6 mM and 1 mM were used to induce GST-MADP1 expression from *E. coli* transformed with clone 2 of pGEX-MADP1 plasmid (Figure 3.10, panel A). The expression level of the recombinant protein was observed to be higher when 0.6 mM of IPTG was used for induction compared to 1 mM. A second experiment was performed to compare the expression level of GST-MADP1 at 0.6 mM and 0.8 mM IPTG (Figure 3.10, panel B). The result was almost the same, with 0.6 mM induction producing a slightly greater amount of protein. However, in both

experiments, the recombinant protein could only be detected in the insoluble fraction (P) by coomassie blue staining although the soluble fraction (S) was observed by probing with anti-GST, to contain a similar amount of GST-MADP1. However, even if the same amount of protein was present in the soluble fraction, the amount was not enough to undergo purification and tag cleavage.

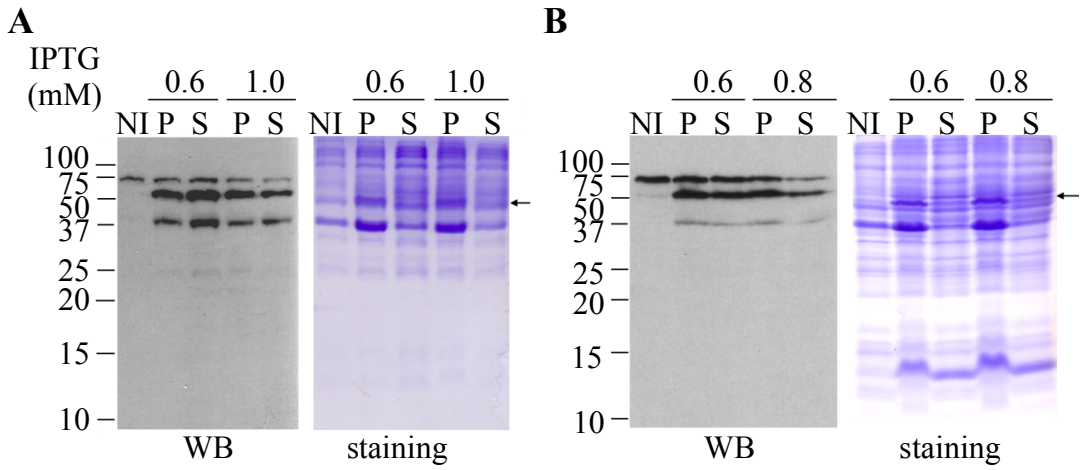

Figure 3.10: Lowering of IPTG concentration to 0.6 and 0.8 mM increased the expression of GST-MADP1 but is still not detectable by coomassie blue staining. Optimization of induction conditions I. *E. coli* transformed with clone 2 of pGEX-MADP1 was induced to express recombinant GST-MADP1 at 30°C for 3 hours with different contrations of IPTG. The samples were resolved on a 12% SDS-PAGE gel and protein expression profile of each induction was analyzed by total protein staining with coomassie brilliant blue or western blot with anti-GST antibody. (A) Expression profile of induction with 0.6 mM and 1.0 mM IPTG. (B) Expression profile of induction with 0.6 mM and 0.8 mM IPTG. WB: western blot, staining: coomassie brilliant blue staining. This experiment was performed once.

In the third and last experiment, the induction temperature was lowered to 27°C, duration increased to 4 hours and 0.6 mM of IPTG was used to induce recombinant protein expression (Figure 3.11). No improvement to the expression level of GST-MADP1 was detected.

In view of the poor result obtained from the expression of either GST-MADP1 or HIS-MADP1 recombinant protein in the bacteria system, it was abandoned in favour of mammalian expression system which was more likely to produce stable recombinant proteins although the yield would be greatly compromised.

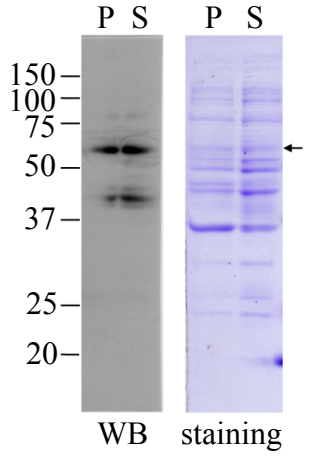

Figure 3.11: Lowering of induction temperature to 27°C did not further increase the expression of GST-MADP1. Optimization of induction conditions II. *E. coli* transformed with clone 2 of pGEX-MADP1 was induced to express recombinant GST-MADP1 at 27°C for 4 hours with 0.6 mM IPTG. Samples were resolved using a 10% SDS-PAGE gel and the protein expression profile was analyzed by total protein staining with coomassie brilliant blue or western blot with anti-GST antibody. This experiment was performed once.

3.2.2 Mammalian Expression Of MADP1 N-Terminally Tagged With FLAG

To select a cell line for expressing the recombinant protein FLAG-MADP1, a trial experiment using three cell lines commonly used in the laboratory was performed. FLAG (from vector pXJ40Flag) or FLAG-MADP1 (from plasmid pXJ40Flag-Madp1) proteins were over-expressed in Vero, H1299 and HuH-7 cells grown in 6-well plates without Vaccinia/T7 virus for 24 hours. The cells were lysed and the lysate was resolved by SDS-PAGE and western blot was performed with anti-FLAG-HRP antibody as shown in Figure 3.12.

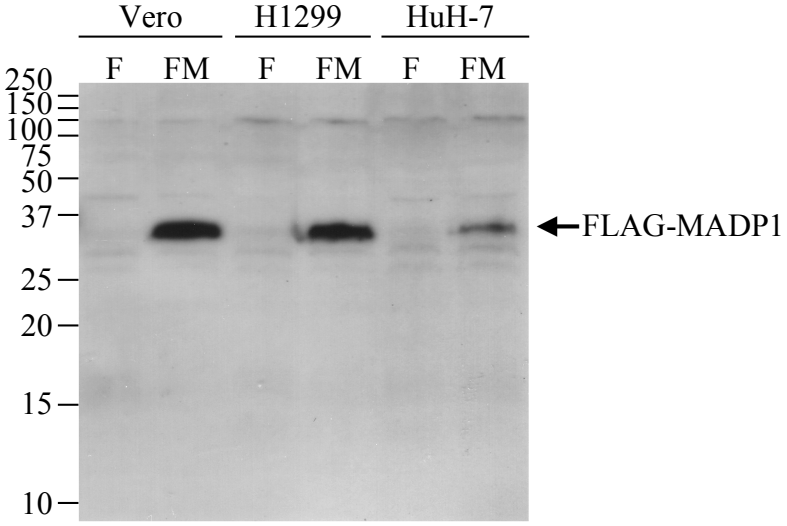

Figure 3.12: FLAG-MADP1 expression was higher in Vero and H1299 cells compared to HuH-7 cells. Trial over-expression of FLAG-MADP1 in Vero, H1299 and HuH-7 cells. Cells grown in 6-well plates were infected with Vaccinia/T7 virus and transfected with 0.4 µg of plasmid DNA pXJ40Flag or pXJ40Flag-Madp1 using Effectene® for 24 hours. Cells were lysed with 200 µl of lysis buffer, 20 µl of each lysate was resolved on a 12% gel and transferred onto a nitrocellulose membrane. Recombinant protein FLAG-MADP1 (indicated by an arrow) was detected after probing with anti-FLAG-HRP. Samples were labeled by the identity of over-expressed protein, F: FLAG tag and FM: FLAG-MADP1. A representative result of two independent experiments was shown.

The expression level of recombinant FLAG-MADP1 protein was found to be comparable in Vero and H1299 cells but much lesser in HuH-7 cells, so the latter was not used for the subsequent experiments. It was surprising that the expression level of FLAG-MADP1 in Vero was as high as H1299 as the former cell line was usually associated with low over-expression levels. Hence, it was decided that H1299 would be used for subsequent experiments as the expression level achieved by Vero could be non-reproducible.

3.2.3 North-western blot of FLAG-MADP1 and the 5'-UTRs of SARS-CoV and IBV.

FLAG tag (negative control) and FLAG-MADP1 were over-expressed in H1299 cells grown in a 6-well plate in the presence of Vaccinia/T7 virus for 24 hours to increase the protein yield. The cells were harvested and lysates were purified using anti-FLAG® M2 affinity gel and eluted with 3X FLAG® peptide. The eluted samples were resolved using SDS-PAGE and north-western blot was performed using either DIG-labeled SARS-CoV or IBV full-length 5'-UTR (+) probes. The expression of the recombinant protein was assessed by western blot with anti-FLAG-HRP as shown in Figure 3.13, panel B contained multiple bands (smaller mass), which were pre-mature termination products common to over-expression system using Vaccinia/T7 virus.

The north-western blot did not show a clear band corresponding to the estimated size of FLAG-MADP1 when probed with both 5'-UTRs, as was obtained from the western blot (top band) of the same samples. Although there appeared to be a dense band in the north-western blot for IBV 5'-UTR (+) (Figure 3.13, panel A) which might correspond to the second band seen on the western blot (Figure 3.13, panel B), the

band appeared in the negative control sample, F, as well. The identities of the multiple bands seen on the north-western blot for both probes (lanes marked FM) were unknown but could be associated with MADP1 (as co-purified bands) as they were not found in the lanes that were loaded with negative control purified lysate (lanes marked F). In conclusion, north-western blot was not sensitive enough to detect the low amounts of FLAG-MADP1 over-expressed even with Vaccinia/T7 virus.

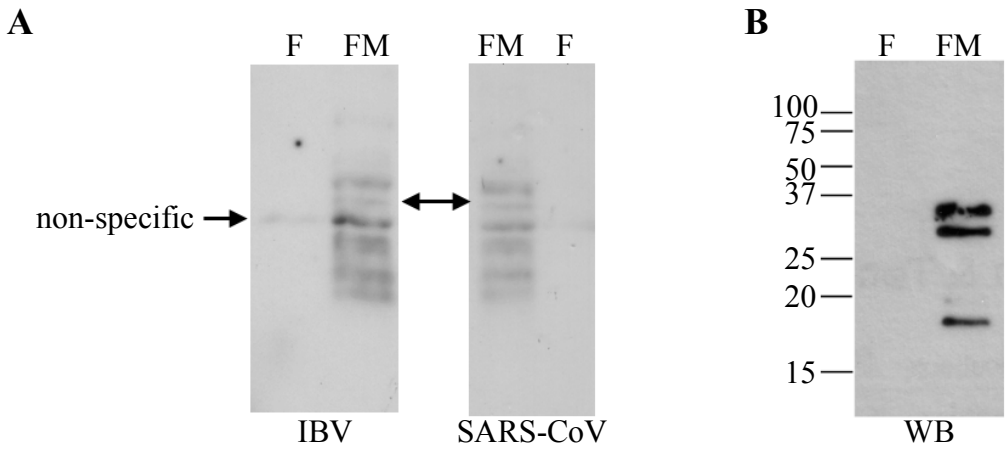

Figure 3.13: FLAG-MADP1 could not be detected by north-western blotting using both IBV and SARS-CoV 5'-UTR (+) probes. (A) North-western blot of affinity purified FLAG-MADP1 probed with 5'-UTR (+) of IBV or SARS-CoV. The bands corresponding to full-length FLAG-MADP1 on both blots were indicated by the double headed arrow. (B) Western blot (WB) of affinity purified FLAG-MADP1 used in north-western blot detected by anti-FLAG-HRP antibody. A representative result of three independent experiments was shown.

3.2.4 MADP1 interacts with SARS-CoV 5'-UTR (+) and IBV 5'-UTR (+)

A different method based on the ability of interacting proteins to co-purify with biotin-labeled RNA probes using streptavidin beads was used to assess the interaction between FLAG-MADP1 recombinant protein and the 5'-UTR (+) from SARS-CoV and IBV. The full-length 5'-UTR (+) probes synthesized as biotin-labeled RNA by *in vitro* transcription and FLAG-MADP1 over-expressed in H1299 cells in the presence

of Vaccinia/T7 virus were used for the assay. As this was the first time this method was used in the laboratory, all fractions were analyzed to ensure that the conditions were optimized. The samples were resolved by SDS-PAGE and western blot was used for the detection of FLAG-MADP1 (Figure 3.14).

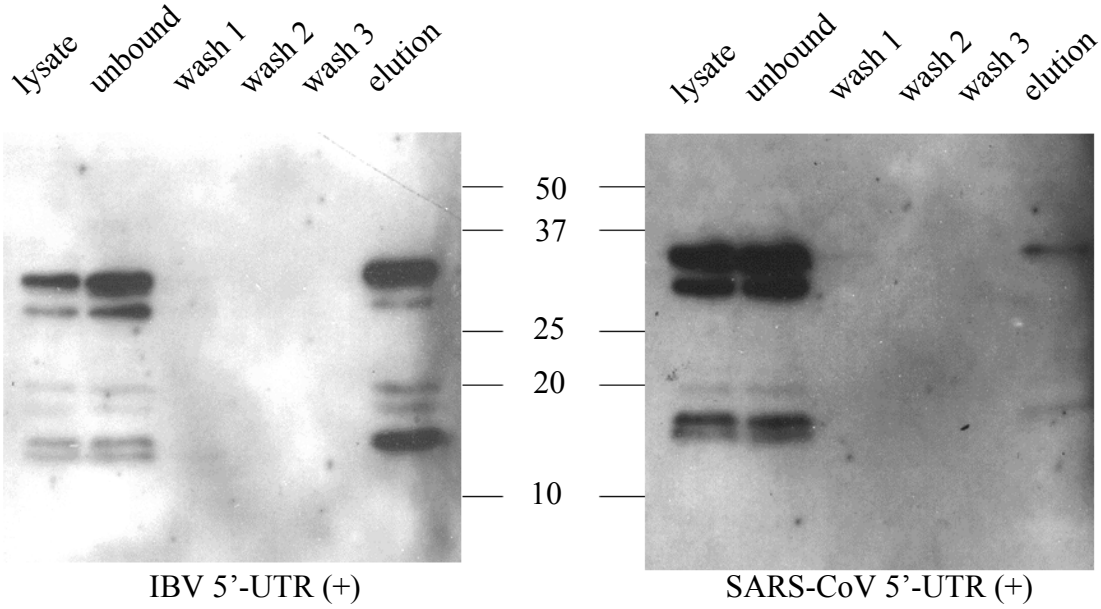

Figure 3.14: MADP1 interacts with the 5'-UTR (+) of IBV and SARS-CoV. Lysate of H1299 cells over-expressing FLAG-MADP1 was mixed with biotin-labeled RNA probes and the mixture was affinity purified by streptavidin beads. The beads were washed thrice and co-purified proteins eluted with 2X SDS loading dye. All eluted proteins, 10 µl of cell lysate and 20 µl of all other fractions were resolved with a 12% SDS-PAGE gel and western blot was performed with anti-FLAG-HRP antibody. A representative result of two independent experiments was shown.

The strength of interaction between MADP1 and the RNA probe was assessed by a comparison of the relative band intensity corresponding to full-length FLAG-MADP1 for the cell lysate loaded and the eluted proteins. The SARS-CoV 5'-UTR (+) appeared to interact weakly with MADP1 (Figure 3.14, right panel). Although the interaction observed for SARS-CoV 5'-UTR (+) was weak, it indicated that the binding was likely specific since the amounts detected in the three washes were

negligible compared to the amount detected in the eluted sample. IBV 5'-UTR (+) on the otherhand, was exhibiting an unquestionably stronger interaction with MADP1 compared to its SARS-CoV counterpart.

As the interaction observed for SARS-CoV 5'-UTR with MADP1 was much weaker than expected, it could complicate further analyses of the interaction when mutations targeted at obliterating the interaction were performed. Hence, the subsequent mapping of interaction domains were based on the interaction between IBV 5'-UTR (+) and MADP1.

3.3 MADP1 Translocated to the Cytoplasm during IBV Infection

Although the interaction between MADP1 and both SARS-CoV and IBV 5'-UTR (+) appeared to be true, the possibility of a nuclear protein participating in coronavirus RNA synthesis which occurs in the cytoplasm in virus-induced DMVs needed verification. As a previous report on MADP1 only noted its nuclear (excluding nucleolus) localization, there was no indication that the protein could be transported out of the nucleus. Hence, to confirm if the interaction between the IBV 5'-UTR (+) and MADP1 was possible in infected cells, a cell fractionation experiment was performed to assess the cellular distribution of MADP1 during an IBV infection.

3.3.1 MADP1 was present in the cytosol during IBV infection

For this purpose, 2 cell lines, H1299 and Vero cells, were selected as H1299 cells would be used for most transfection-related experiments and Vero was the cell line

the strain of IBV used had been adapted to. The cells grown in a 6-well plate were either infected with IBV virus stock at a multiplicity of infection (MOI) of approximately 1 or with the same volume of mock virus stock for 10 hours. The cells were fractionated using CelLytic™ NuCLEAR™ Extraction Kit and both nuclear and cytoplasmic fractions were resolved by SDS-PAGE. Nuclear marker Histone H1 and cytoplasmic marker β–tubulin were probed with the appropriate antibodies. A made-to-order serum antibody produced in rabbit was used to detect endogenous MADP1.

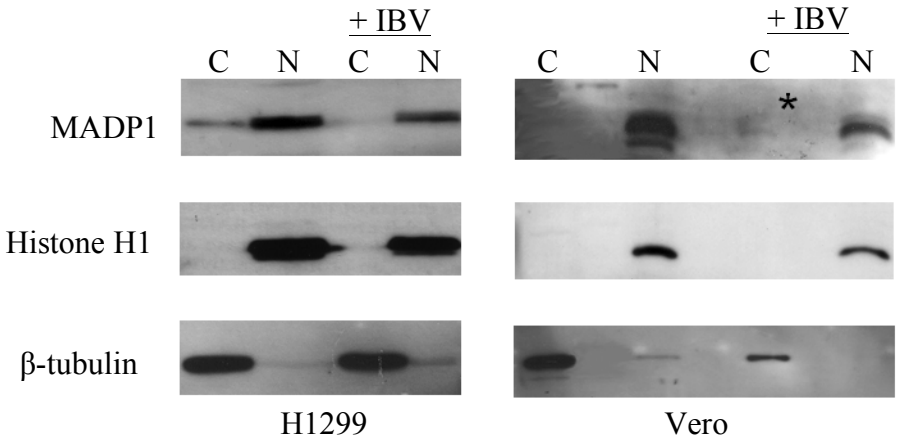

Figure 3.15: MADP1 localized predominantly in the nucleus but was detectable in the cytoplasm. H1299 and Vero cells were infected with IBV virus stock at MOI ≈ 1 (+IBV) or with an equal volume of mock virus stock for 10 hours then cell fractionation was performed for each sample. 10% of the respective fractions were resolved by a 12% SDS-PAGE gel and western blot was performed with antibodies to histone H1, β-tubulin and MADP1. C: cytoplasmic fraction, N: nuclear fraction. A representative result of three independent experiments was shown.

In H1299 cells (Figure 3.15, left panel), MADP1 localized predominantly in the nuclear fraction but was present in the cytoplasm as well, with or without IBV infection. Although the amount of MADP1 present in the cytosol appeared lower in the presence of IBV infection than without, densitometric analysis revealed that the C/N ratios were consistent at 25% and 29% respectively. The lower amount of MADP1 in the cytosol could have been due to a difference in cell numbers at 10 hours

post infection as the mock virus infected cells could continue replication while the IBV infected cells experienced cell cycle arrest, which resulted in their inability to replicate.

In Vero cells (Figure 3.15, right panel), MADP1 did not appear to be present in the cytoplasmic fraction for the mock virus infected. However, a minute amount of MADP1 was detected in the cytosol for the IBV infected sample (indicated by an asterisk). Densitometric analysis of the detected bands has revealed an increase of the C/N ratio from 3.6% to 18.7% after IBV infection. This increased presence of MADP1 resulting from IBV infection was significant considering the lack of histone H1 contamination in the cytoplasmic fractions.

3.3.2 MADP1 translocates to the cytoplasm during IBV infection

Although the cell fractionation study indicated the presence of MADP1 in the cytosol at least during IBV infection, it was unable to prove that the host protein was present at regions with active viral RNA synthesis, the viral replicase/transcriptase complex (RTC). To determine if MADP1 was able to co-localize with the viral RTCs, indirect immunofluorescence confocal microscopy was performed. The serum antibody for MADP1 was not suitable for immunofluorescence detection of the endogenous protein, so MADP1 was over-expressed as recombinant protein FLAG-MADP1, its detection made by polyclonal rabbit anti-FLAG^{TM} antibody. The active RTCs were labeled with bromouridine triphosphate (BrUTP) and detection was made by a monoclonal mouse antibody to bromodeoxyuridine (BrdU) which cross-reacts with BrUTP.

Cells infected with IBV were treated with actinomycin D at 3 hours post infection (h.p.i.) for 4 hours to inhibit host transcription and BrUTP was introduced by transfection to label newly synthesized RNAs for 3 hours before the cells were fixed. Immunofluorescence detection was performed by probing with both primary antibodies then Alexa Fluor® 488 conjugated anti-rabbit and Alexa Fluor® 594 conjugated anti-mouse secondary antibodies.

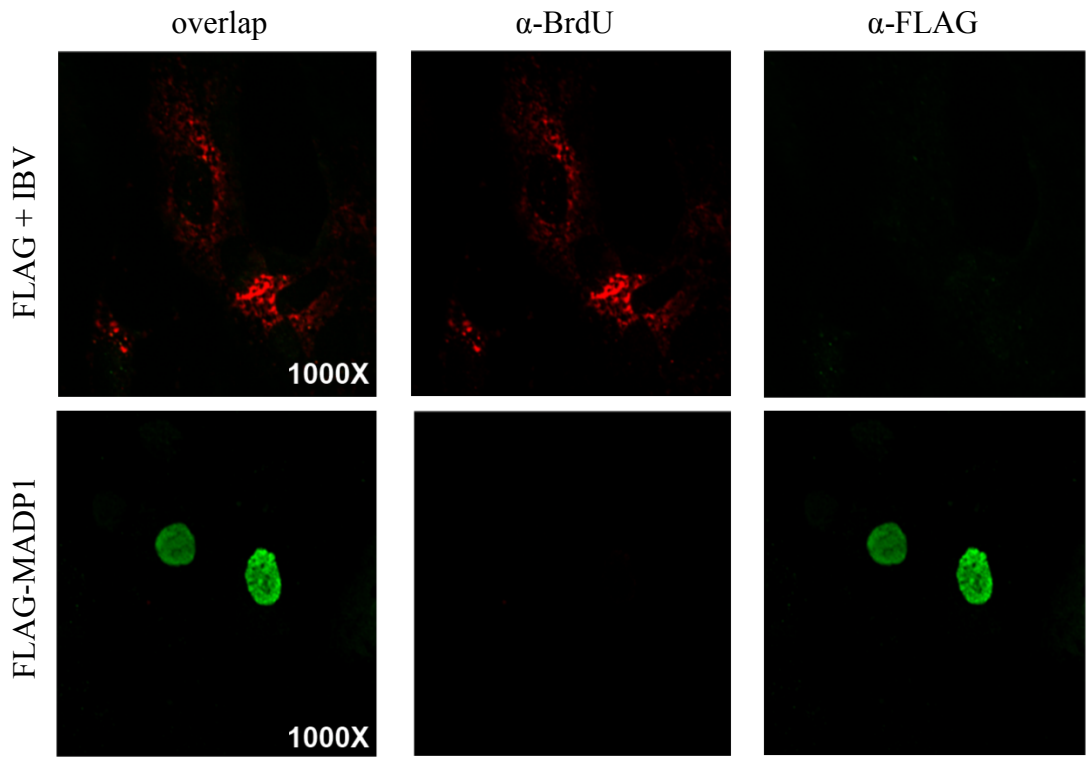

Figure 3.16: Negative controls for indirect immuno-fluorescent detection of BrUTP and FLAG-MADP1. Top panel: Vero cells over-expressing FLAG which were infected with IBV were stained with anti-BrdU only. Bottom panel: Vero cells over-expressing FLAG-MADP1 which were mock virus infected were stained with anti-FLAG only. A representative set of images from three independent experiments was shown (between three to six images were taken for each experiment).

Two negative Controls (Figure 3.16) were included in the experiment. The first was IBV infected FLAG expressing Vero cells (upper panel) which displayed only positive staining for BrUTP (red) in the cytoplasm as punctate structures. The second

was mock virus infected FLAG-MADP1 expressing Vero cells (lower panel) which displayed only positive staining for FLAG-MADP1 in the cell nuclei (green). Taken together, the two negative controls indicated that detection by both anti-BrdU and anti-FLAG were specific for BrUTP and FLAG-MADP1 respectively.

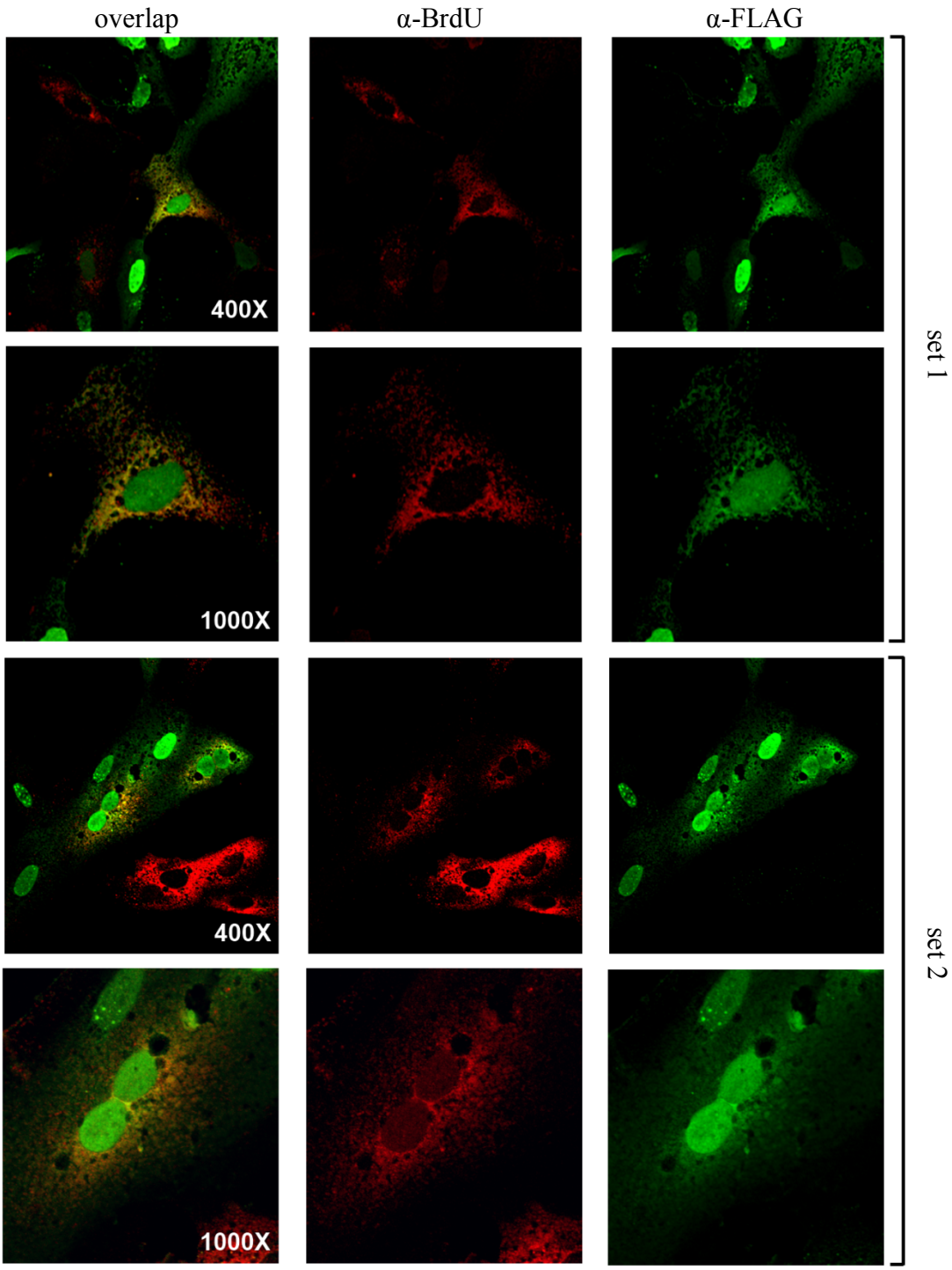

Figure 3.17: FLAG-MADP1 was present in the cytoplasm of Vero cells during IBV infection. Indirect immunofluorescence visualization of FLAG-MADP1 and BrUTP labeled RNA in IBV-infected Vero cells. FLAG-MADP1 was stained by Alexa Fluor 488 (green), BrUTP was stained by Alexa Fluor 594 (red) and overlapping staining (yellow) in the overlapped images indicated points of overlapping signals. Two sets of representative images were selected to show the extent of colocalization. Cells were visualized at 400X magnification and selected fields were magnified at 1000X. Two representative sets of images from three independent experiments was shown (between two to four images of different sections were taken for each experiment).

Two sets of representative images of IBV-infected FLAG-MADP1 expressing Vero cells were shown in Figure 3.17 (set 1 and set 2) at 400X and 1000X magnification. In both sets of images, FLAG-MADP1 (green) displayed a pre-dominantly nuclear staining with some cytoplasmic staining as punctate structures that appeared to be slightly more concentrated in the perinuclear region. BrUTP (red) staining was observed as punctate structures in the cytoplasm which exhibited stronger signals in the perinuclear region. The overlap images (left column) showed some yellow regions (green + red), indicating the presence of both stains at the same positions. This implied that FLAG-MADP1 could be located in close proximity to *de novo* synthesized RNA labeled by BrUTP. Although the overlap was far from complete, and a co-localization in the perinuclear region could not be confirmed, the cellular distribution of FLAG-MADP1 was clearly affected by IBV infection.

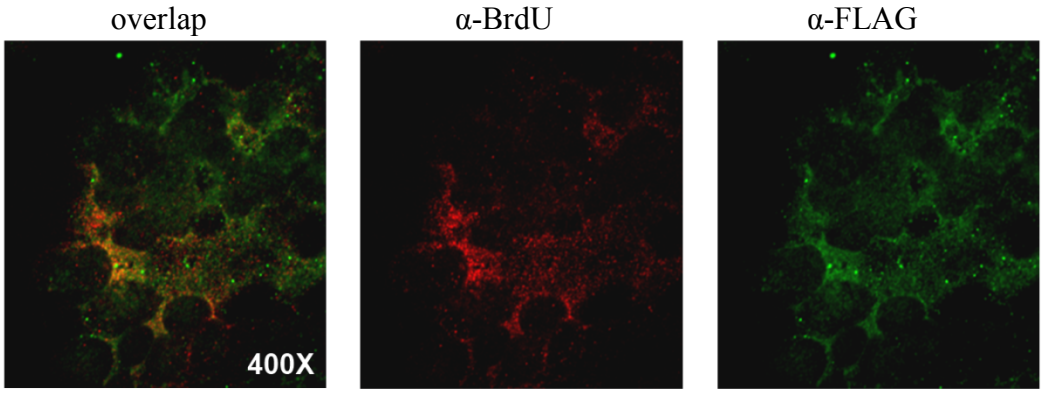

Figure 3.18: FLAG-MADP1 was present in the cytoplasm of H1299 cells during IBV infection. Indirect immunofluorescence visualization of FLAG-MADP1 and BrUTP labeled RNA in IBV-infected H1299 cells. FLAG-MADP1 was stained by Alexa Fluor 488 (green), BrUTP was stained by Alexa Fluor 594 (red) and overlapping staining (yellow) in the overlapped images indicated points of overlapping signals. Cells were visualized at 400X magnification. A representative set of images from three independent experiments was shown (between two to four images were taken for each experiment).

The same observation could be made in H1299 cells as shown in Figure 3.18 (left image). However, as the infection proceeded much faster in H1299 cells, fusion cells were formed so no single infected cells were observed. BrUTP staining (middle image) and regions stained for both BrUTP and FLAG-MADP1 (yellow) appeared to be concentrated near one particular nucleus, which likely belonged to the original infected cell before the syncytium was formed. It was also noted that in H1299 cells, FLAG-MADP1 appeared to be almost absent from most nuclei in the syncytium (right image) during IBV infection.

Although the immunofluorescence data were insufficient to show that MADP1 could colocalize with *de novo* synthesized viral RNA (in the presence of actinomycin D) in the cytosol, there was a distinct change in the staining pattern for MADP1 after the cells were infected with IBV. This was in addition to the results from cell fractionation experiment that MADP1 was present in the cytosol in low amounts at least during IBV infection in both Vero and H1299 cells. As the labeling of RNA lasted only three hours just before the cells were fixed, the stained punctate structures would likely indicate the positions of active RTCs since the retired RTCs which stopped RNA synthesis would not have been labeled. The close proximity of FLAG-MADP1 with active RTCs may indicate the significance in its interaction with viral RNA in the virus infected cells, although further analysis would be required to confirm if close proximity of MADP1 to the newly synthesized RNA indicates its association with the RTCs.

3.4 MADP1 Interacts Specifically with IBV 5'-UTR (+)

Although MADP1 was able to copurify with biotin-labeled IBV 5'-UTR (+) in the biotin-pull-down assay, it was not known if the interaction was specific or if MADP1 could be a non-specific RNA binding protein. To investigate the specificity of the RNA-binding activity of MADP1, a binding competition assay, based on the biotin pull-down assay, was performed. Unlabeled IBV 5'-UTR (+) (IBV genome nt 1 to 528) RNA and negative-sense EGFP coding sequence nt 1 to 528 (EGFP (-)) were synthesized by *in vitro* transcription to be used as specific and non-specific RNA competitors respectively. As a control, the binding of IBV N protein, a non-specific RNA-binding protein, to one of its biological targets, the IBV 3'-UTR (+) was examined. Unlabeled IBV 3'-UTR (+) (IBV genome nt 27106 to 27611) was synthesized by *in vitro* transcription to be used as the specific RNA competitor while unlabeled EGFP (-) RNA was used as the non-specific RNA competitor.

For both specific and non-specific competition assays, different amounts of unlabeled probes (0 μM, 0.5 μM, 1.0 μM, 1.5 μM and 2.0 μM final) were mixed with a fixed amount (0.1 μM final) of biotin-labeled probes (5'-UTR (+) and 3'-UTR (+)) prior to the addition of cell lysate from FLAG-MADP1 or FLAG-IBV N over-expressing H1299 cells respectively. Each mixture was incubated 30 minutes at room temperature before streptavidin beads were added. The proteins that co-purified with biotin-labeled RNA were resolved by SDS-PAGE and probed for FLAG-MADP1 using anti-FLAG-HRP antibody.

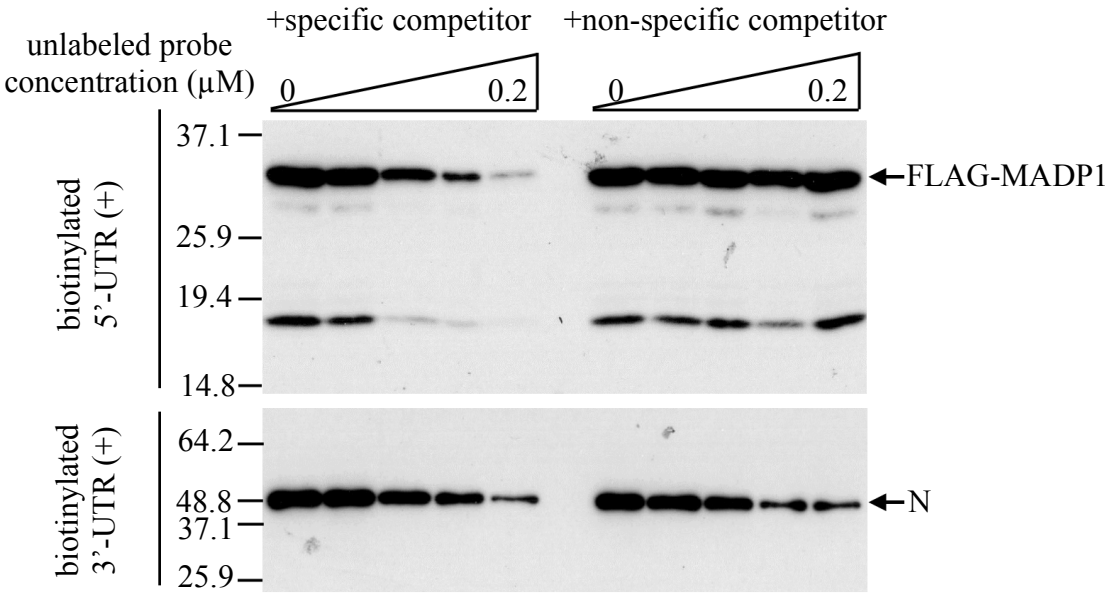

Figure 3.19: MADP1 interacts specifically with IBV 5'-UTR (+). Increasing concentrations of unlabeled specific RNA competitor (IBV 5'-UTR (+)) decreased the binding of MADP1 to biotinylated IBV 5'-UTR. Increasing concentrations of unlabeled non-specific RNA competitor (EGFP (-) did not affect the interaction. The binding of non-specific RNA-binding protein, IBV N, to its biotinylated biological target, IBV 3'-UTR (+) was affected by increasing concentrations of both its specific RNA competitor (IBV 3'-UTR (+)) and non-specific RNA competitor (EGFP (-)). A representative result of three independent experiments was shown.

The binding of MADP1 to biotinylated 5'-UTR (+) decreased in the presence of an increasing concentration of specific RNA competitor, unlabeled 5'-UTR (+) (Figure 3.19, top panel). The binding was reduced to about 50% when the concentration of the specific competitor equaled that of the biotinylated 5'-UTR (+) (0.1 μM). When twice the amount (0.2 μM) of unlabeled probe was present, the binding of MADP1 to biotinylated 5'-UTR (+) suffered at least a 10-fold reduction. Conversely, the presence of non-specific RNA competitor, EGFP (-) did not affect the binding of MADP1 to biotinylated IBV 5'-UTR at the maximum concentration used (0.2 μM) (Figure 3.19, top panel).

For the control experiment, both unlabeled IBV 3'-UTR (+) (specific competitor) and EGFP (-) (non-specific competitor) probes decreased the binding of IBV N to its biotinylated biological target, IBV 3'-UTR (+) RNA. This was vastly different from the observation made from the interaction between MADP1 and biotinylated IBV 5'-UTR (+), which could only be affected by the presence of unlabeled specific RNA. Hence, it could be concluded that the interaction between MADP1 and IBV 5'-UTR was of a specific nature and not a result of non-specific RNA-binding activity exhibited by MADP1.

3.5 Stem Loop I of IBV 5'-UTR (+) is required to interact with MADP1

To map the binding site of MADP1 on the IBV 5'-UTR (+), biotinylated RNA spanning different regions of the sequence were synthesized by *in vitro* transcription for use in biotin-pull down assays using FLAG-MADP1 over-expressing H1299 cell lysate. The probes which were created for the mapping of the MADP1 binding site were shown in Figure 3.20.

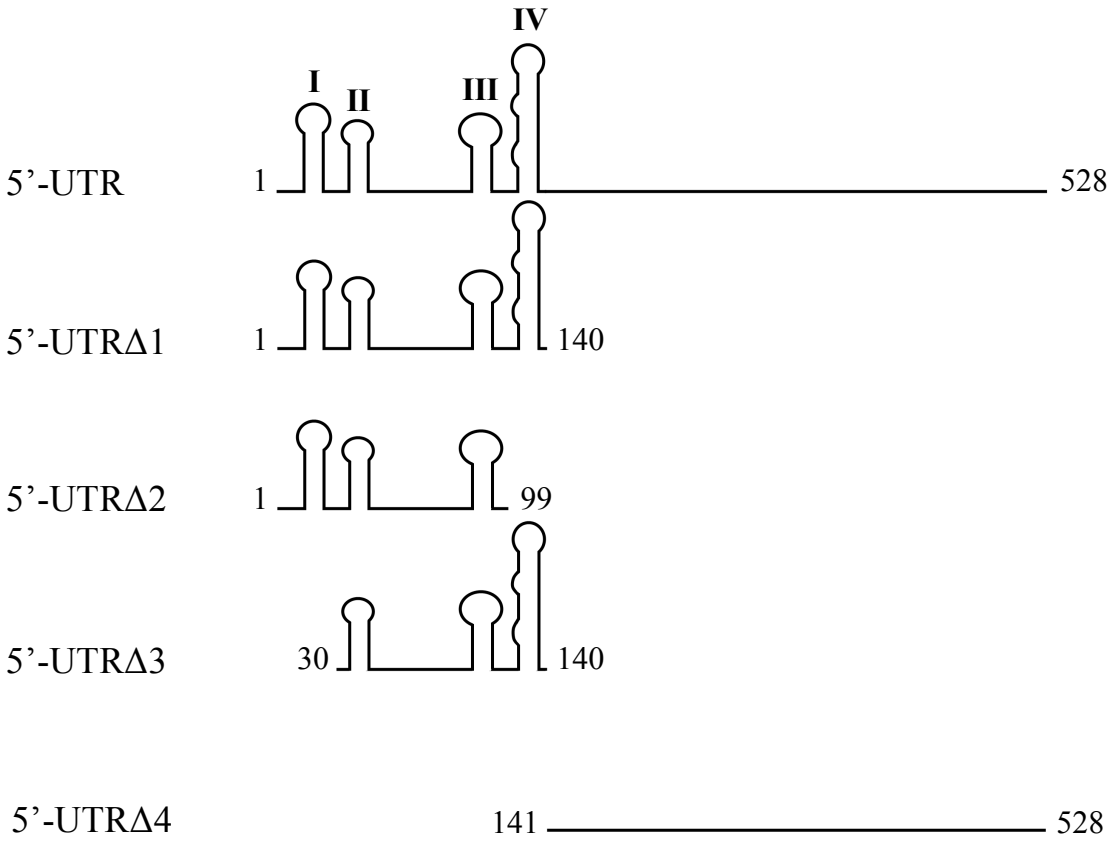

Figure 3.20: Schematic diagram of biotinylated probes synthesized used to map the MADP1 binding site on IBV 5'-UTR (+). All probes were produced by *in vitro* transcription with PCR templates spanning the indicated regions. 5'-UTR spanned the entire 5'-UTR. 5'-UTRΔ1, 5'-UTRΔ2 and 5'-UTRΔ3 spanned nucleotides 1-140, 1-99 and 30-140 respectively while 5'-UTRΔ4 spanned nucleotides 141-528. Predicted secondary structures for the first 140 nucleotides were indicated.

3.5.1 The first 140 nucleotide residues of IBV 5'-UTR (+) is required to interact with MADP1

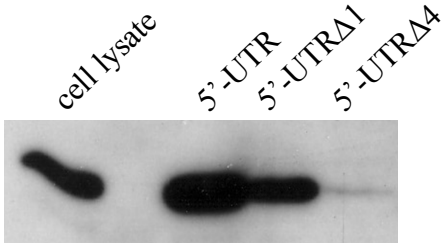

Figure 3.21: The binding site for MADP1 lies in the first 140 nucleotides of the IBV 5'-UTR (+). Biotin pull-down assay performed with probes 5'-UTR (full length IBV 5'-UTR, nucleotides 1-528), 5'-UTRΔ 1 (nucleotides 1-140) and 5'-UTRΔ4 (nucleotides 141-528). A representative result of three independent experiments was shown.

Two biotinylated probes, 5'-UTRΔ1 and 5'-UTRΔ4 (Figure 3.21) were assessed for their binding to MADP1 first to determine if the binding site for MADP1 was located in the 5' one-third or the 3' two-thirds of the IBV 5'-UTR (+). Comparing the relative binding efficiency of the three probes, 5'-UTR, 5'-UTRΔ1 and 5'-UTRΔ4, it was observed that 5'-UTRΔ1 while 5'-UTRΔ4 did not retain much interaction with MADP1, 5'-UTRΔ1 was able to maintain its interaction, although it appeared to be less efficient compared to that observed for full length 5'-UTR (probe 5'-UTR). This implied the binding site for MADP1 was encoded within the first 140 nt of the IBV 5'-UTR (+).

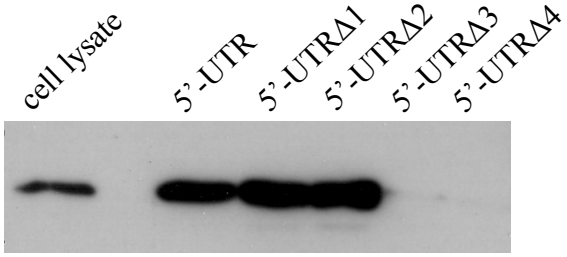

Figure 3.22: Stem-loop I was required to retain the interaction between biotinylated RNA and MADP1. Biotin pull-down assay was performed with the probes 5'-UTR, 5'-UTRΔ1 to 4. The probes 5'-UTRΔ3 (nucleotides 30-140) and 5'-UTRΔ4 (nucleotides 141-528) were unable to interact with MADP1. A representative result of three independent experiments was shown.

3.5.2 Stem-loop I of the IBV 5'-UTR is required to interact with MADP1

The first 140 nt of the IBV 5'-UTR contains four predicted stem loop structures, stem loops I to IV, indicated in Figure 3.20 (5'-UTR) which are well conserved across the three genera of coronaviruses. In an attempt to pin-point the secondary structure(s) responsible for the interaction between IBV 5'-UTR (+) and MADP1, two additional probes, 5'-UTRΔ2 and 5'-UTRΔ3 were assessed for their interaction with MADP1 together with probes 5'-UTR, 5'-UTRΔ1 and 5'-UTRΔ4 (Figure 3.22).

As shown earlier in Figure 3.21, 5'-UTRΔ4 which was unable to interact with MADP1 was included in this assay to serve as a control for negative binding. It was observed that probes 5'-UTR (full length), 5'-UTRΔ1 (nt 1-140) and 5'-UTRΔ2 (nt 1-99) were able to bind MADP1 efficiently while 5'-UTRΔ3 (nt 30-140) and 5'-UTRΔ4 (nt 141-528) did not bind MADP1. While probes 5'-UTR and 5'-UTRΔ4 served as controls for positive and negative interaction with MADP1, probes 5'-UTRΔ1, 5'-UTRΔ2 and 5'-UTRΔ3 contained a different set of secondary structures each. 5'-UTRΔ1 contained stem loops I to IV, 5'-UTRΔ2 contained stem loops I to III and 5'-UTRΔ3 contained stem loops II to IV.

Since probes 5'-UTRΔ1 and 5'-UTRΔ2 could both bind to MADP1, stem loop IV would likely not be required for the interaction. In addition, the observation that 5'-UTRΔ3 could not bind to MADP1 indicated that a critical secondary structure required for the interaction was not present on the probe but present on probes 5'-UTRΔ1 and 5'-UTRΔ2. These observations had narrowed down the secondary structure responsible for the interaction to stem loop I.

3.5.3 The integrity of stem-loop I structure is essential to maintain its interaction with MADP1

As stem loop I of the IBV 5'-UTR (+) was determined to be the binding site for MADP1, and that 5'-UTRΔ2 (nt 1-99) was the shortest tested probe which could bind MADP1 at high efficiency, a mutant probe 5'-UTRΔ2M1, was synthesized based on the probe 5'-UTRΔ2. The two-residue mutation changed nt 11 and 12 from "GA" to "CU" and was predicted to destabilize the structure of stem loop I by creating unpaired bases in the mid-stem region (Figure 3.23).

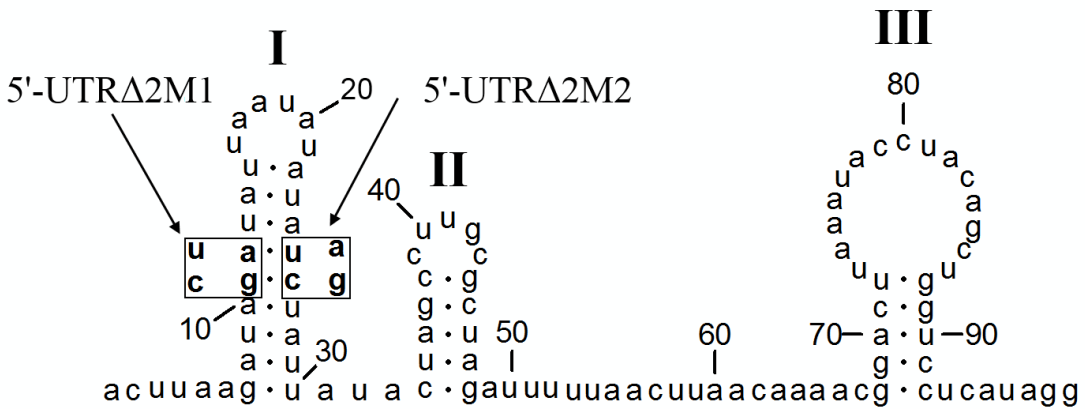

Figure 3.23: Two mutations introduced to probe 5'-UTRΔ2 to create mutant probes 5'-UTRΔ2M1 and 5'-UTRΔ2M2. 5'-UTR Δ2M1 contains a two-residue mutation which was predicted to destabilized stem loop I while 5'-UTRΔ2M2 contains an additional two-residue mutation which was predicted to restore the structure of stem loop I.

A second mutant probe 5'-UTRΔ2M2, which contained an additional two-residue mutation in mutant probe 5'-UTRΔ2M1 changing nt 25 and 25 from "UC" to "AG". This change was predicted to reinstate the stem loop I structure through the restoration of base pairing in the mid-stem region, residue 11 with residue 26 and residue 12 with residue 25. Both mutants were assessed for their binding efficiency to

MADP1 with the biotin pull-down assay using FLAG-MADP1 over-expressing H1299 cell lysate or negative control EGFP over-expressing H1299 cell lysate.

As shown in Figure 3.24, the interaction between MADP1 and IBV 5'-UTR (nt 1-99) was obliterated when the probe contained a destabilized stem loop I, 5'-UTRΔ2M1. On the otherhand, the interaction was restored, albeit partially, when the mutant probe which contained an additional mutation to restore the stem loop I structure, 5'-UTRΔ2M2, was used. The inability of 5'-UTRΔ2M2 in fully restoring the interaction between MADP1 and IBV 5'-UTR (nt 1-99), despite having restored the secondary structure, could indicate an importance of the primary nucleic acid sequence of stem loop I as a critical determinant for the interaction.

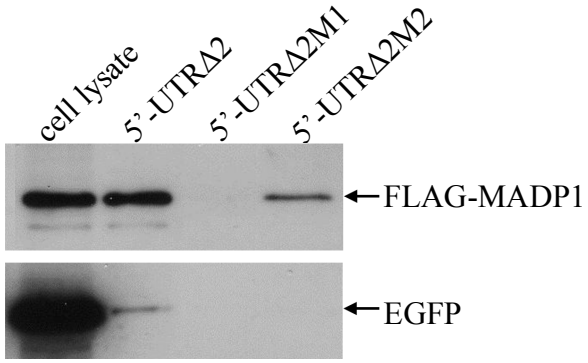

Figure 3.24: The secondary structure of stem loop I was essential to bind MADP1. Biotin pull-down assay with probes 5'-UTRΔ2, 5'-UTRΔ2M1 and 5'-UTRΔ2M2. Mutant probe 5'-UTRΔ2M1 did not interact with MADP1 but 5'-UTRΔ2M2 could bind MADP1. MADP1 interacted with 5'-UTRΔ2M2 at a lower efficiency compared to 5'-UTRΔ2 (positive control). EGFP (negative control) did not interact efficiently with all three probes tested. A representative result of four independent experiments was shown.

For non-RNA binding protein, EGFP, the band observed in the lane loaded with sample from the pull-down assay with probe 5'-UTRΔ2 was likely due to a leakage from the adjacent, cell lysate as the amount was extremely low, relative to the amount

of EGFP in the cell lysate and EGFP had not been observed to interact with any RNA probes in the earlier assays.

With these results, we could confirm that stem loop I of the IBV 5'-UTR (+) is the binding site for MADP1.

3.6 The RNA Recognition Motif Domain of MADP1 is required to interact with IBV 5'-UTR (+)

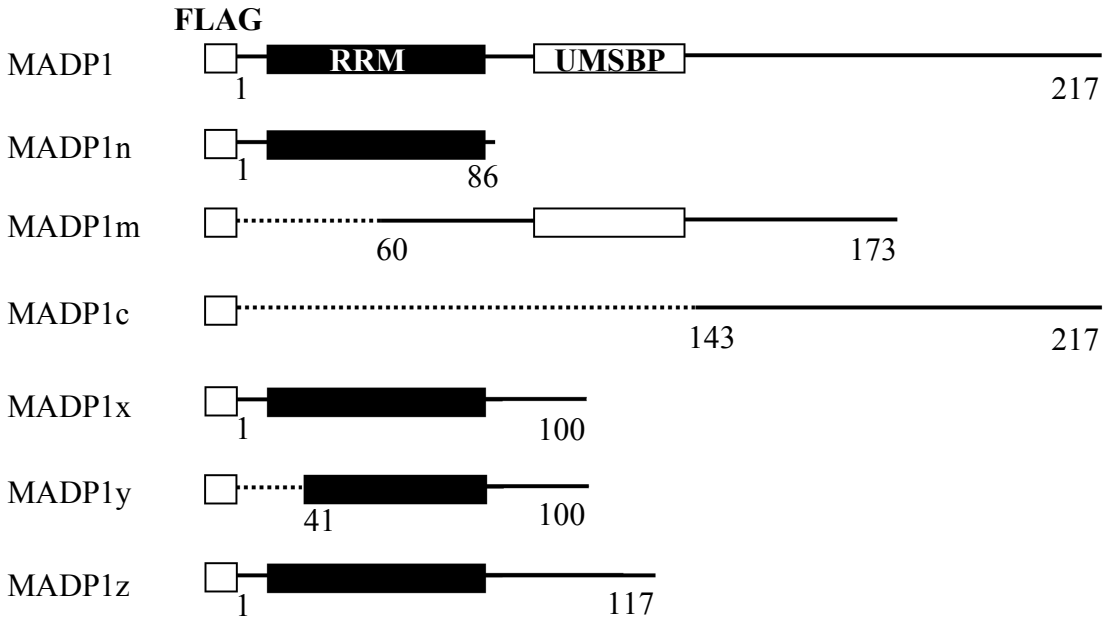

Figure 3.25: Schematic diagram of MADP1 truncation mutants used in the determination of domain responsible for interacting with IBV 5'-UTR (+). Wild-type full length MADP1 (MADP1) contains two conserved domains, the RNA recognition motif (RRM) and the universal minicircle sequence binding protein (UMSBP) domains. All proteins were N-terminally tagged with FLAG-epitope and amino acid residue numbers were indicated.

MADP1 protein was predicted to contain two nucleic acid binding domains, the RNA recognition motif (RRM) domain (residues 11 to 84) and a provisional universal minicircle sequence binding protein (UMSBP) domain (residues 97 to 123). In order

to determine the domain responsible for interacting with IBV 5'-UTR, a series of truncation mutants of MADP1, shown as a schematic diagram in Figure 3.25, were created to assess each of their RNA-binding activity with full length 5'-UTR (+) as the binding partner. EGFP protein was used as the negative control.

3.6.1 The IBV 5'-UTR (+) binding activity was mapped to the RRM domain of MADP1

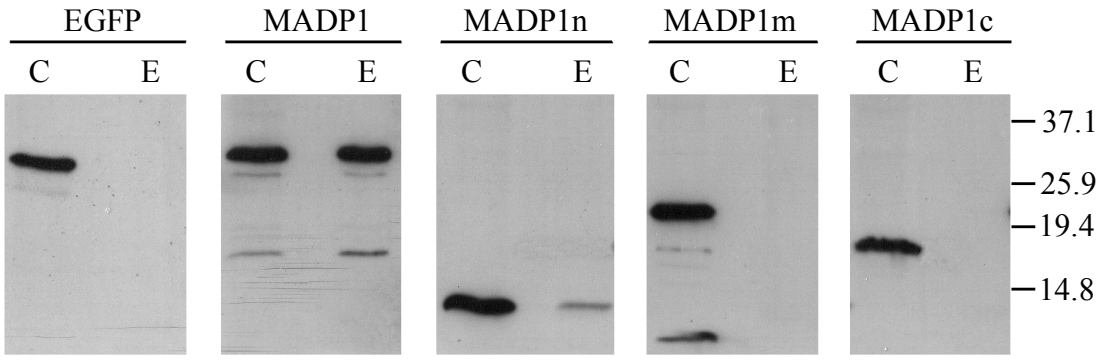

Figure 3.26: The RRM domain interacted weakly with IBV 5'-UTR (+). Biotin pull-down assay of three MADP1 truncation mutants, MADP1n (RRM domain) MADP1m (UMSBP domain) and MADP1c (C-terminus) performed with biotinylated probe 5'-UTR. MADP1m and MADP1c did not interact with the biotinylated probe and the interaction of MADP1n with the biotinylated was much weaker compared to full-length MADP1 (MADP1). EGFP (negative control) did not bind to the biotinylated probe. C: cell lysate, E: eluted proteins bound to streptavidin beads. A representative result of four independent experiments was shown.

The first three truncated mutants, MADP1n, MADP1m and MADP1c which spanned the RRM domain (N-terminus), UMSBP domain (middle) and the C-terminus which contained mostly phosphorylation sites were assessed for their RNA-binding to IBV 5'-UTR (+), using biotin pull-down assay, to determine the domain responsible for interaction. As shown in Figure 3.26, it appeared the UMSBP domain (MADP1m) and the C-terminus (MADP1c) were unable to bind IBV 5'-UTR (+). Although the

RRM domain (MADP1n) was able to interact with IBV 5'-UTR (+), the interaction was much weaker compared to that with the full-length MADP1 protein. This observation indicated the importance of the peptide sequence beyond the RRM domain in achieving its full RNA-binding capacity.

Therefore, three additional mutants based on MADP1n (Figure 3.25), were created and assessed for their RNA-binding activity with the biotin pull-down assay using biotinylated 5'-UTR as the RNA probe. The mutants MADP1x and MADP1z were extensions of MADP1n by 14 and 31 amino acid residues respectively while MADP1y was a variation of MADP1x with a 40 amino acid residue deletion at its N-terminal. Both MADP1x and MADP1z exhibited efficient binding to the biotinylated IBV 5'-UTR (+) while MADP1y bound weakly (Figure 3.27).

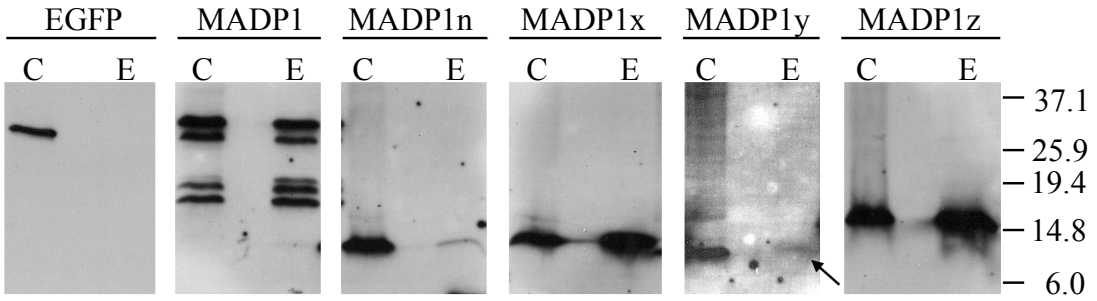

Figure 3.27: Extension by a minimum of 14 amino acid residues of RRM domain or MADP1n (amino acid residues 1 to 86), was required to achieve a RNA-binding activity comparable to that of full-length MADP1. MADP1x (amino acid residues 1 to 100) and MADP1z (amino acid residues 1 to 117) both bound efficiently to biotinylated IBV 5'-UTR (+). N-terminally truncated MADP1y (amino acid residues 41-100) did not bind to the biotinylated probe efficiently. C: cell lysate, E: eluted proteins bound to streptavidin beads. A representative result of four independent experiments was shown.

This observation showed that the peptide sequence beyond the RRM is critical for its function in RNA-binding and that the minimum number of additional amino acid residues is 16 (up to residue number 100). These additional residues could have been

required to ensure correct protein folding which would have been crucial to the domain function. Also, the 40 residue N-terminal truncation proved detrimental to the RNA-binding function of the RRM as represented by the poor RNA-binding efficiency exhibited by MADP1y. This observation confirmed that the RRM interacts with IBV 5'-UTR (+) as the truncation at the N-terminus would have disrupted the structure of the domain and affected its function in RNA-binding.

3.6.2 The active site of MADP1 RRM domain is required to interact with IBV 5'-UTR (+)

To confirm if the RRM domain is required for the IBV 5'-UTR (+) to bind MADP1, mutations to disrupt the active site of the domain would be required. The RRM domain active site of MADP1 was predicted to be made up of three residues, tyrosine 13, valine 53 and phenylalanine 55. Valine and phenylalanine would have been required to interact with the bases via hydrophobic interactions or base stacking respectively while positively charged tyrosine would likely act as an anchor for the negatively charged phosphate backbone. Hence, three mutants of MADP1 which had one, two or all three active site residues replaced by a neutral charged alanine residue were created. The tyrosine 13 residue was substituted in the Y mutant (Y13→A), valine 53 and phenylalanine 55 residues were substituted in VF mutant (V53→A, F55→A), while the YVF mutant had all three active site residues substituted replaced (Y13→A, V53→A, F55→A). The mutants which were over-expressed as FLAG-tagged proteins were assessed for their interaction with IBV 5'-UTR (+) using biotin pull-down assay alongside wild-type FLAG-tagged MADP1.

All three mutants were found to exhibit lower RNA-binding to the biotinylated 5'-UTR probe compared to wild-type MADP1 (Figure 3.28). Single and double residue mutants, Y and VF were co-purified with the biotinylated probe with similar efficiencies while the triple residue mutant YVF was co-purified at a much lower efficiency. These observations have demonstrated that the domain which served as the interacting partner to IBV 5'-UTR (+) was the RRM, not the UMSBP domain nor the C-terminus as the preservation of its active site residues was critical to the ability of full-length MADP1 protein to bind its target. Also, the interaction was the result of all three active site residues interacting with the RNA.

In conclusion, the experimental results have affirmed that the RRM domain of MADP1 interacts with IBV 5'-UTR (+) and that a minimum of 16 additional amino acid residues beyond the domain were required to preserve its RNA-binding activity.

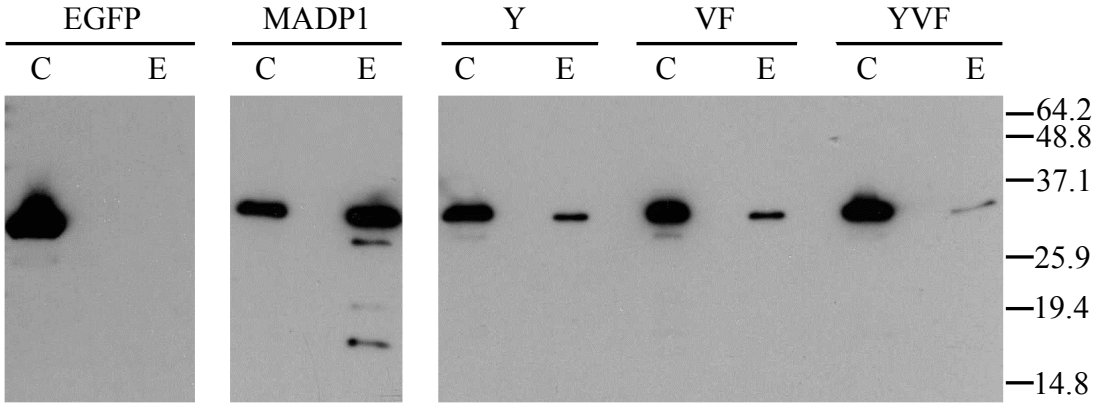

Figure 3.28: The MADP1 RRM domain active site residues are essential for its ability to bind to IBV 5'-UTR (+). Single (Y), double (VF) or triple (YVF) residue substitution mutants of MADP1 were used in a biotin pull-down assay with biotinylated 5'-UTR probe. Both Y and VF mutants showed a decreased binding to the biotinylated probe and YVF mutant showed a drastic decrease in its ability to bind to the probe. C: cell lysate, E: eluted proteins bound to streptavidin beads. A representative result of three independent experiments was shown.

3.7 Transient Gene Silencing of MADP1 Reduced Viral Replication and Transcription

Although the interaction between MADP1 and IBV 5'-UTR (+) was determined to be specific and had been validated to have a possibility in occurring during virus infection, the significance of MADP1 in viral RNA synthesis had yet to be determined. The first strategy employed to demonstrate the significance of MADP1 was to determine the effect of gene silencing on IBV infection in cultured cells.

3.7.1 Optimization of MADP1 gene silencing

Gene silencing was first attempted using transfection reagent Lipofectamine® RNAiMAX on both Vero and H1299 cells. A trial knockdown experiment was performed on both cell lines with a range of concentrations of siRNA to MADP1 (siMADP1): 0 nM, 1 nM, 5 nM, 15 nM, 30 nM and 50 nM. The cells were transfected twice, 24 hours apart and RNA was extracted from the cells 48 hours after the first transfection. RT was performed with an oligo-dT primer and PCR performed with the primers 5'MADP1_SmaI and 3'MADP1_SmaI.

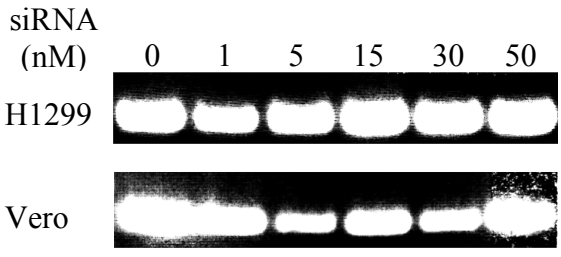

Figure 3.29: Silencing of MADP1 with Lipofectamine® RNAiMAX in H1299 and Vero cells. Different concentrations of siMADP1 were transfected into the cells. 2 µg of total RNA was used for RT and 2 µl of RT product used for PCR. All samples were resolved by agarose gel electrophoresis on a 1% gel and stained with ethidium bromide. A representative result of two independent experiments was shown.

It was observed that although about 50% reduction in mRNA level of MADP1 was achieved in Vero cells at 5 nM siRNA concentration, the silencing efficiency was not high enough to see a visible effect on IBV infection (Figure 3.29). Silencing using Lipofectamine® RNAiMAX reagent was poor in H1299 cells. Hence, a second transfection reagent, Dharma*FECT*® was assessed for its silencing efficiency in the two cell lines. The reagent had been tested in a wide range cell lines by the manufacturer, it was indicated that Dharma*FECT*® 2 and Dharma*FECT*® 3 were prescribed for H1299 and Vero cells respectively. A single siRNA concentration was used for the trial silencing experiment, 100 mM of siMADP1 or siRNA to EGFP gene (siEGFP) was transfected into the cells twice, 24 hours apart and RNA was extracted at 48 hours after the first transfection. RT-PCR was performed with the same primers as with the trial for Lipofectamine® RNAiMAX.

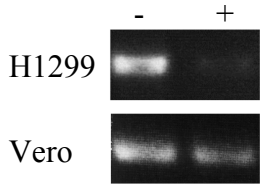

Figure 3.30: MADP1 was efficiently silenced in H1299 cells but less efficiently in Vero cells using Dharma*FECT*® Transfection Reagents. Silencing of MADP1 with Dharma*FECT*® 2 and 3 Transfection Reagents in H1299 and Vero cells respectively. 2 µg of total RNA was used for RT and 1 µl of RT product used for PCR. All samples were resolved by agarose gel electrophoresis on a 1% gel and stained with ethidium bromide. (-) indicates samples transfected with siEGFP and (+) indicates samples transfected with siMADP1. A representative result of two independent experiments was shown.

As shown in Figure 3.30, a high silencing efficiency was achieved in H1299 cells but that for Vero cells was still not high enough. Since a high gene silencing efficiency could only be achieved in H1299, it was chosen as the cell line with which subsequent functional studies were conducted.

3.7.2 MADP1 silencing in H1299 cells reduced luciferase gene expression of IBV-Luc virus

To determine the impact of MADP1 silencing in H1299 cells on IBV infection, a time course experiment was conducted. A recombinant IBV virus which had its accessory gene 3 (encoding 3a and 3b proteins) replaced by the firefly luciferase gene (339), IBV-Luc, was used to provide a quantitative measure of the efficiency of IBV infection. H1299 cells grown to a confluency of 30% in 6-well plates were transfected twice with 100 nM of siMADP1 or siEGFP using Dharma*FECT*® 2, 24 hours apart. The cells were then infected with recombinant IBV-Luc at MOI ≈ 1 in serum-free medium 72 hours after the first transfection. The cells were incubated at 37°C, in an atmosphere of 5% CO_2 for 2 hours before the virus was removed and replaced with fresh serum-free medium. Cells continued to be incubated at 37°C, 5% CO_2 until they were ready to be harvested at 4, 8, 12, 16, 20 or 24 hours post infection (h.p.i.) by lysis with 200 µl of Lysis Buffer for luciferase assay.

Samples representative of the point of infection (0 h.p.i.) were incubated at 37°C, 5% CO_2 for 5 minutes before they were harvested. Mock infected samples were infected with mock virus stock, of the same volume as IBV-Luc used for infected samples, incubated at 37°C for 2 hours before it was removed and replaced with fresh serum-free medium. The mock infected samples were harvested only at 24 h.p.i..

Luciferase activity, expressed as Relative Luminescence Unit per ml (RLU/ml) of the infected cell lysates was used as an indication of viral replication as illustrated in Figure 3.31. Peak luciferase activity was attained by siEGFP transfected cells was 2.23 x 10^4 RLU/ml while that for siMADP1 transfected cells was only 8.00 x 10^2 RLU/ml at 20 h.p.i.. These observations have shown that at low levels of MADP1 expression, expression of virus genes were reduced, and that the spread of the infection could have been hampered, therefore resulting in a 20-fold reduction of maximum luciferase activity achieved.

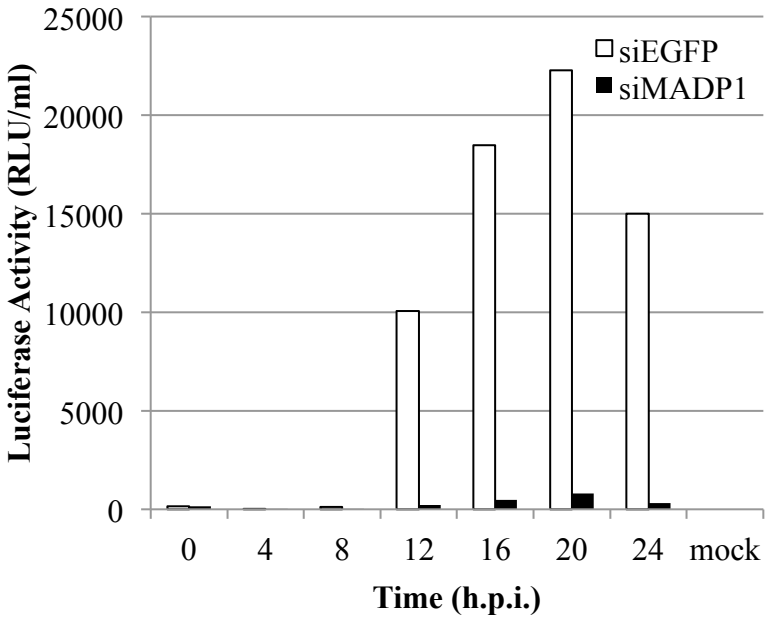

Figure 3.31: Silencing of MADP1 in H1299 cells reduced firefly luciferase activity produced by IBV-Luc infection. H1299 cells transfected with siEGFP (control) or siMADP1 were infected with IBV-Luc virus. Luciferase activity of the cells were measured with 5 µl of lysate and expressed as Relative Luminescence Units per milliliter of lysate (RLU/ml). Samples measured were harvested at 0, 4, 8, 12, 16, 20, 24 hours post infection (h.p.i.). Error bars with standard deviation between the readings were included but too narrow to be seen. Maximum luciferase activity in MADP1 silenced cells was less than 5% of what was achieved in control cells transfected with siEGFP. A representative result of four independent experiments was shown.

3.7.3 Low efficiency silencing of MADP1 in Vero cells had little impact on luciferase gene expression of IBV-Luc virus

As the impact of MADP1 gene silencing in H1299 cells evident, Vero cells, in which a much lower silencing efficiency could be achieved, was also used in a trial time course experiment to assess how much impact would a slight reduction in MADP1 gene expression have on IBV infection. Vero cells grown to a confluency of 30% were transfected with twice with 100 nM of siMADP1 or siEGFP using Dharma*FECT*® 3 and infected with the same protocol as described for H1299 cells in section 3.7.2. Cells were incubated at 37°C, 5% CO_2 until they were ready to be harvested at 4, 8, 12, 16, 20 or 24 hours post infection (h.p.i.) by lysis with 200 µl of Lysis Buffer for luciferase assay. Samples representative of the point of infection (0 h.p.i.) and mock infected samples were prepared as described in section 3.7.2.

It was observed that only about 30% reduction in peak firefly luciferase activity was achieved in cells transfected with siMADP1 compared to negative control, siEGFP transfected cells (Figure 3.32). This implied that the low gene silencing efficiency achieved in Vero cells resulted in a correspondingly weak impact on IBV infection. This was a contrast from the results obtained in H1299 cells which exhibited high gene silencing efficiency. In addition, peak luciferase activity was achieved at the same time point for both siEGFP and siMADP1 transfected cells, which implied that the virus spread was most likely not affected. Since a high silencing efficiency was not achievable for Vero cells, further analyses of the impact of MADP1 gene silencing in cultured cells on IBV replication were performed with H1299 cells only.

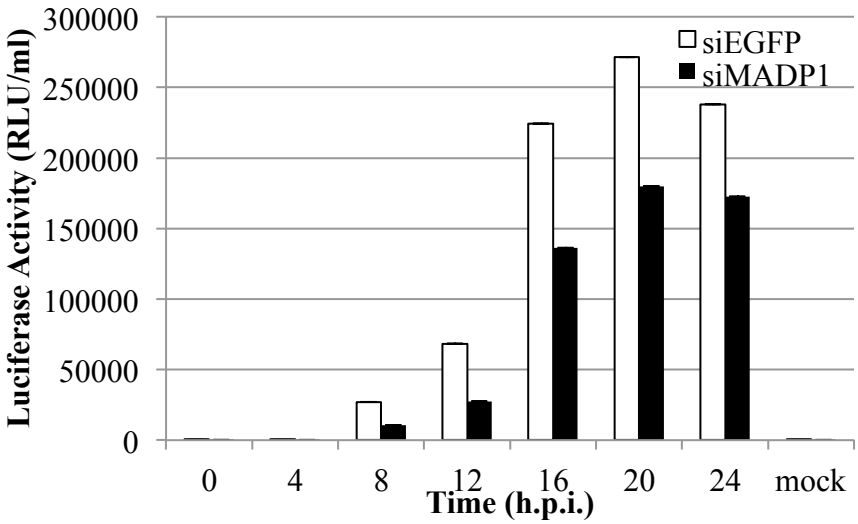

Figure 3.32: Silencing of MADP1 in Vero cells slightly reduced firefly luciferase activity produced by IBV-Luc infection. Vero cells transfected with siEGFP (control) or siMADP1 were infected with IBV-Luc virus. Luciferase activity of the cells were measured with 5 µl of lysate and expressed as Relative Luminescence Units per milliliter of lysate (RLU/ml). Samples measured were harvested at 0, 4, 8, 12, 16, 20, 24 hours post infection (h.p.i.). Error bars with standard deviation between the readings were included but too narrow to be seen. Maximum luciferase activity in MADP1 silenced cells was less than 70% of what was achieved in control cells transfected with siEGFP. A representative result of three independent experiments was shown.

3.7.4 The silencing of MADP1 gene correlates to a reduction in virus titre and viral protein expression

To further examine the impact of MADP1 silencing upon IBV replication in H1299 cells, time course experiments were performed using IBV-Luc virus several times and the most representative set of data was chosen to be presented. The impact of MADP1 gene silencing on IBV replication on general was analyzed by virus titration and viral protein production in addition to luciferase gene expression of cells infected with IBV-Luc virus. Monolayers of H1299 cells grown in 6-well plates to a confluency of 30% was transfected with either siEGFP (control) or siMADP1 using Dharma*FECT*® 2 twice. The medium containing the transfection mix was replaced with fresh culture

medium (with serum) 24 hours after the second transfection. The cells were infected 72 hours after the first transfection and the virus was replaced with fresh serum-free medium 2 hours after infection.

Viability of the transfected cells just before infection was determined to be approximately 92%, as assessed by cell counting coupled with trypan blue staining using Countess® Automated Cell Counter from Invitrogen (Carlsbad, CA, USA), for both types of transfected cells. Samples were harvested at 4, 8, 12, 16, 20 and 24 hours post-infection with the appropriate method. For virus titration, the cells with its medium were subjected to three freeze/thaw cycles and 0 h.p.i. samples were harvested after 5 minutes of incubation with the virus at 37°C. Mock-infected samples were not collected for virus titration assay. For luciferase assay and viral protein analysis, the cells were lysed with 200 µl of Lysis Buffer.

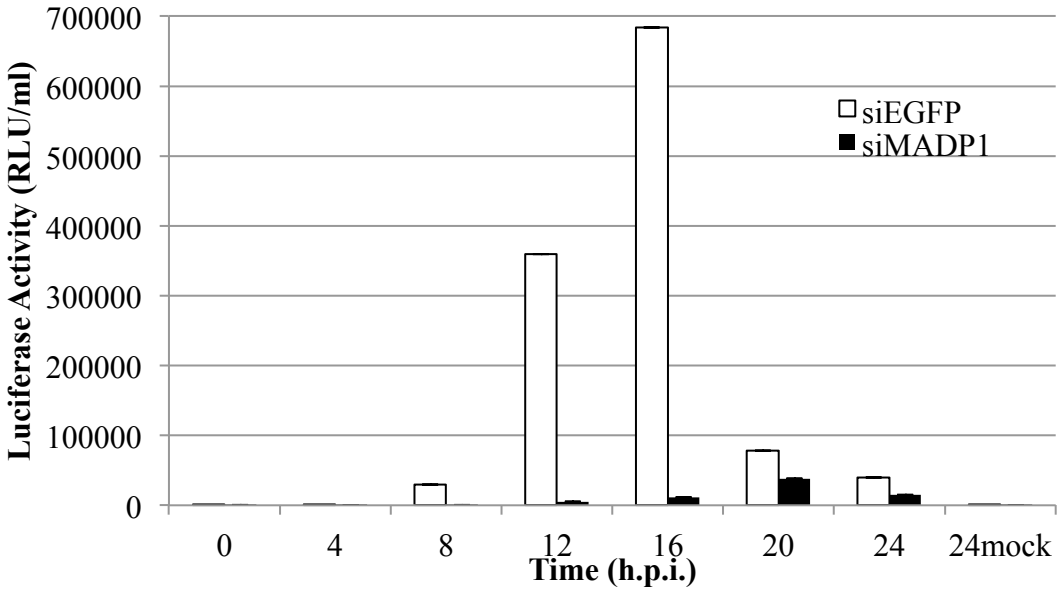

Figure 3.33: Replacement of culture medium after transfection increased luciferase activities of cells infected with IBV-Luc virus. Luciferase activity of the cells were measured with 5 µl of lysate and expressed as RLU/ml. Samples measured were harvested at 0, 4, 8, 12, 16, 20, 24 h.p.i.. Error bars with standard deviation between the readings were included but too narrow to be seen Maximum luciferase activity in MADP1 silenced cells was less than 6% of what was achieved in control cells transfected with siEGFP. A representative result of four independent experiments was shown.

As the experiment protocol was changed slightly, with the inclusion of an additional medium change 24 hours after the second siRNA transfection, 24 hours before the virus infection, the luciferase gene expression was assessed by luciferase assay using the cell lysate samples as shown in Figure 3.33. It was found to show a similar trend as reported in section 3.7.2 earlier.

From the luciferase assay results, it appeared that the additional medium change included in the experiment increased the luciferase activities attained by the assayed samples and shifted the peak luciferase activity recorded for siEGFP transfected cells, from 20 h.p.i. to 16 h.p.i.. These observations could be an indication of an improvement in the general condition of the cells which resulted in greater infectivity of the virus in the transfected cells. In addition, there was a drastic drop in luciferase activity from 16 h.p.i. to 20 h.p.i. for siEGFP transfected cells which was due to the widespread detachment of infected cells as a result of cell death. This could also be attributed to the greater infectivity of the virus, resulting in a faster progression of infection compared to what was presented in Figure 3.31, which no such drastic change in luciferase activity was recorded.

Virus titration was performed using an end-point dilution assay and calculating the 50% tissue culture infectious dose ($TCID_{50}$), or the dilution of virus at which 50% of cultured cells would be infected. Log_{10} $TCID_{50}$ values calculated for samples harvested at each time point were plotted on a graph as shown in Figure 3.34.

The amount of virus present in the medium during infection (0 h.p.i.) was similar for both kinds of transfected cells and both of them experienced a drop in virus titre at 4 h.p.i. to a similar level. The drop in virus titre was most likely due to the removal of virus at 2 h.p.i. compounded by degradation of input virus particles before progeny virus was produced. It was observed at the end of the infection (24 h.p.i.), siMADP1 transfected cells produced a virus titre what was more than 10-fold lower compared to siEGFP transfected cells. The averaged peak virus titre produced by siMADP1 transfected cells was also more than 10-fold below that of siEGFP transfected cells although both occurred at the same time point, 12 h.p.i.. These observations demonstrated that despite having a similar amount of input virus (0 and 4 h.p.i.), H1299 cells with less MADP1 protein expression produced virus titres that were consistently lower than cells which had normal MADP1 protein expression (from 8 h.p.i. to 24 h.p.i.).

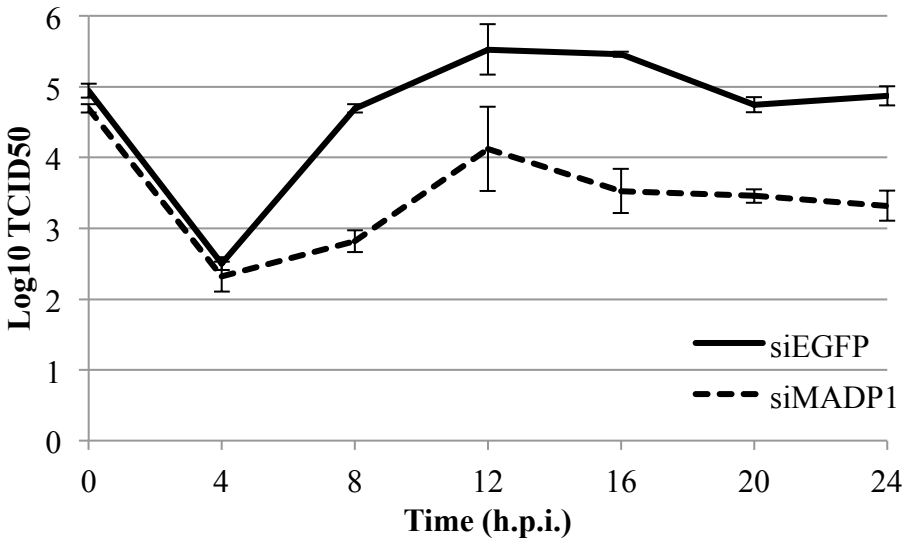

Figure 3.34: The silencing of MADP1 gene expression reduced the production of infectious particles. Virus titres at each specified time point for both siEGFP and siMADP1 transfected cells were represented as $\log_{10}$ $TCID_{50}$ values. Graph was plotted with the average values obtained from three titration assays and the error bars with standard deviation between the results were included. A representative result of four independent experiments was shown.

Western blot analysis on the viral structural proteins, 20 µl (10%) of lysate for each sample was resolved by SDS-PAGE using either an 8% or a 12% gel. For an assessment of viral protein production, the detection of IBV S and N proteins were performed with polyclonal serum antibodies, α-S and α-N. Polyclonal serum antibody to MADP1 (α-MADP1) was used to detect endogeneous MADP1. Actin and β-tubulin used as loading controls were detected with commercial antibodies, α-actin and α-β-tubulin, respectively. Samples for 20 h.p.i. and 24 h.p.i. of siEGFP transfected cells (MADP1 (+)) were not included as most of the cells have detached by 20 h.p.i. so the total protein loaded would be too different from the rest of the samples.

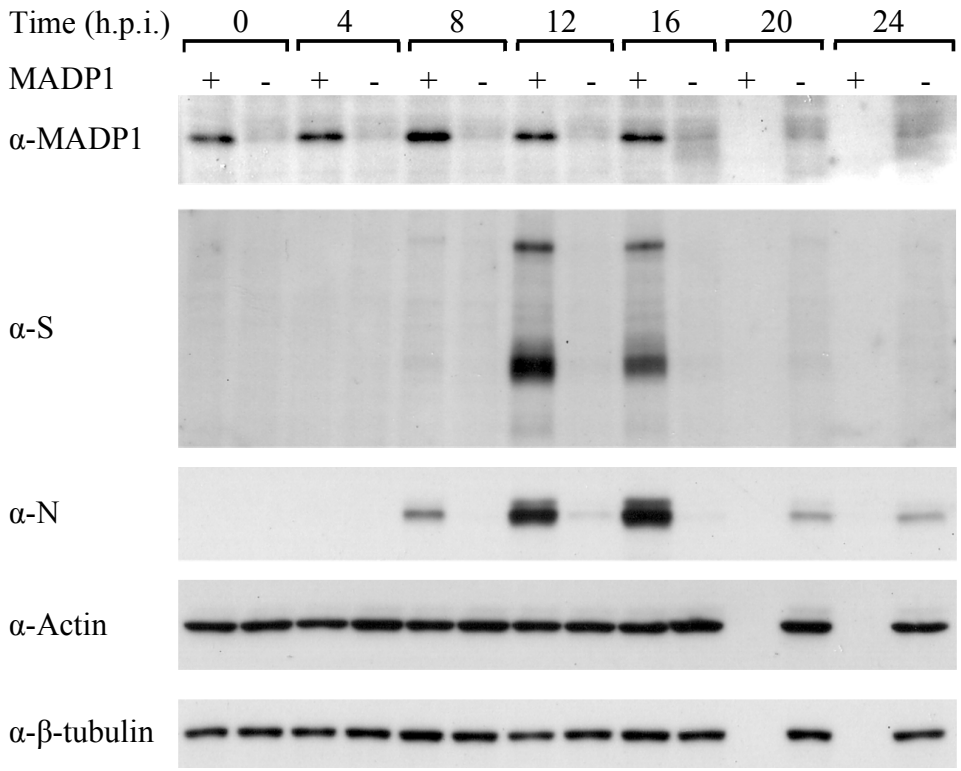

Figure 3.35: The silencing of MADP1 in H1299 cells with siMADP1 reduced the expression of viral structural genes S and N drastically. Samples which expressed normal level of MADP1 (siEGFP transfected) were indicated with (+) and samples which had MADP1 silenced (siMADP1 transfected) were indicated with (-). 20 h.p.i. and 24 h.p.i. samples for siEGFP transfected cells were not included as most cells have detached by 20 h.p.i.. A representative result of four independent experiments was shown.

As depicted in Figure 3.35, viral structural protein, S, was only detectable in siMADP1 transfected cells (MADP1 (-)) from 16 h.p.i. onwards at extremely low levels and N protein from 12 h.p.i. onwards, also at a low level. Densitometric analyses on the blots indicated a reduction by more than 80% of structural protein expression in MADP1 (-) cells compared to siEGFP transfected cells (MADP1 (+)).The expression of MADP1 was also reduced by about 50 to 80% in MADP1 (-) cells.

These results corresponded well to the results from luciferase assays performed on the same samples (Figure 3.33) which indicated an extremely low level of viral protein production. Hence, it could be concluded that the silencing of MADP1 in H1299 cells on general exerted a great impact on the production of viral proteins and the progeny virus particles.

3.7.5 Silencing of MADP1 with siRNA resulted in the absence of CPE upon IBV infection

Direct visualization of the infected cells at the stipulated time points was also conducted before the samples were harvested for the various analyses. Infected cells were observed by phase contrast microscopy at a magnification of 100X and images were captured with a digital microscope camera attached to the light microscope. Representative images captured four chosen time points, 0 h.p.i., 12 h.p.i., 16 h.p.i. and 20 h.p.i. which exhibited the most changes in cell morphologies were presented in Figure 3.36.

H1299 transfected with siEGFP (control) exhibited cytopathic effects (CPE) from 12 h.p.i. which reached a peak at 16 h.p.i. when all the cells formed syncytia, followed by the detachment of dead cells at 20 h.p.i.. The image captured of siEGFP transfected cells at 20 h.p.i. in particular supported the conclusion that the drastic drop of luciferase activity recorded for siEGFP transfected cells at 20 h.p.i. in section 3.7.4 was due to the detachment of dead cells. Also, the peak luciferase activity recorded coincided with the attainment of 100% CPE in siEGFP transfected cells.

CPE was conspicuously absent in cells transfected with siMADP1 at every time point observed which was a stark contrast to what was observed for the control experiment. This was true even at 20 h.p.i., when the peak luciferase activity was recorded in section 3.7.4 for the siMADP1 transfected cells. This observation indicated that the spread of IBV infection was mitigated by the silencing of MADP1 gene expression with siMADP1.

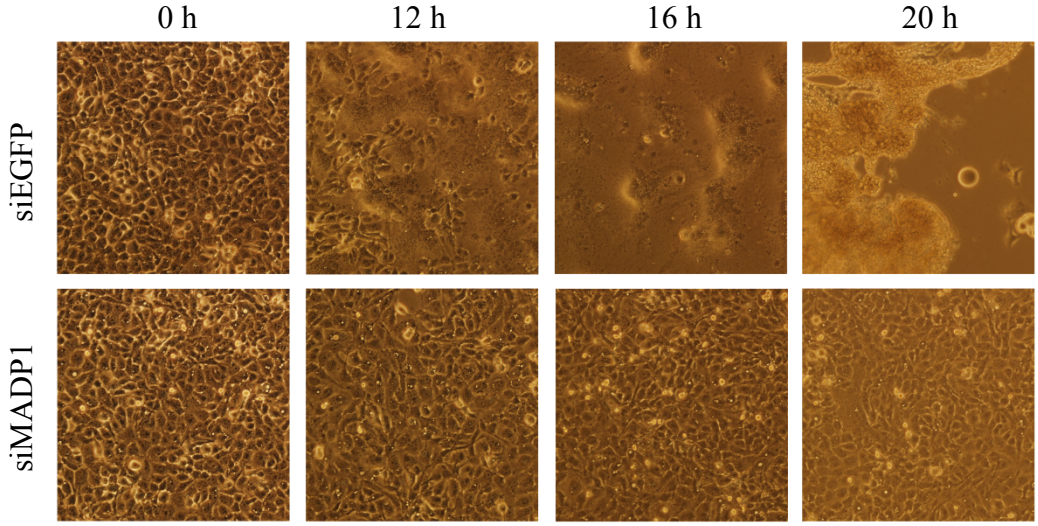

Figure 3.36: Silencing of MADP1 using siRNA resulted in the absence of cytopathic effects (CPE) after infection with IBV-Luc virus. H1299 cells transfected with siEGFP exhibited regular CPE while none appeared in cells transfected with siMADP1. A representative set of images from four independent experiments was shown.

3.7.6 IBV RNA replication and transcription were reduced in MADP1-silenced cells.

Samples for RNA analyses were also harvested using Trizol® from the same time course experiment described in section 3.7.4. RT-PCR was performed to amplify both positive and negative sense sgRNAs (mRNA 4 and 5) as well as negative sense gRNA (mRNA 1) as described in section 2.14. RT-PCR was not performed on 20 h.p.i. and 24 h.p.i. siEGFP transfected samples (MADP1 (+)) as the infected most cells have already detached and no RNA could be extracted. The amplified PCR products were resolved by agarose gel electrophoresis using a 1% gel and stained by ethidium bromide as shown in Figure 3.37.

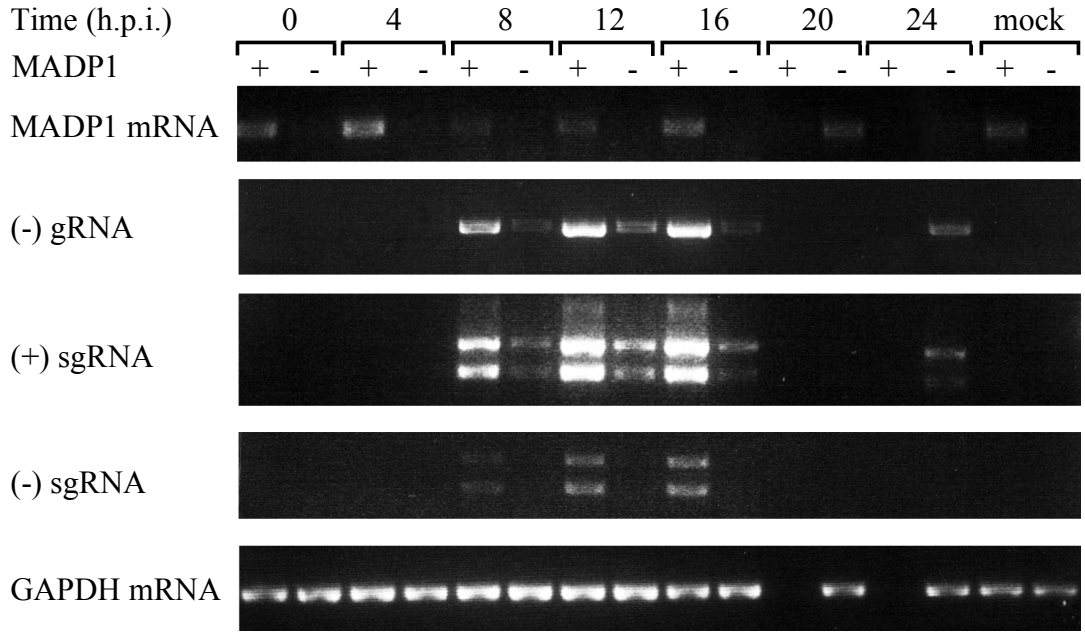

Figure 3.37: MADP1 silencing with siMADP1 reduced the amount of viral gRNA and sgRNAs produced. H1299 cells were transfected twice with siEGFP (MADP1 (+)) or siMADP1 (MADP1 (-)) and infected with IBV-Luc virus. Samples were harvested at 4 h-intervals, and mock-infected cells were used as negative control. A representative result of duplicate PCRs from four independent experiments was shown.

The silencing of MADP1 expression using siMADP1 clearly diminished the amount of viral mRNAs produced during the infection by IBV-Luc virus. Densitometric analyses identified a reduction between 40-80% of MADP1 mRNA achieved by siMADP1 which varied between the time points assessed. The lower levels of MADP1 mRNA in siMADP1 transfected cells (MADP1 (-) samples) correlated with a reduction of between 70-90% of negative stranded viral gRNA (gRNA (-)), 40-80% of negative stranded sgRNA (sgRNA (-)) and 50-90% of positive stranded sgRNA (sgRNA (+)) compared to siEGFP transfected cells (MADP1 (+) samples). These observations point out the significance of MADP1 in viral RNA synthesis at an early stage, negative strand sgRNA synthesis.

3.8 The Impact of MADP1 Silencing on IBV Infection using siRNA was not an Off-Target Effect

The experiments conducted to assess the impact of MADP1 silencing on IBV infection were performed with a high concentration of siRNA with a single target sequence, siMADP1, which had not been tested for additional effects other than a reduction in MADP1 protein expression. Hence, an additional experiment was performed to rule out the possibility that the compromised infectivity phenotype seen in siMADP1 cells was not due to an off-target effect of the siRNA used.

3.8.1 MADP1 silencing using siRNA pools reduced luciferase gene expression in IBV-Luc infected H1299 cells

Table 3.1: Volumes (in microlitres) of each 50 μM siRNA used in the different siRNA pool combinations.

Combi/siRNA	**siMADP1**	**si1**	**si2**	**si3**	**si4**
siCombi1	0.5	0.5	0.5	0.5	0.5
siCombi2	0.5	1	1	-	-
siCombi3	-	0.5	1	1	-
siCombi4	-	-	0.5	1	1
siCombi5	1	-	-	0.5	1
siCombi6	1	1	-	-	0.5

Evaluation of the effect of MADP1 silencing on IBV-Luc virus infection was performed with siRNA pools composed of four commercial siRNAs and siMADP1, each targeting a different region of the MADP1 mRNA in different combinations. H1299 cells grown to a confluency of 30% were transfected twice with 250 pmoles of siEGFP, siMADP1 or one of the six siRNA pools (siCombi1 to 6), 24 hours apart. The composition of each siRNA pool is listed in Table 3.1.

The medium containing the transfection mix was changed to fresh culture medium (containing serum) 24 hours after the second transfection and the cells were infected with IBV-Luc virus at MOI ≈ 1. Infected cells were harvested with 200 μl of Lysis Buffer at 20 h.p.i. and luciferase assay was performed to determine the firefly luciferase activity in each sample.

As shown in Figure 3.38, all siRNA pools used, which contained three out of a total of five siRNA duplexes, were able to reduce luciferase activity by more than 65% compared to siEGFP transfected cells. Marked reductions of luciferase activity by more than 90% was seen in four of the siRNA pools used (siCombi1, siCombi2, siCombi5 and siCombi6), which were comparable to what was achieved by homogeneous siMADP1. Although it was noted that combinations which did not contain siMADP1 (siCombi 3 and siCombi4) exhibited higher levels of luciferase activity (about 30% of siEGFP), the effect seen was still significant.

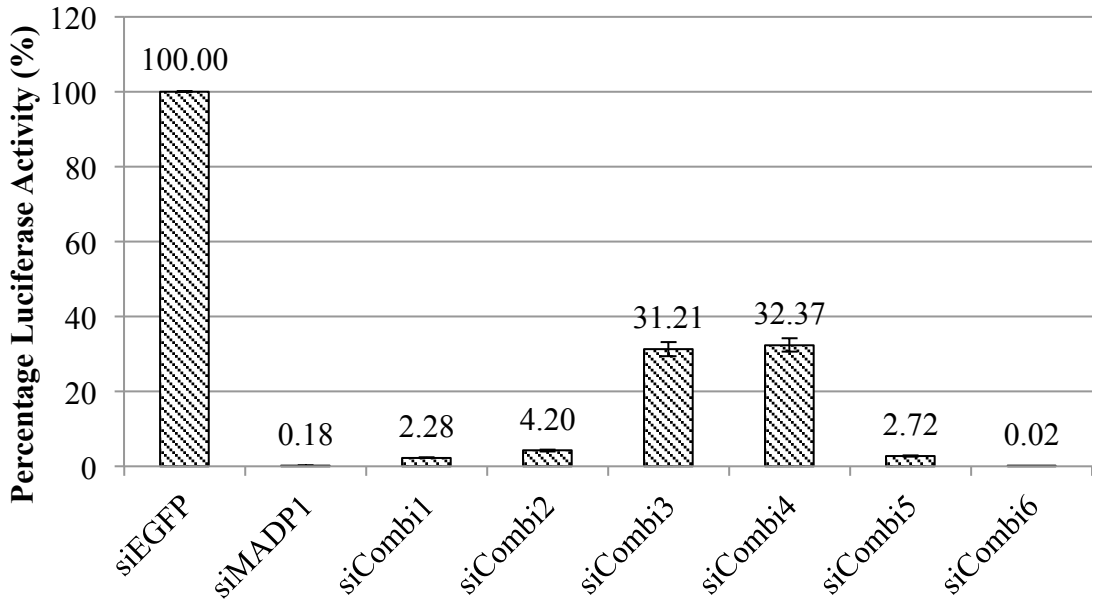

Figure 3.38: Silencing of MADP1 using different combinations of siRNA pools reduced luciferase expression from IBV-Luc recombinant virus. 250 pmol of either siRNA to EGFP or siRNA pools against Madp1 were transfected into H1299 cells twice and infected with IBV-Luc recombinant virus at 72 h after the first transfection. The averaged luciferase activity of siRNA pool or siMADP1 transfected cells were expressed as a percentage of what was obtained by siEGFP transfected cells and standard deviation of three separate measurements of each sample were included as error bars. A representative result of two independent experiments was shown.

3.9 Expression of a Silencing-Resistant mutant MADP1 in a stable MADP1 Knock-Down Cell Clone Enhances IBV Replication

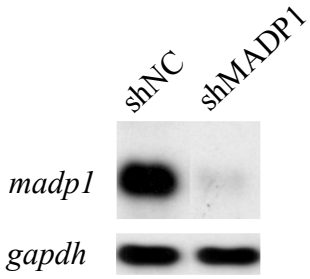

Figure 3.39: The mRNA level of MADP1 in shMADP1 cells were much lower compared to shNC cells. Northern blotting of total RNA extracted from shNC and shMADP1 cells detected using DIG-labeled double-stranded DNA probes. A representative result of two independent experiments was shown.

A stable cell clone expressing short hairpin RNA to MADP1 (shMadp1), which had the same target sequence as siMADP1, was selected from H1299 cells. A stable cell clone expressing short hairpin RNA which does not target any human gene (shNC) was also selected from H1299 cells using the same conditions. The mRNA levels of MADP1 (*madp1*) and housekeeping gene GAPDH (*gapdh*) were confirmed using northern blot in Figure 3.39 which showed that *madp1* was much lower in shMADP1 cells compared to shNC cells.

3.9.1 IBV RNA synthesis was reduced in stable MADP1 knock-down cells

To ensure that the stable cell clone exhibits a similar phenotype to transiently silenced cells, the effect of MADP1 knock-down on IBV infection was established by comparing the amount of viral RNA synthesized during an infection in shMADP1 cells with that of shNC cells. Both shMADP1 and shNC cells grown to confluency were infected with wild-type IBV virus and the virus-containing medium was replaced at 2 h.p.i.. Samples were harvested by lysis with Trizol® at 8, 10, 12, 14, 16,

20 h.p.i. and total RNA was extracted from each of them. 0 h.p.i. samples were harvested after 5 minutes of incubation with the virus-containing medium. Northern blot was performed using DIG-labeled double-stranded DNA probe which hybridizes to both positive and negative sense IBV 3'-UTR, present in all viral mRNAs. Housekeeping gene GAPDH mRNA (*gapdh*) was also detected to serve as a loading control.

As presented in Figure 3.40, the results reflected that on general, silencing of MADP1 with shMADP1 reduced the total viral mRNA production up to 16 h.p.i.. All species of sgRNA (*mRNA 2* to *mRNA 6*) were equally affected. The amount of gRNA (*mRNA 1*) was extremely low and the bands were too weak to be visualized, hence it was not indicated on the blot. The total amount of virus mRNA was higher in shMADP1 cells compared to shNC cells at 20 h.p.i. due to the greater efficiency of the virus infection in shNC cells which resulted in most cells having experienced cell death and have detached while the infection continued in shMADP1 cells which were still surviving.

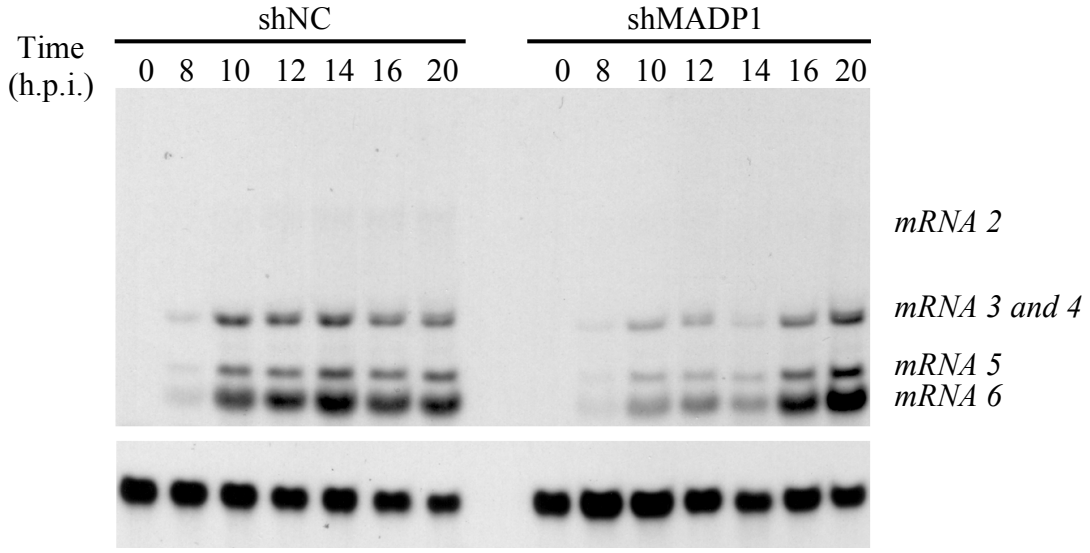

Figure 3.40: The production of virus-specific mRNAs was reduced in shMADP1 cells compared to shNC cells. Northern blot of IBV infected shNC and shMADP1 cells showing viral mRNAs 2 to 6 and GAPDH mRNA (*gapdh*). A representative result of two independent experiments was shown.

3.9.2 Over-expression of silencing-resistant MADP1 in shMADP1 cells enhanced IBV replication

The shMadp1 cells were transfected with constructs expressing FLAG-tagged wild type MADP1 (FM), triple residue mutant (FM(YVF)), two mRNA mutants resistant to silencing by shMADP1 based on wild type MADP1 (FMmut) and the triple residue mutant (FMmut(YVF)), negative vector controls expressing FLAG (F) and EGFP (E). The two silencing-resistant mutants were constructed by mutating the siRNA-targeting sequence with degenerate codons at several positions, so that the protein sequence of MADP1 was maintained while rendering the mRNA resistant to the effect of the shRNA. The transfected cells were subsequently infected with IBV-Luc recombinant virus and harvested at 19 h.p.i. with 200 µl of Lysis Buffer.

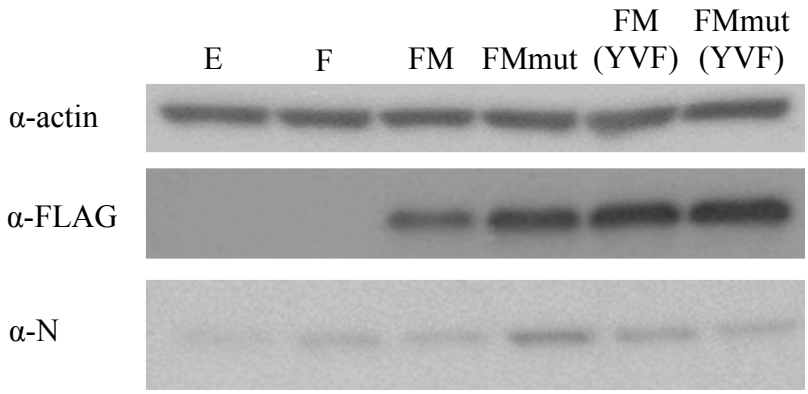

Figure 3.41: Over-expression of shRNA-resistant MADP1 in stable MADP1 knock-down cells (shMADP1) enhanced viral protein production. IBV N protein was used as an indicator of viral protein production and actin as a loading control. Over-expressed MADP1 proteins were detected with an antibody to the FLAG-epitope tag. A representative result of five independent experiments was shown.

Western blot was performed and over-expressed MADP1 was detected with commercial α-FLAG-HRP antibody, IBV N protein was detected with a polyclonal serum antibody, α-N and loading control actin was detected with a commercial α-

actin antibody. The results showed an obvious increase in the amount of IBV N expression in shMADP1 cells over-expressing silencing-resistant wild-type MADP1 (FMmut) as well as a slight increase in cells over-expressing both normal triple residue mutant (FM(YVF)) and silencing-resistant triple residue mutant (FMmut(YVF)) (Figure 3.41).

An assessment of the luciferase activity of total cell lysates presented in Figure 3.42 showed that the over-expression of triple residue mutants FM(YVF) and FMmut(YVF) resulted in a slight increase of the luciferase activity in shMADP1 cells by about 15%. Over-expression of silencing-resistant wild-type MADP1 (FMmut) on the otherhand resulted in a more drastic increase of the luciferase activity, by about 40% compared to control cells over-expressing FLAG (F) only. As expected, the over-expression of wild-type MADP1 (FM) did not result in a deviation from the luciferase activity recorded for cells over-expressing FLAG (F). It was however noted that the over-expression of EGFP resulted in a decrease of luciferase activity compared to FLAG expressing cells (F). This phenotype could have arisen from the cellular toxicity of the protein when expressed at high levels.

The observations made in this section as well as section 3.8 provide evidence that the phenotype observed from the silencing of MADP1 in H1299 cells using siMADP1 (sections 3.7.4, 3.7.5 and 3.7.6) on IBV infection was not the result of an off-target effect from the siRNA used. These findings affirmed the impact of MADP1 on coronavirus RNA synthesis through its interaction with the positive sense 5'UTR of IBV in H1299 cells.

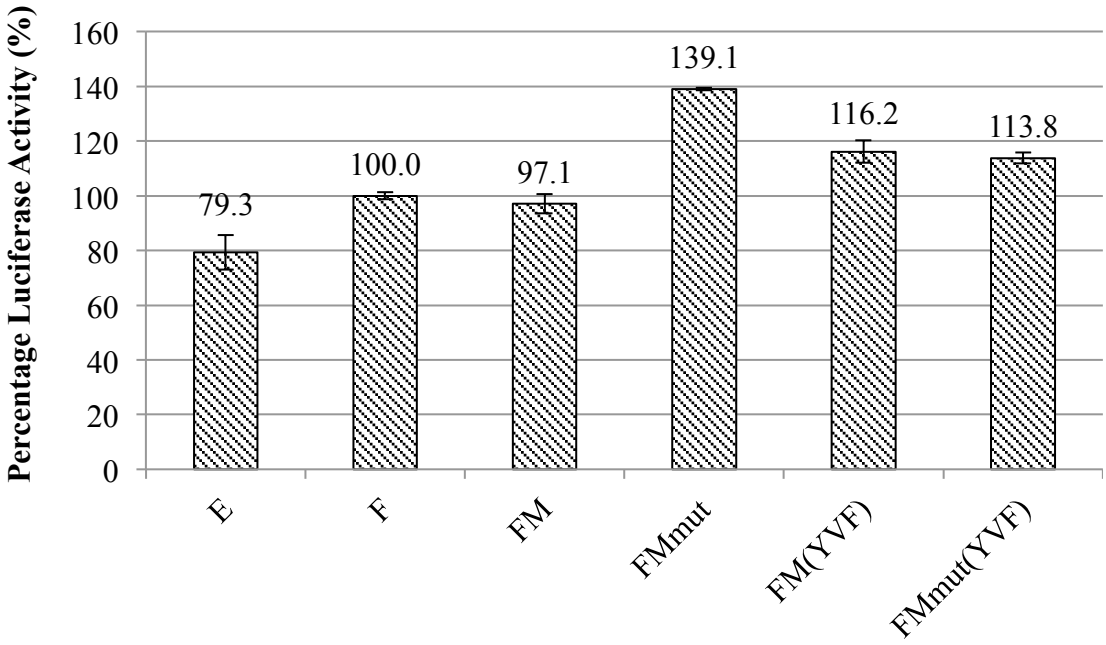

Figure 3.42: Over-expression of shRNA resistant MADP1 enhanced viral infectivity as indicated by the increase in luciferase activity. Averaged luciferase activity recorded for each cell lysate showed a marked increase in luciferase activity when silencing-resistant MADP1 was over-expressed in shMADP1 cells. Luciferase activity of FLAG over-expressing cells (F) was used as a benchmark for 100% activity. Luciferase activity recorded for cells expressing MADP1 proteins and EGFP were expressed as percentages of what was achieved for F. Standard deviation of three separate recordings was included. A representative result of five independent experiments was shown.

3.10 MADP1 Interacts Weakly with Human Coronavirus OC43 (HCoV-OC43) 5'-UTR (+)

The screen in which MADP1 was identified as a candidate that could interact with the coronavirus untranslated region was performed with the SARS-CoV 5'-UTR (+). It was later observed that although MADP1 interacted with both SARS-CoV and IBV 5'-UTR using the biotin pull-down assay described in section 3.2.4, the interaction was rather weak for the former. A comparison of predicted stem loop I structures from both coronaviruses indicated a marked difference in both their primary sequence and secondary structure as illustrated in Figure 3.43. Hence, a third coronavirus, HCoV-OC43 (accession AY391777), whose stem loop I structure and sequence deviated further from IBV than SARS-CoV, was also assessed for its binding to MADP1.

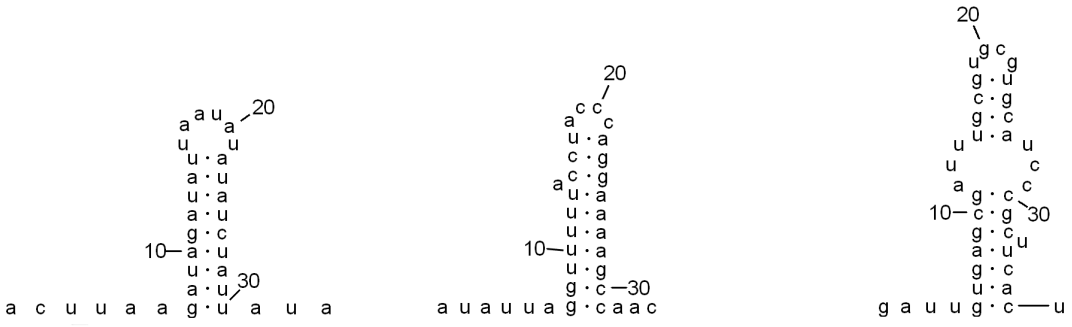

Figure 3.43: Predicted stem loop I structures from IBV, SARS-CoV and HCoV-OC43.

A biotin pull-down assay was performed using FLAG-MADP1 or EGFP over-expressing H1299 cell lysates with biotinylated IBV, SARS-CoV or HCoV-OC43 full-length 5'-UTR (+) probes. As shown in Figure 3.44, it was found that the binding of MADP1 to the 5' UTR of HCoV-OC43 was as weak, if not weaker than SARS-

CoV. All three probes did not bind to negative control EGFP. A comparison of the predicted stem loop I structures revealed that the stem loop I of HCoV-OC43 contained a bulge which encompassed a larger area of the stem compared to SARS-CoV while bulges caused by unpaired bases in the stem region were conspicuously absent from the IBV stem loop I. In addition to the lack of structural similarity between the stem loop I of the three coronaviruses, there was a lack of sequence similarity as well (Figure 3.44).

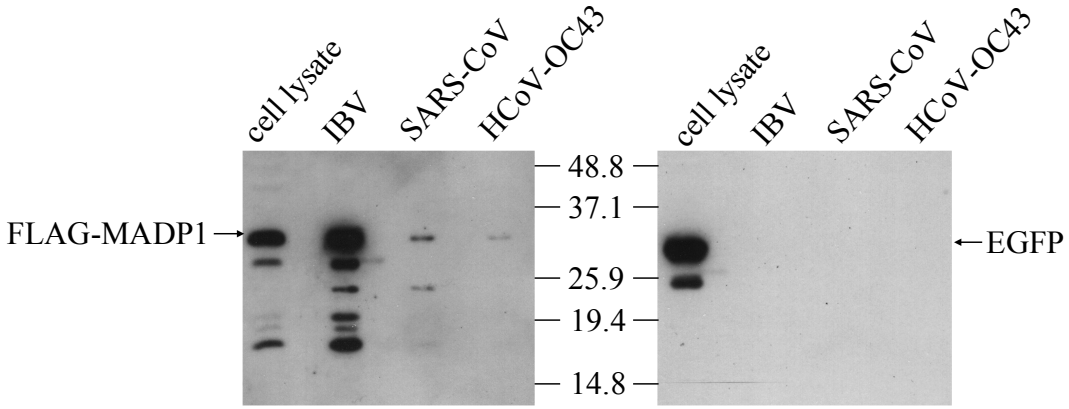

Figure 3.44: MADP1 binds weakly to both SARS-CoV and HCoV-OC43 5'-UTR (+) in a biotin pull-down assay. Biotin pull-down assay was performed using over-expressed FLAG-MADP1 or EGFP (negative control) with biotinylated 5'-UTR (+) probes of the three coronaviruses. IBV 5'-UTR bound strongly to MADP1 while the other two probes only interacted weakly. Bound proteins were resolved by SDS-PAGE with a 12% gel and western blot detection was performed with α-FLAG-HRP (FLAG-MADP1) or α-EGFP. A representative result of three independent experiments was shown.

3.11 MADP1 Interacts with IBV 3'-UTR (+)

The interaction between MADP1 and the IBV 5'-UTR (+) had been studied in-depth in the earlier sections of this chapter but it was not known if MADP1 could interact with other untranslated regions of the IBV genome. HnRNP A1 as mentioned in section 1.3.5, was reported to be required for viral RNA transcription and could interact with multiple untranslated regions of the MHV genome in both polarity. Hence, it was of interest to investigate if MADP1 too, could interact with more than one untranslated region of the IBV genome. A biotin pull-down assay was performed with FLAG-MADP1 or EGFP (non-binding control) over-expressing H1299 cell lysate and biotinylated full-length IBV 5'-UTR (+), 5'-UTR (-) and 3'-UTR (+) probes. The proteins bound by the streptavidin beads were resolved by SDS-PAGE. Western blot was performed and FLAG-MADP1 was detected with α-FLAG-HRP, EGFP with α-EGFP antibodies.

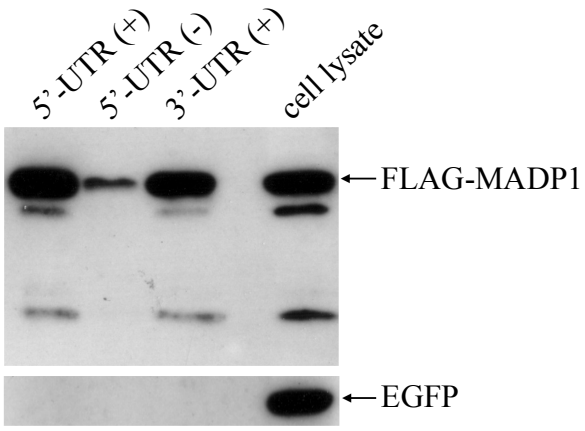

Figure 3.45: MADP1 interacted strongly with both 5'-UTR (+) and 3'-UTR (+) but weakly with 5'-UTR (-). MADP1 was co-purified with IBV 5'-UTR (-) at low efficiency and 3'-UTR (+) at high efficiency in a biotin pull-down assay. EGFP did not co-purify with any of the probes used. Biotin pull-down assay was performed with biotinylated RNA of the IBV 5'-UTR (+), 5'-UTR (-) and 3'-UTR (+). Bound proteins were resolved using a 12% gel by SDS-PAGE and detected using the appropriate antibodies by western blot. A representative result of three independent experiments was shown.

As illustrated in Figure 3.45, MADP1 bound to most efficiently to 5'-UTR (+) followed by 3'-UTR (+) with which it also exhibited strong binding, then 5'-UTR (-) which it bound relatively weakly. No binding was observed for EGFP to all biotinylated probes used in the assay. This piece of information emphasized the possibility that MADP1 could also interact with IBV 3'-UTR (+) during viral RNA synthesis.

3.12 A Correlation of MADP1 Expression Level to IBV Infectivity could not be Established

Gene expression profiles vary between different cell lines and the infectivity of viruses of each cells differs as well. It would certainly institute MADP1 as a critical genetic marker for infection susceptibility if a correlation could be established between its expression levels to the infectivity of the cell line by IBV. This prompted a trial experiment to assess expression level of MADP1 in several human cell lines (mostly of carcinoma origin) and to check if the cell lines could be infected by IBV virus. Adherent cells grown to between 90% and 100% confluency in 60 mm dishes were lysed with 200 µl of 2X SDS loading dye. Suspension cells were grown to confluency when clumping was observed, sedimented by centrifugation at 1000 rpm for 3 minutes then lysed. The cell lysates were resolved by SDS-PAGE and detection of MADP1 and loading control actin was performed using polyclonal serum antibody α-MADP1 and commercial α-actin antibodies.

As shown in Figure 3.46, an interesting observation was made in the detection of higher molecular weight bands in the cell lines HuH-4 (hepato-cellularcarcinoma), MRC-5 (lung fibroblast) and Sk-Hep1 (hepato-adenocarcinoma) which was also present in H1299 (lung cancer). The molecular weight of the band suggested that it could be a dimer of MADP1 which could not be dissociated by the reducing agent DTT which was present in the loading dye. This was interesting as MADP1 did contain a RRM dimerization site at amino acid residues 83 and 84. Bands of molecular weights corresponding to neither the monomeric or dimeric mass of MADP1 were detected for the cell lines HCT116 (colorectal carcinoma), U937

(histiocytic lymphoma) and Y79 (retinoblastoma). As the identities of such higher molecular weight bands were unknown, it could only be speculated that they correspond to post-translationally modified MADP1.

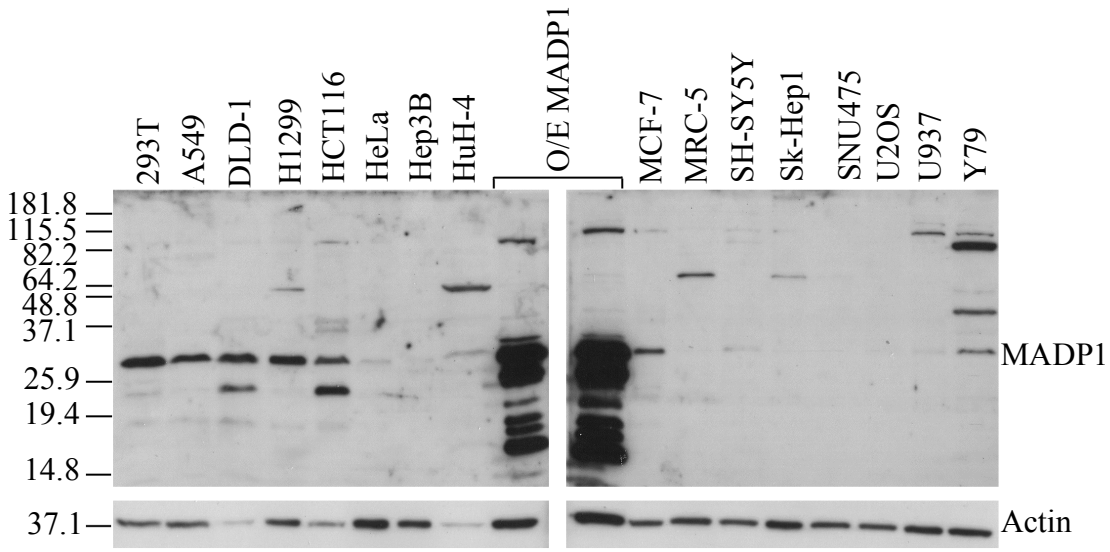

Figure 3.46: Western blot showing the amount of MADP1 and actin in 16 different cell lines. Over-expressed (O/E) MADP1 was included as a control for MADP1 detection by the antibody. Samples were resolved on two separate gels of the same percentage but antibody incubations and detection were performed together. A representative result of three independent experiments was shown.

Table 3.2: Band densities of MADP1 (normalized with band densities of actin for each cell line) in 16 cell lines classified by tissue of origin.

Tissue	**Cell Line (Band Density)**	**Tissue**	**Cell Line (Band Density)**
Liver	Hep3B (0.13), HuH-4 (1.05), Sk-Hep1 (0.01), SNU475 (0.01)	Cervix	HeLa (0.08)
Lung	A549 (1.5), H1299 (1.73), MRC-5 (0.02)	CNS	SH-SY5Y (0.10)
Colon	DLD-1 (7.83), HCT116 (2.01)	Bone	U2OS (0.08)
Kidney	293T (2.42)	Monocyte	U937 (0.03)
Breast	MCF-7 (0.72)	Retina	Y79 (0.36)

For densitometric analysis, only the band of the molecular mass 31 kDa was considered for quantitation for MADP1. Band density of MADP1 was normalized to

the amount of actin detected for each cell line and the cell lines were classified by their tissue of origin in Table 3.2.

CPE was observed in all cell lines except SNU475 (hepato-cellular carcinoma), U937 and Y79. Cell death was observed in SH-SY5Y but it could not be determined if it was due to CPE or that the cells did not survive due to the removal of serum during infection. Extensive CPE was observed for 293T, H1299, HeLa, Hep3B, MRC-5, Sk-Hep1 and U2OS. Moderate CPE was observed for DLD-1, HCT116 and HuH-4 and limited CPE was observed for A549. It appeared that tissues which do not form part of the normal tissue tropism of IBV could also be infected and that no clear relationship could be established between the infectivity of IBV and MADP1 expression or the type of tissue the cells originated from. This could be partly due to the fact that almost all of the cells were derived from cancerous tissues, with the exception of MRC-5, which expressed an altered proteome that could include the differential expression of MADP1. Hence, the results derived from this trial experiment were inconclusive and a correlation between the expression of MADP1 and IBV infectivity could not be established.

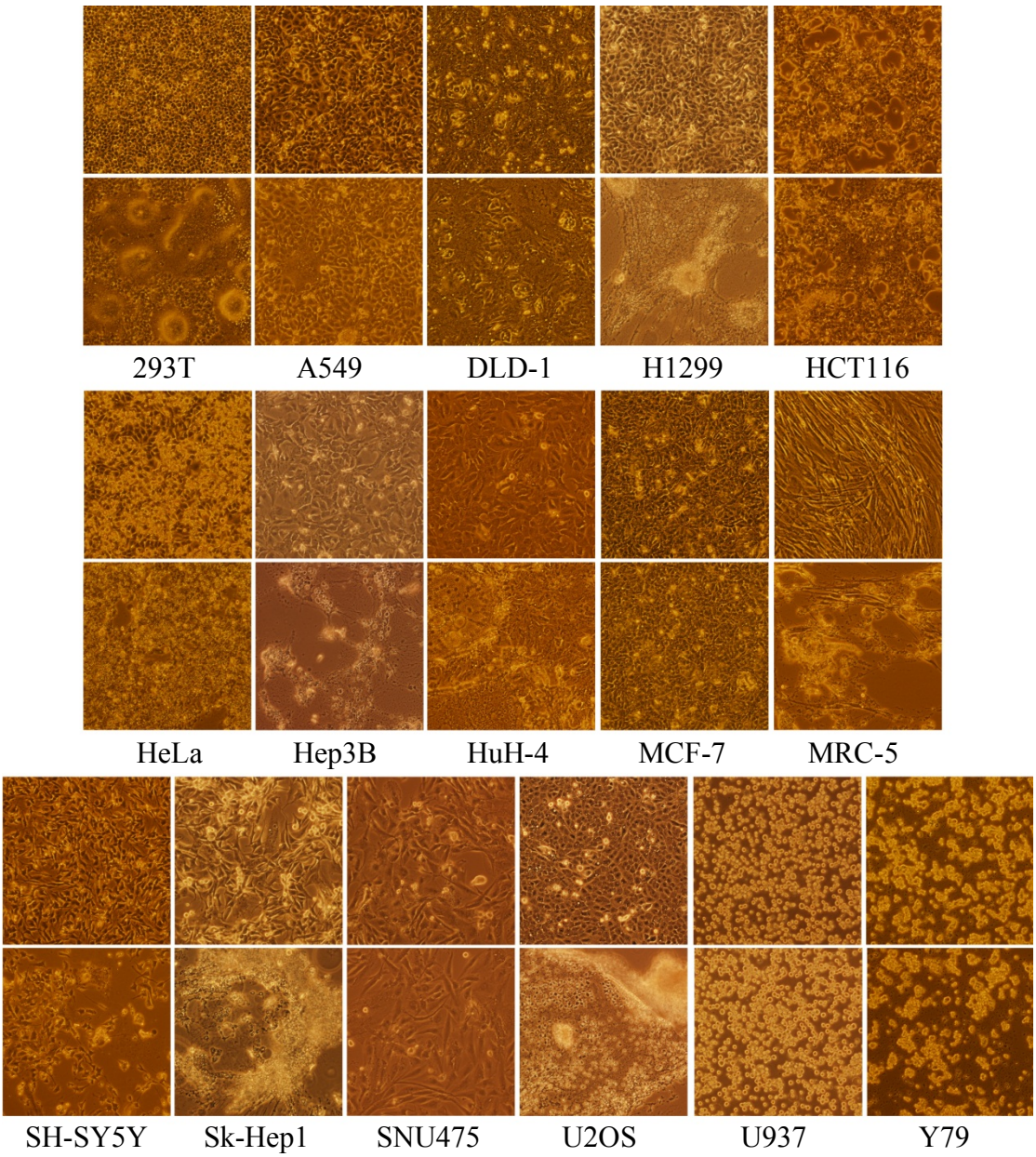

Figure 3.47: All cell lines exhibited CPE upon IBV infection except SNU475, U937 and Y79. Images captured of 16 different cell lines infected with IBV at 0 h.p.i. (top image) or 24 h.p.i. (bottom image). Extensive CPE was observed for 293T, H1299, HeLa, Hep3B, MRC-5, Sk-Hep1 and U2OS. Moderate CPE was observed for DLD-1, HCT116 and HuH-4. Low CPE was observed for A549 and no discernable difference was observed for SNU475, U937 and Y79. Cell death was observed for SH-SY5Y but it could not be determined if it was caused by CPE or the lack of serum. A representative set of images taken from two independent experiments was shown.

3.13 Discussion

Previous studies on the involvement of host proteins in viral RNA synthesis have revealed a number of proteins which are able to interact with the untranslated regions of viral genomes (299,307-309,314,340). Some of these proteins may also interact with other viral proteins as well (303,304).

In this study, the interaction between human MADP1 and the SARS-CoV and IBV 5'-UTR was initially identified in the yeast (*S. cerevisiae*) system and subsequently confirmed using an *in vitro* RNA pull-down assay with IBV 5'-UTR. MADP1 (Genbank, BAB56132), a member of the U11/12 alternative snRNP of the minor spliceosome, was shown to be localized to the nucleoplasm but excluded from the nucleolus, but its role in RNA splicing remains to be determined (337). The GenBank entry of MADP1 stated that it contains two conserved RNA-binding domains, the RNA recognition motif (RRM) and universal minicircle sequence binding protein (UMSBP) domains (a zinc finger CCHC-type) (338). In addition, the GenBank entry for MADP1 also stated that the MADP1 RRM conserved domain interacts with nucleic acid residues via aromatic and hydrophobic side chains at its active site, which in the case supplied by phenylalanine 55 and valine 53, respectively. Tyrosine 13 may have acted as an anchor for the phosphate backbone via electrostatic interactions.

A deeper look at the details of this interaction revealed that the RNA recognition motif, but not the zinc finger motif, of MADP1, is responsible for the interaction (Figure 3.26 and Figure 3.27). Using a competitive RNA binding assay based on the RNA pull-down assay, it was found that the interaction between MADP1 and IBV 5'-UTR (+) was specific (Figure 3.19). This conclusion was derived from the

observation of a non-specific unlabeled RNA probe, EGFP (-), being unable to compete for binding to MADP1 with the biotinylated IBV 5'-UTR (+) probe. The three active-site residues predicted for MADP1 were also subsequently shown to be vital for MADP1 to bind IBV 5'-UTR (+) (Figure 3.28). These findings collectively asserted the interaction between MADP1 and the IBV 5'-UTR (+). In addition, the binding site for MADP1 on the IBV 5'-UTR had been determined in this study to be its stem loop I (Figure 3.22) and that the integrity of the stem loop structure is vital for the interaction to occur (Figure 3.24).

Although MADP1 was reported to be a nuclear protein (338), it could be detected in the cytoplasm of IBV-infected cells by both indirect immunofluorescence and western blot. The staining pattern for MADP1 coincidentally, appeared to partially overlap with that of *de novo* synthesized viral RNA, which marks the location of the viral RTCs in infected cells, in the presence of actinomycin D. Although a colocalization of MADP1 and viral RTCs could not be established, it was clear that MADP1 translocated to the cytoplasm during IBV infection.

Functional studies were conducted and it was found that the silencing of MADP1 resulted in a marked reduction in syncytium formation upon IBV infection (Figure 3.36). A closer examination revealed that the synthesis of both gRNA and sgRNAs was compromised (Figure 3.37), resulting in a drastic reduction of viral structural protein expression and release of progeny virus particles, hence the overall reduction of viral infectivity in the cells. Hence, it could be concluded that MADP1 is required for viral RNA synthesis, including negative-strand synthesis, which occurs via discontinuous transcription.

As the functional studies were conducted using an untested, homogeneous siRNA, it was not known if the phenotype observed from the silencing was due to an off-target effect of the siRNA sequence used. A validation experiment using siRNA pools targeting different regions of MADP1, which was meant to minimize off-target effects (Figure 3.38). The results showed that the phenotype of reduced viral infectivity was reproducible with different siRNAs targeting the same gene.

Across different coronaviruses, the leader sequence situated in the extreme 5' end of the genome, is composed of stem loops I and II. Mutations introduced into either stem loop I or II resulted in non-viable viruses, impaired (sense and anti-sense) sgRNA synthesis, but not the full-length gRNA synthesis (74,75). It was, however, observed in this study that silencing of MADP1 did render an impact on gRNA synthesis, although to a lesser extent compared to sgRNA synthesis. This might have been a secondary effect of decreased sgRNA synthesis, as proteins encoded by sgRNAs may enhance viral RNA replication (135), or gRNA synthesis.

The leader sequence of coronaviruses spans the first two stem loops of the 5'-UTR, nucleotide residues 1 to 64 in IBV. The predicted structure of stem loop II indicated a strong secondary interaction, which is highly conserved across different groups of coronaviruses. The predicted stem loop I structure, on the other hand, appears to fold into a hairpin of low thermodynamic stability, shows a wider sequence variation and is characterized by the presence of bulges, non-canonical base pairing as well as a prevalence of A-U base pairing (341). It has been shown in MHV that the structural liability of stem loop I is a critical driving force in the 5'- and 3'-UTR interaction (75).

Comparing the predicted stem loop I structures of IBV to SARS-CoV and HCoV-OC43 (Figure 3.43), it was noted that there exists a difference in the loop sequence. In addition, IBV stem-loop I has a shorter stem and bulges are conspicuously absent, although the structure may be as unstable thermodynamically as that of SARS-CoV and HCoV-OC43, due to the extremely high prevalence of weak base pairing between A and U as well as the presence of a non-canonical base pair at the base of the stem (341). A trial experiment revealed that betacoronaviruses HCoV-OC43, SARS-CoV and gammacoronavirus IBV 5'-UTR (+) all bound to MADP1, albeit with different affinities (Figure 3.44). Hence, sequence and structural differences may be one of the possible explanations for the observation of a weaker binding between MADP1 and SARS-CoV or HCoV-OC43 5'-UTR than with IBV 5'-UTR. In fact, the relatively weaker binding of MADP1 to the stem loop I restoring mutant (5'-UTRΔ2M2) demonstrated in this study (Figure 3.24) supports that primary sequences in the 5'-UTR may play a certain role in this interaction.

While it seems that the strength of interaction between MADP1 and the coronavirus 5'-UTR is likely dependent upon both primary sequence and secondary structure of the RNA, the functional implication of the relatively weaker interaction between SARS-CoV 5'-UTR and MADP1 remains to be determined. This was not completed due to the lack of a higher containment facility required for the handling of live SARS-CoV. It is, therefore, yet to be demonstrated if this weaker binding dictates less dependency on MADP1 in SARS-CoV RNA replication and infectivity.

It was shown in section 3.11, in a trial experiment that MADP1 not only interacts with IBV 5'-UTR (+), it could also interact with other untranslated regions of the IBV

genome, strongly with the 3'-UTR (+) and weakly with 5'-UTR (-) (Figure 3.45). This new finding seemed to support the proposed function of MADP1 in viral negative-strand synthesis as hnRNP A1, a very well documented host protein for its function in MHV RNA synthesis, also interacted with coronavirus MHV genome at multiple regulatory regions (299). This common trait of multiple-site interactions between the hnRNP A1 and MADP1 with coronavirus MHV and IBV genomes respectively, could possibly facilitate the occurrence of template-switching during discontinuous transcription. The interaction of MADP1 with the other untranslated regions of IBV, especially the 3'-UTR (+), would need to be further characterized to confirm this finding before any conclusions could be drawn.

Current evidence indicates that MADP1 is compartmentalized in the nuclei of cultured cells (338), markedly differing from the cytoplasmic, perinuclear localization of the coronavirus RTCs (342-344). As there was no report on the possibility of MADP1 shuttling between the nucleus and cytoplasm, our observation using indirect immunofluorescence that over-expressed MADP1 upon IBV infection became partially localized in the cytoplasm may represent a first report that MADP1 could be localized outside the nucleus (Figure 3.15 and Figure 3.17). This could have been achieved with either an existing shuttling mechanism used by a nuclear protein or the assistance of viral factors. For example, IBV N protein is known to enter the nucleus while maintaining a predominantly cytoplasmic localization (232,345). Alternatively, binding of viral RNA may partially retain the newly synthesized MADP1 in the cytoplasm, as observed in this study.

It was observed that the over-expression of Flag-tagged MADP1 was unable to fully restore IBV infection in MADP1-knockdown cells, even though the expression level of the introduced MADP1 construct far surpassed the endogenous level, as observed by Western blot analysis. Considering the fact that only 30% of cells were transfected and over-expressed MADP1 protein despite the presence of a higher level of the protein in the transfected cells, it is understandable that the expression of viral proteins could not be restored after combining both transfected and untransfected cells. Interestingly, over-expression of silencing-sensitive MADP1 (FM) was unable to cause an increase in virus infection, comparing to what was observed for silencing-resistant MADP1 (FMmut) in shMadp1 cells, even though their expression levels were comparable. This lends further support to the conclusion that MADP1 is actively involved in the replication and infectivity of IBV.

It was found that the expression level of MADP1 could not be correlated to originating tissues of different cell lines. A correlation of MADP1 expression levels to the infectivity of IBV in the different cell lines was also unable to be established. Cell lines which originated from tissues not part of the regular tissue tropism of IBV could be infected as well. Hence, no clear relationship could be established between the infectivity of IBV and MADP1 expression or the type of tissue the cells originated from. This was most probably due to the fact that almost all of the cells were derived from cancerous tissues, with the exception of MRC-5. Such cell lines would express an altered proteome that could also include the differential expression of MADP1.

In a prior report, it was shown that MADP1 could be selectively upregulated in the hepatocarcinoma cell line, HepG2, compared to normal liver cells (338). Hence, the

results derived from this trial experiment were inconclusive and a correlation between the expression of MADP1 and IBV infectivity could not be established.

Chapter 4 Interaction Between Non-Structural Proteins With Viral RNA And Proteins.

As mentioned earlier in Chapter 3, efficient replication and transcription of the viral genome is required for infection to progress. The key player in this part of the coronavirus life cycle is the virus-encoded replicase gene. Replicase gene, the 5'-most ORF of the coronavirus genome is translated into the polyproteins pp1a and pp1ab which are auto-proteolytically processed into 15 (IBV) or 16 non-structural proteins in other coronaviruses, the replicase gene products. Among these non-structural proteins are the key enzymes critical to the virus' ability to replicate its genome and propagate in the host cell, including the RNA-dependent RNA polymerase (RdRP) or nsp12, which is presumably central to the ability of the coronavirus to synthesize viral mRNAs.

Enzymatic activities required for most of the key processes in coronavirus RNA synthesis have been mapped to the some of the non-structural proteins. However, information on their specific interactions with the viral genome or other non-structural proteins is limited. In addition, it is not known if the non-structural proteins which were not yet assigned with key functions in coronavirus RNA synthesis could be participating in viral RNA replication or transcription.

Hence, a two-pronged approach was adopted to study viral proteins and protein-RNA interactions in coronavirus RNA synthesis. To elucidate RNA-protein interactions, an attempt was made to detect the presence of RNA-binding activity in any of the non-structural proteins of IBV, which had not been reported to possess such an activity. This was done using available constructs over-expressing individual non-structural proteins in a biotin pull-down assay with biotinylated probes. The second method

used was to conduct a screen for protein-protein interactions between non-structural proteins and the viral polymerase, nsp12.

4.1 Biotin pull-down screen for RNA-binding activity of non-structural proteins

Plasmids based on the vector pXJ40-FLAG inserted with nucleotide sequences of the non-structural proteins either in tandem (nsp7/8 fusion and nsp8/9 fusion) or individually were used to over-express the proteins in H1299 cells coupled with Vaccinia/T7 virus infection. The cell lysates were used in biotin pull-down assays with biotinylated 5'-UTR (+), 5'-UTR (-) or 3'-UTR (+) RNA probes. As the focus of the study was on negative strand RNA synthesis, only the positive sense UTRs and the 5'-UTR (-), which contains the anti-leader TRS important for strand-transfer during discontinuous transcription of negative strands, were included in the screen. The proteins bound to the streptavidin beads were resolved by SDS-PAGE and detected by western blot using α-FLAG-HRP antibody. Negative control, non-binding protein, EGFP was also included in each screen.

4.1.1 Non-structural proteins nsp2, nsp5 and nsp10 may interact with IBV 5'-UTR (+)

For the screen conducted using biotinylated, IBV 5'-UTR (+), individual non-structural proteins, two fusion proteins, nsp7/8 and nsp8/9, and EGFP were over-expressed in Vaccinia/T7 recombinant virus infected H1299 cells on 60 mm dishes. Cells were lysed with 250 µl Lysis Buffer and used immediately. Biotin pull-down assay was performed with 0.1 µM (final concentration) biotinylated IBV 5'-UTR (+)

probe with 150 µl cell lysate. Streptavidin beads were used to purify the biotinylated RNA from the mixture and additional proteins bound to the beads through interactions with the bound RNA were eluted with 2X SDS loading dye. For western blot analysis, 10 µl of cell lysate and all of the eluted proteins were denatured and resolved by SDS-PAGE. Detection of the FLAG-tagged non-structural proteins and EGFP were performed with α-FLAG-HRP antibody and α-EGFP antibody respectively.

As shown in Figure 4.1, the non-structural proteins that were able to co-purify with the biotinylated probe in the assay were nsp2, nsp10 and to a lesser extent, nsp5. The clones for nsp8 and nsp9 were not available at the time of this assay so only the fusion proteins nsp7/8 and nsp8/9 were used. Non-structural proteins that were not shown were either not detectable in the cell lysate, in the case of nsp6 and nsp13, or not successfully cloned, in the case of nsp3 and nsp4.

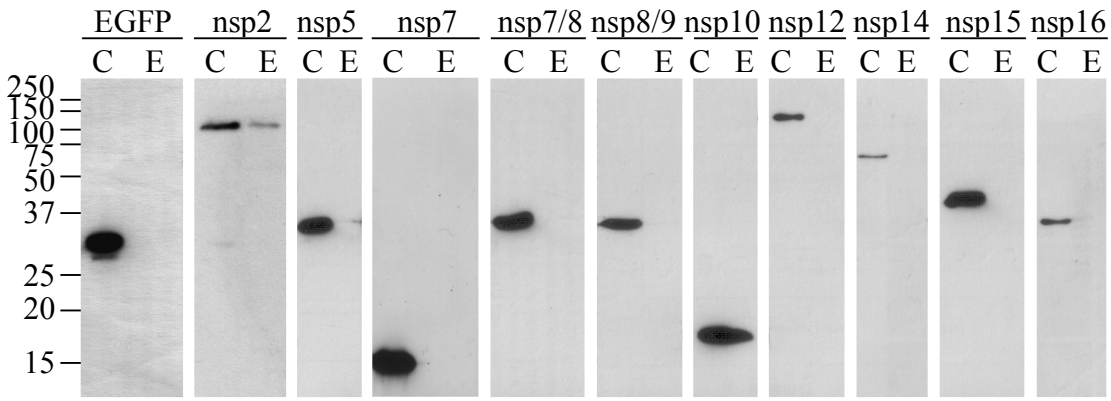

Figure 4.1: IBV nsp2, nsp5 and nsp10 showed binding activity to its 5'-UTR (+). Biotin pull-down assay of non-structural proteins with IBV 5'-UTR (+). Cell lysates of H1299 cells ver-expressing different non-structural proteins were incubated with biotinylated 5'-UTR (+) probes and purified using streptavidin beads. Bound proteins were resolved by SDS-PAGE and western blot was performed. Proteins which did not express were not presented. C: cell lysate, E: elution. A representative result of two independent experiments was shown.

4.1.2 Non-structural proteins nsp5 and nsp10 may interact with IBV 5'-UTR (-)

All non-structural proteins except nsp3, nsp4, nsp6, nsp13 and EGFP were over-expressed in Vaccinia/T7 recombinant virus infected H1299 cells grown on 60 mm dishes. The cell lysates were used in biotin pull-down assays with biotinylated 5'-UTR (-) probe to screen for interacting proteins. Proteins which co-purified with the biotinylated RNA probe were eluted from the beads with 2X SDS loading dye and resolved by SDS-PAGE. Detection was performed as described in section 4.1.1 and the result for this set of biotin pull-down assays is presented in Figure 4.2.

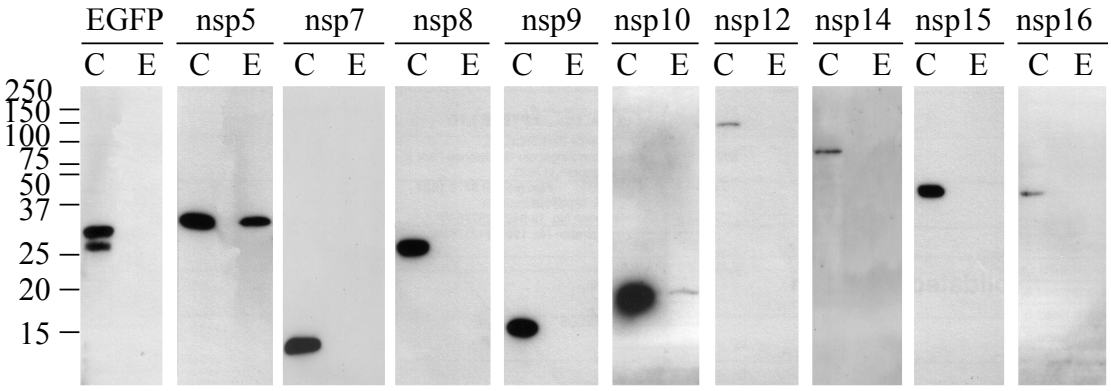

Figure 4.2: IBV nsp5 and nsp10 showed binding activity to its 5'-UTR (-). Biotin pull-down assay of non-structural proteins with IBV 5'-UTR (-). Cell lysates of H1299 cells ver-expressing different non-structural proteins were incubated with biotinylated 5'-UTR (-) probes and purified using streptavidin beads. Bound proteins were resolved by SDS-PAGE and western blot was performed. The expression of nsp2 was not detectable for this assay and was excluded. C: cell lysate, E: elution. A representative result of two independent experiments was shown.

For this screen, the expression of nsp12 although detectable, was extremely weak, hence it could not be determined if it co-purified with IBV 5'-UTR (-). As the expression level of nsp2 was too low to be detected for this particular screen, it was omitted from the presented figure. Out of the several non-structural proteins assayed,

non-structural proteins nsp5 and nsp10 were found to be interacting with IBV 5'-UTR (-).

4.1.3 Non-structural proteins nsp5, nsp8 and nsp9 may interact with IBV 3'-UTR (+)

For the last screen for non-structural proteins interacting with IBV 3'-UTR (+), all non-structural proteins except nsp3, nsp4, nsp6, nsp13 and EGFP were over-expressed in Vaccinia/T7 recombinant virus infected H1299 cells grown on 60 mm dishes. The cell lysates were used in biotin pull-down assays with biotinylated 3'-UTR (-) probe and proteins which copurified with the biotinylated RNA probe were eluted from the beads with 2X SDS loading dye, resolved by SDS-PAGE and detection was performed as described in section 4.1.1.

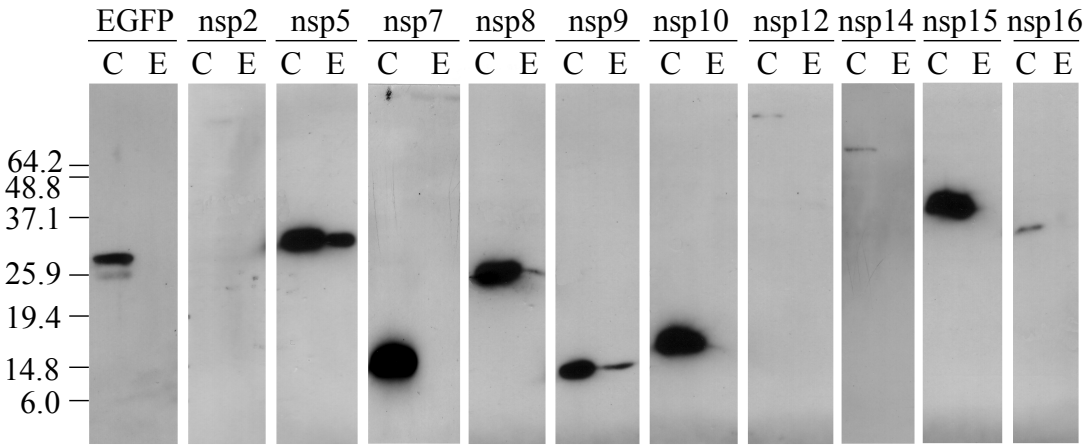

Figure 4.3: IBV nsp5, nsp8 and nsp9 showed binding activity to IBV 3'-UTR (+). Biotin pull-down assay of non-structural proteins with IBV 3'-UTR (+). Cell lysates of H1299 cells ver-expressing different non-structural proteins were incubated with biotinylated 3'-UTR (+) probes and purified using streptavidin beads. Bound proteins were resolved by SDS-PAGE and western blot was performed. C: cell lysate, E: elution. A representative result of two independent experiments was shown.

As presented in Figure 4.3, nsp5 showed strong interaction , nsp8 and nsp9 showed a moderate level of interaction with IBV 3'-UTR. The expression levels of nsp2, nsp12 and nsp14 for this assay were too low for any RNA-binding to be observed and it could not be concluded if they interacted with the biotinylated probe.

4.1.4 Candidates identified from the screen which could interact with IBV 5'-UTR (+), 5'-UTR (-) or 3'-UTR (+)

In summary, out of the 11 non-structural proteins tested, only nsp2, nsp5, nsp8, nsp9 and nsp10 were able to interact with one or more of the untranslated regions of IBV. Out of these five replicase gene products, only nsp2 and nsp5 have not been reported to possess RNA-binding activity. Existing literature reported that the coronavirus nsp8 possessed non-specific RNA-dependent RNA polymerase activity and was proposed to function as a primase, synthesizing short ribonucleotide chains, or primers, which are required for transcription initiation by the coronavirus RNA-dependent RNA polymerase nsp12 (103). This implied that nsp8 could bind to RNA in a non-specific manner. Although it was not surprising to find nsp8 interacting with IBV 3'-UTR (+), it was noted that the interaction observed was very weak and was not detected for all three RNA probes tested. This could have resulted from experimental variance if nsp8 could weakly bind RNA non-specifically as the three screens were not conducted at the same time.

The coronavirus nsp9 was shown to be a weak, non-specific single-stranded nucleic acid binding protein (ssDNA and ssRNA) (106,108). Hence, it was interesting that nsp9 was found to interact weakly only with IBV 3'-UTR (+) and not at all with the

5’-UTR in both polarity. As nsp9 had not been proven not to bind specifically with particular regions of the coronavirus genome, there is still a possibility of it being able to bind RNA in a specific manner and that the 3’-UTR (+) could have been its specific interaction partner. Conversely, the low affinity binding could imply that the weak affinity binding to the biotinylated probe was of a non-specific nature. Further studies would be required to verify the specificity of the interaction.

The crystal structure of nsp10 showed that it contains two zinc-finger motifs (109), forms a dodecameric complex (110) and functions as a stimulatory factor to nsp16, the 2’-O-methyltransferase which catalyzes the conversion of the cap-0 structure on m7GpppA-RNA to a cap-1 structure (121). It was also shown to exhibit low-affinity binding to single stranded RNA (ssRNA), double stranded RNA and DNA (dsRNA and dsDNA) in the absence of other viral proteins (109). Hence, in a case similar to nsp9, the binding of nsp10 to IBV 5’-UTR (-) could also be of low-specificity.

Nsp2 was found to interact with IBV 5’-UTR (+) and it could not be concluded if it bound to IBV 5’-UTR (-) and 3’-UTR (+). Although nsp2 was not reported to be a RNA-binding protein, it had been demonstrated as a weak antagonist of PKR antagonist (219), a dsRNA-activated kinase. The mechanism of this antagonism has yet to be determined hence nsp2 acting as a competitive dsRNA-binding protein to prevent PKR activation by dsRNA synthesized by the virus during replication and transcription is not beyond the bounds of possibility.

It was intriguing to find nsp5 interacting with all three probes tested, of which its interactions with the 5’-UTR (-) and 3’-UTR (+) were rather strong. Nsp5 is a 3C-like protease, one of the proteases involved in the proteolytic processing of the replicase

gene products. Having no prior reports of it possessing RNA-binding activity, this represents a novel piece of information with regards to the function of nsp5 in addition to its role as a protease if the interactions could be validated. Hence, nsp5 along with nsp2 were chosen to have their RNA-binding activity assessed again to confirm the interactions.

4.1.5 Interactions of nsp5 with viral RNA could not be confirmed and nsp2 exhibited weak binding for viral RNA

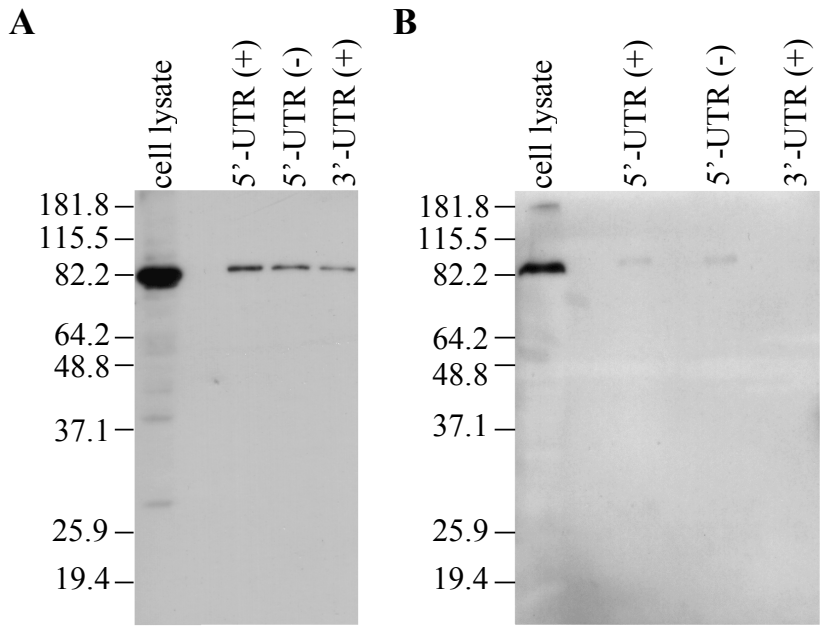

Figure 4.4: IBV nsp2 was confirmed to interact weakly with the single stranded viral UTRs. Selected results of repeated biotin pull-down assays performed for nsp2. The efficiency of RNA-binding for nsp2 was generally low. Binding to IBV 3'-UTR (+) could only be detected when a higher amount of nsp2 was present in the lysate. Panel A: High nsp2 expression. Panel B: Low nsp2 expression. Two representative results of four independent experiments were shown.

Biotin pull-down assays were performed for nsp2 and nsp5 with biotinylated RNA probes of IBV 5'-UTR (+), 5'-UTR (-) and 3'-UTR (+) to confirm if the interactions observed in the three screens (section 4.1.1, 4.1.2 and 4.1.3) were valid. The assays

were performed several times for both proteins and it was found that the expression level of nsp2 differs between different experiments. This could have been due to the pronounced effect of different transfection efficiencies more visible when the expression was generally low. Figure 4.4 shows two sets of results of the biotin pull-down assays performed for nsp2.

On the otherhand, the expression level of nsp5 in the cell lysate was generally high enough for detection by western blot. However, as shown in Figure 4.5, the RNA-binding efficiency of nsp5 appeared to be much weaker (Panel A) at best or even nullified (Panel B).

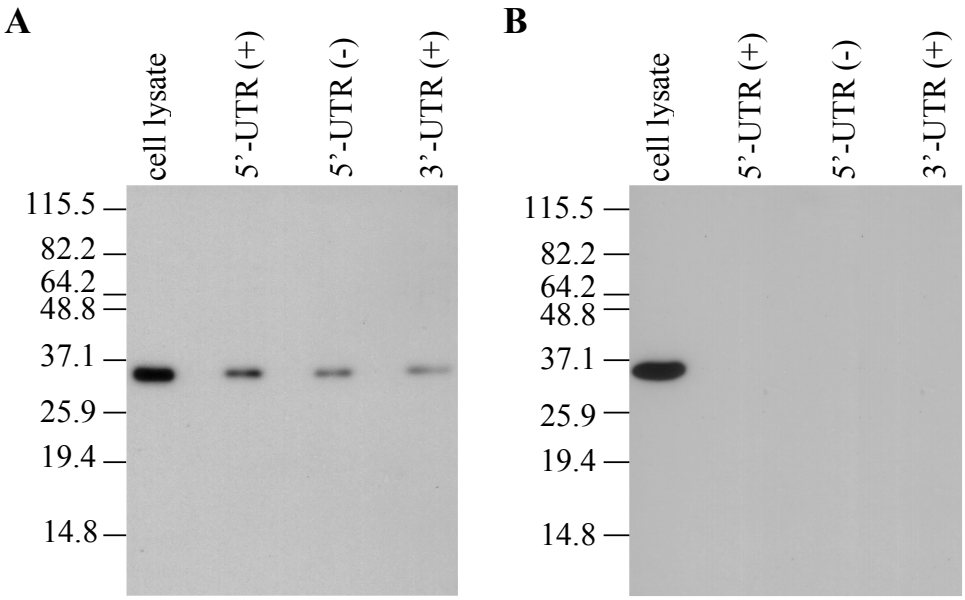

Figure 4.5: IBV nsp5 was not confirmed to interact with the single-stranded viral UTRs. Selected results of repeated biotin pull-down assays performed for nsp5. Panel A: low efficiency RNA-binding was observed for nsp5. Panel B: no RNA-binding was detected for nsp5 in this experiment. Two representative results of five independent experiments were shown.

The results from these confirmatory interaction pull-down assays indicated that nsp2 does exhibit low-efficiency ssRNA-binding activity the nature of which would need

to be verified. As it could interact weakly with both strands of the IBV 5'-UTR, there lies a possibility that it may bind to a double-stranded 5'-UTR. These would need further confirmation with other assays using dsRNA probes instead. However, the proposed function of a dsRNA-binding nsp2 would most likely be linked to PKR antagonism, which was not the aim of the study, no follow up was planned.

Additional assays performed for nsp5 painted a completely different picture for the RNA-binding activity of the protein. Most of the repeated assays performed for nsp5 showed no RNA-binding for any biotinylated probe tested and it was likely that nsp5 did not bind RNA and the bands observed during the screen could be an experimental artifact.

4.2 Screen for non-structural proteins interacting with nsp12

An IBV recombinant virus which expressed N-terminally HA-epitope tagged nsp12 (HA-RdRP recombinant virus) was created by another lab member using reverse genetics. This virus was used to infect confluent Vero and H1299 cells to prepare the infected cell lysates for the screen. The expression level of nsp12 in Vero cells infected with wild-type IBV or HA-RdRP recombinant IBV as well as its IP efficiency with α-HA coated beads (HA-beads) was determined by western blot using a polyclonal serum antibody to nsp12 (α-RdRP) before the screen. This was done to ensure that the protocol was able to precipitate the HA-tagged protein efficiently enough for detection of other coprecipitated proteins.

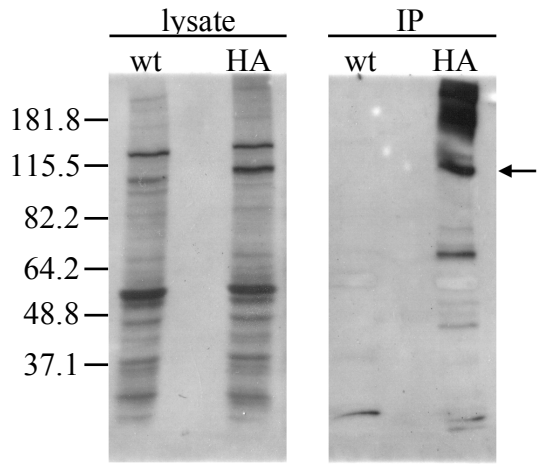

Figure 4.6: Only HA-nsp12 was present in the sample after IP with HA-beads. Western blot showing nsp12 detected by serum antibody, α-RdRP in the cell lysates (lysate) of wild-type (wt) IBV or HA-RdRP recombinant (HA) IBV infected Vero cells and after immuno-precipitation with HA-beads (IP). A representative result of two independent experiments was shown.

As shown in Figure 4.6, the expression of nsp12 and HA-nsp12 in wild-type virus and HA-RdRP virus infected cells were comparable and only HA-nsp12 was precipitated by HA-beads.

4.2.1 Nsp8 coprecipitated with nsp12

Confluent Vero and H1299 cells grown in 80 cm^2 flasks were infected with either wild-type IBV or HA-RdRP recombinant IBV. The cells were harvested at 9 h.p.i. and 16 h.p.i. for Vero, at 9 h.p.i. for H1299 by lysis with 800 µl of Lysis Buffer for each flask. HA-beads (20 µl of 50% slurry) were added to 500 µl of each lysate to precipitate HA-nsp12 and any other interacting proteins from the lysates. The bound proteins were eluted with 55 µl of 2X SDS loading dye and resolved by SDS-PAGE using an 8% or 15% gel (20 µl per lane) together with 20 µl of each cell lysate. Detection of coprecipitated proteins was performed by western blot using available anti-sera for some non-structural proteins of IBV as well as structural proteins S and N and accessory proteins ORF 3a, 3b and 5b.

The results of the co-IP detection were presented in Figure 4.7 and Figure 4.8 for H1299 cells and Vero cells respectively. Many of the anti-sera used were unable to detect the correct bands in the cell lysates which could be due to the low expression level of the proteins during IBV infection in addition to the low levels of antibody in the serum. For the structural proteins, S was not detected in the IP samples and N was detected in both wild-type (wt) and HA-RdRP recombinant (HA) IBV infected cells. Although it appeared that the amount coprecipitated in HA-RdRP IBV infected

samples was higher compared to wild-type IBV infected samples, the amount detected in the cell lysates was also higher. So it was unlikely for N to have been specifically coprecipitated by an interaction with nsp12.

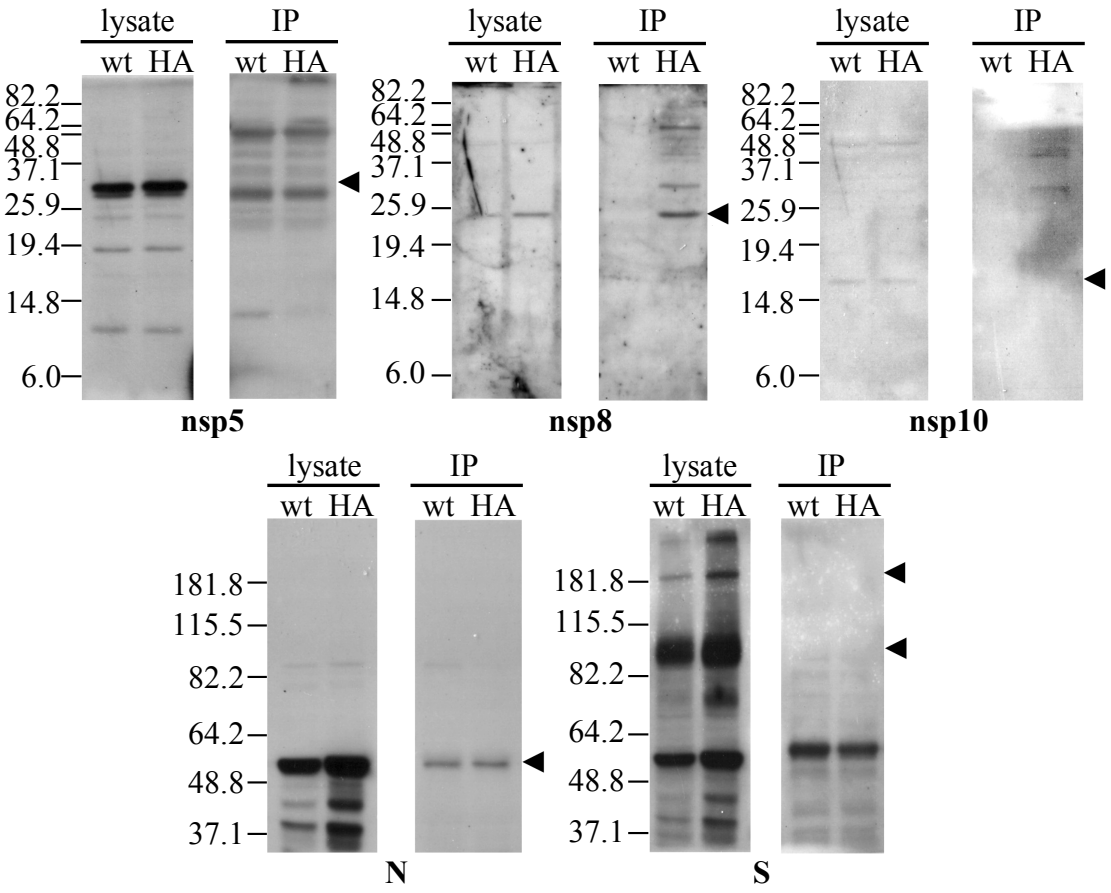

Figure 4.7: IBV nsp8 co-precipitated with nsp12 in infected H1299 cells. Western blot detection of IBV proteins with serum antibodies to the respective proteins in the cell lysates (lysate) of wild-type (wt) or HA-RdRP recombinant IBV (HA) infected H1299 cells and samples after immunoprecipitation with HA-beads (IP) . Only serum antibodies which were able to detect the correct bands in the lysates were presented. Positions of the bands were indicated by arrowheads. Anti-sera which were used but not presented were for the following proteins: nsp2, nsp3, nsp3/4 , nsp7, nsp13, ORF 3a, ORF 3b, ORF 5a. A representative result of two independent experiments was shown.

Nsp5 was strongly detected in the cell lysates but a band corresponding to its molecular mass was not detectable in the IP samples although many other bands were detected. For both H1299 and Vero cells, a high molecular weight band of

undetermined mass was detected in HA-beads precipitated samples. The identity of the band was likely a partially processed product of pp1a or pp1ab, which included nsp5 that was detected by the antibody. Nsp8 was detected by the anti-sera to be present in only HA-beads precipitated HA-RdRP IBV infected cell lysates and not HA-beads precipitated wild-type IBV infected cell lysates. The co-precipitation was detected in both H1299 and Vero cells. Hence, nsp8 was the only protein found to be coprecipitated with HA-nsp12 using HA-beads.

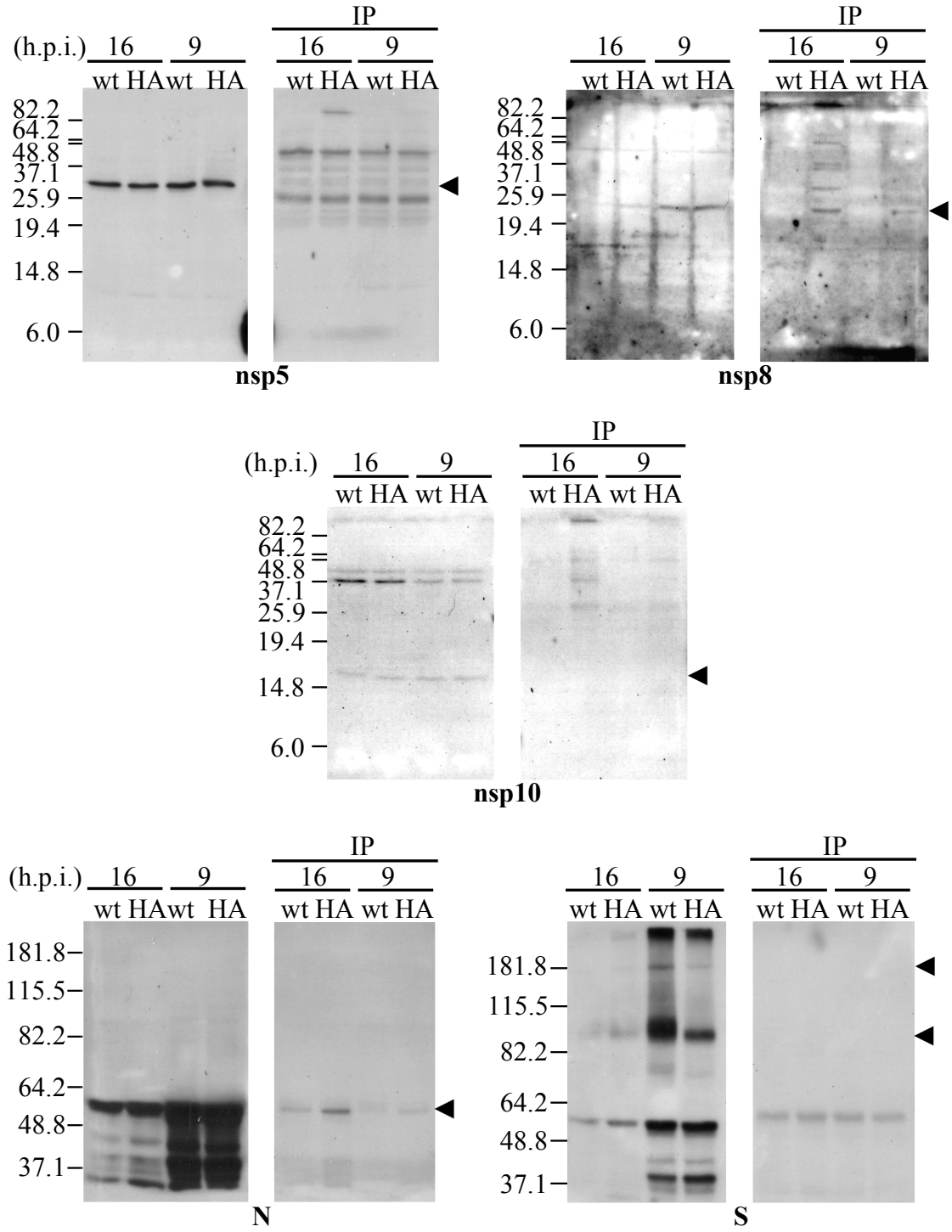

Figure 4.8: IBV nsp8 co-precipitated with nsp12 in infected Vero cells. Western blot detection of IBV proteins with serum antibodies to the respective proteins in the cell lysates (lysate) of wild-type (wt) or HA-RdRP recombinant IBV (HA) infected Vero cells and samples after immunoprecipitation with HA-beads (HA). Only serum antibodies which were able to detect the correct bands in the lysates were presented. Positions of the bands were indicated by arrowheads. Anti-sera which were used but not presented were the same as that for H1299 infected cells. A representative result of two independent experiments was shown.

4.2.2 The co-precipitation of nsp8 and nsp12 is confirmed

To confirm if nsp8 interacts with nsp12, the IP of nsp12 was repeated with HA-beads. In addition, a reciprocal precipitation was performed using anti-nsp8 serum antibody. The lysates were prepared as described in section 4.2.1 except that the cells were only harvested at 9 h.p.i.. The bead-bound proteins were eluted with 55 µl 2X SDS loading dye and resolved by SDS-PAGE using an 8% or 15% gel (20 µl per lane) together with 20 µl of each cell lysate. Detection of nsp8 was performed for proteins precipitated by HA-beads and the detection of nsp12 was performed for proteins precipitated by anti-nsp8 antibody.

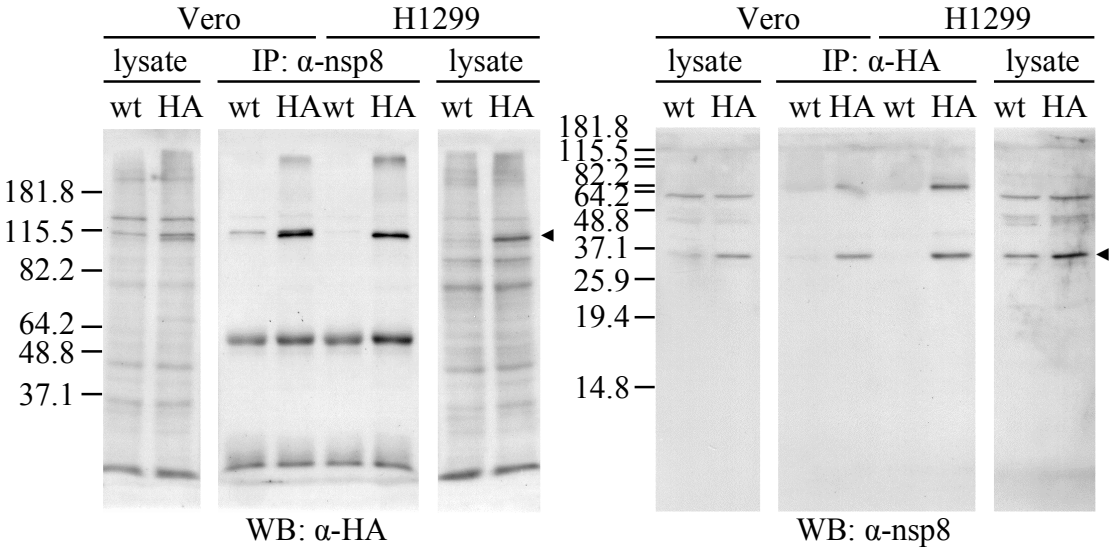

Figure 4.9: IBV nsp8 coprecipitates with HA-nsp12 and vice versa. Immuno-precipitation of wild-type IBV (wt) or HA-RdRP (HA) recombinant IBV infected Vero and H1299 cell lysates. Immuno-precipitation was performed with either α-nsp8 (rabbit serum) (left panel) or HA-beads (right panel). Detection of nsp8 (right panel) and nsp12 (left panel) were performed with α-nsp8 and α-HA-HRP antibodies respectively and their positions were indicated by arrowheads. A representative result of three independent experiments was shown.

As observed from the results of the IP in Figure 4.9, in addition to the detection of HA-nsp12 in HA-RdRP recombinant IBV infected cell lysate after precipitation with α-nsp8, a band corresponding to a similar molecular mass was also detected in wild-type IBV infected cell lysates after precipitation (very weak for H1299).

A closer examination revealed that there was an additional band detected in all cell lysates of a molecular mass slightly higher than HA-nsp12 (left panel). Hence, to confirm that the band predicted to be HA-nsp12 was accurate, and that the higher molecular weight band was indeed a non-specific band detected by the antibody, the blot for IP using HA-beads was checked for the presence of HA-nsp12 using α-HA-HRP antibody. The blot depicted in Figure 4.10 detected the same band in all lanes which were loaded with IP samples. Hence, the band was confirmed to be a non-specific band detected by the antibody used for western blot. Since the additional band was confirmed to be non-specific, the observation that nsp12 was coprecipitated by α-nsp8 was accurate. Hence, the interaction between nsp8 and nsp12 has been validated.

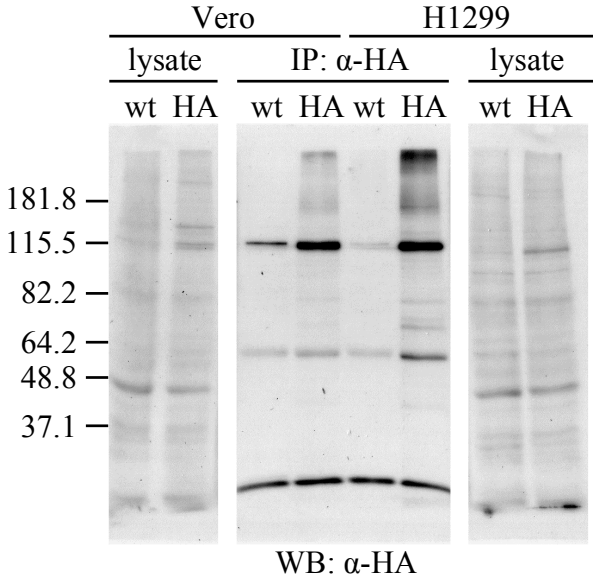

Figure 4.10: Higher molecular weight band observed from the IP was a non-specific band. Cell lysates precipitated with HA-beads was probed with α-HA-HRP antibody. A representative result of three independent experiments was shown.

Although the interaction between nsp8 and nsp12 had been reported before for SARS-CoV (133), it was not reported in other coronaviruses and the interaction had not been subjected to an in-depth study. Hence, the interaction between nsp8 and nsp12 was to be further characterized.

4.2.3 The interaction between nsp8 and nsp12 is not RNA-dependent

IP was performed using co-expressed nsp8 and nsp12 to confirm their interaction. The proteins were co-expressed as a FLAG-tagged protein for nsp8 (FLAG-nsp8) and a Myc-tagged protein for nsp12 (Myc-nsp12) in H1299 cells infected with Vaccinia/T7 virus. As controls, dual vector transfected samples (FLAG + Myc) and single vector transfected samples (FLAG-nsp8 + Myc and FLAG + Myc-nsp12) were used. The IP was performed with α-Myc coated beads (Myc-beads) and the bound proteins were resolved by SDS-PAGE together with 20 µl of the cell lysates. Western blot (WB) was performed using α-FLAG-HRP and α-Myc-HRP antibodies to detect the precipitated proteins as shown in Figure 4.11.

FLAG-nsp8 was detected at almost equal amounts whether it was expressed together with Myc only (FLAG-nsp8 + Myc) or with Myc-nsp12 (FLAG-nsp8 + Myc-nsp12) but was detected in the IP samples only when it was co-expressed with Myc-nsp12 (Figure 4.11, left panel. The ≈ 50 kDa band detected in all IP samples was likely to be the heavy chain eluted from the beads during sample preparation for SDS-PAGE. Also, Myc-nsp12 was detected in both the cell lysates and IP samples (Figure 4.11, right panel). As the appearance of FLAG-nsp8 in the IP sample occurred only in the

presence of Myc-nsp12, it was be concluded that FLAG-nsp8 was coprecipitated with Myc-nsp12 by interacting with it.

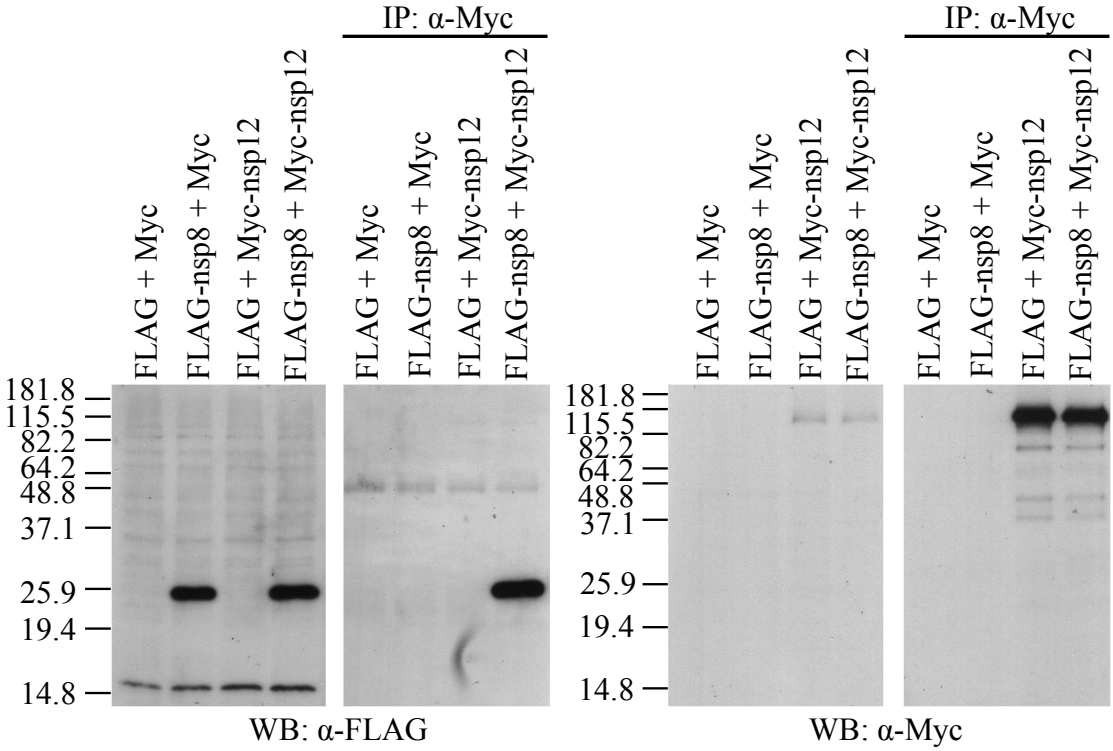

Figure 4.11: FLAG-nsp8 was precipitated by Myc-beads only when it was co-expressed with Myc-nsp12. Western blot detection was performed with α-FLAG (left panel) and α-Myc (right panel) antibodies. IP: immuno-precipitated samples, WB: western blot. A representative result of two independent experiments was shown.

Nsp8 was shown to be exhibit RNA-binding activity in section 4.1.3 earlier and was also reported by other groups to function as a primase for the viral RdRP, nsp12. Since both of them are RNA-synthesizing enzymes and would likely be interacting with viral RNA and it was not known if their interaction was direct or RNA-dependent. Hence, another IP was performed with cell lysates that were either treated (+RNase A) or not treated (-RNase A) with 50 μg/ml of RNase A at 37°C for one hour before the addition of α-Myc (Myc-beads) or α-FLAG (FLAG-beads) coated beads. The results of the IP as shown in Figure 4.12, were identical with or without

RNase A treatment, nsp8 was still precipitated when RNA had been removed. Hence, it was confirmed that nsp8 interacts directly with nsp12 and not indirectly through their individual interactions with RNA.

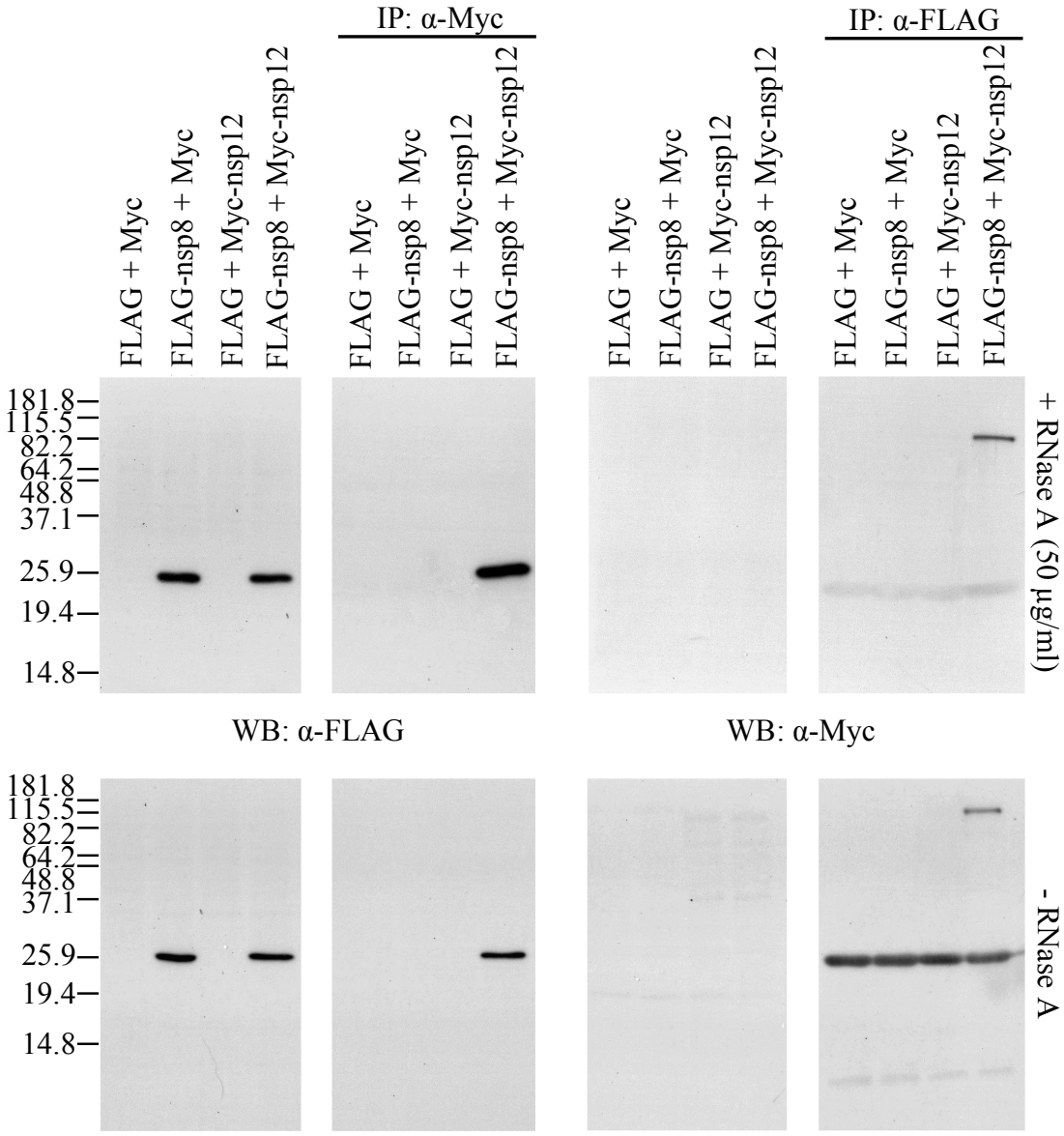

Figure 4.12: FLAG-nsp8 and Myc-nsp12 co-precipitates with or without RNase A treatment. RNase A treated or untreated cell lysates were subjected to IP with either FLAG-beads or Myc-beads and precipitated proteins were detected with the respective antibodies. A representative result of two independent experiments was shown.

4.3 Nsp8 interacts with the N- and C-terminal portions of nsp12

Since the interaction between nsp8 and nsp12 had been confirmed, the domain responsible for the interaction on nsp12 was to be mapped. Three Myc-tagged mutants of nsp12 were created as shown in Figure 4.13.

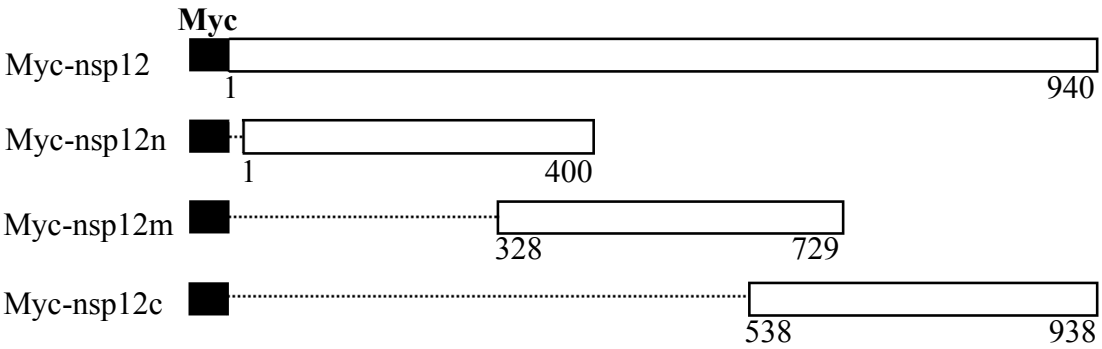

Figure 4.13: Schematic diagram of Myc-tagged nsp12 truncation mutant proteins. Numerals indicate amino acid positions.

The three mutants and full length nsp12 (Myc-nsp12) were either co-expressed with a vector control expressing FLAG-epitope only or a construct expressing FLAG-nsp8. The cell lysates were precipitated with FLAG-beads and the bound proteins were resolved by SDS-PAGE and detection was made with α-Myc-HRP antibody. The cell lysates were also probed to assess the expression levels of the different nsp12 mutants.

It could be observed from the results of the IP that all Myc-tagged truncation mutants and full-length nsp12 were coprecipitated by FLAG-beads except for Myc-nsp12m (amino acid residues 328 – 729) (Figure 4.14, right panel). The absence of Myc-tagged protein co-precipitation in samples which were co-expressed with FLAG-epitope, indicated that the coprecipitation of Myc-nsp12n and Myc-nsp12c were dependent on the presence and their interaction with FLAG-nsp8, as was the case for

Myc-nsp12. The lysates were examined for the expression levels of the respective Myc-tagged proteins as well (Figure 4.14, left panel).

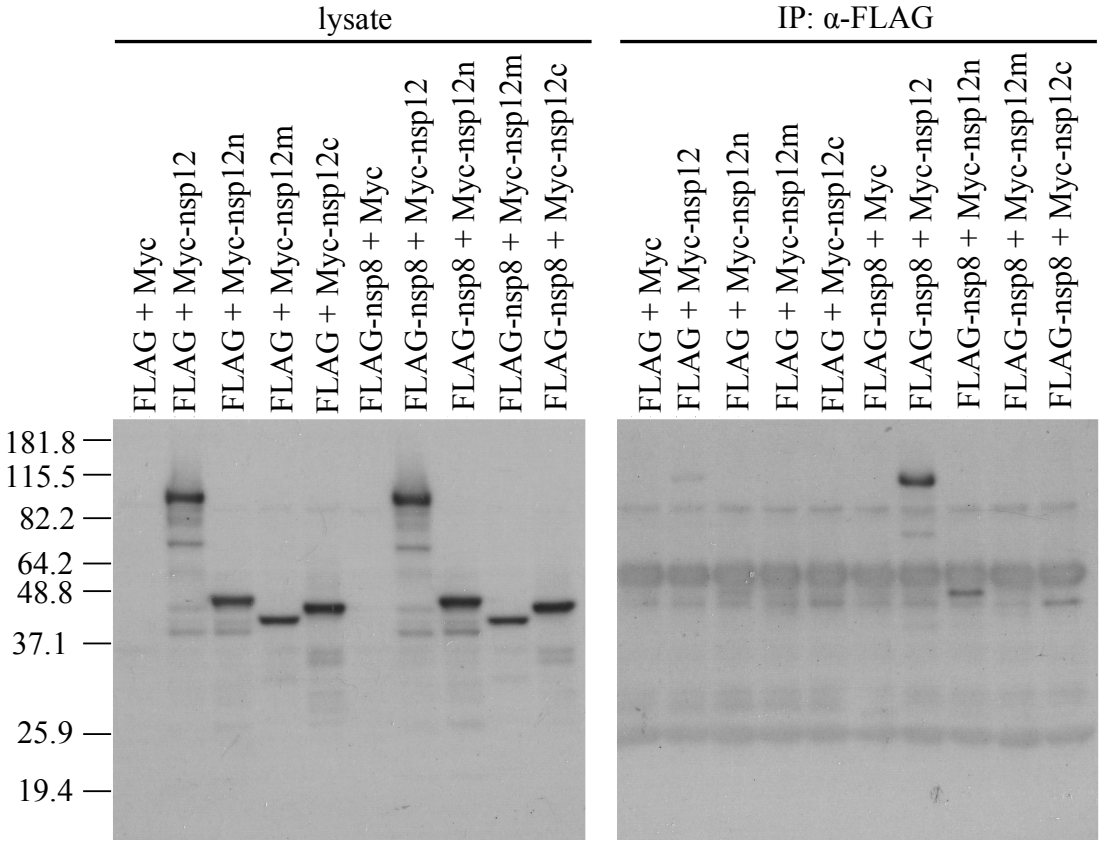

Figure 4.14: The N- and C-terminal portions of IBV nsp12 co-precipitated with FLAG-nsp8 using FLAG-beads. Full-length and truncated nsp12 proteins or Myc (vector control) were co-expressed with FLAG (vector control) or FLAG-nsp8. The cell lysates were precipitated with FLAG-beads and bound proteins were analyzed with western blotting using α-Myc. Full-length nsp12 and mutants nsp12n (residues 9 – 400), nsp12c (residues 538 – 938) were co-precipitated by the beads. A representative result of three independent experiments was shown.

4.4 Discussion

In summary, IBV nsp2, nsp8, nsp9 and nsp10 have been shown to exhibit RNA-binding activity to either of the UTRs. Also, from the results of the IP screen, it was

revealed that IBV nsp8 interacts with nsp12 at two points, the N- and C-termini of the latter.

Studying viral RNA-protein interactions using the biotin pull-down assay was hampered by the difficulty of cloning certain viral non-structural proteins like nsp3 and nsp4, as well as the insolubility of nsp6, a protein containing multiple transmembrane domains of the replicase gene (126). In addition, the low expression levels of nsp12, nsp13 and nsp14 in cultured cell made it difficult to detect any RNA-protein interactions. One previously undocumented interaction, that between nsp2 and viral RNA, was unfounded by the screen. This finding adhered to a previous report of nsp2 possibly being an antagonist to PKR (219), which requires double-stranded RNA for activation. Since current evidence is not indicative on an active role of nsp2 in viral RNA synthesis, the RNA-binding activity of nsp2 was not further studied.

The screen also showed that previously documented RNA-binding activities of nsp9 and nsp10 which surprisingly, did not bind to all three probes tested as both were determined to be of a non-specific nature (106,108,109). This could however be explained by the generally weak interactions between these two proteins and RNA that could escape detection in one or more of the screens. The interaction between nsp8 and IBV 3'-UTR (+) may have provided another piece of evidence that nsp8 is heavily involved in viral RNA synthesis, as a RNA-primer synthesizing enzyme for nsp12. Although the interaction was only shown for the protein with IBV 3'-UTR, it was notable that the interaction was also weak like that of nsp9 and nsp10. Hence, it cannot be concluded that nsp8 only bound to the 3'-UTR.

The approach taken to study viral protein-protein interactions was also hampered by the availability of sensitive anti-sera to viral proteins, especially that of the less immunogenic non-structural proteins and accessory proteins. Compounded by the fact that the non-structural proteins were also expressed in much lower amounts compared to structural proteins like S and N which were easily detected, their detection in cell lysates proved to be much more difficult. Out of the five proteins which could be detected by the available anti-sera, only nsp8 was identified as a binding partner to nsp12. This interaction had been reported in an ORFeome screen for SARS-CoV (133). Since it has not been proven to exist in other coronaviruses, reporting the same interaction in IBV suggested that it is highly probable that the interaction holds true across the three genera.

The nsp8 binding activity of nsp12 appeared to be present in both truncation mutants Myc-nsp12n and Myc-nsp12c (Figure 4.14), its N- and C-terminal. Coincidentally, it had been reported for SARS-CoV that both a p12 fragment in its N-terminal and a p64 fragment in its C-terminal were required for the exhibition of RdRP activity by nsp12 (346). The p12 and p64 fragments were shown to form a stable complex in the same report and the p12 fragment had been suggested by the authors to play a role in primer-binding while the p64 fragment contains the polymerase activity. Therefore, the ability of nsp8 to interact with truncation mutant Myc-nsp12n (residues 9 to 400) seemed to act a piece of supporting evidence for the role of the p12 fragment in primer-binding. This offers an interesting perspective on the coordination between coronavirus nsp8 and nsp12 in viral RNA synthesis.

Chapter 5 Conclusions and Future Directions

The main focus of this thesis is the investigation of the interaction of host protein, MADP1, with the coronavirus genome, the significance of its interaction with IBV 5'-UTR (+) as well as that of viral proteins in coronavirus RNA synthesis. This chapter is dedicated to the summarization of findings described in Chapters 3 and 4, discussion of the significance of these findings and suggestions for future work to be done. Since coronavirus RNA synthesis occurs early in the replication cycle, the information presented by these studies could reveal new strategies to drug design targeted to coronaviruses.

In the case of MADP1, a drug designed to inhibit its binding to the coronavirus 5'-UTR could possibly arrest the infection at an early stage, thus reducing the extent of virus-associated morbidity. Viral non-structural proteins are believed to be an integral part of the viral replicase complex. In-depth knowledge of their functions and interactions with other viral components could facilitate the development of critical processes into effective therapeutic targets. For the interaction between nsp8 and nsp12, an inhibition of their interaction could become a strategy to reduce the efficiency of viral RNA synthesis.

5.1 Main Conclusions

5.1.1 Identification of host proteins interacting with coronavirus by yeast 3-hybrid screen

- MADP1 (alias ZCRB1) was identified to interact with SARS-CoV 5'-UTR (+).

- HAX1 was identified to interact with SARS-CoV 5'-UTR (-).
- RPL27a was identified to interact with SARS-CoV 3'-UTR (+).

5.1.2 Biochemical characterization of the interaction between MADP1 and the IBV 5'-UTR

- Using a RNA pull-down assay based on the interaction between biotinylated RNA and streptavidin beads, MADP1 was shown to exhibit a strong interaction with IBV 5'-UTR (+). The interaction was shown to be sequence-specific and the secondary structure, stem loop I, served as the MADP1 binding site.
- The RNA recognition domain (RRM) of MADP1 was shown to be the domain responsible for interacting with IBV genome and that the active site residues were vital to its RNA-binding activity.

5.1.3 MADP1 in IBV RNA synthesis

- Using both cell fractionation and indirect immunofluorescence detection, it was demonstrated that MADP1 was either translocated from the nucleus to the cytoplasm or selectively retained in the cytoplasm during IBV infection.
- Silencing of MADP1 with siRNA resulted in a decimated infection by IBV exemplified by the reduction of luciferase gene expression by recombinant IBV-Luc virus, viral structural protein expression, synthesis of both genomic (- gRNA) and subgenomic (+ sgRNA and – sgRNA) mRNA, and the absence of syncytium formation. This phenotype was subsequently shown to be valid and not an off-target effect of the siRNA.

- The over-expression of a silencing-resistant MADP1 enhanced IBV infection in stable MADP1 knockdown cells.

5.1.4 Interaction of coronavirus nsps with the 5'- and 3'-UTRs

- During the screen, IBV nsp2, nsp5 and nsp10 were found to interact with the 5'-UTR (+).
- IBV nsp5 and nsp10 were found to interact with the 5'-UTR (-).
- IBV nsp5, nsp8 and nsp9 were found to interact with the 3'-UTR (+).
- Nsp2 was confirmed to interact weakly with the 5'-UTR (+) and 5'-UTR (-).
- The RNA-binding activity of nsp5 could not be confirmed

5.1.5 Interaction of coronavirus nsp12 with other viral proteins

- Nsp8 was shown to coprecipitate with nsp12 and their interaction occurred directly, independent on the presence of RNA.
- The N- and C-terminal of nsp12 but not the middle section was shown to interact with nsp8.

5.2 General Discussion

5.2.1 The yeast three-hybrid screen for human proteins interacting with SARS-CoV untranslated regions

The number of initial hits generated by the yeast three-hybrid screen was relatively low, at about four hundred colonies for the 5'-UTR (+) and two hundred and fifty colonies for the 5'-UTR (-) and 3'-UTR (-). This was in comparison to the well documented yeast two-hybrid system which could generate thousands of initial hits for a genome-wide screen of protein-protein interactions. The number of false positives for reporter gene activation, *HIS3*, appeared to be on the high side as strong reporter gene activating colonies dwindled to between six and seven (about 2% of initial hits) for each bait-RNA sequence after the secondary screen. This led to the conclusion that the lower number of initial hits would most likely be a result of poor transformation efficiencies or cell densities of the competent cells prepared which culminated in a limited representation of the genome being screened.

After the colony PCRs to identify the fragment contained in library plasmid, only one colony for each bait-RNA sequence remained as some appeared to contain fragments which were either too short to be translated into a peptide long enough to be representative of the protein the sequence was derived from or that the mRNA sequence encoded by the plasmid was anti-sense. Although only three proteins, MADP1, HAX1 and RPL27a, were identified from the screen, the discovery of MADP1 interacting with SARS-CoV 5'-UTR (+) proved to be an interesting lead to study.

5.2.2 Over-expression of MADP1 in different systems

The initial screen which identified MADP1 as a candidate for further characterization was performed in yeast, a eukaryotic cell system. Early attempts to express the protein using the bacteria expression system were met with problems in obtaining a consistent, high expression of the protein in the soluble fraction. The problem could not be rectified with a change of the fusion tag as well. Changing the over-expression system to a mammalian cell, driven by T7 polymerase, appeared to result in the increased stability of the protein. This could imply the presence of post-translational modifications in MADP1 which served to enhance its stability. Since there were no reports of the post-translational modifications of MADP1, a prediction on Eukaryotic Linear Motif server (ELM) based on the amino acid sequence of MADP1 revealed the presence of multiple phosphorylation sites as well as a sumoylation site (AKIE) from residues 176 to 179. Although it is not known if MADP1 is indeed sumoylated, this may be a possible explanation for the perceived instability of MADP1 in *E. coli* which are, by nature, unable to sumoylate proteins.

5.2.3 The cellular distribution of over-expressed MADP1 during IBV infection

Both cellular fractionation and indirect immunofluorescence indicated an increased presence of MADP1 in the cytoplasm, a deviation from its regular nuclear localization (338), during IBV infection. Coimmunofluorescence detection was performed for MADP1 with *de novo* synthesized viral RNA labeled by BrUTP. Although a colocalization of the two entities could not be confirmed, they did appear to partially overlap in their staining patterns. Regrettably, an antibody for immunofluorescence

detection of MADP1 was unavailable; hence, no visual information on the cellular distribution of the endogeneous protein could be obtained. This would have amplified the significance of the observed change in distribution during infection.

BrUTP labeling was used as a surrogate marker for the viral RTCs instead of anti-sera to viral non-structural proteins which are present in the complex as they were not sensitive enough to be used for immunofluorescence assays. Although the problem of detection of fully synthesized viral RNA not bound to any RTCs could disrupt the staining pattern, the three hour time-frame imposed for the RNA labeling and the immediate fixation of cells thereafter minimized any of such effect. Since only RNA synthesized during this three hour time frame would be labeled, it was likely that the labeled RNA remained associated or in the vicinity of actively synthesizing RTCs.

5.2.4 MADP1 as an enhancer of IBV RNA synthesis

The results obtained from the functional studies performed for MADP1 in IBV infections supported the conclusion that the interaction with IBV 5'-UTR (+) culminated in its involvement in viral RNA synthesis. Although splicing has been ruled out as a possible mechanism by which discontinuous transcription in coronavirus negative strand synthesis occur, the involvement of a spliceosome-associated protein in viral RNA synthesis could be beneficial to the virus even as the function of MADP1 in the human minor spliceosome remained a mystery.

It had been demonstrated that MADP1 expression levels in a single cell type influenced the efficiency of viral RNA synthesis, including that of negative-sense subgenomic mRNAs and the overall progress of the infection. Although the over-

expression of silencing-resistant MADP1 did not restore IBV infection in stable MADP1 knockdown cells to a level comparable to that in normal cells, it did exert a certain effect in enhancing IBV infection in the former. Taking into account that normally, only about 30% of the cells were transfected, the seemingly high expression level of MADP1 in the knockdown cells is not a true reflection of the entire population. Most of the cells did not express MADP1 and therefore negated the enhancement of IBV infection by cells expressing silencing-resistant MADP1 to a certain extent. In addition, expression of silencing sensitive MADP1 was determined to be close to that of silencing-resistant MADP1 in the stable knockdown cells but did not result in an enhancement of IBV infection. This observation made it more certain that the difference was due to the expression of silencing resistant MADP1 in cells infected by IBV.

5.2.5 Screening for RNA-binding proteins using biotin pull-down assay

Overall, the results obtained from the screen coincide well with current reports of RNA-binding activity in non-structural proteins of other coronaviruses. However, the sensitivity of the assay could be an obstacle to the reproducibility of the detection of weak and non-specific RNA-protein interactions. That would have been subjected to minute differences in variables like washing conditions and amount of beads used for each assay. These variations could be easily controlled within the same assay but it may prove to be a more difficult task if more samples were involved. Hence, it seemed to serve better as an *in vitro* confirmatory assay, like how it was used for confirming the interaction between MADP1 and IBV 5'-UTR, where the number of samples involved would be lesser than as part of a screening protocol.

5.2.6 Functional conservation of MADP1 in RNA synthesis of different coronaviruses in different host species

Most studies on host involvement in coronavirus RNA synthesis were so far performed using MHV (307,308,313,340), a betacoronavirus. Identification of the interaction between MADP1 and 5'-UTR as well as its functional involvement in coronavirus replication, in this study, therefore may represent the first host protein identified to play a role in viral RNA synthesis by interacting with the 5'-UTR of the viral RNA in a gammacoronavirus. The functional implication of the interaction between MADP1 and IBV 5'-UTR may also be extended to the rest of the members of the coronavirus family. In the case of hnRNP A1, it was initially reported to be functionally important for viral RNA synthesis for group II virus MHV (299,304). Subsequently, its involvement in viral RNA synthesis was also confirmed in TGEV, a group I coronavirus (309).

This discovery that MADP1 could interact with the 3'-UTR (+) as well allowed a comparison of MADP1 to hnRNP A1 to be drawn, the latter being the first reported, and best characterized host factor in coronavirus MHV discontinuous transcription. Although it has been reported that other hnRNPs could replace hnRNP A1 in coronavirus RNA synthesis (306), the binding sites of MADP1 and hnRNP A1 only partially overlap as the latter was reported to bind negative-sense IG sequences, 5'-UTR (-) and 3'-UTR (+) (299,300,307). Hence MADP1 may play its role as a separate entity, not as an equivalent of hnRNP A1 in gammacoronavirus IBV and there is likelihood that MADP1 could play a role in the RNA synthesis of other coronaviruses as well.

It may seem unconventional that functional studies described in chapter 3 involving IBV, a chicken coronavirus, and a human protein, MADP1, were conducted using human and African green monkey cells. However, it is noteworthy that MADP1 (HomoloGene 12095) is conserved in humans (*Homo sapiens*), chimpanzees (*Pan troglodytes*), wolves (*Canis lupus*), cattle (*Bos Taurus*), mice (*Mus musculus*), rats (*Rattus norvegicus*) and chickens (*Gallus gallus*). The African green monkey genome is not available at NCBI, but an alignment search using basic local alignment search tool (BLAST) of the MADP1 amino acid sequence against the closest available non-human primate, the rhesus macaque (*Macaca mulatta*) RefSeq Protein library yielded a 99% sequence similarity between the two species. The chicken homolog of MADP1 on the other hand, bears 85% amino acid sequence similarity, but with an almost identical match in the N-terminal 120 amino acids, to its human counterpart. As the mapped interaction domain lies in the N-terminus, it is highly likely that the homologs from other species could replace human MADP1 in the interaction and functional studies. Hence, the results obtained for these studies conducted in human and African green monkey cells are definitely of relevance to IBV.

5.2.7 Potential involvement of MADP1 in coronavirus RNA transcription

An important conclusion from the functional studies of MADP1 in human cells is its role in IBV negative-strand subgenomic RNA synthesis. In the discontinuous model of transcription for coronaviruses described in Figure 1.7 (93), transcription initiation occurs at the 3'-UTR then the replicase complex encounters and transcribes the body TRS sequence (TRS-B). Complementary base-pairing between the CS of the nascent cTRS-B and the template TRS-L, at the 5'-leader, stalls the complex and allows the

nascent strand to either anneal to the TRS-L or to its original template location (88-91). In the former situation, the template has been switched to the 5'-leader but the template remains the same for the latter. Transcription continues until the complex reaches the 5'-end of the genome or until the replicase complex encounters another TRS-B sequence.

In principle, the template switching event requires the presence of the 5'-leader sequence in the vicinity or in contact with the stalled replicase complex at one of the cTRS-B sequences to occur. As the coronavirus genome is extreme long, ranging between 27 and 32 kilobases, with the TRS-B sequences occurring within the 3' one-third of the genome, it would require assistance for the 5'-UTR to be brought near the replicase complex stalled at these points along the transcribed genome instead of leaving it to chance. It had been proposed previously that stem loop I of the coronavirus 5'-UTR is important in the maintenance of a 5'- UTR to 3'-UTR interaction which is critical specifically for discontinuous transcription of negative-sense sgRNAs to occur (75). Therefore, it seemed befitting that the facilitation of 5'-UTR to 3'-UTR interaction during discontinuous transcription be the proposed role for MADP1 following the discovery that it was able to interact strongly with the stem loop I of the IBV 5'-UTR (+) and possibly with the 3'-UTR (+) of the IBV genome as well.

It was indicated in the GenBank entry of MADP1 that it contains a RRM dimerization site, composed of two amino acid residues, at the end of the domain. If MADP1 does form dimers, and that both monomers could interact with the 5'-UTR (+) and 3'-UTR (+), it seemed likely that MADP1 could be the bridge between these two distal RNA

sequences. The absence of MADP1 would then result in highly inefficient template transfer and disrupt the synthesis of negative-sense sub-genome length mRNAs while it may or may not affect the synthesis of negative-sense genome length mRNAs. That which has been demonstrated by the silencing of MADP1 in the functional studies conducted in IBV infected H1299 cells.

In addition to the ability of interacting with multiple regions of the MHV genome, hnRNP A1 also interacted with the nucleocapsid protein of both SARS-CoV and MHV (302,303). That being said, if interactions of MADP1 with viral proteins or other host proteins implicated in coronavirus discontinuous transcription could be documented, it would bolster the significance of MADP1 in coronavirus discontinuous transcription and to paint a better picture of how it functions in the RTC as a whole and in particular, the facilitation of template transfer.

5.2.8 Potential mode of cooperation between nsp8 and nsp12 in RNA synthesis

Information pertaining to how the coronavirus negative-strand synthesis initiation occurs has been limited and only in the recent years has more information been available with regards to the source of the primer required for the RdRP (nsp12) to function (101). The nsp7-nsp8 hexadecameric complex which has been shown to be the second RdRP of the coronavirus that requires no primer to function and synthesizes short length RNA non-specifically fulfilled the role as the primase synthesizing short RNA primers for nsp12 (103).

An examination of the interaction between nsp8 and nsp12 has revealed that the interaction occurs at two points, the N- and C-terminal of nsp12. Coincidentally, it

was reported that a p12 fragment from at the N-terminus and a p64 fragment at the C-terminus of nsp12 were reported to be required for RdRP activity (346). A likely model that would fit the mapped interactions would indicate a direct interaction between the N- and C-terminals of nsp12 with the nsp7-nsp8 complex. In this model, the nsp7-nsp8 complex would first synthesize a RNA-primer of a sufficient length, which would be exposed to and binds to the N-terminus of nsp12, brought in close proximity through its interaction with nsp8. The extension of the RNA could then be catalyzed by the polymerase domain in the C-terminus of nsp12, which would also be oriented in close proximity to the end of the RNA-primer through its interactions at its N-terminus with nsp8. This arrangement of the two RdRPs would ensure the high efficiency of the replicase complex as the RNA primers synthesized by nsp8 could be utilized by nsp12 immediately for transcription elongation.

5.3 Future Directions

5.3.1 Characterization of interactions involving MADP1 with other viral proteins and host proteins known to function in viral RNA synthesis

The involvement of MADP1 in coronavirus RNA synthesis and its significance have been demonstrated in this thesis using the tissue culture system. Further studies with a MADP1 knock-out animal system, which is currently not available, would be beneficial to affirm the role of MADP1 in coronavirus RNA synthesis. A possible function of MADP1 in coronavirus negative-strand synthesis has also been proposed with the results obtained thus far.

Additional work, especially in the characterization of the interaction between MADP1 and 3'-UTR (+), other viral proteins or even host proteins known to be involved in coronavirus transcription, would be required to substantiate the proposed model. Characterizing the interaction between MADP1 and the 3'-UTR (+) could be carried out in a similar manner as what had been presented in this thesis for the 5'-UTR (+). On the otherhand, a screen by co-IP and verification with indirect immunofluorescence could be employed to ascertain the identities of viral or host proteins interacting with MADP1 during IBV infections. The results from these studies would together, provide a clearer illustration of how MADP1 works in the viral RTC.

5.3.2 Confirming the colocalization of MADP1 with viral proteins in the RTC

In addition to the studies suggested above, it would be beneficial to obtain colocalization data for MADP1 and the viral RTC. This could possibly be accomplished by employing fluorescence resonance energy transfer (FRET) analysis to provide quantitative data on the localization of MADP1 and a vital component of the viral RTC, for example, nsp8 or nsp12. This would ascertain if MADP1 is indeed colocalizing with the viral RTC, thus providing additional evidence that MADP1 is indeed required for viral RNA synthesis.

5.3.3 Functional analysis of MADP1 in other coronavirus infections

While the role of MADP1 in IBV RNA synthesis is unquestionable, the question if it is also required for other coronaviruses remains. The interaction between MADP1 and the 5'-UTR (+) of IBV was observed to be exceptionally strong compared to that of SARS-CoV or HCoV-OC43. As other host or viral proteins could possibly affect binding affinity between MADP1 and the RNA substrate in a cell system, whether the weak interaction demonstrated for the two betacoronaviruses amount to a lower dependency or independency of MADP1 for RNA synthesis would need to be examined with functional studies in virus infected cells.

5.3.4 Further characterization and structural confirmation of the interaction between nsp8 and nsp12

Some detail on the enzymatic core of the viral RTC, has also been illustrated, including a proposed model of the two RdRPs working in tandem, which ensures the

efficiency of the replicase complex. However, further characterization of the interaction between nsp8 and nsp12 is still required to ascertain if the proposed model is valid. Structural information, especially the resolution of the nsp12 structure would be of particular importance in confirming if the interactions detected between its N- and C-terminals and nsp8 are spatially possible. However, as none of the structures of coronavirus nsp12 has been solved till date, only predictions of its structure are available. This would be one of the most important studies required for the elucidation of cooperation between nsp8 and nsp12. Likewise, the interaction site on nsp8 should also be mapped as its interaction with nsp12 would only be meaningful if it is confined to the exterior of the hexadecameric complex.

In addition, functional studies by introducing mutations at the interaction sites could be performed to ascertain if the interaction between nsp8 and nsp12 is crucial for the processivity of the replicase complex.

References

1. Brian, D.A. and Baric, R.S. (2005) Coronavirus genome structure and replication. *Curr Top Microbiol Immunol*, **287**, 1-30.

2. Youn, S., Leibowitz, J.L. and Collisson, E.W. (2005) In vitro assembled, recombinant infectious bronchitis viruses demonstrate that the 5a open reading frame is not essential for replication. *Virology*, **332**, 206-215.

3. Yokomori, K. and Lai, M.M. (1991) Mouse hepatitis virus S RNA sequence reveals that nonstructural proteins ns4 and ns5a are not essential for murine coronavirus replication. *J Virol*, **65**, 5605-5608.

4. Fischer, F., Peng, D., Hingley, S.T., Weiss, S.R. and Masters, P.S. (1997) The internal open reading frame within the nucleocapsid gene of mouse hepatitis virus encodes a structural protein that is not essential for viral replication. *J Virol*, **71**, 996-1003.

5. Bosch, B.J., van der Zee, R., de Haan, C.A. and Rottier, P.J. (2003) The coronavirus spike protein is a class I virus fusion protein: structural and functional characterization of the fusion core complex. *J Virol*, **77**, 8801-8811.

6. Cavanagh, D., Davis, P.J., Pappin, D.J., Binns, M.M., Boursnell, M.E. and Brown, T.D. (1986) Coronavirus IBV: partial amino terminal sequencing of spike polypeptide S2 identifies the sequence Arg-Arg-Phe-Arg-Arg at the cleavage site of the spike precursor propolypeptide of IBV strains Beaudette and M41. *Virus Res*, **4**, 133-143.

7. Bonavia, A., Zelus, B.D., Wentworth, D.E., Talbot, P.J. and Holmes, K.V. (2003) Identification of a receptor-binding domain of the spike glycoprotein of human coronavirus HCoV-229E. *J Virol*, **77**, 2530-2538.

8. Gallagher, T.M. and Buchmeier, M.J. (2001) Coronavirus spike proteins in viral entry and pathogenesis. *Virology*, **279**, 371-374.

9. Casais, R., Dove, B., Cavanagh, D. and Britton, P. (2003) Recombinant avian infectious bronchitis virus expressing a heterologous spike gene demonstrates that the spike protein is a determinant of cell tropism. *J Virol*, **77**, 9084-9089.

10. Yokomori, K., Banner, L.R. and Lai, M.M. (1991) Heterogeneity of gene expression of the hemagglutinin-esterase (HE) protein of murine coronaviruses. *Virology*, **183**, 647-657.

11. Luytjes, W., Bredenbeek, P.J., Noten, A.F., Horzinek, M.C. and Spaan, W.J. (1988) Sequence of mouse hepatitis virus A59 mRNA 2: indications for RNA recombination between coronaviruses and influenza C virus. *Virology*, **166**, 415-422.

12. Shieh, C.K., Lee, H.J., Yokomori, K., La Monica, N., Makino, S. and Lai, M.M. (1989) Identification of a new transcriptional initiation site and the corresponding functional gene 2b in the murine coronavirus RNA genome. *J Virol*, **63**, 3729-3736.

13. Sugiyama, K., Ishikawa, R. and Fukuhara, N. (1986) Structural polypeptides of the murine coronavirus DVIM. *Arch Virol*, **89**, 245-254.

14. Vlasak, R., Luytjes, W., Leider, J., Spaan, W. and Palese, P. (1988) The E3 protein of bovine coronavirus is a receptor-destroying enzyme with acetylesterase activity. *J Virol*, **62**, 4686-4690.

15. Schultze, B., Wahn, K., Klenk, H.D. and Herrler, G. (1991) Isolated HE-protein from hemagglutinating encephalomyelitis virus and bovine coronavirus has receptor-destroying and receptor-binding activity. *Virology*, **180**, 221-228.

16. Schultze, B., Gross, H.J., Brossmer, R. and Herrler, G. (1991) The S protein of bovine coronavirus is a hemagglutinin recognizing 9-O-acetylated sialic acid as a receptor determinant. *J Virol*, **65**, 6232-6237.

17. Kunkel, F. and Herrler, G. (1993) Structural and functional analysis of the surface protein of human coronavirus OC43. *Virology*, **195**, 195-202.

18. Zuniga, S., Sola, I., Moreno, J.L., Sabella, P., Plana-Duran, J. and Enjuanes, L. (2007) Coronavirus nucleocapsid protein is an RNA chaperone. *Virology*, **357**, 215-227.

19. Chang, C.K., Sue, S.C., Yu, T.H., Hsieh, C.M., Tsai, C.K., Chiang, Y.C., Lee, S.J., Hsiao, H.H., Wu, W.J., Chang, W.L. *et al.* (2006) Modular organization of SARS coronavirus nucleocapsid protein. *J Biomed Sci*, **13**, 59-72.

20. Surjit, M., Liu, B., Kumar, P., Chow, V.T. and Lal, S.K. (2004) The nucleocapsid protein of the SARS coronavirus is capable of self-association through a C-terminal 209 amino acid interaction domain. *Biochem Biophys Res Commun*, **317**, 1030-1036.

21. Yu, I.M., Oldham, M.L., Zhang, J. and Chen, J. (2006) Crystal structure of the severe acute respiratory syndrome (SARS) coronavirus nucleocapsid protein dimerization domain reveals evolutionary linkage between corona- and arteriviridae. *J Biol Chem*, **281**, 17134-17139.

22. Yu, I.M., Gustafson, C.L., Diao, J., Burgner, J.W., 2nd, Li, Z., Zhang, J. and Chen, J. (2005) Recombinant severe acute respiratory syndrome (SARS) coronavirus nucleocapsid protein forms a dimer through its C-terminal domain. *J Biol Chem*, **280**, 23280-23286.

23. Hsieh, P.K., Chang, S.C., Huang, C.C., Lee, T.T., Hsiao, C.W., Kou, Y.H., Chen, I.Y., Chang, C.K., Huang, T.H. and Chang, M.F. (2005) Assembly of

severe acute respiratory syndrome coronavirus RNA packaging signal into virus-like particles is nucleocapsid dependent. *J Virol*, **79**, 13848-13855.

24. Chen, C.Y., Chang, C.K., Chang, Y.W., Sue, S.C., Bai, H.I., Riang, L., Hsiao, C.D. and Huang, T.H. (2007) Structure of the SARS coronavirus nucleocapsid protein RNA-binding dimerization domain suggests a mechanism for helical packaging of viral RNA. *J Mol Biol*, **368**, 1075-1086.

25. Luo, H., Chen, J., Chen, K., Shen, X. and Jiang, H. (2006) Carboxyl terminus of severe acute respiratory syndrome coronavirus nucleocapsid protein: self-association analysis and nucleic acid binding characterization. *Biochemistry*, **45**, 11827-11835.

26. Klumperman, J., Locker, J.K., Meijer, A., Horzinek, M.C., Geuze, H.J. and Rottier, P.J. (1994) Coronavirus M proteins accumulate in the Golgi complex beyond the site of virion budding. *J Virol*, **68**, 6523-6534.

27. Nguyen, V.P. and Hogue, B.G. (1997) Protein interactions during coronavirus assembly. *J Virol*, **71**, 9278-9284.

28. Narayanan, K., Maeda, A., Maeda, J. and Makino, S. (2000) Characterization of the coronavirus M protein and nucleocapsid interaction in infected cells. *J Virol*, **74**, 8127-8134.

29. Tseng, Y.T., Wang, S.M., Huang, K.J., Lee, A.I., Chiang, C.C. and Wang, C.T. (2010) Self-assembly of severe acute respiratory syndrome coronavirus membrane protein. *J Biol Chem*, **285**, 12862-12872.

30. de Haan, C.A., Vennema, H. and Rottier, P.J. (2000) Assembly of the coronavirus envelope: homotypic interactions between the M proteins. *J Virol*, **74**, 4967-4978.

31. Corse, E. and Machamer, C.E. (2000) Infectious bronchitis virus E protein is targeted to the Golgi complex and directs release of virus-like particles. *J Virol*, **74**, 4319-4326.

32. Bos, E.C., Luytjes, W., van der Meulen, H.V., Koerten, H.K. and Spaan, W.J. (1996) The production of recombinant infectious DI-particles of a murine coronavirus in the absence of helper virus. *Virology*, **218**, 52-60.

33. Vennema, H., Godeke, G.J., Rossen, J.W., Voorhout, W.F., Horzinek, M.C., Opstelten, D.J. and Rottier, P.J. (1996) Nucleocapsid-independent assembly of coronavirus-like particles by co-expression of viral envelope protein genes. *EMBO J*, **15**, 2020-2028.

34. Baudoux, P., Carrat, C., Besnardeau, L., Charley, B. and Laude, H. (1998) Coronavirus pseudoparticles formed with recombinant M and E proteins induce alpha interferon synthesis by leukocytes. *J Virol*, **72**, 8636-8643.

35. Maeda, J., Maeda, A. and Makino, S. (1999) Release of coronavirus E protein in membrane vesicles from virus-infected cells and E protein-expressing cells. *Virology*, **263**, 265-272.

36. Fischer, F., Stegen, C.F., Masters, P.S. and Samsonoff, W.A. (1998) Analysis of constructed E gene mutants of mouse hepatitis virus confirms a pivotal role for E protein in coronavirus assembly. *J Virol*, **72**, 7885-7894.

37. Snijder, E.J., van der Meer, Y., Zevenhoven-Dobbe, J., Onderwater, J.J., van der Meulen, J., Koerten, H.K. and Mommaas, A.M. (2006) Ultrastructure and origin of membrane vesicles associated with the severe acute respiratory syndrome coronavirus replication complex. *J Virol*, **80**, 5927-5940.

38. Gosert, R., Kanjanahaluethai, A., Egger, D., Bienz, K. and Baker, S.C. (2002) RNA replication of mouse hepatitis virus takes place at double-membrane vesicles. *J Virol*, **76**, 3697-3708.

39. Brockway, S.M., Clay, C.T., Lu, X.T. and Denison, M.R. (2003) Characterization of the expression, intracellular localization, and replication complex association of the putative mouse hepatitis virus RNA-dependent RNA polymerase. *J Virol*, **77**, 10515-10527.

40. Stadler, K., Masignani, V., Eickmann, M., Becker, S., Abrignani, S., Klenk, H.D. and Rappuoli, R. (2003) SARS--beginning to understand a new virus. *Nat Rev Microbiol*, **1**, 209-218.

41. Chu, V.C., McElroy, L.J., Chu, V., Bauman, B.E. and Whittaker, G.R. (2006) The avian coronavirus infectious bronchitis virus undergoes direct low-pH-dependent fusion activation during entry into host cells. *J Virol*, **80**, 3180-3188.

42. Eifart, P., Ludwig, K., Bottcher, C., de Haan, C.A., Rottier, P.J., Korte, T. and Herrmann, A. (2007) Role of endocytosis and low pH in murine hepatitis virus strain A59 cell entry. *J Virol*, **81**, 10758-10768.

43. Gallagher, T.M., Escarmis, C. and Buchmeier, M.J. (1991) Alteration of the pH dependence of coronavirus-induced cell fusion: effect of mutations in the spike glycoprotein. *J Virol*, **65**, 1916-1928.

44. Kooi, C., Cervin, M. and Anderson, R. (1991) Differentiation of acid-pH-dependent and -nondependent entry pathways for mouse hepatitis virus. *Virology*, **180**, 108-119.

45. Hofmann, H., Pyrc, K., van der Hoek, L., Geier, M., Berkhout, B. and Pohlmann, S. (2005) Human coronavirus NL63 employs the severe acute respiratory syndrome coronavirus receptor for cellular entry. *Proc Natl Acad Sci U S A*, **102**, 7988-7993.

46. Li, W., Moore, M.J., Vasilieva, N., Sui, J., Wong, S.K., Berne, M.A., Somasundaran, M., Sullivan, J.L., Luzuriaga, K., Greenough, T.C. *et al.*

(2003) Angiotensin-converting enzyme 2 is a functional receptor for the SARS coronavirus. *Nature*, **426**, 450-454.

47. Wu, K., Li, W., Peng, G. and Li, F. (2009) Crystal structure of NL63 respiratory coronavirus receptor-binding domain complexed with its human receptor. *Proc Natl Acad Sci U S A*, **106**, 19970-19974.

48. Winter, C., Schwegmann-Wessels, C., Cavanagh, D., Neumann, U. and Herrler, G. (2006) Sialic acid is a receptor determinant for infection of cells by avian Infectious bronchitis virus. *J Gen Virol*, **87**, 1209-1216.

49. Simmons, G., Gosalia, D.N., Rennekamp, A.J., Reeves, J.D., Diamond, S.L. and Bates, P. (2005) Inhibitors of cathepsin L prevent severe acute respiratory syndrome coronavirus entry. *Proc Natl Acad Sci U S A*, **102**, 11876-11881.

50. Matsuyama, S., Ujike, M., Morikawa, S., Tashiro, M. and Taguchi, F. (2005) Protease-mediated enhancement of severe acute respiratory syndrome coronavirus infection. *Proc Natl Acad Sci U S A*, **102**, 12543-12547.

51. Du, L., Kao, R.Y., Zhou, Y., He, Y., Zhao, G., Wong, C., Jiang, S., Yuen, K.Y., Jin, D.Y. and Zheng, B.J. (2007) Cleavage of spike protein of SARS coronavirus by protease factor Xa is associated with viral infectivity. *Biochem Biophys Res Commun*, **359**, 174-179.

52. Belouzard, S., Chu, V.C. and Whittaker, G.R. (2009) Activation of the SARS coronavirus spike protein via sequential proteolytic cleavage at two distinct sites. *Proc Natl Acad Sci U S A*, **106**, 5871-5876.

53. Shulla, A., Heald-Sargent, T., Subramanya, G., Zhao, J., Perlman, S. and Gallagher, T. (2011) A transmembrane serine protease is linked to the severe acute respiratory syndrome coronavirus receptor and activates virus entry. *J Virol*, **85**, 873-882.

54. Matsuyama, S. and Taguchi, F. (2009) Two-step conformational changes in a coronavirus envelope glycoprotein mediated by receptor binding and proteolysis. *J Virol*, **83**, 11133-11141.

55. Yamada, Y. and Liu, D.X. (2009) Proteolytic activation of the spike protein at a novel RRRR/S motif is implicated in furin-dependent entry, syncytium formation, and infectivity of coronavirus infectious bronchitis virus in cultured cells. *J Virol*, **83**, 8744-8758.

56. Brierley, I., Boursnell, M.E., Binns, M.M., Bilimoria, B., Blok, V.C., Brown, T.D. and Inglis, S.C. (1987) An efficient ribosomal frame-shifting signal in the polymerase-encoding region of the coronavirus IBV. *EMBO J*, **6**, 3779-3785.

57. Bredenbeek, P.J., Pachuk, C.J., Noten, A.F., Charite, J., Luytjes, W., Weiss, S.R. and Spaan, W.J. (1990) The primary structure and expression of the second open reading frame of the polymerase gene of the coronavirus MHV-

A59; a highly conserved polymerase is expressed by an efficient ribosomal frameshifting mechanism. *Nucleic Acids Res*, **18**, 1825-1832.

58. Herold, J., Raabe, T., Schelle-Prinz, B. and Siddell, S.G. (1993) Nucleotide sequence of the human coronavirus 229E RNA polymerase locus. *Virology*, **195**, 680-691.

59. Ziebuhr, J., Snijder, E.J. and Gorbalenya, A.E. (2000) Virus-encoded proteinases and proteolytic processing in the Nidovirales. *J Gen Virol*, **81**, 853-879.

60. Prentice, E., McAuliffe, J., Lu, X., Subbarao, K. and Denison, M.R. (2004) Identification and characterization of severe acute respiratory syndrome coronavirus replicase proteins. *J Virol*, **78**, 9977-9986.

61. Gorbalenya, A.E., Enjuanes, L., Ziebuhr, J. and Snijder, E.J. (2006) Nidovirales: evolving the largest RNA virus genome. *Virus Res*, **117**, 17-37.

62. Kim, J.C., Spence, R.A., Currier, P.F., Lu, X. and Denison, M.R. (1995) Coronavirus protein processing and RNA synthesis is inhibited by the cysteine proteinase inhibitor E64d. *Virology*, **208**, 1-8.

63. Boursnell, M.E., Brown, T.D., Foulds, I.J., Green, P.F., Tomley, F.M. and Binns, M.M. (1987) Completion of the sequence of the genome of the coronavirus avian infectious bronchitis virus. *J Gen Virol*, **68 (Pt 1)**, 57-77.

64. Fang, S.G., Shen, H., Wang, J., Tay, F.P. and Liu, D.X. (2008) Proteolytic processing of polyproteins 1a and 1ab between non-structural proteins 10 and 11/12 of Coronavirus infectious bronchitis virus is dispensable for viral replication in cultured cells. *Virology*, **379**, 175-180.

65. Fang, S., Shen, H., Wang, J., Tay, F.P. and Liu, D.X. (2010) Functional and genetic studies of the substrate specificity of coronavirus infectious bronchitis virus 3C-like proteinase. *J Virol*, **84**, 7325-7336.

66. Sawicki, S.G., Sawicki, D.L., Younker, D., Meyer, Y., Thiel, V., Stokes, H. and Siddell, S.G. (2005) Functional and genetic analysis of coronavirus replicase-transcriptase proteins. *PLoS Pathog*, **1**, e39.

67. Sawicki, S.G. and Sawicki, D.L. (1998) A new model for coronavirus transcription. *Adv Exp Med Biol*, **440**, 215-219.

68. Sawicki, S.G. and Sawicki, D.L. (1990) Coronavirus transcription: subgenomic mouse hepatitis virus replicative intermediates function in RNA synthesis. *J Virol*, **64**, 1050-1056.

69. Schaad, M.C. and Baric, R.S. (1994) Genetics of mouse hepatitis virus transcription: evidence that subgenomic negative strands are functional templates. *J Virol*, **68**, 8169-8179.

70. Sethna, P.B., Hung, S.L. and Brian, D.A. (1989) Coronavirus subgenomic minus-strand RNAs and the potential for mRNA replicons. *Proc Natl Acad Sci U S A*, **86**, 5626-5630.

71. Sawicki, S.G., Sawicki, D.L. and Siddell, S.G. (2007) A contemporary view of coronavirus transcription. *J Virol*, **81**, 20-29.

72. Herold, J. and Andino, R. (2001) Poliovirus RNA replication requires genome circularization through a protein-protein bridge. *Mol Cell*, **7**, 581-591.

73. Chen, S.C. and Olsthoorn, R.C. (2010) Group-specific structural features of the 5'-proximal sequences of coronavirus genomic RNAs. *Virology*, **401**, 29-41.

74. Liu, P., Li, L., Millership, J.J., Kang, H., Leibowitz, J.L. and Giedroc, D.P. (2007) A U-turn motif-containing stem-loop in the coronavirus 5' untranslated region plays a functional role in replication. *RNA*, **13**, 763-780.

75. Li, L., Kang, H., Liu, P., Makkinje, N., Williamson, S.T., Leibowitz, J.L. and Giedroc, D.P. (2008) Structural lability in stem-loop 1 drives a 5' UTR-3' UTR interaction in coronavirus replication. *J Mol Biol*, **377**, 790-803.

76. Tahara, S.M., Dietlin, T.A., Bergmann, C.C., Nelson, G.W., Kyuwa, S., Anthony, R.P. and Stohlman, S.A. (1994) Coronavirus translational regulation: leader affects mRNA efficiency. *Virology*, **202**, 621-630.

77. Raman, S., Bouma, P., Williams, G.D. and Brian, D.A. (2003) Stem-loop III in the 5' untranslated region is a cis-acting element in bovine coronavirus defective interfering RNA replication. *J Virol*, **77**, 6720-6730.

78. Raman, S. and Brian, D.A. (2005) Stem-loop IV in the 5' untranslated region is a cis-acting element in bovine coronavirus defective interfering RNA replication. *J Virol*, **79**, 12434-12446.

79. Zust, R., Miller, T.B., Goebel, S.J., Thiel, V. and Masters, P.S. (2008) Genetic interactions between an essential 3' cis-acting RNA pseudoknot, replicase gene products, and the extreme 3' end of the mouse coronavirus genome. *J Virol*, **82**, 1214-1228.

80. Hsue, B. and Masters, P.S. (1997) A bulged stem-loop structure in the 3' untranslated region of the genome of the coronavirus mouse hepatitis virus is essential for replication. *J Virol*, **71**, 7567-7578.

81. Hsue, B., Hartshorne, T. and Masters, P.S. (2000) Characterization of an essential RNA secondary structure in the 3' untranslated region of the murine coronavirus genome. *J Virol*, **74**, 6911-6921.

82. Dye, C. and Siddell, S.G. (2005) Genomic RNA sequence of Feline coronavirus strain FIPV WSU-79/1146. *J Gen Virol*, **86**, 2249-2253.

83. Dalton, K., Casais, R., Shaw, K., Stirrups, K., Evans, S., Britton, P., Brown, T.D. and Cavanagh, D. (2001) cis-acting sequences required for coronavirus infectious bronchitis virus defective-RNA replication and packaging. *J Virol*, **75**, 125-133.

84. Williams, G.D., Chang, R.Y. and Brian, D.A. (1999) A phylogenetically conserved hairpin-type 3' untranslated region pseudoknot functions in coronavirus RNA replication. *J Virol*, **73**, 8349-8355.

85. Lin, Y.J., Liao, C.L. and Lai, M.M. (1994) Identification of the cis-acting signal for minus-strand RNA synthesis of a murine coronavirus: implications for the role of minus-strand RNA in RNA replication and transcription. *J Virol*, **68**, 8131-8140.

86. Sola, I., Moreno, J.L., Zuniga, S., Alonso, S. and Enjuanes, L. (2005) Role of nucleotides immediately flanking the transcription-regulating sequence core in coronavirus subgenomic mRNA synthesis. *J Virol*, **79**, 2506-2516.

87. Alonso, S., Izeta, A., Sola, I. and Enjuanes, L. (2002) Transcription regulatory sequences and mRNA expression levels in the coronavirus transmissible gastroenteritis virus. *J Virol*, **76**, 1293-1308.

88. Pasternak, A.O., van den Born, E., Spaan, W.J. and Snijder, E.J. (2001) Sequence requirements for RNA strand transfer during nidovirus discontinuous subgenomic RNA synthesis. *EMBO J*, **20**, 7220-7228.

89. van Marle, G., Dobbe, J.C., Gultyaev, A.P., Luytjes, W., Spaan, W.J. and Snijder, E.J. (1999) Arterivirus discontinuous mRNA transcription is guided by base pairing between sense and antisense transcription-regulating sequences. *Proc Natl Acad Sci U S A*, **96**, 12056-12061.

90. Zuniga, S., Sola, I., Alonso, S. and Enjuanes, L. (2004) Sequence motifs involved in the regulation of discontinuous coronavirus subgenomic RNA synthesis. *J Virol*, **78**, 980-994.

91. Grossoehme, N.E., Li, L., Keane, S.C., Liu, P., Dann, C.E., 3rd, Leibowitz, J.L. and Giedroc, D.P. (2009) Coronavirus N protein N-terminal domain (NTD) specifically binds the transcriptional regulatory sequence (TRS) and melts TRS-cTRS RNA duplexes. *J Mol Biol*, **394**, 544-557.

92. Zhang, X. and Lai, M.M. (1996) A 5'-proximal RNA sequence of murine coronavirus as a potential initiation site for genomic-length mRNA transcription. *J Virol*, **70**, 705-711.

93. Enjuanes, L., Almazan, F., Sola, I. and Zuniga, S. (2006) Biochemical aspects of coronavirus replication and virus-host interaction. *Annu Rev Microbiol*, **60**, 211-230.

94. Hussain, S., Pan, J., Chen, Y., Yang, Y., Xu, J., Peng, Y., Wu, Y., Li, Z., Zhu, Y., Tien, P. *et al.* (2005) Identification of novel subgenomic RNAs and

noncanonical transcription initiation signals of severe acute respiratory syndrome coronavirus. *J Virol*, **79**, 5288-5295.

95. Wu, H.Y., Ozdarendeli, A. and Brian, D.A. (2006) Bovine coronavirus 5'-proximal genomic acceptor hotspot for discontinuous transcription is 65 nucleotides wide. *J Virol*, **80**, 2183-2193.

96. Dufour, D., Mateos-Gomez, P.A., Enjuanes, L., Gallego, J. and Sola, I. (2011) Structure and functional relevance of a transcription-regulating sequence involved in coronavirus discontinuous RNA synthesis. *J Virol*, **85**, 4963-4973.

97. Sawicki, S.G. and Sawicki, D.L. (1986) Coronavirus minus-strand RNA synthesis and effect of cycloheximide on coronavirus RNA synthesis. *J Virol*, **57**, 328-334.

98. Ziebuhr, J. (2005) The coronavirus replicase. *Curr Top Microbiol Immunol*, **287**, 57-94.

99. Tanner, J.A., Watt, R.M., Chai, Y.B., Lu, L.Y., Lin, M.C., Peiris, J.S., Poon, L.L., Kung, H.F. and Huang, J.D. (2003) The severe acute respiratory syndrome (SARS) coronavirus NTPase/helicase belongs to a distinct class of 5' to 3' viral helicases. *J Biol Chem*, **278**, 39578-39582.

100. Lee, N.R., Kwon, H.M., Park, K., Oh, S., Jeong, Y.J. and Kim, D.E. (2010) Cooperative translocation enhances the unwinding of duplex DNA by SARS coronavirus helicase nsP13. *Nucleic Acids Res*, **38**, 7626-7636.

101. te Velthuis, A.J., Arnold, J.J., Cameron, C.E., van den Worm, S.H. and Snijder, E.J. (2010) The RNA polymerase activity of SARS-coronavirus nsp12 is primer dependent. *Nucleic Acids Res*, **38**, 203-214.

102. Fang, S., Chen, B., Tay, F.P., Ng, B.S. and Liu, D.X. (2007) An arginine-to-proline mutation in a domain with undefined functions within the helicase protein (Nsp13) is lethal to the coronavirus infectious bronchitis virus in cultured cells. *Virology*, **358**, 136-147.

103. Imbert, I., Guillemot, J.C., Bourhis, J.M., Bussetta, C., Coutard, B., Egloff, M.P., Ferron, F., Gorbalenya, A.E. and Canard, B. (2006) A second, non-canonical RNA-dependent RNA polymerase in SARS coronavirus. *EMBO J*, **25**, 4933-4942.

104. Zhai, Y., Sun, F., Li, X., Pang, H., Xu, X., Bartlam, M. and Rao, Z. (2005) Insights into SARS-CoV transcription and replication from the structure of the nsp7-nsp8 hexadecamer. *Nat Struct Mol Biol*, **12**, 980-986.

105. Bost, A.G., Carnahan, R.H., Lu, X.T. and Denison, M.R. (2000) Four proteins processed from the replicase gene polyprotein of mouse hepatitis virus colocalize in the cell periphery and adjacent to sites of virion assembly. *J Virol*, **74**, 3379-3387.

106. Egloff, M.P., Ferron, F., Campanacci, V., Longhi, S., Rancurel, C., Dutartre, H., Snijder, E.J., Gorbalenya, A.E., Cambillau, C. and Canard, B. (2004) The severe acute respiratory syndrome-coronavirus replicative protein nsp9 is a single-stranded RNA-binding subunit unique in the RNA virus world. *Proc Natl Acad Sci U S A*, **101**, 3792-3796.

107. Sutton, G., Fry, E., Carter, L., Sainsbury, S., Walter, T., Nettleship, J., Berrow, N., Owens, R., Gilbert, R., Davidson, A. *et al.* (2004) The nsp9 replicase protein of SARS-coronavirus, structure and functional insights. *Structure*, **12**, 341-353.

108. Chen, B., Fang, S., Tam, J.P. and Liu, D.X. (2009) Formation of stable homodimer via the C-terminal alpha-helical domain of coronavirus nonstructural protein 9 is critical for its function in viral replication. *Virology*, **383**, 328-337.

109. Joseph, J.S., Saikatendu, K.S., Subramanian, V., Neuman, B.W., Brooun, A., Griffith, M., Moy, K., Yadav, M.K., Velasquez, J., Buchmeier, M.J. *et al.* (2006) Crystal structure of nonstructural protein 10 from the severe acute respiratory syndrome coronavirus reveals a novel fold with two zinc-binding motifs. *J Virol*, **80**, 7894-7901.

110. Su, D., Lou, Z., Sun, F., Zhai, Y., Yang, H., Zhang, R., Joachimiak, A., Zhang, X.C., Bartlam, M. and Rao, Z. (2006) Dodecamer structure of severe acute respiratory syndrome coronavirus nonstructural protein nsp10. *J Virol*, **80**, 7902-7908.

111. Donaldson, E.F., Sims, A.C., Graham, R.L., Denison, M.R. and Baric, R.S. (2007) Murine hepatitis virus replicase protein nsp10 is a critical regulator of viral RNA synthesis. *J Virol*, **81**, 6356-6368.

112. Nedialkova, D.D., Ulferts, R., van den Born, E., Lauber, C., Gorbalenya, A.E., Ziebuhr, J. and Snijder, E.J. (2009) Biochemical characterization of arterivirus nonstructural protein 11 reveals the nidovirus-wide conservation of a replicative endoribonuclease. *J Virol*, **83**, 5671-5682.

113. Ivanov, K.A., Hertzig, T., Rozanov, M., Bayer, S., Thiel, V., Gorbalenya, A.E. and Ziebuhr, J. (2004) Major genetic marker of nidoviruses encodes a replicative endoribonuclease. *Proc Natl Acad Sci U S A*, **101**, 12694-12699.

114. Eckerle, L.D., Lu, X., Sperry, S.M., Choi, L. and Denison, M.R. (2007) High fidelity of murine hepatitis virus replication is decreased in nsp14 exoribonuclease mutants. *J Virol*, **81**, 12135-12144.

115. Minskaia, E., Hertzig, T., Gorbalenya, A.E., Campanacci, V., Cambillau, C., Canard, B. and Ziebuhr, J. (2006) Discovery of an RNA virus 3'->5' exoribonuclease that is critically involved in coronavirus RNA synthesis. *Proc Natl Acad Sci U S A*, **103**, 5108-5113.

116. Ivanov, K.A. and Ziebuhr, J. (2004) Human coronavirus 229E nonstructural protein 13: characterization of duplex-unwinding, nucleoside triphosphatase, and RNA 5'-triphosphatase activities. *J Virol*, **78**, 7833-7838.

117. Chen, Y., Cai, H., Pan, J., Xiang, N., Tien, P., Ahola, T. and Guo, D. (2009) Functional screen reveals SARS coronavirus nonstructural protein nsp14 as a novel cap N7 methyltransferase. *Proc Natl Acad Sci U S A*, **106**, 3484-3489.

118. Decroly, E., Debarnot, C., Ferron, F., Bouvet, M., Coutard, B., Imbert, I., Gluais, L., Papageorgiou, N., Sharff, A., Bricogne, G. *et al.* (2011) Crystal Structure and Functional Analysis of the SARS-Coronavirus RNA Cap 2'-O-Methyltransferase nsp10/nsp16 Complex. *PLoS Pathog*, **7**, e1002059.

119. Lugari, A., Betzi, S., Decroly, E., Bonnaud, E., Hermant, A., Guillemot, J.C., Debarnot, C., Borg, J.P., Bouvet, M., Canard, B. *et al.* (2010) Molecular mapping of the RNA Cap 2'-O-methyltransferase activation interface between severe acute respiratory syndrome coronavirus nsp10 and nsp16. *J Biol Chem*, **285**, 33230-33241.

120. Chen, Y., Su, C., Ke, M., Jin, X., Xu, L., Zhang, Z., Wu, A., Sun, Y., Yang, Z., Tien, P. *et al.* (2011) Biochemical and structural insights into the mechanisms of SARS coronavirus RNA ribose 2'-O-methylation by nsp16/nsp10 protein complex. *PLoS Pathog*, **7**, e1002294.

121. Decroly, E., Imbert, I., Coutard, B., Bouvet, M., Selisko, B., Alvarez, K., Gorbalenya, A.E., Snijder, E.J. and Canard, B. (2008) Coronavirus nonstructural protein 16 is a cap-0 binding enzyme possessing (nucleoside-2'O)-methyltransferase activity. *J Virol*, **82**, 8071-8084.

122. Piotrowski, Y., Hansen, G., Boomaars-van der Zanden, A.L., Snijder, E.J., Gorbalenya, A.E. and Hilgenfeld, R. (2009) Crystal structures of the X-domains of a Group-1 and a Group-3 coronavirus reveal that ADP-ribose-binding may not be a conserved property. *Protein Sci*, **18**, 6-16.

123. Xu, Y., Cong, L., Chen, C., Wei, L., Zhao, Q., Xu, X., Ma, Y., Bartlam, M. and Rao, Z. (2009) Crystal structures of two coronavirus ADP-ribose-1"-monophosphatases and their complexes with ADP-Ribose: a systematic structural analysis of the viral ADRP domain. *J Virol*, **83**, 1083-1092.

124. Wojdyla, J.A., Manolaridis, I., Snijder, E.J., Gorbalenya, A.E., Coutard, B., Piotrowski, Y., Hilgenfeld, R. and Tucker, P.A. (2009) Structure of the X (ADRP) domain of nsp3 from feline coronavirus. *Acta Crystallogr D Biol Crystallogr*, **65**, 1292-1300.

125. Xu, X., Lou, Z., Ma, Y., Chen, X., Yang, Z., Tong, X., Zhao, Q., Xu, Y., Deng, H., Bartlam, M. *et al.* (2009) Crystal structure of the C-terminal cytoplasmic domain of non-structural protein 4 from mouse hepatitis virus A59. *PLoS One*, **4**, e6217.

126. Oostra, M., Hagemeijer, M.C., van Gent, M., Bekker, C.P., te Lintelo, E.G., Rottier, P.J. and de Haan, C.A. (2008) Topology and membrane anchoring of the coronavirus replication complex: not all hydrophobic domains of nsp3 and nsp6 are membrane spanning. *J Virol*, **82**, 12392-12405.

127. Manolaridis, I., Wojdyla, J.A., Panjikar, S., Snijder, E.J., Gorbalenya, A.E., Berglind, H., Nordlund, P., Coutard, B. and Tucker, P.A. (2009) Structure of the C-terminal domain of nsp4 from feline coronavirus. *Acta Crystallogr D Biol Crystallogr*, **65**, 839-846.

128. Hagemeijer, M.C., Ulasli, M., Vonk, A.M., Reggiori, F., Rottier, P.J. and de Haan, C.A. (2011) Mobility and interactions of coronavirus nonstructural protein 4. *J Virol*, **85**, 4572-4577.

129. Oostra, M., te Lintelo, E.G., Deijs, M., Verheije, M.H., Rottier, P.J. and de Haan, C.A. (2007) Localization and membrane topology of coronavirus nonstructural protein 4: involvement of the early secretory pathway in replication. *J Virol*, **81**, 12323-12336.

130. Kanjanahaluethai, A., Chen, Z., Jukneliene, D. and Baker, S.C. (2007) Membrane topology of murine coronavirus replicase nonstructural protein 3. *Virology*, **361**, 391-401.

131. Harcourt, B.H., Jukneliene, D., Kanjanahaluethai, A., Bechill, J., Severson, K.M., Smith, C.M., Rota, P.A. and Baker, S.C. (2004) Identification of severe acute respiratory syndrome coronavirus replicase products and characterization of papain-like protease activity. *J Virol*, **78**, 13600-13612.

132. Sparks, J.S., Lu, X. and Denison, M.R. (2007) Genetic analysis of Murine hepatitis virus nsp4 in virus replication. *J Virol*, **81**, 12554-12563.

133. von Brunn, A., Teepe, C., Simpson, J.C., Pepperkok, R., Friedel, C.C., Zimmer, R., Roberts, R., Baric, R. and Haas, J. (2007) Analysis of intraviral protein-protein interactions of the SARS coronavirus ORFeome. *PLoS One*, **2**, e459.

134. Verheije, M.H., Hagemeijer, M.C., Ulasli, M., Reggiori, F., Rottier, P.J., Masters, P.S. and de Haan, C.A. (2010) The coronavirus nucleocapsid protein is dynamically associated with the replication-transcription complexes. *J Virol*, **84**, 11575-11579.

135. Schelle, B., Karl, N., Ludewig, B., Siddell, S.G. and Thiel, V. (2005) Selective replication of coronavirus genomes that express nucleocapsid protein. *J Virol*, **79**, 6620-6630.

136. Zuniga, S., Cruz, J.L., Sola, I., Mateos-Gomez, P.A., Palacio, L. and Enjuanes, L. (2010) Coronavirus nucleocapsid protein facilitates template switching and is required for efficient transcription. *J Virol*, **84**, 2169-2175.

137. Niemann, H. and Klenk, H.D. (1981) Coronavirus glycoprotein E1, a new type of viral glycoprotein. *J Mol Biol*, **153**, 993-1010.

138. Schmidt, M.F. (1982) Acylation of viral spike glycoproteins: a feature of enveloped RNA viruses. *Virology*, **116**, 327-338.

139. van Berlo, M.F., van den Brink, W.J., Horzinek, M.C. and van der Zeijst, B.A. (1987) Fatty acid acylation of viral proteins in murine hepatitis virus-infected cells. Brief report. *Arch Virol*, **95**, 123-128.

140. Delmas, B. and Laude, H. (1990) Assembly of coronavirus spike protein into trimers and its role in epitope expression. *J Virol*, **64**, 5367-5375.

141. Lopez, L.A., Jones, A., Arndt, W.D. and Hogue, B.G. (2006) Subcellular localization of SARS-CoV structural proteins. *Adv Exp Med Biol*, **581**, 297-300.

142. Nal, B., Chan, C., Kien, F., Siu, L., Tse, J., Chu, K., Kam, J., Staropoli, I., Crescenzo-Chaigne, B., Escriou, N. *et al.* (2005) Differential maturation and subcellular localization of severe acute respiratory syndrome coronavirus surface proteins S, M and E. *J Gen Virol*, **86**, 1423-1434.

143. Gallagher, T.M., Buchmeier, M.J. and Perlman, S. (1993) Dissemination of MHV4 (strain JHM) infection does not require specific coronavirus receptors. *Adv Exp Med Biol*, **342**, 279-284.

144. Corse, E. and Machamer, C.E. (2002) The cytoplasmic tail of infectious bronchitis virus E protein directs Golgi targeting. *J Virol*, **76**, 1273-1284.

145. Boscarino, J.A., Logan, H.L., Lacny, J.J. and Gallagher, T.M. (2008) Envelope protein palmitoylations are crucial for murine coronavirus assembly. *J Virol*, **82**, 2989-2999.

146. Liao, Y., Yuan, Q., Torres, J., Tam, J.P. and Liu, D.X. (2006) Biochemical and functional characterization of the membrane association and membrane permeabilizing activity of the severe acute respiratory syndrome coronavirus envelope protein. *Virology*, **349**, 264-275.

147. Cohen, J.R., Lin, L.D. and Machamer, C.E. (2011) Identification of a Golgi complex-targeting signal in the cytoplasmic tail of the severe acute respiratory syndrome coronavirus envelope protein. *J Virol*, **85**, 5794-5803.

148. Machamer, C.E., Mentone, S.A., Rose, J.K. and Farquhar, M.G. (1990) The E1 glycoprotein of an avian coronavirus is targeted to the cis Golgi complex. *Proc Natl Acad Sci U S A*, **87**, 6944-6948.

149. Locker, J.K., Griffiths, G., Horzinek, M.C. and Rottier, P.J. (1992) O-glycosylation of the coronavirus M protein. Differential localization of sialyltransferases in N- and O-linked glycosylation. *J Biol Chem*, **267**, 14094-14101.

150. Swift, A.M. and Machamer, C.E. (1991) A Golgi retention signal in a membrane-spanning domain of coronavirus E1 protein. *J Cell Biol*, **115**, 19-30.

151. Locker, J.K., Klumperman, J., Oorschot, V., Horzinek, M.C., Geuze, H.J. and Rottier, P.J. (1994) The cytoplasmic tail of mouse hepatitis virus M protein is essential but not sufficient for its retention in the Golgi complex. *J Biol Chem*, **269**, 28263-28269.

152. Baric, R.S., Nelson, G.W., Fleming, J.O., Deans, R.J., Keck, J.G., Casteel, N. and Stohlman, S.A. (1988) Interactions between coronavirus nucleocapsid protein and viral RNAs: implications for viral transcription. *J Virol*, **62**, 4280-4287.

153. Cavanagh, D., Shaw, K. and Zhao, X. (1993) Analysis of messenger RNA within virions of IBV. *Adv Exp Med Biol*, **342**, 123-128.

154. Hofmann, M.A., Sethna, P.B. and Brian, D.A. (1990) Bovine coronavirus mRNA replication continues throughout persistent infection in cell culture. *J Virol*, **64**, 4108-4114.

155. Sethna, P.B., Hofmann, M.A. and Brian, D.A. (1991) Minus-strand copies of replicating coronavirus mRNAs contain antileaders. *J Virol*, **65**, 320-325.

156. Zhao, X., Shaw, K. and Cavanagh, D. (1993) Presence of subgenomic mRNAs in virions of coronavirus IBV. *Virology*, **196**, 172-178.

157. Lai, M.M. and Stohlman, S.A. (1978) RNA of mouse hepatitis virus. *J Virol*, **26**, 236-242.

158. Makino, S., Shieh, C.K., Keck, J.G. and Lai, M.M. (1988) Defective-interfering particles of murine coronavirus: mechanism of synthesis of defective viral RNAs. *Virology*, **163**, 104-111.

159. Makino, S., Yokomori, K. and Lai, M.M. (1990) Analysis of efficiently packaged defective interfering RNAs of murine coronavirus: localization of a possible RNA-packaging signal. *J Virol*, **64**, 6045-6053.

160. Fosmire, J.A., Hwang, K. and Makino, S. (1992) Identification and characterization of a coronavirus packaging signal. *J Virol*, **66**, 3522-3530.

161. van der Most, R.G., Bredenbeek, P.J. and Spaan, W.J. (1991) A domain at the 3' end of the polymerase gene is essential for encapsidation of coronavirus defective interfering RNAs. *J Virol*, **65**, 3219-3226.

162. Woo, K., Joo, M., Narayanan, K., Kim, K.H. and Makino, S. (1997) Murine coronavirus packaging signal confers packaging to nonviral RNA. *J Virol*, **71**, 824-827.

163. Escors, D., Izeta, A., Capiscol, C. and Enjuanes, L. (2003) Transmissible gastroenteritis coronavirus packaging signal is located at the 5' end of the virus genome. *J Virol*, **77**, 7890-7902.

164. Cologna, R. and Hogue, B.G. (2000) Identification of a bovine coronavirus packaging signal. *J Virol*, **74**, 580-583.

165. Dalton, K., Penzes, Z., Wroe, C., Stirrups, K., Evans, S., Shaw, K., Brown, T.D., Britton, P. and Cavanagh, D. (1998) Sequence elements involved in the rescue of IBV defective RNA CD-91. *Adv Exp Med Biol*, **440**, 253-257.

166. Narayanan, K., Chen, C.J., Maeda, J. and Makino, S. (2003) Nucleocapsid-independent specific viral RNA packaging via viral envelope protein and viral RNA signal. *J Virol*, **77**, 2922-2927.

167. Opstelten, D.J., Raamsman, M.J., Wolfs, K., Horzinek, M.C. and Rottier, P.J. (1995) Envelope glycoprotein interactions in coronavirus assembly. *J Cell Biol*, **131**, 339-349.

168. Corse, E. and Machamer, C.E. (2003) The cytoplasmic tails of infectious bronchitis virus E and M proteins mediate their interaction. *Virology*, **312**, 25-34.

169. Lim, K.P. and Liu, D.X. (2001) The missing link in coronavirus assembly. Retention of the avian coronavirus infectious bronchitis virus envelope protein in the pre-Golgi compartments and physical interaction between the envelope and membrane proteins. *J Biol Chem*, **276**, 17515-17523.

170. Ortego, J., Ceriani, J.E., Patino, C., Plana, J. and Enjuanes, L. (2007) Absence of E protein arrests transmissible gastroenteritis coronavirus maturation in the secretory pathway. *Virology*, **368**, 296-308.

171. Torres, J., Wang, J., Parthasarathy, K. and Liu, D.X. (2005) The transmembrane oligomers of coronavirus protein E. *Biophys J*, **88**, 1283-1290.

172. Wilson, L., McKinlay, C., Gage, P. and Ewart, G. (2004) SARS coronavirus E protein forms cation-selective ion channels. *Virology*, **330**, 322-331.

173. Wilson, L., Gage, P. and Ewart, G. (2006) Hexamethylene amiloride blocks E protein ion channels and inhibits coronavirus replication. *Virology*, **353**, 294-306.

174. Ruch, T.R. and Machamer, C.E. (2011) The hydrophobic domain of infectious bronchitis virus E protein alters the host secretory pathway and is important for release of infectious virus. *J Virol*, **85**, 675-685.

175. Nakamura, N., Tanaka, S., Teko, Y., Mitsui, K. and Kanazawa, H. (2005) Four Na+/H+ exchanger isoforms are distributed to Golgi and post-Golgi compartments and are involved in organelle pH regulation. *J Biol Chem*, **280**, 1561-1572.

176. Medzhitov, R. and Janeway, C.A., Jr. (1997) Innate immunity: the virtues of a nonclonal system of recognition. *Cell*, **91**, 295-298.

177. Janeway, C.A., Jr. (1989) Approaching the asymptote? Evolution and revolution in immunology. *Cold Spring Harb Symp Quant Biol*, **54 Pt 1**, 1-13.

178. Perry, A.K., Chen, G., Zheng, D., Tang, H. and Cheng, G. (2005) The host type I interferon response to viral and bacterial infections. *Cell Res*, **15**, 407-422.

179. Uematsu, S. and Akira, S. (2006) Toll-like receptors and innate immunity. *J Mol Med (Berl)*, **84**, 712-725.

180. Kawai, T. and Akira, S. (2011) Toll-like receptors and their crosstalk with other innate receptors in infection and immunity. *Immunity*, **34**, 637-650.

181. Yoneyama, M., Kikuchi, M., Natsukawa, T., Shinobu, N., Imaizumi, T., Miyagishi, M., Taira, K., Akira, S. and Fujita, T. (2004) The RNA helicase RIG-I has an essential function in double-stranded RNA-induced innate antiviral responses. *Nat Immunol*, **5**, 730-737.

182. Loo, Y.M. and Gale, M., Jr. (2011) Immune signaling by RIG-I-like receptors. *Immunity*, **34**, 680-692.

183. Shimada, T., Kawai, T., Takeda, K., Matsumoto, M., Inoue, J., Tatsumi, Y., Kanamaru, A. and Akira, S. (1999) IKK-i, a novel lipopolysaccharide-inducible kinase that is related to IkappaB kinases. *Int Immunol*, **11**, 1357-1362.

184. Tojima, Y., Fujimoto, A., Delhase, M., Chen, Y., Hatakeyama, S., Nakayama, K., Kaneko, Y., Nimura, Y., Motoyama, N., Ikeda, K. *et al.* (2000) NAK is an IkappaB kinase-activating kinase. *Nature*, **404**, 778-782.

185. Hemmi, H., Takeuchi, O., Sato, S., Yamamoto, M., Kaisho, T., Sanjo, H., Kawai, T., Hoshino, K., Takeda, K. and Akira, S. (2004) The roles of two IkappaB kinase-related kinases in lipopolysaccharide and double stranded RNA signaling and viral infection. *J Exp Med*, **199**, 1641-1650.

186. Fitzgerald, K.A., McWhirter, S.M., Faia, K.L., Rowe, D.C., Latz, E., Golenbock, D.T., Coyle, A.J., Liao, S.M. and Maniatis, T. (2003) IKKepsilon and TBK1 are essential components of the IRF3 signaling pathway. *Nat Immunol*, **4**, 491-496.

187. Sharma, S., tenOever, B.R., Grandvaux, N., Zhou, G.P., Lin, R. and Hiscott, J. (2003) Triggering the interferon antiviral response through an IKK-related pathway. *Science*, **300**, 1148-1151.

188. Alexopoulou, L., Holt, A.C., Medzhitov, R. and Flavell, R.A. (2001) Recognition of double-stranded RNA and activation of NF-kappaB by Toll-like receptor 3. *Nature*, **413**, 732-738.

189. Karin, M. and Ben-Neriah, Y. (2000) Phosphorylation meets ubiquitination: the control of NF-[kappa]B activity. *Annu Rev Immunol*, **18**, 621-663.

190. Peters, R.T., Liao, S.M. and Maniatis, T. (2000) IKKepsilon is part of a novel PMA-inducible IkappaB kinase complex. *Mol Cell*, **5**, 513-522.

191. Bonnard, M., Mirtsos, C., Suzuki, S., Graham, K., Huang, J., Ng, M., Itie, A., Wakeham, A., Shahinian, A., Henzel, W.J. *et al.* (2000) Deficiency of T2K leads to apoptotic liver degeneration and impaired NF-kappaB-dependent gene transcription. *EMBO J*, **19**, 4976-4985.

192. Hiscott, J., Pitha, P., Genin, P., Nguyen, H., Heylbroeck, C., Mamane, Y., Algarte, M. and Lin, R. (1999) Triggering the interferon response: the role of IRF-3 transcription factor. *J Interferon Cytokine Res*, **19**, 1-13.

193. Taniguchi, T., Ogasawara, K., Takaoka, A. and Tanaka, N. (2001) IRF family of transcription factors as regulators of host defense. *Annu Rev Immunol*, **19**, 623-655.

194. Hornung, V., Ellegast, J., Kim, S., Brzozka, K., Jung, A., Kato, H., Poeck, H., Akira, S., Conzelmann, K.K., Schlee, M. *et al.* (2006) 5'-Triphosphate RNA is the ligand for RIG-I. *Science*, **314**, 994-997.

195. Pichlmair, A., Schulz, O., Tan, C.P., Naslund, T.I., Liljestrom, P., Weber, F. and Reis e Sousa, C. (2006) RIG-I-mediated antiviral responses to single-stranded RNA bearing 5'-phosphates. *Science*, **314**, 997-1001.

196. Kato, H., Takeuchi, O., Mikamo-Satoh, E., Hirai, R., Kawai, T., Matsushita, K., Hiiragi, A., Dermody, T.S., Fujita, T. and Akira, S. (2008) Length-dependent recognition of double-stranded ribonucleic acids by retinoic acid-inducible gene-I and melanoma differentiation-associated gene 5. *J Exp Med*, **205**, 1601-1610.

197. Schlee, M., Roth, A., Hornung, V., Hagmann, C.A., Wimmenauer, V., Barchet, W., Coch, C., Janke, M., Mihailovic, A., Wardle, G. *et al.* (2009) Recognition of 5' triphosphate by RIG-I helicase requires short blunt double-stranded RNA as contained in panhandle of negative-strand virus. *Immunity*, **31**, 25-34.

198. Gitlin, L., Barchet, W., Gilfillan, S., Cella, M., Beutler, B., Flavell, R.A., Diamond, M.S. and Colonna, M. (2006) Essential role of mda-5 in type I IFN responses to polyriboinosinic:polyribocytidylic acid and encephalomyocarditis picornavirus. *Proc Natl Acad Sci U S A*, **103**, 8459-8464.

199. Zust, R., Cervantes-Barragan, L., Habjan, M., Maier, R., Neuman, B.W., Ziebuhr, J., Szretter, K.J., Baker, S.C., Barchet, W., Diamond, M.S. *et al.* (2011) Ribose 2'-O-methylation provides a molecular signature for the distinction of self and non-self mRNA dependent on the RNA sensor Mda5. *Nat Immunol*, **12**, 137-143.

200. Li, J., Liu, Y. and Zhang, X. (2010) Murine coronavirus induces type I interferon in oligodendrocytes through recognition by RIG-I and MDA5. *J Virol*, **84**, 6472-6482.

201. Zhou, H. and Perlman, S. (2007) Mouse hepatitis virus does not induce Beta interferon synthesis and does not inhibit its induction by double-stranded RNA. *J Virol*, **81**, 568-574.

202. Versteeg, G.A., Bredenbeek, P.J., van den Worm, S.H. and Spaan, W.J. (2007) Group 2 coronaviruses prevent immediate early interferon induction by protection of viral RNA from host cell recognition. *Virology*, **361**, 18-26.

203. Ye, Y., Hauns, K., Langland, J.O., Jacobs, B.L. and Hogue, B.G. (2007) Mouse hepatitis coronavirus A59 nucleocapsid protein is a type I interferon antagonist. *J Virol*, **81**, 2554-2563.

204. Lu, X., Pan, J., Tao, J. and Guo, D. (2011) SARS-CoV nucleocapsid protein antagonizes IFN-beta response by targeting initial step of IFN-beta induction pathway, and its C-terminal region is critical for the antagonism. *Virus Genes*, **42**, 37-45.

205. Siu, K.L., Kok, K.H., Ng, M.H., Poon, V.K., Yuen, K.Y., Zheng, B.J. and Jin, D.Y. (2009) Severe acute respiratory syndrome coronavirus M protein inhibits type I interferon production by impeding the formation of TRAF3.TANK.TBK1/IKKepsilon complex. *J Biol Chem*, **284**, 16202-16209.

206. Fang, X., Gao, J., Zheng, H., Li, B., Kong, L., Zhang, Y., Wang, W., Zeng, Y. and Ye, L. (2007) The membrane protein of SARS-CoV suppresses NF-kappaB activation. *J Med Virol*, **79**, 1431-1439.

207. Lindner, H.A., Fotouhi-Ardakani, N., Lytvyn, V., Lachance, P., Sulea, T. and Menard, R. (2005) The papain-like protease from the severe acute respiratory syndrome coronavirus is a deubiquitinating enzyme. *J Virol*, **79**, 15199-15208.

208. Chen, Z., Wang, Y., Ratia, K., Mesecar, A.D., Wilkinson, K.D. and Baker, S.C. (2007) Proteolytic processing and deubiquitinating activity of papain-like proteases of human coronavirus NL63. *J Virol*, **81**, 6007-6018.

209. Wojdyla, J.A., Manolaridis, I., van Kasteren, P.B., Kikkert, M., Snijder, E.J., Gorbalenya, A.E. and Tucker, P.A. (2010) Papain-like protease 1 from transmissible gastroenteritis virus: crystal structure and enzymatic activity toward viral and cellular substrates. *J Virol*, **84**, 10063-10073.

210. Wang, G., Chen, G., Zheng, D., Cheng, G. and Tang, H. (2011) PLP2 of mouse hepatitis virus A59 (MHV-A59) targets TBK1 to negatively regulate cellular type I interferon signaling pathway. *PLoS One*, **6**, e17192.

211. Devaraj, S.G., Wang, N., Chen, Z., Tseng, M., Barretto, N., Lin, R., Peters, C.J., Tseng, C.T., Baker, S.C. and Li, K. (2007) Regulation of IRF-3-

dependent innate immunity by the papain-like protease domain of the severe acute respiratory syndrome coronavirus. *J Biol Chem*, **282**, 32208-32221.

212. Clementz, M.A., Chen, Z., Banach, B.S., Wang, Y., Sun, L., Ratia, K., Baez-Santos, Y.M., Wang, J., Takayama, J., Ghosh, A.K. *et al.* (2010) Deubiquitinating and interferon antagonism activities of coronavirus papain-like proteases. *J Virol*, **84**, 4619-4629.

213. Kuri, T., Eriksson, K.K., Putics, A., Zust, R., Snijder, E.J., Davidson, A.D., Siddell, S.G., Thiel, V., Ziebuhr, J. and Weber, F. (2011) The ADP-ribose-1"-monophosphatase domains of SARS-coronavirus and Human coronavirus 229E mediate resistance to antiviral interferon responses. *J Gen Virol*, **29**, 1988-1905.

214. Kamitani, W., Narayanan, K., Huang, C., Lokugamage, K., Ikegami, T., Ito, N., Kubo, H. and Makino, S. (2006) Severe acute respiratory syndrome coronavirus nsp1 protein suppresses host gene expression by promoting host mRNA degradation. *Proc Natl Acad Sci U S A*, **103**, 12885-12890.

215. Zust, R., Cervantes-Barragan, L., Kuri, T., Blakqori, G., Weber, F., Ludewig, B. and Thiel, V. (2007) Coronavirus non-structural protein 1 is a major pathogenicity factor: implications for the rational design of coronavirus vaccines. *PLoS Pathog*, **3**, e109.

216. Narayanan, K., Huang, C., Lokugamage, K., Kamitani, W., Ikegami, T., Tseng, C.T. and Makino, S. (2008) Severe acute respiratory syndrome coronavirus nsp1 suppresses host gene expression, including that of type I interferon, in infected cells. *J Virol*, **82**, 4471-4479.

217. Kamitani, W., Huang, C., Narayanan, K., Lokugamage, K.G. and Makino, S. (2009) A two-pronged strategy to suppress host protein synthesis by SARS coronavirus Nsp1 protein. *Nat Struct Mol Biol*, **16**, 1134-1140.

218. Wathelet, M.G., Orr, M., Frieman, M.B. and Baric, R.S. (2007) Severe acute respiratory syndrome coronavirus evades antiviral signaling: role of nsp1 and rational design of an attenuated strain. *J Virol*, **81**, 11620-11633.

219. Wang, X., Liao, Y., Yap, P.L., Png, K.J., Tam, J.P. and Liu, D.X. (2009) Inhibition of protein kinase R activation and upregulation of GADD34 expression play a synergistic role in facilitating coronavirus replication by maintaining de novo protein synthesis in virus-infected cells. *J Virol*, **83**, 12462-12472.

220. Graham, R.L., Sims, A.C., Baric, R.S. and Denison, M.R. (2006) The nsp2 proteins of mouse hepatitis virus and SARS coronavirus are dispensable for viral replication. *Adv Exp Med Biol*, **581**, 67-72.

221. Graham, R.L., Sims, A.C., Brockway, S.M., Baric, R.S. and Denison, M.R. (2005) The nsp2 replicase proteins of murine hepatitis virus and severe acute

respiratory syndrome coronavirus are dispensable for viral replication. *J Virol*, **79**, 13399-13411.

222. Kopecky-Bromberg, S.A., Martinez-Sobrido, L., Frieman, M., Baric, R.A. and Palese, P. (2007) Severe acute respiratory syndrome coronavirus open reading frame (ORF) 3b, ORF 6, and nucleocapsid proteins function as interferon antagonists. *J Virol*, **81**, 548-557.

223. Frieman, M., Yount, B., Heise, M., Kopecky-Bromberg, S.A., Palese, P. and Baric, R.S. (2007) Severe acute respiratory syndrome coronavirus ORF6 antagonizes STAT1 function by sequestering nuclear import factors on the rough endoplasmic reticulum/Golgi membrane. *J Virol*, **81**, 9812-9824.

224. Varshney, B. and Lal, S.K. (2011) SARS-CoV accessory protein 3b induces AP-1 transcriptional activity through activation of JNK and ERK pathways. *Biochemistry*, **50**, 5419-5425.

225. Minakshi, R., Padhan, K., Rani, M., Khan, N., Ahmad, F. and Jameel, S. (2009) The SARS Coronavirus 3a protein causes endoplasmic reticulum stress and induces ligand-independent downregulation of the type 1 interferon receptor. *PLoS One*, **4**, e8342.

226. Koetzner, C.A., Kuo, L., Goebel, S.J., Dean, A.B., Parker, M.M. and Masters, P.S. (2010) Accessory protein 5a is a major antagonist of the antiviral action of interferon against murine coronavirus. *J Virol*, **84**, 8262-8274.

227. Chen, C.J. and Makino, S. (2004) Murine coronavirus replication induces cell cycle arrest in G0/G1 phase. *J Virol*, **78**, 5658-5669.

228. Dove, B., Brooks, G., Bicknell, K., Wurm, T. and Hiscox, J.A. (2006) Cell cycle perturbations induced by infection with the coronavirus infectious bronchitis virus and their effect on virus replication. *J Virol*, **80**, 4147-4156.

229. Li, F.Q., Tam, J.P. and Liu, D.X. (2007) Cell cycle arrest and apoptosis induced by the coronavirus infectious bronchitis virus in the absence of p53. *Virology*, **365**, 435-445.

230. Chen, H., Wurm, T., Britton, P., Brooks, G. and Hiscox, J.A. (2002) Interaction of the coronavirus nucleoprotein with nucleolar antigens and the host cell. *J Virol*, **76**, 5233-5250.

231. Wurm, T., Chen, H., Hodgson, T., Britton, P., Brooks, G. and Hiscox, J.A. (2001) Localization to the nucleolus is a common feature of coronavirus nucleoproteins, and the protein may disrupt host cell division. *J Virol*, **75**, 9345-9356.

232. Li, F.Q., Xiao, H., Tam, J.P. and Liu, D.X. (2005) Sumoylation of the nucleocapsid protein of severe acute respiratory syndrome coronavirus. *FEBS Lett*, **579**, 2387-2396.

233. Dove, B.K., You, J.H., Reed, M.L., Emmett, S.R., Brooks, G. and Hiscox, J.A. (2006) Changes in nucleolar morphology and proteins during infection with the coronavirus infectious bronchitis virus. *Cell Microbiol*, **8**, 1147-1157.

234. Surjit, M., Liu, B., Chow, V.T. and Lal, S.K. (2006) The nucleocapsid protein of severe acute respiratory syndrome-coronavirus inhibits the activity of cyclin-cyclin-dependent kinase complex and blocks S phase progression in mammalian cells. *J Biol Chem*, **281**, 10669-10681.

235. You, J., Dove, B.K., Enjuanes, L., DeDiego, M.L., Alvarez, E., Howell, G., Heinen, P., Zambon, M. and Hiscox, J.A. (2005) Subcellular localization of the severe acute respiratory syndrome coronavirus nucleocapsid protein. *J Gen Virol*, **86**, 3303-3310.

236. Timani, K.A., Liao, Q., Ye, L., Zeng, Y., Liu, J., Zheng, Y., Yang, X., Lingbao, K., Gao, J. and Zhu, Y. (2005) Nuclear/nucleolar localization properties of C-terminal nucleocapsid protein of SARS coronavirus. *Virus Res*, **114**, 23-34.

237. Harrison, S.M., Dove, B.K., Rothwell, L., Kaiser, P., Tarpey, I., Brooks, G. and Hiscox, J.A. (2007) Characterisation of cyclin D1 down-regulation in coronavirus infected cells. *FEBS Lett*, **581**, 1275-1286.

238. Chen, C.J., Sugiyama, K., Kubo, H., Huang, C. and Makino, S. (2004) Murine coronavirus nonstructural protein p28 arrests cell cycle in G0/G1 phase. *J Virol*, **78**, 10410-10419.

239. Yuan, X., Wu, J., Shan, Y., Yao, Z., Dong, B., Chen, B., Zhao, Z., Wang, S., Chen, J. and Cong, Y. (2006) SARS coronavirus 7a protein blocks cell cycle progression at G0/G1 phase via the cyclin D3/pRb pathway. *Virology*, **346**, 74-85.

240. Yuan, X., Yao, Z., Wu, J., Zhou, Y., Shan, Y., Dong, B., Zhao, Z., Hua, P., Chen, J. and Cong, Y. (2007) G1 phase cell cycle arrest induced by SARS-CoV 3a protein via the cyclin D3/pRb pathway. *Am J Respir Cell Mol Biol*, **37**, 9-19.

241. Yuan, X., Shan, Y., Zhao, Z., Chen, J. and Cong, Y. (2005) G0/G1 arrest and apoptosis induced by SARS-CoV 3b protein in transfected cells. *Virol J*, **2**, 66.

242. Bechill, J., Chen, Z., Brewer, J.W. and Baker, S.C. (2008) Coronavirus infection modulates the unfolded protein response and mediates sustained translational repression. *J Virol*, **82**, 4492-4501.

243. Chan, C.P., Siu, K.L., Chin, K.T., Yuen, K.Y., Zheng, B. and Jin, D.Y. (2006) Modulation of the unfolded protein response by the severe acute respiratory syndrome coronavirus spike protein. *J Virol*, **80**, 9279-9287.

244. Liang, S.H., Zhang, W., McGrath, B.C., Zhang, P. and Cavener, D.R. (2006) PERK (eIF2alpha kinase) is required to activate the stress-activated MAPKs

and induce the expression of immediate-early genes upon disruption of ER calcium homoeostasis. *Biochem J*, **393**, 201-209.

245. Mizutani, T., Fukushi, S., Saijo, M., Kurane, I. and Morikawa, S. (2004) Phosphorylation of p38 MAPK and its downstream targets in SARS coronavirus-infected cells. *Biochem Biophys Res Commun*, **319**, 1228-1234.

246. Banerjee, S., Narayanan, K., Mizutani, T. and Makino, S. (2002) Murine coronavirus replication-induced p38 mitogen-activated protein kinase activation promotes interleukin-6 production and virus replication in cultured cells. *J Virol*, **76**, 5937-5948.

247. Law, P.T., Wong, C.H., Au, T.C., Chuck, C.P., Kong, S.K., Chan, P.K., To, K.F., Lo, A.W., Chan, J.Y., Suen, Y.K. *et al.* (2005) The 3a protein of severe acute respiratory syndrome-associated coronavirus induces apoptosis in Vero E6 cells. *J Gen Virol*, **86**, 1921-1930.

248. Padhan, K., Minakshi, R., Towheed, M.A. and Jameel, S. (2008) Severe acute respiratory syndrome coronavirus 3a protein activates the mitochondrial death pathway through p38 MAP kinase activation. *J Gen Virol*, **89**, 1960-1969.

249. Ye, Z.D., Wong, C.K., Li, P. and Xie, Y. (2010) The role of SARS-CoV protein, ORF-6, in the induction of host cell death. *Hong Kong Med J*, **16**, 22-26.

250. Tan, Y.J., Fielding, B.C., Goh, P.Y., Shen, S., Tan, T.H., Lim, S.G. and Hong, W. (2004) Overexpression of 7a, a protein specifically encoded by the severe acute respiratory syndrome coronavirus, induces apoptosis via a caspase-dependent pathway. *J Virol*, **78**, 14043-14047.

251. Tan, Y.X., Tan, T.H., Lee, M.J., Tham, P.Y., Gunalan, V., Druce, J., Birch, C., Catton, M., Fu, N.Y., Yu, V.C. *et al.* (2007) Induction of apoptosis by the severe acute respiratory syndrome coronavirus 7a protein is dependent on its interaction with the Bcl-XL protein. *J Virol*, **81**, 6346-6355.

252. Kopecky-Bromberg, S.A., Martinez-Sobrido, L. and Palese, P. (2006) 7a protein of severe acute respiratory syndrome coronavirus inhibits cellular protein synthesis and activates p38 mitogen-activated protein kinase. *J Virol*, **80**, 785-793.

253. Vasilenko, N., Moshynskyy, I. and Zakhartchouk, A. (2010) SARS coronavirus protein 7a interacts with human Ap4A-hydrolase. *Virol J*, **7**, 31.

254. McLennan, A.G. (2000) Dinucleoside polyphosphates-friend or foe? *Pharmacol Ther*, **87**, 73-89.

255. Goerlich, O., Foeckler, R. and Holler, E. (1982) Mechanism of synthesis of adenosine(5')tetraphospho(5')adenosine (AppppA) by aminoacyl-tRNA synthetases. *Eur J Biochem*, **126**, 135-142.

256. Zamecnik, P.C., Rapaport, E. and Baril, E.F. (1982) Priming of DNA synthesis by diadenosine 5',5'''-P1,P4-tetraphosphate with a double-stranded octadecamer as a template and DNA polymerase alpha. *Proc Natl Acad Sci U S A*, **79**, 1791-1794.

257. Vartanian, A., Prudovsky, I., Suzuki, H., Dal Pra, I. and Kisselev, L. (1997) Opposite effects of cell differentiation and apoptosis on Ap3A/Ap4A ratio in human cell cultures. *FEBS Lett*, **415**, 160-162.

258. Vartanian, A., Alexandrov, I., Prudowski, I., McLennan, A. and Kisselev, L. (1999) Ap4A induces apoptosis in human cultured cells. *FEBS Lett*, **456**, 175-180.

259. Vartanian, A.A., Suzuki, H. and Poletaev, A.I. (2003) The involvement of diadenosine 5',5'''-P1,P4-tetraphosphate in cell cycle arrest and regulation of apoptosis. *Biochem Pharmacol*, **65**, 227-235.

260. Ye, Z., Wong, C.K., Li, P. and Xie, Y. (2008) A SARS-CoV protein, ORF-6, induces caspase-3 mediated, ER stress and JNK-dependent apoptosis. *Biochim Biophys Acta*, **1780**, 1383-1387.

261. Chen, C.Y., Ping, Y.H., Lee, H.C., Chen, K.H., Lee, Y.M., Chan, Y.J., Lien, T.C., Jap, T.S., Lin, C.H., Kao, L.S. *et al.* (2007) Open reading frame 8a of the human severe acute respiratory syndrome coronavirus not only promotes viral replication but also induces apoptosis. *J Infect Dis*, **196**, 405-415.

262. Khan, S., Fielding, B.C., Tan, T.H., Chou, C.F., Shen, S., Lim, S.G., Hong, W. and Tan, Y.J. (2006) Over-expression of severe acute respiratory syndrome coronavirus 3b protein induces both apoptosis and necrosis in Vero E6 cells. *Virus Res*, **122**, 20-27.

263. Yang, Y., Xiong, Z., Zhang, S., Yan, Y., Nguyen, J., Ng, B., Lu, H., Brendese, J., Yang, F., Wang, H. *et al.* (2005) Bcl-xL inhibits T-cell apoptosis induced by expression of SARS coronavirus E protein in the absence of growth factors. *Biochem J*, **392**, 135-143.

264. Belyavsky, M., Belyavskaya, E., Levy, G.A. and Leibowitz, J.L. (1998) Coronavirus MHV-3-induced apoptosis in macrophages. *Virology*, **250**, 41-49.

265. Chen, C.J. and Makino, S. (2002) Murine coronavirus-induced apoptosis in 17Cl-1 cells involves a mitochondria-mediated pathway and its downstream caspase-8 activation and bid cleavage. *Virology*, **302**, 321-332.

266. Liu, Y., Pu, Y. and Zhang, X. (2006) Role of the mitochondrial signaling pathway in murine coronavirus-induced oligodendrocyte apoptosis. *J Virol*, **80**, 395-403.

267. Liu, Y. and Zhang, X. (2007) Murine coronavirus-induced oligodendrocyte apoptosis is mediated through the activation of the Fas signaling pathway. *Virology*, **360**, 364-375.

268. Liu, Y. and Zhang, X. (2005) Expression of cellular oncogene Bcl-xL prevents coronavirus-induced cell death and converts acute infection to persistent infection in progenitor rat oligodendrocytes. *J Virol*, **79**, 47-56.

269. An, S., Chen, C.J., Yu, X., Leibowitz, J.L. and Makino, S. (1999) Induction of apoptosis in murine coronavirus-infected cultured cells and demonstration of E protein as an apoptosis inducer. *J Virol*, **73**, 7853-7859.

270. Liu, C., Xu, H.Y. and Liu, D.X. (2001) Induction of caspase-dependent apoptosis in cultured cells by the avian coronavirus infectious bronchitis virus. *J Virol*, **75**, 6402-6409.

271. De Martino, L., Marfe, G., Longo, M., Fiorito, F., Montagnaro, S., Iovane, V., Decaro, N. and Pagnini, U. (2010) Bid cleavage, cytochrome c release and caspase activation in canine coronavirus-induced apoptosis. *Vet Microbiol*, **141**, 36-45.

272. Suzuki, K., Matsui, Y., Miura, Y. and Sentsui, H. (2008) Equine coronavirus induces apoptosis in cultured cells. *Vet Microbiol*, **129**, 390-395.

273. Eleouet, J.F., Chilmonczyk, S., Besnardeau, L. and Laude, H. (1998) Transmissible gastroenteritis coronavirus induces programmed cell death in infected cells through a caspase-dependent pathway. *J Virol*, **72**, 4918-4924.

274. Tanahashi, N., Kawahara, H., Murakami, Y. and Tanaka, K. (1999) The proteasome-dependent proteolytic system. *Mol Biol Rep*, **26**, 3-9.

275. Voges, D., Zwickl, P. and Baumeister, W. (1999) The 26S proteasome: a molecular machine designed for controlled proteolysis. *Annu Rev Biochem*, **68**, 1015-1068.

276. Galinier, R., Gout, E., Lortat-Jacob, H., Wood, J. and Chroboczek, J. (2002) Adenovirus protein involved in virus internalization recruits ubiquitin-protein ligases. *Biochemistry*, **41**, 14299-14305.

277. Gao, L., Tu, H., Shi, S.T., Lee, K.J., Asanaka, M., Hwang, S.B. and Lai, M.M. (2003) Interaction with a ubiquitin-like protein enhances the ubiquitination and degradation of hepatitis C virus RNA-dependent RNA polymerase. *J Virol*, **77**, 4149-4159.

278. Harty, R.N., Brown, M.E., McGettigan, J.P., Wang, G., Jayakar, H.R., Huibregtse, J.M., Whitt, M.A. and Schnell, M.J. (2001) Rhabdoviruses and the cellular ubiquitin-proteasome system: a budding interaction. *J Virol*, **75**, 10623-10629.

279. Ros, C., Burckhardt, C.J. and Kempf, C. (2002) Cytoplasmic trafficking of minute virus of mice: low-pH requirement, routing to late endosomes, and proteasome interaction. *J Virol*, **76**, 12634-12645.

280. Schubert, U., Ott, D.E., Chertova, E.N., Welker, R., Tessmer, U., Princiotta, M.F., Bennink, J.R., Krausslich, H.G. and Yewdell, J.W. (2000) Proteasome inhibition interferes with gag polyprotein processing, release, and maturation of HIV-1 and HIV-2. *Proc Natl Acad Sci U S A*, **97**, 13057-13062.

281. Yu, G.Y. and Lai, M.M. (2005) The ubiquitin-proteasome system facilitates the transfer of murine coronavirus from endosome to cytoplasm during virus entry. *J Virol*, **79**, 644-648.

282. Raaben, M., Posthuma, C.C., Verheije, M.H., te Lintelo, E.G., Kikkert, M., Drijfhout, J.W., Snijder, E.J., Rottier, P.J. and de Haan, C.A. (2010) The ubiquitin-proteasome system plays an important role during various stages of the coronavirus infection cycle. *J Virol*, **84**, 7869-7879.

283. Wang, Q., Li, C., Zhang, Q., Wang, T., Li, J., Guan, W., Yu, J., Liang, M. and Li, D. (2010) Interactions of SARS coronavirus nucleocapsid protein with the host cell proteasome subunit p42. *Virol J*, **7**, 99.

284. Raaben, M., Grinwis, G.C., Rottier, P.J. and de Haan, C.A. (2010) The proteasome inhibitor Velcade enhances rather than reduces disease in mouse hepatitis coronavirus-infected mice. *J Virol*, **84**, 7880-7885.

285. Shi, S.T., Schiller, J.J., Kanjanahaluethai, A., Baker, S.C., Oh, J.W. and Lai, M.M. (1999) Colocalization and membrane association of murine hepatitis virus gene 1 products and De novo-synthesized viral RNA in infected cells. *J Virol*, **73**, 5957-5969.

286. Knoops, K., Kikkert, M., Worm, S.H., Zevenhoven-Dobbe, J.C., van der Meer, Y., Koster, A.J., Mommaas, A.M. and Snijder, E.J. (2008) SARS-coronavirus replication is supported by a reticulovesicular network of modified endoplasmic reticulum. *PLoS Biol*, **6**, e226.

287. Verheije, M.H., Raaben, M., Mari, M., Te Lintelo, E.G., Reggiori, F., van Kuppeveld, F.J., Rottier, P.J. and de Haan, C.A. (2008) Mouse hepatitis coronavirus RNA replication depends on GBF1-mediated ARF1 activation. *PLoS Pathog*, **4**, e1000088.

288. Knoops, K., Swett-Tapia, C., van den Worm, S.H., Te Velthuis, A.J., Koster, A.J., Mommaas, A.M., Snijder, E.J. and Kikkert, M. (2010) Integrity of the early secretory pathway promotes, but is not required for, severe acute respiratory syndrome coronavirus RNA synthesis and virus-induced remodeling of endoplasmic reticulum membranes. *J Virol*, **84**, 833-846.

289. Zhao, Z., Thackray, L.B., Miller, B.C., Lynn, T.M., Becker, M.M., Ward, E., Mizushima, N.N., Denison, M.R. and Virgin, H.W.t. (2007) Coronavirus replication does not require the autophagy gene ATG5. *Autophagy*, **3**, 581-585.

290. Prentice, E., Jerome, W.G., Yoshimori, T., Mizushima, N. and Denison, M.R. (2004) Coronavirus replication complex formation utilizes components of cellular autophagy. *J Biol Chem*, **279**, 10136-10141.

291. de Haan, C.A. and Reggiori, F. (2008) Are nidoviruses hijacking the autophagy machinery? *Autophagy*, **4**, 276-279.

292. Reggiori, F., Monastyrska, I., Verheije, M.H., Cali, T., Ulasli, M., Bianchi, S., Bernasconi, R., de Haan, C.A. and Molinari, M. (2010) Coronaviruses Hijack the LC3-I-positive EDEMosomes, ER-derived vesicles exporting short-lived ERAD regulators, for replication. *Cell Host Microbe*, **7**, 500-508.

293. van Hemert, M.J., van den Worm, S.H., Knoops, K., Mommaas, A.M., Gorbalenya, A.E. and Snijder, E.J. (2008) SARS-coronavirus replication/transcription complexes are membrane-protected and need a host factor for activity in vitro. *PLoS Pathog*, **4**, e1000054.

294. Yu, W. and Leibowitz, J.L. (1995) Specific binding of host cellular proteins to multiple sites within the 3' end of mouse hepatitis virus genomic RNA. *J Virol*, **69**, 2016-2023.

295. Furuya, T. and Lai, M.M. (1993) Three different cellular proteins bind to complementary sites on the 5'-end-positive and 3'-end-negative strands of mouse hepatitis virus RNA. *J Virol*, **67**, 7215-7222.

296. Zhang, X. and Lai, M.M. (1995) Interactions between the cytoplasmic proteins and the intergenic (promoter) sequence of mouse hepatitis virus RNA: correlation with the amounts of subgenomic mRNA transcribed. *J Virol*, **69**, 1637-1644.

297. Okunola, H.L. and Krainer, A.R. (2009) Cooperative-binding and splicing-repressive properties of hnRNP A1. *Mol Cell Biol*, **29**, 5620-5631.

298. He, Y. and Smith, R. (2009) Nuclear functions of heterogeneous nuclear ribonucleoproteins A/B. *Cell Mol Life Sci*, **66**, 1239-1256.

299. Li, H.P., Zhang, X., Duncan, R., Comai, L. and Lai, M.M. (1997) Heterogeneous nuclear ribonucleoprotein A1 binds to the transcription-regulatory region of mouse hepatitis virus RNA. *Proc Natl Acad Sci U S A*, **94**, 9544-9549.

300. Zhang, X., Li, H.P., Xue, W. and Lai, M.M. (1998) Cellular protein hnRNP-A1 interacts with the 3'-end and the intergenic sequence of mouse hepatitis virus negative-strand RNA to form a ribonucleoprotein complex. *Adv Exp Med Biol*, **440**, 227-234.

301. Zhang, X., Li, H.P., Xue, W. and Lai, M.M. (1999) Formation of a ribonucleoprotein complex of mouse hepatitis virus involving heterogeneous nuclear ribonucleoprotein A1 and transcription-regulatory elements of viral RNA. *Virology*, **264**, 115-124.

302. Wang, Y. and Zhang, X. (1999) The nucleocapsid protein of coronavirus mouse hepatitis virus interacts with the cellular heterogeneous nuclear ribonucleoprotein A1 in vitro and in vivo. *Virology*, **265**, 96-109.

303. Luo, H., Chen, Q., Chen, J., Chen, K., Shen, X. and Jiang, H. (2005) The nucleocapsid protein of SARS coronavirus has a high binding affinity to the human cellular heterogeneous nuclear ribonucleoprotein A1. *FEBS Lett*, **579**, 2623-2628.

304. Shi, S.T., Huang, P., Li, H.P. and Lai, M.M. (2000) Heterogeneous nuclear ribonucleoprotein A1 regulates RNA synthesis of a cytoplasmic virus. *EMBO J*, **19**, 4701-4711.

305. Shen, X. and Masters, P.S. (2001) Evaluation of the role of heterogeneous nuclear ribonucleoprotein A1 as a host factor in murine coronavirus discontinuous transcription and genome replication. *Proc Natl Acad Sci U S A*, **98**, 2717-2722.

306. Shi, S.T., Yu, G.Y. and Lai, M.M. (2003) Multiple type A/B heterogeneous nuclear ribonucleoproteins (hnRNPs) can replace hnRNP A1 in mouse hepatitis virus RNA synthesis. *J Virol*, **77**, 10584-10593.

307. Huang, P. and Lai, M.M. (2001) Heterogeneous nuclear ribonucleoprotein a1 binds to the 3'-untranslated region and mediates potential 5'-3'-end cross talks of mouse hepatitis virus RNA. *J Virol*, **75**, 5009-5017.

308. Li, H.P., Huang, P., Park, S. and Lai, M.M. (1999) Polypyrimidine tract-binding protein binds to the leader RNA of mouse hepatitis virus and serves as a regulator of viral transcription. *J Virol*, **73**, 772-777.

309. Galan, C., Sola, I., Nogales, A., Thomas, B., Akoulitchev, A., Enjuanes, L. and Almazan, F. (2009) Host cell proteins interacting with the 3' end of TGEV coronavirus genome influence virus replication. *Virology*, **391**, 304-314.

310. Huang, P. and Lai, M.M. (1999) Polypyrimidine tract-binding protein binds to the complementary strand of the mouse hepatitis virus 3' untranslated region, thereby altering RNA conformation. *J Virol*, **73**, 9110-9116.

311. Choi, K.S., Huang, P. and Lai, M.M. (2002) Polypyrimidine-tract-binding protein affects transcription but not translation of mouse hepatitis virus RNA. *Virology*, **303**, 58-68.

312. Sola, I., Galan, C., Mateos-Gomez, P.A., Palacio, L., Zuniga, S., Cruz, J.L., Almazan, F. and Enjuanes, L. (2011) The polypyrimidine tract-binding protein affects coronavirus RNA accumulation levels and relocalizes viral RNAs to novel cytoplasmic domains different from replication-transcription sites. *J Virol*, **85**, 5136-5149.

313. Choi, K.S., Mizutani, A. and Lai, M.M. (2004) SYNCRIP, a member of the heterogeneous nuclear ribonucleoprotein family, is involved in mouse hepatitis virus RNA synthesis. *J Virol*, **78**, 13153-13162.

314. Spagnolo, J.F. and Hogue, B.G. (2000) Host protein interactions with the 3' end of bovine coronavirus RNA and the requirement of the poly(A) tail for coronavirus defective genome replication. *J Virol*, **74**, 5053-5065.

315. Nanda, S.K. and Leibowitz, J.L. (2001) Mitochondrial aconitase binds to the 3' untranslated region of the mouse hepatitis virus genome. *J Virol*, **75**, 3352-3362.

316. Theil, E.C., McKenzie, R.A. and Sierzputowska-Gracz, H. (1994) Structure and function of IREs, the noncoding mRNA sequences regulating synthesis of ferritin, transferrin receptor and (erythroid) 5-aminolevulinate synthase. *Adv Exp Med Biol*, **356**, 111-118.

317. Klausner, R.D., Rouault, T.A. and Harford, J.B. (1993) Regulating the fate of mRNA: the control of cellular iron metabolism. *Cell*, **72**, 19-28.

318. Cordin, O., Banroques, J., Tanner, N.K. and Linder, P. (2006) The DEAD-box protein family of RNA helicases. *Gene*, **367**, 17-37.

319. Xu, L., Khadijah, S., Fang, S., Wang, L., Tay, F.P. and Liu, D.X. (2010) The cellular RNA helicase DDX1 interacts with coronavirus nonstructural protein 14 and enhances viral replication. *J Virol*, **84**, 8571-8583.

320. Vennema, H., Heijnen, L., Zijderveld, A., Horzinek, M.C. and Spaan, W.J. (1990) Intracellular transport of recombinant coronavirus spike proteins: implications for virus assembly. *J Virol*, **64**, 339-346.

321. Tomley, F.M., Mockett, A.P., Boursnell, M.E., Binns, M.M., Cook, J.K., Brown, T.D. and Smith, G.L. (1987) Expression of the infectious bronchitis virus spike protein by recombinant vaccinia virus and induction of neutralizing antibodies in vaccinated mice. *J Gen Virol*, **68 (Pt 9)**, 2291-2298.

322. Cosson, P. and Letourneur, F. (1994) Coatomer interaction with di-lysine endoplasmic reticulum retention motifs. *Science*, **263**, 1629-1631.

323. McBride, C.E., Li, J. and Machamer, C.E. (2007) The cytoplasmic tail of the severe acute respiratory syndrome coronavirus spike protein contains a novel endoplasmic reticulum retrieval signal that binds COPI and promotes interaction with membrane protein. *J Virol*, **81**, 2418-2428.

324. Youn, S., Collisson, E.W. and Machamer, C.E. (2005) Contribution of trafficking signals in the cytoplasmic tail of the infectious bronchitis virus spike protein to virus infection. *J Virol*, **79**, 13209-13217.

325. Lontok, E., Corse, E. and Machamer, C.E. (2004) Intracellular targeting signals contribute to localization of coronavirus spike proteins near the virus assembly site. *J Virol*, **78**, 5913-5922.

326. Lee, M.C., Miller, E.A., Goldberg, J., Orci, L. and Schekman, R. (2004) Bi-directional protein transport between the ER and Golgi. *Annu Rev Cell Dev Biol*, **20**, 87-123.

327. Teasdale, R.D. and Jackson, M.R. (1996) Signal-mediated sorting of membrane proteins between the endoplasmic reticulum and the golgi apparatus. *Annu Rev Cell Dev Biol*, **12**, 27-54.

328. Wang, J., Fang, S., Xiao, H., Chen, B., Tam, J.P. and Liu, D.X. (2009) Interaction of the coronavirus infectious bronchitis virus membrane protein with beta-actin and its implication in virion assembly and budding. *PLoS One*, **4**, e4908.

329. Valderrama, F., Luna, A., Babia, T., Martinez-Menarguez, J.A., Ballesta, J., Barth, H., Chaponnier, C., Renau-Piqueras, J. and Egea, G. (2000) The golgi-associated COPI-coated buds and vesicles contain beta/gamma -actin. *Proc Natl Acad Sci U S A*, **97**, 1560-1565.

330. Luna, A., Matas, O.B., Martinez-Menarguez, J.A., Mato, E., Duran, J.M., Ballesta, J., Way, M. and Egea, G. (2002) Regulation of protein transport from the Golgi complex to the endoplasmic reticulum by CDC42 and N-WASP. *Mol Biol Cell*, **13**, 866-879.

331. Valderrama, F., Duran, J.M., Babia, T., Barth, H., Renau-Piqueras, J. and Egea, G. (2001) Actin microfilaments facilitate the retrograde transport from the Golgi complex to the endoplasmic reticulum in mammalian cells. *Traffic*, **2**, 717-726.

332. SenGupta, D.J., Zhang, B., Kraemer, B., Pochart, P., Fields, S. and Wickens, M. (1996) A three-hybrid system to detect RNA-protein interactions in vivo. *Proc Natl Acad Sci U S A*, **93**, 8496-8501.

333. Luo, X., Li, Z., Li, X., Wang, G., Liu, W., Dong, S., Cai, S., Tao, D., Yan, Q., Wang, J. *et al.* (2011) hSav1 interacts with HAX1 and attenuates its anti-apoptotic effects in MCF-7 breast cancer cells. *Int J Mol Med*, **28**, 349-355.

334. Han, Y., Chen, Y.S., Liu, Z., Bodyak, N., Rigor, D., Bisping, E., Pu, W.T. and Kang, P.M. (2006) Overexpression of HAX-1 protects cardiac myocytes from apoptosis through caspase-9 inhibition. *Circ Res*, **99**, 415-423.

335. Lee, A.Y., Lee, Y., Park, Y.K., Bae, K.H., Cho, S., Lee do, H., Park, B.C., Kang, S. and Park, S.G. (2008) HS 1-associated protein X-1 is cleaved by caspase-3 during apoptosis. *Mol Cells*, **25**, 86-90.

336. Johns, H.L., Doceul, V., Everett, H., Crooke, H., Charleston, B. and Seago, J. (2010) The classical swine fever virus N-terminal protease N(pro) binds to cellular HAX-1. *J Gen Virol*, **91**, 2677-2686.

337. Will, C.L., Schneider, C., Hossbach, M., Urlaub, H., Rauhut, R., Elbashir, S., Tuschl, T. and Luhrmann, R. (2004) The human 18S U11/U12 snRNP contains a set of novel proteins not found in the U2-dependent spliceosome. *RNA*, **10**, 929-941.

338. Wang, H., Gao, M.X., Li, L., Wang, B., Hori, N. and Sato, K. (2007) Isolation, expression, and characterization of the human ZCRB1 gene mapped to 12q12. *Genomics*, **89**, 59-69.

339. Shen, H., Fang, S.G., Chen, B., Chen, G., Tay, F.P. and Liu, D.X. (2009) Towards construction of viral vectors based on avian coronavirus infectious bronchitis virus for gene delivery and vaccine development. *J Virol Methods*, **160**, 48-56.

340. Nanda, S.K., Johnson, R.F., Liu, Q. and Leibowitz, J.L. (2004) Mitochondrial HSP70, HSP40, and HSP60 bind to the 3' untranslated region of the Murine hepatitis virus genome. *Arch Virol*, **149**, 93-111.

341. Chen, S.C. and Olsthoorn, R.C. Group-specific structural features of the 5'-proximal sequences of coronavirus genomic RNAs. *Virology*, **401**, 29-41.

342. Ng, L.F. and Liu, D.X. (2002) Membrane association and dimerization of a cysteine-rich, 16-kilodalton polypeptide released from the C-terminal region of the coronavirus infectious bronchitis virus 1a polyprotein. *J Virol*, **76**, 6257-6267.

343. Xu, H.Y., Lim, K.P., Shen, S. and Liu, D.X. (2001) Further identification and characterization of novel intermediate and mature cleavage products released from the ORF 1b region of the avian coronavirus infectious bronchitis virus 1a/1b polyprotein. *Virology*, **288**, 212-222.

344. Ng, L.F. and Liu, D.X. (2000) Further characterization of the coronavirus infectious bronchitis virus 3C-like proteinase and determination of a new cleavage site. *Virology*, **272**, 27-39.

345. Hiscox, J.A., Wurm, T., Wilson, L., Britton, P., Cavanagh, D. and Brooks, G. (2001) The coronavirus infectious bronchitis virus nucleoprotein localizes to the nucleolus. *J Virol*, **75**, 506-512.

346. Cheng, A., Zhang, W., Xie, Y., Jiang, W., Arnold, E., Sarafianos, S.G. and Ding, J. (2005) Expression, purification, and characterization of SARS coronavirus RNA polymerase. *Virology*, **335**, 165-176.